FORCE FEEDBACK IN REMOTE TELE-MANIPULATION

by

Robert Bicker

Thesis submitted for the
Degree of Doctor of Philosophy, May 1989.

Department of Mechanical Engineering
University of Newcastle upon Tyne
England

ABSTRACT

It is becoming increasingly necessary to carry out manual operations in environments which are hazardous to humans - using remote manipulator systems that can extend the operators reach. However, manual dexterity can become severely impaired due to the complex relationship that exists between the operator, the remote manipulator system and the task. Under such circumstances, the introduction of force feedback is considered a desirable feature, and is particularly important when attempting to carry out complex assembly operations. The dynamic interaction in the man-machine system can significantly influence performance, and in the past evaluation has been largely by comparative assessment.

In this study, an experimental remote manipulator system, or tele-manipulator system, has been developed which consists of three electrically linked planar manipulator arms, each with three degrees of freedom. An articulated 'master' arm is used to control an identical 'slave' arm, and independently, a second kinematically and dynamically dissimilar slave arm. Fully resolved Generalized Control has been demonstrated using a high speed computer to carry out the necessary position and force transformations between dissimilar master and slave arms in real-time.

Simulation of a one degree of freedom master-slave system has also been carried out, which includes a simple model of the human operator and a task based upon a rigid stop. The results show good agreement with parallel experimental tests, and have provided a firm foundation for developing a fully resolved position/position control scheme, and a unique way of backdriving the master arm.

Preliminary tests were based on a peg-in-hole transfer task, and have identified the effect on performance of force reflection ratio. More recently a novel crank-turning task has been developed to investigate the interaction of system parameters on overall performance.

The results obtained from these experimental studies, backed up by simulation, demonstrate the potential of computer augmented control of remote manipulator systems. The directions for future work include development of real-time control of tele-robotic systems and research into the overall man-machine interaction.

Acknowledgements

I would like to thank my supervisor Professor Leonard Maunder OBE for suggesting this topic, for the advice and guidance given throughout the course of the research, and in his capacity as Director of the Stephenson Engineering Laboratories for making available the technical resources of the Department.

I am particularly indebted to Bob Adamson for manufacturing and building the mechanical rig and for producing some of the diagrams presented in this thesis. I would also like to thank Tommy Kirkbride for help in manufacturing mechanical components and Tony Clarke for producing the electronic assemblies.

Financial support for this work was initially provided by UKAEA - AERE Harwell Laboratory. The suggestions made, and the help received from Geoff Cole during this period was invaluable.

I am especially grateful to my wife Maureen for the continuous support and encouragement she has given me, and the understanding shown over the many nights I have devoted to this work. And finally to my children Paul and Philip, to who I must apologise for perhaps being a little neglectful of them during this period.

Dedication

To my Father

"Telemachos, you are to be no thoughtless man, no coward, if truly the strong force of your father is instilled in you; such a man he was for accomplishing word and action. Your journey then will be no vain thing nor go unaccomplished. But if you are not the seed begotten of him and Penelope, I have no hope that you will accomplish all that you strive for. For few are the children who turn out to be equals of their fathers, and the greater number are worse; few are better than their father is. But since you are to be no thoughtless man, no coward, and the mind of Odysseus has not altogether given out in you, there is some hope that you can bring all these things to fulfilment."

The Odyssey of Homer BOOK II Lines 270-280

CONTENTS

CHAPTER 8 (CONTINUED)

CHAPTER 1

Introduction

The handling of radioactive materials during the pioneering days of the nuclear industry required extreme caution and led to the introduction of glove-boxes to prevent any direct human contact with toxic elements. As both toxicity and radiation levels increased it became necessary to move the operator further away from the task. This led to the introduction of simple tong devices that the operator could use to manipulate flasks whilst situated behind a relatively safe biological shield.

Further developments in nuclear physics created extreme radiation hazards, along with more stringent legislation designed to limit exposure of technicians to 'safe' radiation levels. Thicker and more effective biological shields were designed requiring devices that could be used to carry out tasks at a distance of several metres. The first generation of master-slave manipulators were thus designed specifically for use in what have been termed hot-cells.

These remote manipulators allowed the human operators to safely carry out manipulative tasks in what would otherwise be a hazardous environment. By using an ingenious arrangement of belts and cables the operator could manipulate the 'master-arm' and in so doing produce a corresponding motion of the identical 'slave-arm'.

Sensory perception is of paramount importance in manual operations, and if the quality or the extent of the perception is reduced, a loss of effectiveness is inevitable. In remote manipulation where the master controls are situated at some distance from the slave arm the operator's field of view may be partially obscured, perhaps by thick plate glass windows, which can diminish the operator's visual perception of the scene.

Force feedback is an intrinsic feature of a mechanically linked master-slave manipulator. Its sensitivity, as perceived by the operator is directly related to the efficiency of the transmission. Since force and tactile sensory feedback are

essential for dextrous manual manipulations it can be readily appreciated that sensitivity will be seriously impaired when factors such as compliance, backlash and friction exist in the mechanical transmission of the master-slave system. Furthermore, the more complex the system, the more likely it is to degrade the quality of this type of feedback. Nevertheless, highly trained personnel can achieve good dexterity and articulation when using familiar, but inefficient mechanical equipment.

More demanding applications in the nuclear industry such as in-reactor repair preclude the use of direct mechanical arrangements and have led to the development of electrically linked 'tele-manipulators'. Here the operator, using either switches or joysticks, can manipulate a single degree of freedom of the slave arm remotely and view the scene indirectly using television cameras. However, such developments also created problems in that control of the slave arm in this way did not provide the operator with any force feedback information.

1.1 Advances in remote tele-manipulation

The development of the general purpose force-reflecting servo manipulator [Goertz,1952,1954] has since provided a firm foundation for advances in Remote Systems Technology (RST) and with parallel developments in the design of numerically controlled machine tools made feasible the design of automatic 'robotic devices' that could be pre-programmed to carry out highly repetitive tasks in harsh manufacturing environments.

More recently the applications in remote tele-manipulation have been extended to include undersea exploration and earth orbit missions. The requirements may as such necessitate enhanced operator capability with improved load carrying capacity and increased reach which can be made possible using high gain servo systems.

However, the major impact on the development of remote manipulator systems can be attributed to recent advances in the field of industrial automation. High speed control of an industrial robot designed for automatic assembly requires integration with a range of sophisticated sensors capable of analysing visual, force and tactile information. The computational demands placed on the robot controller to compute,

in real time, the individual joint torques depends largely on the requirements of the control scheme.

The desirable features of industrial robots, ie. autonomous operation and the integration of sophisticated sensory feedback systems are now being adopted in RST. One approach is to utilize a computer to make limited decisions and provide command signals, and in certain instances override the human operator who would otherwise maintain overall control of the system.

It is interesting to note how the evolution of the industrial robot which relied, in part, on the development of the early remote handling devices, is now contributing significantly to the advances in RST.

1.2 Objectives and layout of thesis

The work presented in this thesis has addressed issues related to force feedback in remote tele-manipulation. In particular, one of the main objectives of the research was to design an experimental manipulator system on which to develop alternative bilateral force control strategies. These have been implemented using a high speed digital computer. The effectiveness of alternative control schemes have been established using digital simulation and by studying the interaction with operator performance using tasks designed specifically for this investigation.

The material in Chapters 2 and 3 of the thesis reviews the background to this work and outlines more recent developments in the area of remote tele-manipulation. Chapter 4 describes the criteria used to evaluate the performance of remote tele-manipulator systems and also discusses different types of tasks considered relevant to the investigation.

The different control schemes implemented here are presented in Chapter 5. Particular reference has been made to the 'Generalized Control' scheme [Bejczy & Salisbury,1980; Bejczy & Handlykken,1981], which has been successfully demonstrated for the first time in the UK using the experimental facility developed in this study, [Bicker,1985].

Chapter 6 is devoted to a description of the experimental facility. Several novel features associated with the rig are also outlined. Simulation of a one degree of freedom master-slave system is fully described in Chapter 7. An attempt has been made to incorporate a simple model of the 'human operator' into the simulation. And to evaluate the overall man-machine interaction which has been complemented, as far as possible, by parallel experimental verification in an attempt to achieve good correlation between the model and physical system.

The two principal tasks adopted ie. peg-in-hole and crank-turning, which have been used to evaluate the performance of the different control schemes are fully described in Chapter 8. The test programme which was carried out to assess the influence of such factors as gain and force-reflection ratio is discussed and the results of the tests presented.

The conclusions drawn from the study and recommendations for further work are presented in Chapter 9.

It should be pointed out that during the course of this study, which was begun in 1982, the author has written and presented a number of technical papers on material which has been included in this thesis. A final report [Bicker,1985] was submitted to UKAEA in conclusion of the initial phase of the investigation.

A review of recent advances in remote tele-manipulation, and a description of the experimental facility [Bicker & Maunder,1985] and the preliminary results of the peg-in-hole task [Bicker & Maunder,1986] were presented. The results of a dynamic analysis of the pantograph slave-arm and the introduction of the crank-turning task [Bicker & Maunder;1987a,1987b] have been described. Studies relating to the man-machine interface (funded in part by CEGB), provided a forum to outline the concept behind simulation of a one degree of freedom master-slave system, including a simple model of the 'human operator' [Bicker,Burn & Maunder,1987; Bicker,1989].

Work on the design and control of flexible manipulators [Bicker,Pittarus & Tsakalotos,1987], and the application of vibration monitoring to industrial robots [Bicker,Daadbin & Rosinski,1989] has been developed through this investigation.

CHAPTER 2

Scope of Present Investigation

The research programme was intended to investigate problems in tele-manipulator applications related to the nuclear industry. However, it was recognised that many aspects of the study would be common to other industrial tele-manipulator developments where the environment is hostile to man, ie. where the working space is too restricted for manual operations or where man does not possess sufficient power or reach or some other physical attribute. Micro-manipulators have been designed to perform delicate surgical operations [Causer,1981; Matsushima & Nagai, 1981; Matsushima ,1984] in a restricted workspace. The GEC Handyman [Mosher,1967], is an exosketal device designed to enhance mans capabilities - in this case his strength and reach.

Any tele-manipulator system must of necessity consist of at least the following components:

(i) a tool or end-effector by which the task is to be accomplished,
(ii) some degree of articulation (an 'arm') by which the tool may be moved and oriented as required,
(iii) a command device, by which the operator sends control signals to the 'arm',
(iv) a set of sensing feedback elements fitted to the tool and the arm which can transmit information back to the operator regarding the progress of the task,
(v) a man-machine interface which allows the operator to monitor and control the manipulation in a manner most convenient to him.

It is an unfortunate, though inevitable, consequence of the use of a teleoperator system that the overall performance is degraded and a penalty is paid, partly in the form of extra time to accomplish a task, and partly in the increased liklihood of mistakes. This is due to the fact that no mechanical manipulation system has, or is ever likely to have, the degree of coordination and dexterity found in a skilled human being. Thus,

although teleoperation will always remain less efficient and more mistake prone than comparable skilled manual operations, it is obviously advantageous to look for improvements, to reduce the performance degradation, to minimise the penalty, and to reduce operator fatigue.

An attempt has been made here to assess the value, or otherwise, of force feedback in remote handling devices. The Atomic Energy Research Establishment (AERE) Harwell Laboratories of the United Kingdom Atomic Energy Authority (UKAEA), have considerable experience with the development and application of such devices in hostile nuclear environments. Harwell are currently developing hydraulically actuated master-slave manipulators for heavy duty handling tasks [Cole,1986;Cole & M^{c}Pherson ,1988]. Because of the potentially high risk of damaging equipment as a result of the operator being able to apply very high forces between the end-effector of the slave arm and its environment, force feedback in such an application is considered essential.

It is important that the operator has the ability to discriminate between what can be described as disturbances and the force information that is relevant to the task. In a mechanical MSM, the operator is required to move the master arm, and in doing so produces a corresponding movement of the slave arm. However, because of dynamic effects in the mechanical transmission system it is unlikely that this corresponding movement is exactly as anticipated. The effects of friction (coulomb and viscous), compliance (non-rigid cables and flexible link-arms), inertia and backlash (badly meshed gears and excessive clearance in mechanisms), all contribute to the eventual motion which subsequently degrades the operator's performance. This may be further impaired by restricted viewing through large thick shielding windows or remote camera systems.

The application of bilateral feedback control in remote manipulation systems has been slow to develop. The main reason can be attributed to the very high costs incurred during prototyping development. Of particular interest in this area is the practical application of a 'generalized' control technique where a single master arm can be successfully used with several kinematically and dynamically dissimilar slave arms, employing real-time computer control of all sensory feedback information.

2.1 Force reflection

So that the human operator is made aware of the forces being exerted by the arm on the working environment (both deliberately and accidentally) a degree of force feedback is essential. This force reflection capability can be instrumented and presented to the operator in a number of distinct ways. Forces may be measured directly by strain-gauges attached at strategic points on the slave arm ie. multi-component force/torque sensor mounted on the wrist or individual joint sensors, or they may be calculated by measuring the reaction forces and torques at the manipulator base. Although instrumenting the manipulator base with force sensors is a less direct method than the other, it offers the advantage, in teleoperator design, of removing the sensors from the 'hot' area and so reducing maintenance and repair problems.

The presentation of the force feedback information to the operator can be implemented in a variety of ways. The most direct method is to motorise the master arm and to 'feedback' forces (or torques) to the operator in the same ratios as they are generated at the slave. This has the advantage of giving the operator a similar 'sense of feel' which he experiences when using the mechanical MSM systems, however it is difficult to obtain stable control. Indirect methods might include the feedback of vibratory or acoustic signals or the presentation to the operator of visual displays identifying areas of stress on the arm, [Bejczy,1980]. The efficiency of different schemes can be examined by setting up of benchmark manipulative operations and the recording of operators ease of use, which are discussed in Chapter 4.

2.2 Force related tasks

In the present study several tasks were assessed with a view to evaluating manipulator performance, and two main categories of force related tasks identified:

> **Constrained trajectory tasks** including turning a crank, following a physical contour, or running a nut onto a screw thread. In each case motion of one or more degrees of freedom is restrained by the task geometry, and so may impose relatively large forces on the slave

manipulator. Thus a means of measuring these forces and providing compliance to these indirectly imposed loads would be desirable, for example, torque sensors mounted on each joint could be used to provide overload torque indication to a controller.

Force controlled tasks which include such operations as picking and placing components, sensing obstacles or identifying the nature and magnitude of an applied load. Here multi-component sensing is necessary, and appropriate sensing devices are multi-axis force dynamometers mounted in the wrist or base, or multiple distributed single component sensors located on an arm or link.

Remote manipulator systems are designed so that the slave end-effector has at least six degrees of freedom, ie. it can be translated along each of three orthogonal axes, and rotated about each of the axes. The task degrees of freedom impose a severe restriction on the motion of the manipulator.

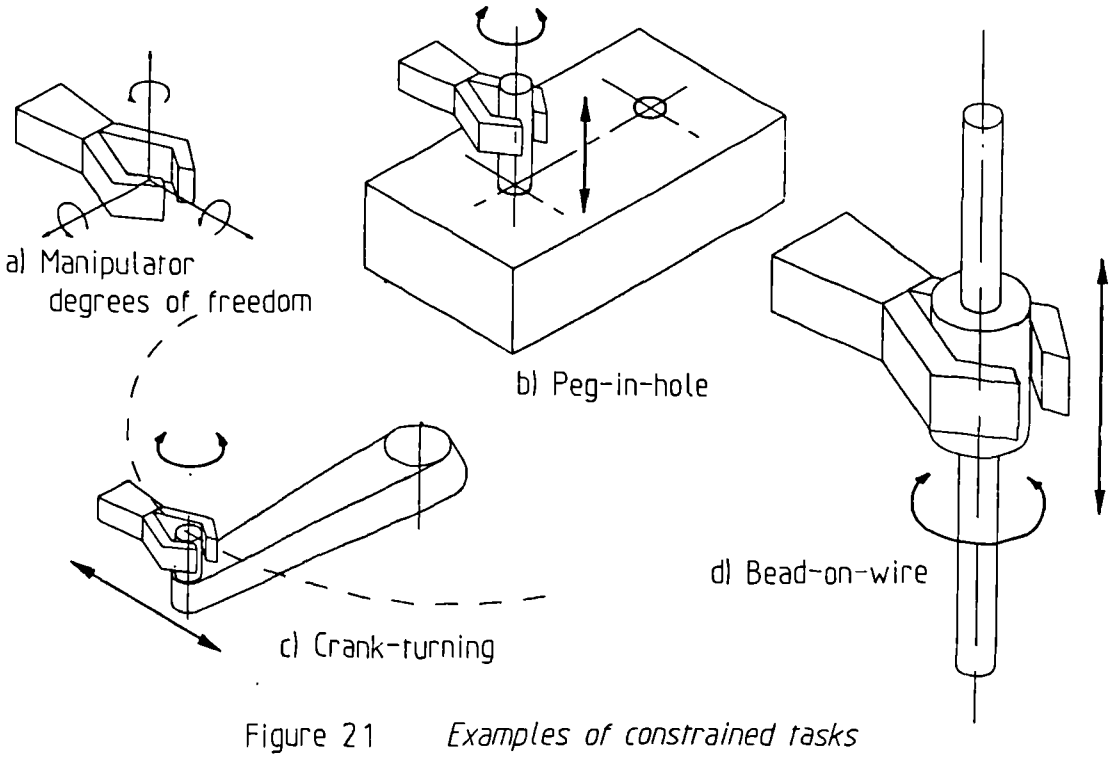

Figure 21 *Examples of constrained tasks*

Examples of constrained trajectory tasks such as peg-in-hole, bead-on-stiff-wire, and crank-turning are illustrated in Figure 2.1. Because the trajectory of the manipulator is modified by the contact forces at the manipulator end-effector, arising as a result of the constraints placed on the motion of the manipulator by the task, the term 'compliance' is often used to describe such manipulative operations. A 'centre of compliance' exists, which is related to the task, and is used to characterize the behaviour of the compliant motion in terms of a 'compliant frame' [Raibert & Craig,1981].

The task degrees of freedom are expressed in an orthogonal coordinate frame, the origin of which is fixed with respect to the centre of compliance. In the peg-in-hole task, the compliance frame is chosen so that the Z-axis is coincident with the axis of the peg, and the origin set near the tip of the peg. The only unconstrained degrees of freedom are translation of, and rotation about the Z-axis, and can thus be position controlled, whereas the remaining freedoms must be force controlled. In the crank-turning task, the Z-axis is aligned with the crank handle, and the X-axis pointing in towards the central crank axis. The degrees of freedom which are position controlled are rotation about the Z-axis and translation along the Y-axis, with the remainder being force controlled. The compliance frame for the bead-on-wire task is chosen so that the Z-axis is directed along the axis of the wire, with the X-axis directed towards the manipulator end-effector, and has position and force controlled axes which are related to the peg-in-hole task.

The constraints placed on the motion of the manipulator by the force controlled freedoms associated with the particular task, and the presence of compliance in the mechanical structure of the manipulator are critical in determining the adequacy of the control scheme. The application of compliant motion control in robot manipulations [Mason,1981;Salisbury & Craig,1981;Raibert & Craig,1981] have addressed issues of active control strategies. Other workers [Watson & Drake,1975;Drake,1977;Whitney,1982] have analyzed parts mating assembly, and describe a passive device, called the Remote Centre Compliance (RCC) which helps prevent jamming or wedging in peg-hole operations.

In remote tele-manipulation the human operator, who is always present, provides the necessary control commands via the input device to carry out the task in hand, and his presence simplifies

the overall control problem. Consequently the performance must be related to the overall man-machine system, and also take into account the requirements of the task.

Two of the tasks described above have been adopted for use in this present investigation. Experiments based on the peg-in-hole and crank-turning tasks have been developed which have provided information relating the performance of a bilateral tele-manipulator system to specific changes in machine parameters, ie. force feedback gain and position feedforward gain. A simple version of the RCC was also designed and used during the testing programme.

CHAPTER 3

Literature Review

The general purpose manipulator has allowed the human operator to extend his 'arms' into potentially hostile environments [Goertz,1952a,1954], and the force reflecting master-slave manipulators (MSM's) have since provided a firm foundation for advances in remote handling and robotics automation, [Galbiati, Mancini & Riamondi, 1964; Flatau, Vertut et al,1972].

The design of mechanically coupled MSM's continues to improve. For example, the high performance Trumotion 'Mini-Manip' [PAR Systems] can easily be inserted through a horizontal cylindrical hole in a vertical shielding wall, and has provision for interchangeable tooling. Devices of this type still account for a large proportion of replica MSM's currently in service, and are used mainly for routine handling of samples having intermediate activity levels.

3.1 Master-slave manipulator development

Compact, replica servo manipulators have been developed for remote maintenance in nuclear installations, and can be gantry mounted on a delivery system for mobile operation. High performance DC servo-motors, harmonic drive gear reduction and cable transmission can offer maximum handling capacity in a light structure, [Flatau 1973,1977].

More recently the Japanese have become actively involved in the development of MSM systems. The Bilarm-83 is a bilateral force reflecting MSM [Yamamoto, Inada et al,1982], and incorporates direct drive technology for each degree of articulation, which it is claimed offers superior reliability over traditional cable/tape transmission. Such systems are designed for applications based on remote maintenance in nuclear facilities and can be crane mounted. A micro-processor controlled bilateral servo-manipulator is currently under development in Japan which has much improved manoeuverability by providing deadweight and

friction compensation in the digital control system [Suzuki et al,1982].

Direct geometric correspondence between master and slave arm automatically resolves the problem of coordinating motion of the end effector or tool mounted on the slave arm. But when restrictions in work space and size exist it may be necessary to make use of alternative strategies, with some limitations in usefulness.

Individual control of joint position or speed using switches or regulators is relatively easy to implement, but coordinated motion of the end effector becomes almost impossible due to the complexity of attempting to resolve motions of several joints simultaneously. It has been established that trained operators can successfully coordinate the motion of up to three joints independently, but not without fatigue quickly diminishing performance.

Velocity or rate control is normally found in applications where large force amplification is required and where environmental constraints prevent direct kinematic correspondence between master and slave arms. Resolved motion rate control (RMRC), [Whitney,1969], provides the ability to carry out the task in world or tool coordinates which are more relevant. The implication is that in a six degree of freedom manipulator all actuators must run simultaneously, at different and time varying rates in order to achieve steady motion along a particular coordinate. The operator simply commands motion along specific trajectories in much the same way that the human reflex system automatically resolves motion of the hands during dextrous manipulations.

Important features of this particular control scheme are that the terminal device can maintain its angular orientation fixed as it moves, or alternatively the angular orientation of the terminal device can be changed at a constant rate about a fixed point in space. The ability to be able to change from a 'world' coordinate frame of reference to a 'tool' coordinate frame is particularly useful. Here the operator can control the approach of the terminal device in 'world' frame then switch to 'tool' frame to undertake a specific task such as tightening or loosening a bolted connection using a spanner or torque wrench.

Irrespective of the coordinate frame, spatial motion and angular orientation can be achieved using dual three-axis joysticks. Most industrial robots employ RMRC for teaching program locations, utilizing either independent switches [Unimation], or three axis joysticks [Asea] on a teach pendant to reposition the manipulator in its workspace in either world or tool coordinates.

The technique relies heavily upon a microcomputer to determine, in real time, the respective joint rates of the slave manipulator by making use of the so called 'Inverse Jacobian' matrix, which is described in Chapter 5. To date the main application for RMRC appears to be in the field of robotics automation where the robot end-effector can be moved under manual control for 'teach and repeat' positioning, and then execute, in the automatic mode, straight line motions at constant velocity. Hydraulically actuated heavy duty manipulators (HDM's), sometimes employ RMRC and are used as an anchor or stiff platform for mounting MSM's in remote locations inside nuclear reactors [Perratt,1987].

Bilateral control of a remote manipulator based on RMRC has not yet been successfully demonstrated, although work at Newcastle is presently addressing this issue [Burn,1989].

3.2 Recent tele-manipulator system control concepts

The development of untethered and unmanned submersibles designed for use in deep ocean exploration studies and for repair and maintenance of large offshore structures is a relatively new area in which remote manipulator systems are being employed. The earth orbit space missions, characterised by the NASA space shuttle program, employs a Shuttle Remote Manipulator System (SRMS) to deploy and capture orbiting satellites. Restrictions in operator cabin size and payload requirements in both undersea and space vehicles preclude full size master-slave control [Bertsche, Pesch & Winget,1977; Doetsch,1977].

The terminal pointer hand controller [Saenger & Pegden,1972] is considered to be an extension of the RMRC technique developed by Whitney. This concept however uses a three degree of freedom hand controller to orient the terminal device of the slave arm. The resulting slave arm velocity is proportional to the position of the hand controller. A terminal mounted camera is also

orientated by the terminal pointer, with rate control provided along the camera viewing axis.

During the initial development of the Space Shuttle remote manipulator system, several alternative control strategies were proposed. One of the recommendations, the X - Reference frame position bilateral control scheme [Booker & Smith,1973] facilitates coordinate indexing, position indexing and variable position gain ratio's to control the large boom manipulator. Whilst these features are important, provision for inertial compensation had to be introduced to permit the slewing of massive satellites with what is a very flexible boom.

The relationships between task specifications, structural elements, control servos and strategies, and the overall design for both industrial and space manipulator systems has been comprehensively assessed [Whitney,1974]. The significance of flexibility in slender manipulators and the requirements for fine motion control have also been evaluated, [Bicker et al,1988].

The developments at the Jet Propulsion Laboratory (JPL), [Bejczy & Brooks,1980; Handlykken & Turner,1980; Bejczy & Salisbury,1980] in kinesthetic man-machine coupling in the form of a general purpose hand controller merits particular attention. The command device has six degrees of freedom, is backdrivable, and the controller and slave arm are geometrically dissimilar. The kinematics of the slave arm being related through mathematical transformations of the master arm joint position variables, calculated in real-time. In a similar manner, force/torque feedback information is presented back to the master arm, resolved again in real time, to give the operator a sense of 'feel' via his hand of the reaction forces/torques exerted between the terminal device and task interaction at the slave arm.

3.3 Supervisory control of remote manipulator systems

Supervisory control of remote manipulators requires a computer to assist the operator and provide additional information regarding the overall status of the system. The system may be capable of carrying out specific manipulative tasks using teach and repeat by programming to ease the operator work load. Smooth interchange between operator and command system must take place,

and the design of general command language implemented is very important [Ferrell & Sheridan,1967; Ferrell,1972;1977; Sheridan, 1976a,1976b].

Distributed microprocessor systems for application in remote manipulator systems are being developed at JPL [Paine,1979] to demonstrate the utility of 'smart' displays that can present graphical information from wrist force and tactile sensors mounted on the slave arm. Voice controlled displays for subsequent integration in supervisory control systems are also under development for use in space applications.

Similar distributed digital control systems are being developed at Oak Ridge National Laboratory [Martin, Satterlee & Bolfing, 1982] to monitor and control a remotely operated dual-arm manipulator and integral closed circuit television. This facility is being funded to support maintenance and repair programs in nuclear installations, and it is recognised that servo-manipulator integration requires improvements in design and flexibility. Future plans include computer augmented remote operation under supervisory control. The implementation of teach-by-doing for autonomous operation of repetitive tasks and automatic camera tracking of the end effector are two areas presently under development. Future plans include automatic control of compliance in the slave manipulator to account for varying loads and slave arm configuration.

The operational Shuttle remote manipulator system is perhaps the most advanced example of a fully integrated man-machine supervisory control system and can be operated from dedicated control and displays with the aid of direct vision and closed circuit television cameras. The operator, in the relative safety of the command cabin can direct the control of the system in one of three operational modes: automatic pre-programmed control; manual augmented control; and, direct drive under fail safe backup control. The autonomous and manual augmented control modes can operate in any one of three coordinate systems: orbiter reference; payload reference; and, end-effector or tool reference [Kumar et al,1979; Brown,1976].

3.4 Tele-robotics

With the recent advances in micro-electronics and subsequent benefits being passed on to the technologies of control and robotics the concept of tele-robotics as distinct from computer aided tele-manipulation has been developed for application in hostile environments. Industrial robotics is beginning to play a significant role where pre-programmed autonomous operation is practical. The main criteria for such application in the nuclear industry is the ability to use equipment having both reliability and a satisfactory radiation tolerance. It has been established that minor modification and gaitering of the robot would provide adequate contamination control [Vertut,1981; Sanders,1977; Abel,1987; Stone,1987]. Integration of suitable real time hand controllers and specialised tooling requirements would of course be necessary.

The substantial saving gained by using enabling technologies for introducing industrial robotics as an alternative to developing advanced tele-manipulators at a prohibitive cost and with limited market potential makes the prospect attractive. Present robotics research programmes are aimed at establishing efficient control algorithms and developing artificial vision, tactile and force sensors with obvious application in remote systems technology.

A tele-robotic installation is presently under development at Newcastle, partly funding by the CEGB, and is based upon a PUMA 560 industrial robot which can be operated remotely by a general purpose hand controller using real-time path control. A hierarchical computer control system is being employed with a supervisory controller capable of communicating with the master and slave arm sub-systems and integrating all sensor data [Burn,1979].

CHAPTER 4

Performance Evaluation of Remote Manipulators

Remote manipulator systems are normally designed to carry out operations in only one hazardous environment ie. space or nuclear. The system must satisfy a very stringent specification in terms of handling capacity, reach, dexterity and high mobility whilst meeting high standards of reliability and maintainability. In many applications it is necessary to design dedicated systems or alternatively tailor existing designs with consequential high development cost. An extensive commissioning programme is considered essential to assess the performance of the system under simulated service conditions prior to its installation.

In view of the complex operator-machine and machine-task interactions it is not surprising that the criteria by which the performance of remote manipulator systems are assessed have in the past generally been based on qualitative tests. Comparison of the time taken to carry out a specific task, or set of tasks manually, being measured against identical tasks carried out with a tele-manipulator.

The human motor system which is combined with highly efficient sensory perception enables complex tasks to be undertaken rapidly and with relative ease. When the manipulator system is interposed between the human and the task a resulting loss in manual dexterity occurs, which is due to many factors. The purpose of most performance testing is to establish the resulting degradation.

For tests to be statistically significant they must be carried out under carefully controlled conditions, and because the 'perfect human' is not available to undergo the tests the results can only be subjective. Sheridan has noted that the relationship between the operator, manipulator, task and subsequent performance is in his opinion quantitatively unknown [Sheridan, 1976c].

4.1 Task performance indices

Previous investigators who have attempted to analyse performance qualitatively, have assessed dexterity using several different criteria.

(i) An index of difficulty - I_d, has been proposed which relates distance moved to final tolerance for a positioning task [Fitts, 1954]. Originally intended for evaluation of human response, the tapping test has been modified to include constrained tasks such as fitting a peg into a hole with different clearance ratios. The original test has also been applied to compare different remote manipulator systems [Ferrell, 1966; Sheridan & Ferrell,1963; M^{c}Govern 1974a; Hill,1979].

(ii) A dexterity quotient - DQ, which is based upon a well defined scoring and timing system and which yields a single number, [Flatau,Greeb & Booker,1973]. The main features of the test includes an exact definition of tasks, procedures to reduce the influence of operator acquired skill, and other related factors.

(iii) A dexterity factor, where the 'dexterity' of a manipulator is compared to the equivalent task undertaken manually [Vertut,1973]. A time efficiency factor, which is always larger than unity, relates the influence of slowing factors to overall performance.

Because of the subjective nature of these 'standard' tests, and the need to maintain strict control and careful planning, it has been proposed that the capability of manipulators could be established by adopting a standardised task and varying parameters of the mechanical transfer function [Jelatis,1976]. Thus the effects of controlled amounts of backlash, damping, compliance and inertia would serve to quantify the performance of master-slave manipulator systems.

4.2 Performance evaluation

Evaluation of remote manipulator systems has in the past been based upon similar criteria to those outlined in the previous

section, and the selection of a particular figure of merit must be related to the operational requirements of the system.

General purpose remote manipulator systems must be able to accomodate a wide range of operational tasks, and evaluation by a systematic test programme has been proposed [Flatau,1972], where each complete test is characterised by a well defined set of typical tasks that must be carried out under carefully controlled conditions. Evaluation based upon this technique can only be qualitative as it is particularly suited to the comparison of different manipulator systems and is not appropriate where specific manipulator characteristics are required to be analysed.

A broad study of manipulator performance has been reported by Vertut, [Vertut,1973]. Provisional evaluation of several different classes of manipulator systems emphasize the importance of bilateral force reflection. Because manipulators come in all shapes and sizes, differences in performance can be qualitatively explained. However, the dynamic characteristics of each manipulator would contribute to the overall assessment and it is not practical to determine what factors are significant.

A comparison of the performance of rate control versus replica master-slave with force reflection has been documented [Wilt,Pieper,Frank & Glenn, 1977], the different control modes were implemented using the same slave arm but with different master controllers. The results of task completion time versus tasks of varying difficulty showed that bilateral control had a distinct advantage over resolved motion rate control.

The task difficulty index proposed by Fitts has been adopted by M^{c}Govern [M^{c}Govern,1974a,1974b] and used to evaluate the performance of two different manipulator systems. The major conclusion drawn from the results of the experimentation were that the index was a valid measure of task difficulty which could be extended over a small reach of operation. However, the results of these were again only qualitative since they attempted to compare two classes of manipulator operating under completely different control modes. In more recent work M^{c}Govern [M^{c}Govern,1977] has assessed the performance of a supervisory control system, and noted that the command language proved to be a limitation, particularly for complex tasks. It was postulated that more efficient languages may yield more positive results.

4.3 Factors influencing performance

4.3.1 Transmission delay

With increasing remoteness between the operator and task, as for example in undersea and space applications, significant transmission delays can be experienced which inevitably leads to a degraded performance as a consequence of reduced stability in the closed loop control system.

For moderate time delays of less than 0.3 seconds, using a remote manipulator system without force feedback, the operator has been found to adopt a strategy that enabled continuous operation based upon a predictive or preview behavioural pattern [Ferrell,1965].

With time delays of up to 3 seconds [Sheridan & Ferrell,1963; Verplank,1976; Freedy & Weltmann,1972] research has found that the operator adopted a move and wait strategy, ie. move open loop and wait for visual and sensory feedback. It has also been noted that, at the expense of time, it was possible to carry out tasks with considerable accuracy using such a strategy.

A more recent study has compared master-slave and resolved motion rate control using a peg transfer task in the presence of time delays of similar magnitude [Starr,1979]. It was found that master-slave control provided better performance in the absence of any time delay, although increasing amounts of time delay degraded performance more rapidly than rate control, especially with an increase in task difficulty. Overall, it was concluded that RMRC was considered to be more effective with a corresponding reduction in operator fatigue being reported.

To date little published data is available regarding the influence of transmission delay on MSM systems where bilateral control is employed. Some early work [Ferrell,1965] has indicated difficulty in achieving satisfactory stable operation, and results were not compared with the equivalent unilateral control system. More recent work [Vertut,1981] is still in its infancy and as yet no meaningful results have been published. In both studies, tests were carried using simple one degree of freedom systems.

4.3.2 Manipulator dynamics

As previously mentioned, the effects of backlash, friction and other dynamic characteristics are often ignored when evaluating manipulator performance. Analysis of system response variables in undersea manipulators has been reported [Bertsche et al,1977], and has led to the systematic development of design alternatives and definition of response variables which were judged to be most critical in terms of their potential effect on a force reflecting manipulator system.

However, recent work [Book & Field,1980; Book & Hannema,1981] has extended this work and attempted to quantify the effects of particular dynamic characteristics necessary to provide a given performance at a given task. Controlled single factor tests have been performed by simulating the characteristics of interest and implementing them in the dynamics via the joint control system. A two degree of freedom, unilateral MSM was developed for the programme and a positioning test adopted based on that of Fitts. The preliminary results appear to support the variations in performance in both a logical and consistent manner.

CHAPTER 5

Control of Remote Manipulators

The most common way of controlling 'hot-lab' remote manipulators is usually by passive mechanical linkages. The operator manipulates a full-scale replica of the remote slave arm to carry out precise tasks and the system has the attributes of both direct spatial correspondence and intrinsic force feedback. The electrically linked master-slave manipulator system solves the problem of coordinating the motion if master and slave are geometrically similar since joint actuators can be driven by corresponding joint transducers. Similarly, force reflection can be achieved by sensing torque demands at each joint and driving corresponding joint actuators mounted on the master arm.

The ability to control kinematically and dynamically dissimilar arms has been termed 'generalized control' [Bejczy,1980]. A six degree of freedom universal hand controller was developed at JPL to establish 'kinesthetic coupling' [Bejczy & Salisbury, 1980] between the operator and a 6 degree of freedom slave manipulator. The hand controller acts as a position control input device by utilizing a computer to carry out complex mathematical transformations to calculate the corresponding slave arm joint position commands in real-time, and so maintain the necessary coordination between hand controller and slave arm.

A multi-component force/torque sensor was mounted on the wrist of the slave manipulator, and a computer was used to carry out the appropriate force/torque transformations between slave-arm and hand controller, and so establishing the kinesthetic coupling, permitting the operator to'feel' the task he is controlling.

In this chapter, the stability characteristics of a simple one degree of freedom master-slave system are presented in terms of its frequency response using digital simulation [Simbol,1987], based upon position/force and position/position bilateral control schemes. The stability of the two methods has been considered for varying amounts of viscous friction and force feedback gains, and the influence of noise in the control loop assessed. The

The concept of generalized control is applied to a study of a one degree of freedom system with dissimilar master and slave. The mathematical requirements for multi-axis generalized control schemes are presented, and a detailed analysis of the concept based on a three degree of freedom system is described. Implementation based on digital control has also been addressed.

5.1 Single axis master-slave control

The typical master slave manipulator system relies upon the use of identical master and slave arms with independent servo control loops associated with corresponding joints. Such a system can be represented in its simplest form as a one d.o.f. unilateral position controller employing velocity damping as shown diagrammatically in Figure 5.1.

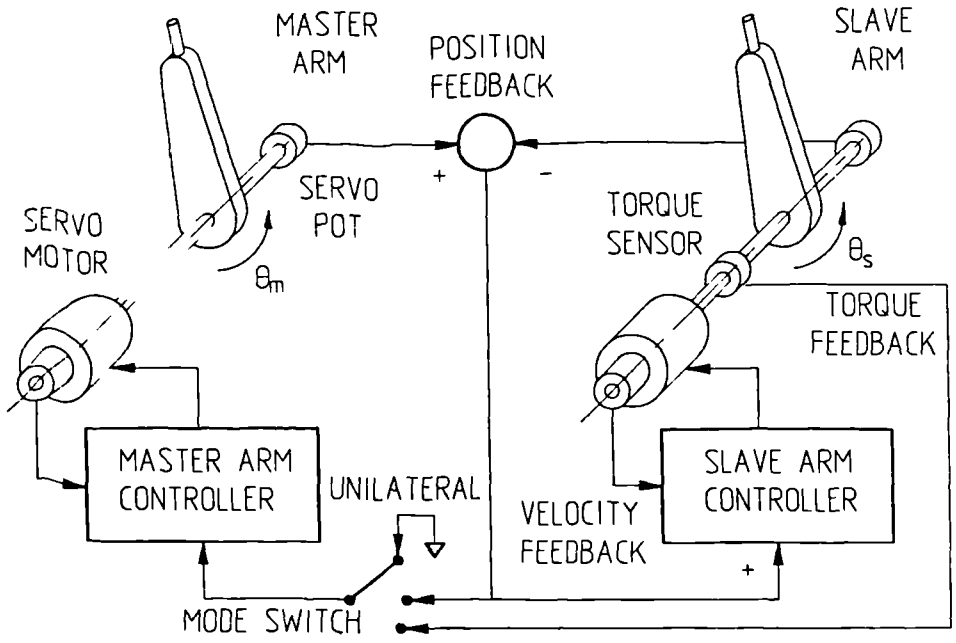

Figure 51 *Schematic of 1 d.o.f master-slave system*

Two modes of bilateral control have been considered, namely, position/force and position/position control.

5.1.1 Position/force control

The equivalent block diagram for a one degree of freedom position/force MSM system is shown in Figure 5.2. The operators hand exerts a torque T_h, which moves the master arm, having a transfer function $G_m(S)$ through an angle θ_m, where 'S' denotes the Laplace variable. The position control loop, has a gain K_p between the master and slave, and drives the slave arm, with transfer function $G_s(S)$ through an angle θ_s. If the arm comes into contact with a rigid obstacle located at θ_t then a reaction torque T_s will result, which is related to the stiffness of the slave arm, K_s. Velocity damping can be introduced, or may already be present in the form of viscous friction, K_v. The addition of force feedback, making the system bilateral is made possible by the introduction of a suitable torque sensor, of gain K_f, the output of which is fedback to the master arm to react against the operator input torque.

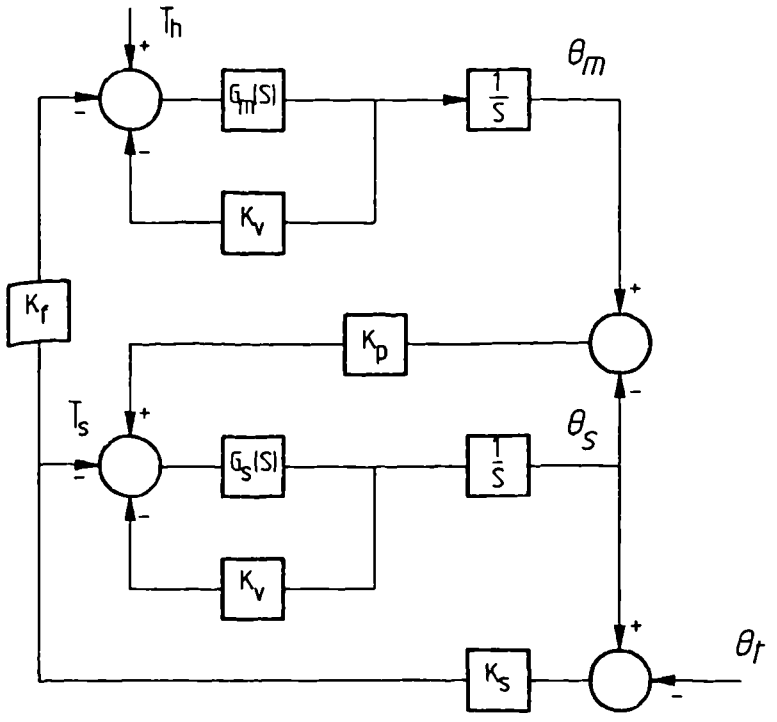

Figure 5.2 *Block diagram of position/force control*

Analysis of an identical master-slave system when $G_m(S) = G_s(S) = K/S$, where K is inversely proportional to the system inertia, can be used to determine a measure of the system performance for the transfer function θ_m/T_h when the slave arm is in contact with an obstacle located at $\theta_t = 0$. It can be shown that

$$\frac{\theta_m}{T_h} = \frac{S^2+SKK_v+K(K_p+K_s)}{S^4/K+2S^3K_v+S^2(KK_v^2+K_p+K_s)+SKK_v(K_p+K_s)+K_fK_pK_sK} \quad \ldots\ldots\{5.1\}$$

The stability of the system, defined by equation {5.1} can be obtained by equating T_h to zero, giving the characteristic equation

$$S^4/K+2S^3K_v+S^2(KK_v^2+K_p+K_s)+SKK_v(K_p+K_s)+K_fK_pK_sK = 0 \quad \ldots\ldots\{5.2\}$$

The stability criteria is given by

$$KK_v^2(K_p+K_s)+(K_p+K_s)^2/2 > 2K_fK_sK_p \quad \ldots\ldots\{5.3\}$$

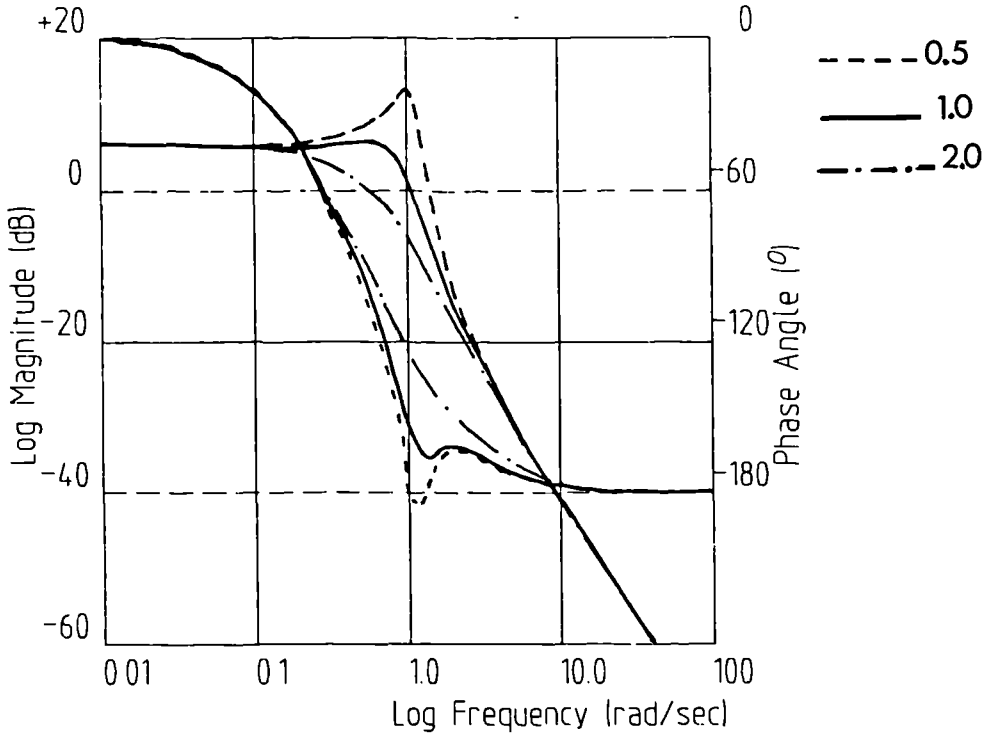

Figure 5.3 *Frequency response - variable K_v*

By inspection of the inequality {5.3}, the following observations can be made when all gain coefficients are positive:

(i) without force feedback, ie. $K_f = 0$, the system is stable for all gains,

(ii) without damping ie. $K_v = 0$, and with $K_f = 1$ the system is stable for all values of K_p and K_s,

(iii) if $K = K_v = K_p = K_s = 1$, then stability will be achieved when $K_f < 2$.

The frequency response of the system for various values of damping K_v, and with all other gain coefficients equated to 1 is shown in Figure 5.3. The results imply that damping values of approximately 1 produce a reasonably flat response up to a cut-off frequency of 1 radian/second. By letting $K_v = 1$ and varying the force feedback gain K_f, the frequency response obtained is shown in Figure 5.4, confirming that instability occurs with a force feedback gain of 2. Figure 5.5 shows the Nyquist plots for $K_f = 1.0$ and 1.5. With increasing K_f the plots rapidly approach the $-1 +/- j0$ point, ie. tending towards instability.

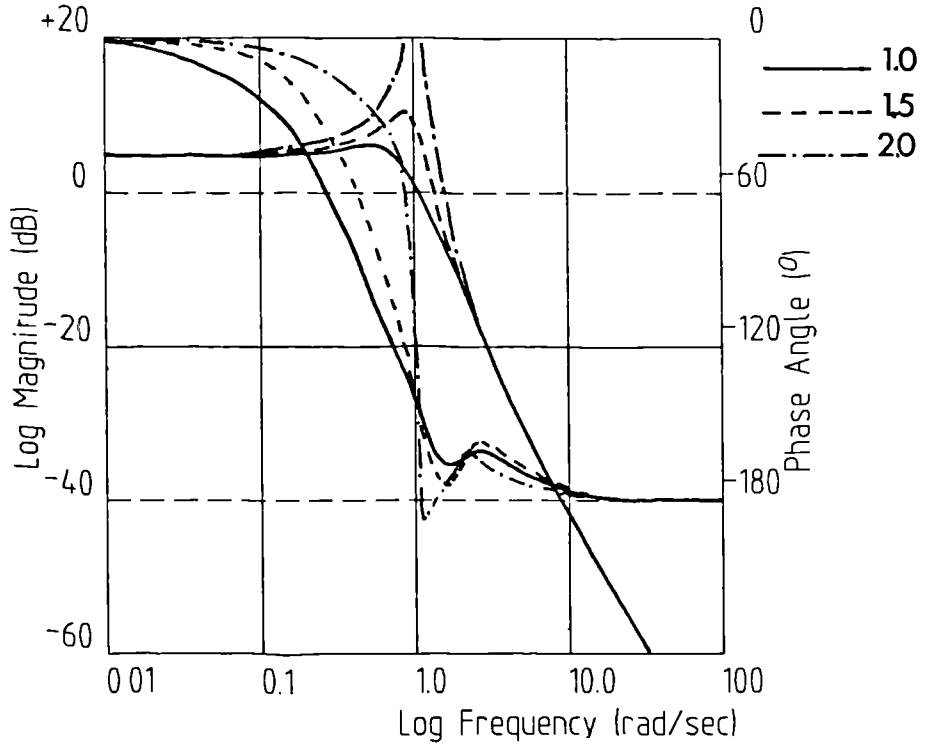

Figure 5.4 *Frequency response - variable K_f*

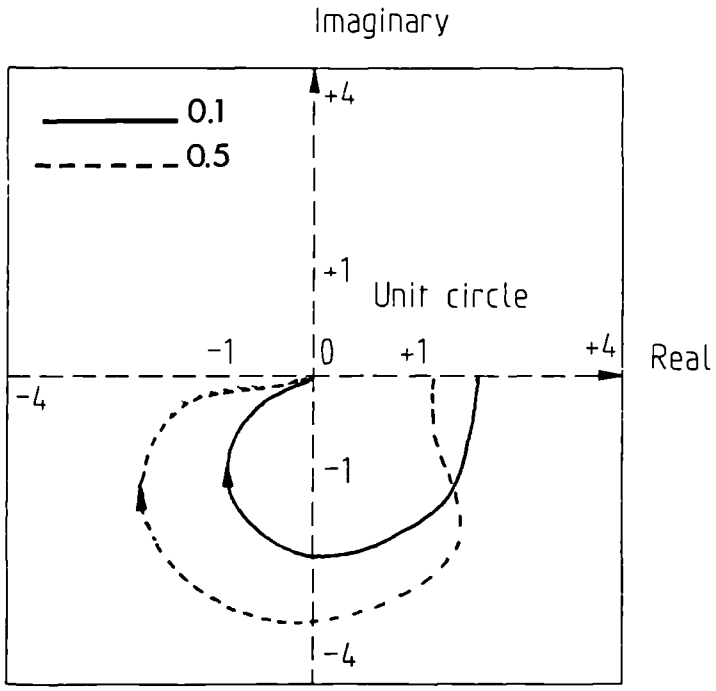

Figure 5.5 *Nyquist plot for variable K_f*

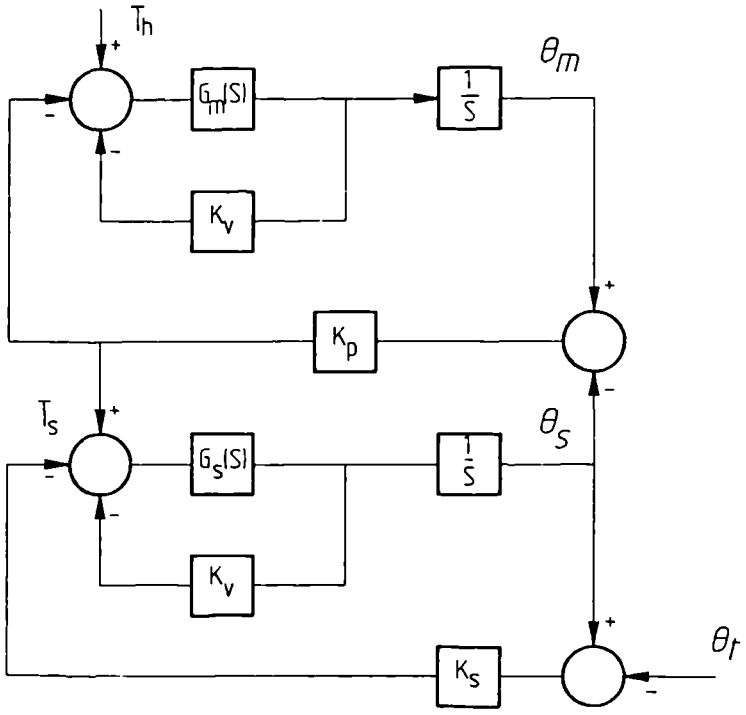

Figure 5 6 *Block diagram of position/position control*

5.1.2 Position/position control

The block diagram for a simplified single degree of freedom position/position control strategy is shown in Figure 5.6, which relies upon two coupled position feedback loops acting on corresponding joints of a master-slave system. The slave to master position feedback provides the necessary compensating force feedback when the slave arm is in contact with an obstacle, without using a force sensor. The feedback 'force' being proportional to the slave to master position error.

For identical master and slave arms ie. $G_m(S) = G_s(S) = K/S$, and assuming the slave arm is in contact with an obstacle positioned at $\theta_t = 0$, the system performance can again be evaluated using the transfer function θ_m/T_h where

$$\frac{\theta_m}{T_h} = \frac{S^2+SKK_v+K(K_p+K_s)}{S^4/K+2S^3K_v+S^2(2K_p+K_s+KK_v^2)+SKK_v(2K_p+K_s)+KK_pK_s} \qquad \ldots\ldots\{5.4\}$$

Letting $T_h = 0$, gives the characteristic equation

$$S^4/K+2S^3K_v+S^2(2K_p+K_s+KK_v^2)+SKK_v(2K_p+K_s)+KK_pK_s = 0 \qquad \ldots\ldots\{5.5\}$$

This yields the stability criteria

$$K_p+K_s/2+KK_v^2 > 0$$

and

$$2K_p^2+2KK_pK_v^2+K_s^2/2 > 0 \qquad \ldots\ldots\{5.6\}$$

The frequency response of the system for different values of K_v is shown in Figure 5.7, the resonant peaks indicate the presence of dominant poles. Figure 5.8 gives the equivalent Nyquist plots for $K_v = 0.1$ and 0.5. Notice that although the lower frequency mode is dominant, the higher frequency mode has a marked affect on the gain and phase margins.

A comparison of Figures 5.3 and 5.7 indicates that better stability is obtained in the position/position control mode, when all gains are unity.

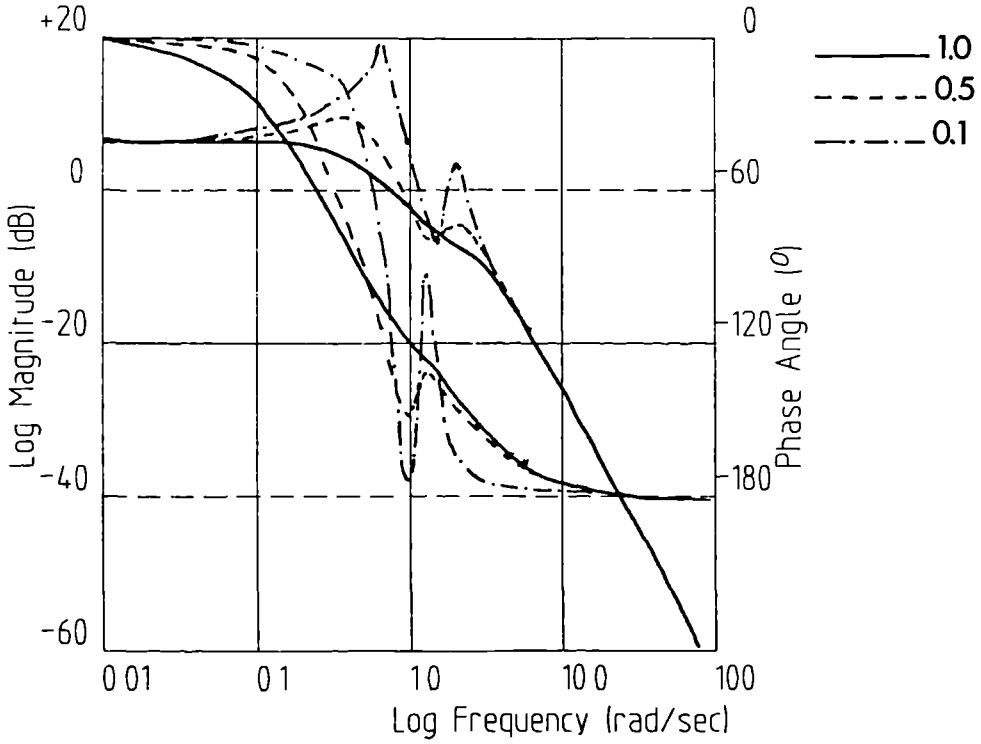

Figure 5 7 *Frequency response - variable K_v*

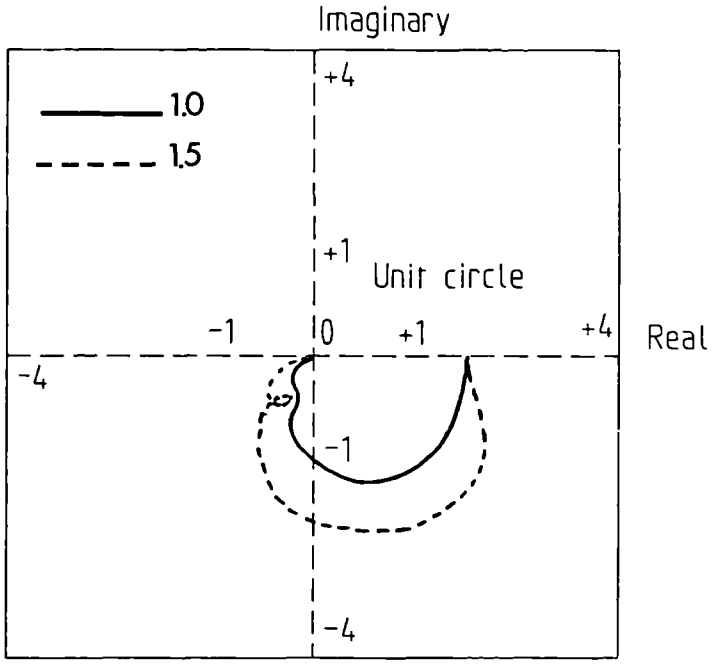

Figure **5.8** *Nyquist plot for variable K_v*

5.1.3 Effect of noise

The relative stability of two different control methods has been assessed in the previous section along with the effect of external disturbances acting on the system. However, control systems are also subjected to undesirable noise which may be generated inside the various feedback loops or occur as a result of changes in the environment affecting transducers and associated cabling.

The presence of unwanted random noise in the position/force feedback master-slave system can be represented as noise in both the position feedback $\mathbf{n_1(S)}$, and force feedback $\mathbf{n_2(S)}$, as shown in Figure 5.9.

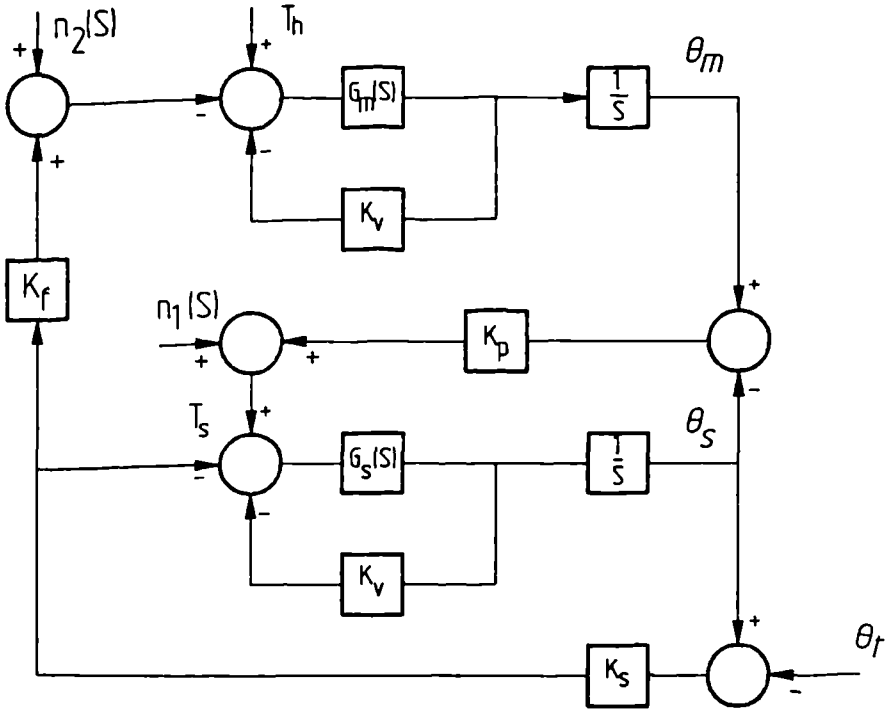

Figure 5.9 *Effect of noise in position/force control system*

It can easily be shown that

$$(T_h-n_2)(S/H_s+K_vS+K_s+K_p)-n_1 = \theta_m((S/H_m+K_vS)(S/H_s+K_s+K_p)+K_fK_sK_p)$$

.....{5.7}

and clearly the noise which is generated in both feedback loops can influence the overall transfer function. Letting the input T_h and $n_2(S)$ be zero, and since the system is linear by applying the principle of superposition, the noise input $n_1(S)$ can be considered as the principal input. The disturbance input transfer function can be written as

$$\frac{\theta_m}{n_1} = \frac{1}{S^4/K+2^3K_v+S^2(2K_pK_s+KK_v^2+SKK_v(2K_p+K_s)+KK_pK_s}$$

.....{5.8}

When compared with the transfer function θ_m/T_h from equation {5.1} it can be seen that the characteristic equations are identical, as expected, but that the numerator functions are different. A disturbance input does not affect the stability of the system but can affect the transient response and also introduce steady state errors which will influence the sensitivity of the system.

Considering the presence of noise in the force feedback loop gives the disturbance input transfer function in terms of θ_m/n_2, and with T_h and n_1 both zero, yields the identical RHS to equation {5.1}.

A control system can be modelled as an idealised low-pass filter that is capable of passing all inputs and rejecting any unwanted disturbances. In practice the effects of noise are not totally cancelled which calls for the careful design of control loops and filtering to bring about their attenuation.

It is difficult to predict in advance the characteristics of induced noise, and consequently it is necessary to make provision for noise reduction by using adequate shielding on instrument cables and eliminating inductive and common impedance coupling or ground loops on sensitive analog circuits. The interface between transducer outputs and electronic circuits often requires the inclusion of analog filters particularly when output devices such

as motors operating at high power levels generate large voltage and current spikes. In the case of coupled digital and analog subsystems it is necessary to make use of special analog filters to eliminate aliasing.

5.2 Single-axis generalized control

A simple one degree of freedom model of a bilateral control scheme between dissimilar master and slave arms is shown schematically in Figure 5.10. Because of kinematic and dynamic differences between the master and slave arms some form of scaling, which may not be linear, would be required to successfully implement the control. The block diagram of Figure 5.11 assumes that the slave arm is only capable of linear motion along the x-coordinate.

The kinematic relationship between master and slave require a transformation from joint to world space, as follows

$$x_s = L.\text{Sin}\,\theta_m$$

$$dx_s/dt = L.\text{Cos}\,\theta_m.d\,\theta_m/dt$$

and

$$d^2x_s/dt^2 = L.\text{Cos}\,\theta_m.d^2\theta_m/dt^2 - L.\text{Sin}\,\theta_m.(d\,\theta_m/dt)^2$$

.....{5.9}

The equivalent force transformation between joint and world space can be represented by

$$F_s = T_h(\text{Cos}\,\theta_m/L)$$

.....{5.10}

The block diagram equivalent of the one degree of freedom generalized control system requires a force transformation between world and joint space ie. the inverse of equation {5.10}, such that

$$T_h = K_f.F_s(\text{Cos}\,\theta_m/L)^{-1}$$

.....{5.11}

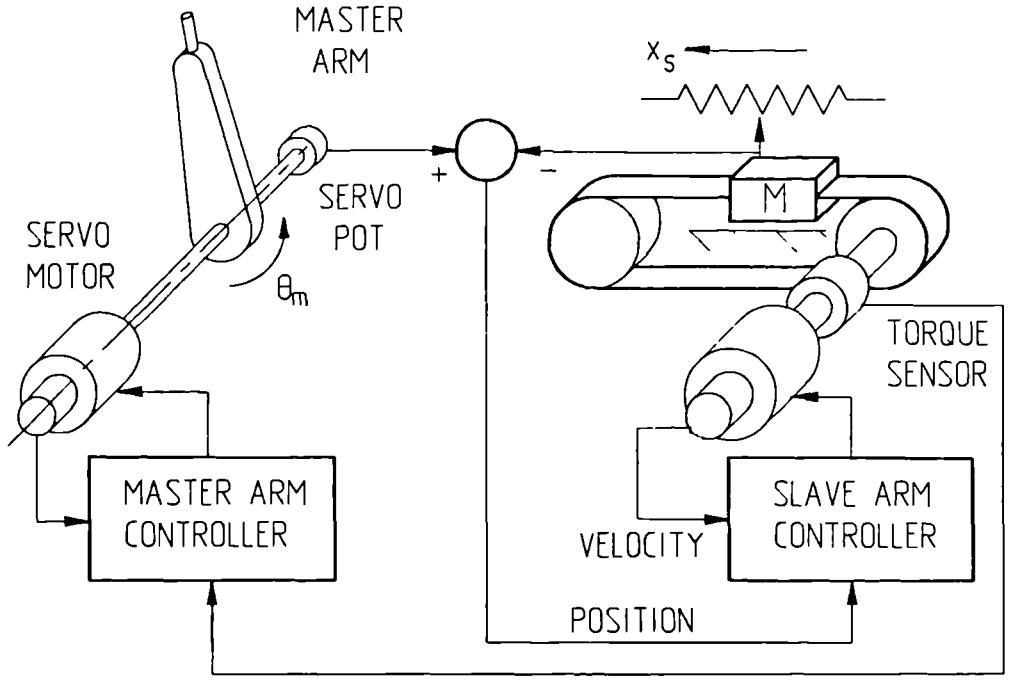

F gure 5 10 *Schematic of 1 d.o.f generalized control system*

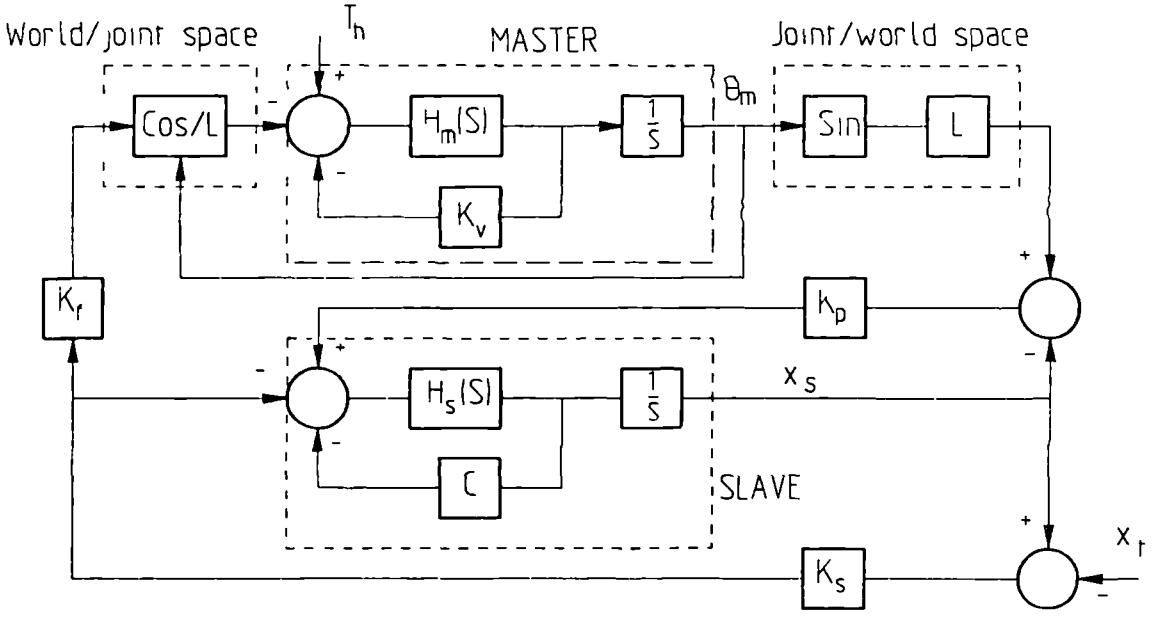

Figure 5.11 *Block diagram of 1 d.o.f generalized control*

The hand torque T_h is related to the master arm displacement θ_m, by assuming the slave arm is in contact with an obstacle $x_t = 0$, as follows

$$T_h = \frac{\theta_m[JMS^4+(JC+MK_v)S^3+(CK_v+JK_s+JK_p)S^2+K_v(K_p+K_s)S]+L^2K_sK_pK_f\text{Tan}\theta_m}{MS^2+CS+(K_p+K_s)} \quad \ldots\ldots\{5.12\}$$

The presence of the non-linear term, $\text{Tan}\,\theta_m$ makes the analysis more difficult. However for small displacements $\text{Tan}\,\theta_m = \theta_m$, thus linearising the system, giving the overall transfer function

$$\frac{\theta_m}{T_h} = \frac{MS^2+CS+(K_p+K_s)}{JMS^4+S^3(JC+MK_v)+S^2(CK_v+JK_s+JK_p)+S(K_s+K_p)K_v+L^2K_sK_fK_p} \quad \ldots\ldots\{5.13\}$$

Using the characteristic equation derived from {5.13}, the stability criterion is given by the inequality

$$K_vC(K_p+K_s)(J^2K_p+J^2K_s+JCK_v+MK_v) > K_fK_sK_pL^2 \quad \ldots\ldots\{5.14\}$$

In the absence of the bilateral loop K_f, the system becomes unilateral, and for positive coefficients the left hand side will always be positive. Equation {5.12} is analogous to {5.1}. If the respective inertia's of the master and slave are $J = M = 1/K$, and damping coefficients are related, such that $C = K_v$ and $L = 1$ the same result is obtained.

For small deviations from the zero position, the response of the one degree of freedom generalized control scheme can be considered linear. As such the stability criteria obtained when modelling a 'conventional' position/force master slave system is equally valid. However, in a multi-axis control system the implementation demands the use of a digital computer, and consequently the effects of sampling frequency and quantization will have a marked influence on stability.

5.3 Multi-axis generalized control

The single degree of freedom model of generalized control required the use of both direct and indirect position and force

transformations to make possible fully resolved bilateral position-force control. For a multi-axis generalized control scheme the slave arm end-effector can only follow the Cartesian movement of the operators hand if the simultaneous solution of direct kinematics of the master arm and the inverse kinematic transformation of the slave arm can be computed in real-time. Similarly, contact of the slave arm end-effector with the environment will generate Cartesian forces (and torques) which must be sensed by suitable force /torque transducers mounted at each joint or else by a multi-component sensor mounted on the wrist of the slave arm. So that the operator can 'feel' the force/torque reaction the slave-arm/environment interactive forces must be resolved into corresponding joint torques at the master arm. A diagrammatic representation of multi-axis generalized control is shown in Figure 5.12.

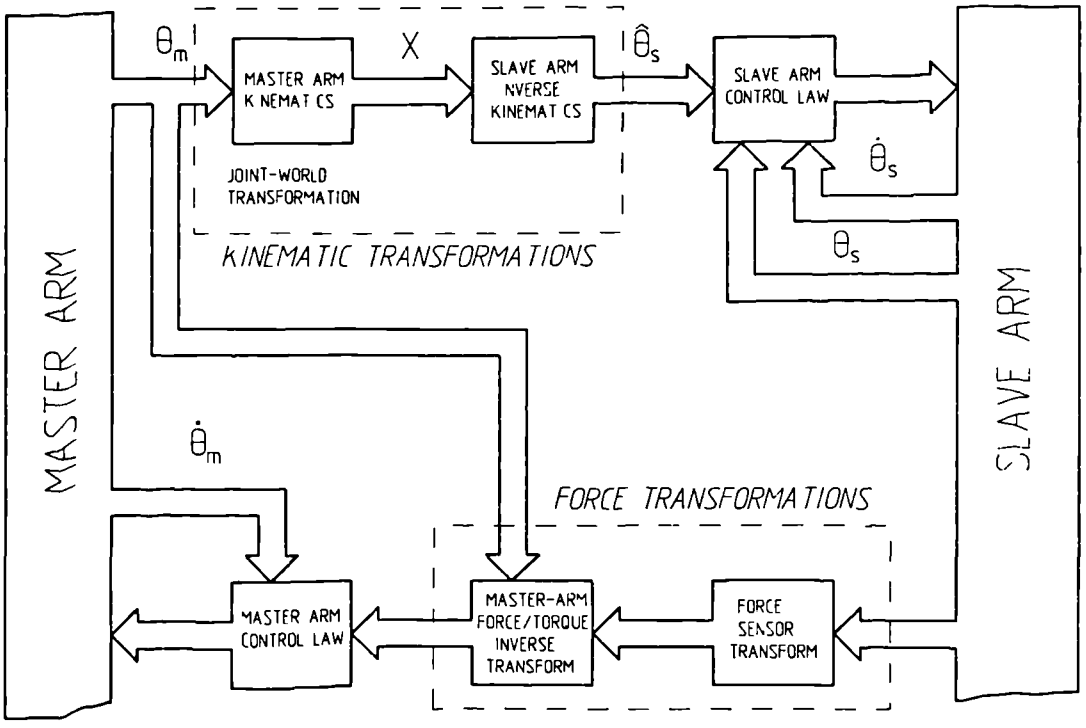

Figure 5.12 *Schematic of Generalized Control*

Position transducers are normally mounted at each joint of both master and slave arms, and the Denavit & Hartenberg notation [Denavit & Hartenberg, 1955] can be used to systematically describe the kinematic relationships between joint coordinates and base coordinate frames of both manipulator arms. The inverse kinematic solution ie. the problem of finding the joint displacements which correspond to the hand transformation, is not straightforward and no general algorithm can be used. The technique used here to determine the geometric solution unambiguously is based on the method outlined by Asada [Asada,1986].

The problem of resolving forces/torques can be achieved by obtaining the manipulator Jacobian, which is associated with differential changes in the position of a manipulator arm. Depending upon the type of feedback employed, the inverse Jacobian may also have to be calculated which may be computationally expense and subject to singularities, and if possible is avoided.

5.3.1 Denavit-Hartenberg notation

To implement fully resolved position control between a dissimilar master and slave arm requires the simultaneous solution of direct kinematics of the master and slave arm, treating both arms as a series of rigid bodies connected as open kinematic chains, in a kinematic structure. Most industrial robots and manipulators can be considered as open kinematic chains, although closed form or parallel robot structures have also been designed.

Each member of the open kinematic chain can be numbered consecutively from the base (0), which is normally fixed, to the terminal joint (n). The end-effector position and orientation can be analyzed by assessing the position and orientation of each link from the base to the terminal link. The Denavit-Hartenberg notation is normally used to systematically describe the kinematic relationships. The method is based upon a 4 x 4 matrix representation of rigid position and orientation as shown in Figure 5.13.

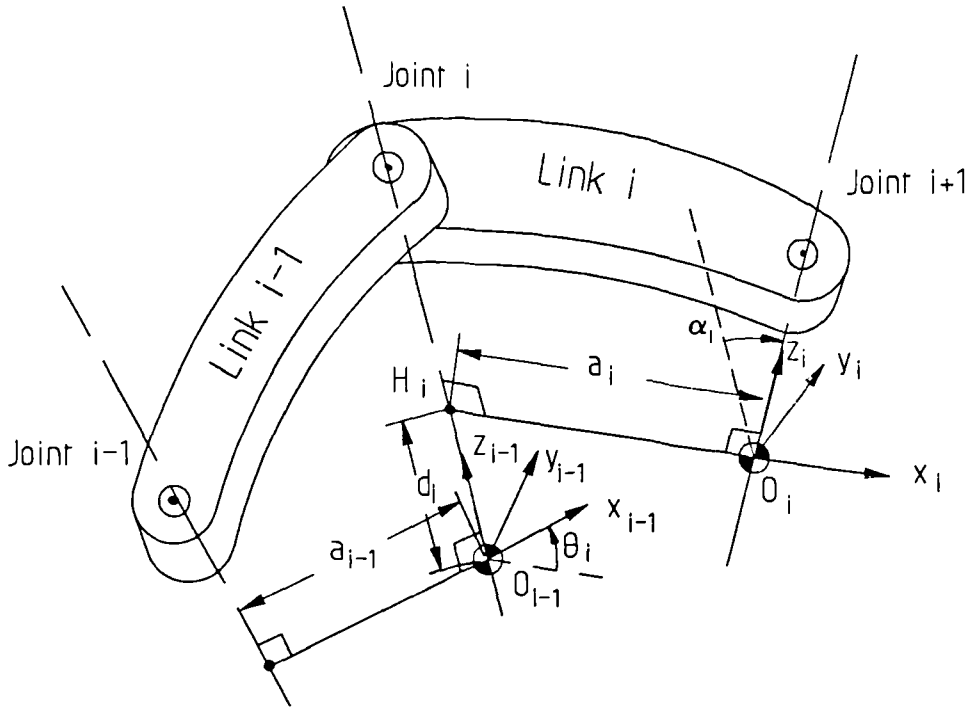

Figure 5 13 *Denavit-Hartenberg notation*

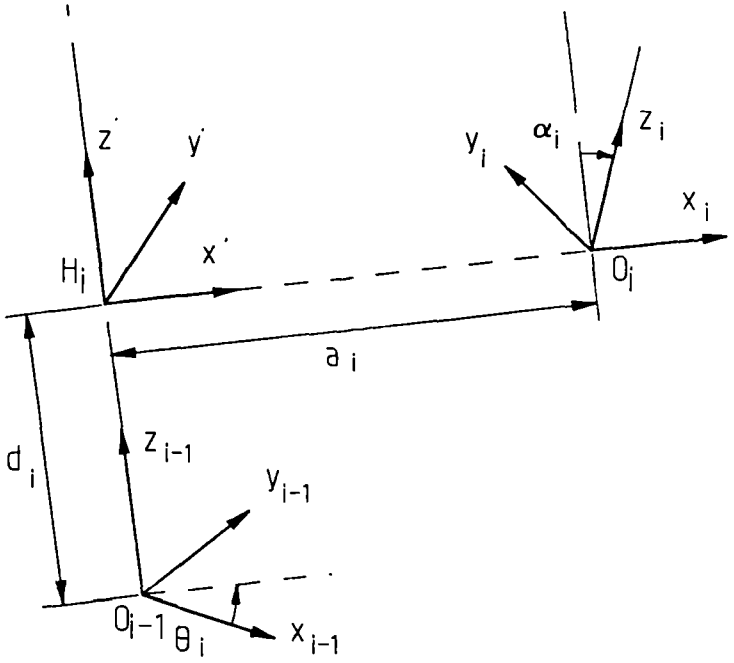

Figure 5 14 *Relationship between coordinate frames*

The relative location of the two frames can be completely described by the following four parameters:

a_i - the length of unique common perpendicular H_iO_i,
θ_i - the angle between the axes x_{i-1} and x_i about the common perpendicular,
d_i - the distance between the origin O_{i-1} and H_i,
α_i - the angle between the joint axis z_i and the common perpendicular.

The parameters a_i and α_i are determined by the geometry of the link : a_i represents a link length and α_i is the twist angle between the two joint axes. Figure 5.14 shows the relationship between the two adjacent coordinate frames.

There are two types of joint mechanism used in manipulator arms 'revolute' (or rotary) and 'prismatic' (or linear), with corresponding variables θ_i and d_i.

If vector R_i represents a 4 x 1 position vector for link i, then the relationship between the coordinate systems of R_i and R_{i-1} can be expressed as

$$R_{i-1} = A_i^{i-1} \times R_i \qquad \text{.....\{5.15\}}$$

where the matrix A_i^{i-1} represents the position and orientation of frame i relative to frame i-1, and is given by:

$$A_i^{i-1} = \begin{bmatrix} \text{Cos}\,\theta_i & -\text{Sin}\,\theta_i\text{Cos}\,\alpha_i & \text{Sin}\,\theta_i\text{Sin}\,\alpha_i & a_i\text{Cos}\,\alpha_i \\ \text{Sin}\,\theta_i & \text{Cos}\,\theta_i\text{Cos}\,\alpha_i & -\text{Cos}\,\theta_i\text{Sin}\,\alpha_i & a_i\text{Sin}\,\alpha_i \\ 0 & \text{Sin}\,\alpha_i & \text{Cos}\,\alpha_i & d_i \\ 0 & 0 & 0 & 1 \end{bmatrix}$$

.....{5.16}

Letting R_0 be the base coordinate system then any link coordinate can be related to R_0 by

$$R_0 = A_1^0 * A_2^1 * A_3^2 * \ldots * A_i^{i-1} * R_i \qquad \text{.....\{5.17\}}$$

or

$$R_0 = T_i^{i-1} * R_i$$

where

$$T_i^{i-1} = A_1^0 * A_2^1 * A_3^2 * \ldots * A_i^{i-1} \quad \ldots\ldots\{5.18\}$$

For a 6 link manipulator the transformation becomes, (dropping the superscript notation)

$$T_6 = A_1 * A_2 * A_3 * A_4 * A_5 * A_6 \quad \ldots\ldots\{5.19\}$$

which represents the end-effector position and orientation in base coordinates as a function of joint displacements. This solution, which is unique, is referred to as the direct kinematic problem [Paul, 1972].

5.3.2 Inverse kinematic transformation

The arm solution, ie. the problem of finding the joint displacements which correspond to the hand transformation is referred to as the inverse kinematics problem [Asada & Slotine,1986]. For certain manipulator configurations multiple inverse solutions may occur for the same end-effector position and orientation, whilst in some configurations the inverse solution may not exist. A manipulator arm requires a minimum of six degrees of freedom both to position and orientate its end-effector in its workspace. By pre-multiplying both sides of equation {5.19} by the inverse of A_1^0, denoted A_1^{-1} gives,

$$A_1^{-1} . T_6 = {}_1T_6$$

where

$${}_1T_6 = A_2 . A_3 . A_4 . A_5 . A_6 \quad \ldots\ldots\{5.20\}$$

The left hand side is a function of the elements of T_6 and the first joint variable. The right hand side consists of elements that include all the other joint displacements. To solve the kinematic equations it is necessary to compare the fourth column vectors of the matrices on both sides of the equation, which

should yield a set of simultaneous equations. However the solution is not generally unique, and it is necessary to use arctangent functions to find angles rather than using sine functions because of the inaccuracies resulting if the joint angles are close to zero. The solution works well for simple manipulators, ie. non-redundant with three intersecting wrist axes.

Unlike the direct kinematic solution, the inverse solution cannot be obtained using a general algorithm since it is trignometric in nature, and it is necessary to determine the geometric solution unambiguously.

Both the direct and inverse kinematic solutions for the planar manipulator arms designed for this study have been obtained using this technique. For general purpose manipulators the methods outlined by Paul [Paul,1981] will produce equations in a direct and systematic manner.

5.3.3 The manipulator Jacobian

In the case of a non-redundant 6 link manipulator, differential changes in the position and orientation of the end-effector (in base coordinates) represented by a 6 x 1 vector $d\mathbf{X}$ can be related to the differential changes in joint coordinates dq_i. For a manipulator having both revolute and prismatic joints, dq_i would correspond to differential rotation and translation respectively, and can be represented by a 6 x 1 vector $d\theta$.

The infinitesmal motion relationships can be determined by partial differentiation of the T_6 transformation as a function of all joint coordinates. For a 6 link manipulator, the differential change in position is written as a 6 x 6 matrix consisting of differential rotation and translation vector elements, and is known as the manipulator Jacobian, denoted J, whose elements are dependent upon the instantaneous configuration of the manipulator, where

$$d\mathbf{X} = \mathbf{J}.d\theta \qquad \text{.....\{5.21\}}$$

The Jacobian can also be used to represent the relationships between the joint velocities and the resulting end-effector velocities, such that

$$dX/dt = J.d\theta/dt \qquad .....\{5.22\}$$

The solution of equations 5.21 and 5.22 may be required in order to obtain a desired differential change in position and orientation or to obtain a desired end-effector velocity. The solution involves finding the inverse Jacobian, denoted J^{-1}, if it exists, and involves complicated mathematical relationships for all but simple manipulators which may make the solution very impractical. RMRC [Whitney,1969], relies on finding the inverse J^{-1} in real-time in order to determine the individual joint velocities consistent with a defined end-effector velocity, such that

$$d\theta/dt = J^{-1}.dX/dt \qquad .....\{5.23\}$$

However, since the Jacobian varies with arm configuration it is possible that it may become singular and as such the rank of the matrix J may degenerate ie. where the determinant of J is zero, and the inverse does not exist. Under these circumstances certain joint velocities can become very large as they attempt to meet the demanded speed, and ultimately movement of the end-effector along or about a particular direction will not be possible. Alternative inverse solutions are available which are easier to evaluate and can be computed in real-time [Paul, Shimano & Mayer,1981a,1981b].

5.3.4 Force/torque transformations

When the slave arm end-effector is in contact with its environment then interactive forces and moments will occur at the interface as a result of applied actuator joint torques. In the bilateral mode, the interactive forces are sensed and reflected back to the operator via the master arm to produce corresponding forces and moments which act on the operator's hand, and as such provide the so called 'kinesthetic coupling' between the operator and the slave manipulator/environment. The quality of the force feedback and related control system will influence the operator's perception of the actual contact forces.

The force transformations between static end-point reaction forces and manipulator static joint torques (or forces for prismatic joints), are computed using the Principle of Virtual Work. The end-point contact forces (and moments) can be represented by a vector

$$F = (F_x \; F_y \; F_z \; M_x \; M_y \; M_z)^T$$

.....{5.24}

where T denotes the vector transpose. The equivalent joint drive torques for a 'n' joint manipulator is given by the vector

$$\tau = (\tau_1 \;\; \tau_2 \;\; \tau_3 \;\; \cdots \; \tau_n)^T$$

.....{5.25}

Assuming that a small 'virtual' displacement, in Cartesian space

$$D = (d_x \;\; d_y \;\; d_z \;\; \delta_x \;\; \delta_y \;\; \delta_z)^T$$

.....{5.26}

corresponds to a displacement in the manipulator joint space, given by

$$\delta_q = (\delta_{q1} \;\; \delta_{q2} \;\; \delta_{q3} \;\; \cdots \; \delta_{qn})^T$$

.....{5.27}

then the virtual work is given by

$$\delta W = \tau^T . \delta_q - F^T D$$

.....{5.28}

The virtual displacements δq and D are related by the manipulator Jacobian, such that $D = J \, \delta_q$, thus

$$\delta W = (\tau - J^T F)^T . \delta_q$$

.....{5.29}

5.4 Implementation of a 3-axis generalized control scheme

The specification initially called for the development of a 3 degree of freedom generalized control scheme, although the number of degrees of freedom would ultimately be increased to 5 by the addition of joints at the base and and wrist. The hand controller is an all revolute, type 3R, planar manipulator arm whilst the dissimilar slave includes a prismatic joint based on a unique pantograph mechanism, and is of type RPR.

5.4.1 Kinematic transformations

In order to implement fully resolved position control between master and slave arms, the kinematic transformations which are required between the master arm terminal joint and a base coordinate frame have been evaluated using the Denavit-Hartenberg method described earlier.

Kinematic Equations for 3R master arm

Figure 5.15 illustrates all the joints and suitable coordinate frames for the master arm. The base frame identifies the absolute coordinates x_0, y_0, and z_0. Because the master arm is of all revolute construction all joint variables are angles θ_i.

Link No.	α_i	a_i	d_i	θ_i
1	0	L_1	0	θ_1
2	0	L_2	0	θ_2
3	0	L_3	0	θ_3

Table 5.1 Link parameters for Articulated master arm

The position and orientation of link i relative to link i-1 can be described as a function of the joint variables, using the 4x4 matrix $A_i^{i-1}(\theta_i)$ by substitution of the link parameters from Table 5.1, as follows

$$A_1^0(\theta_1) = \begin{bmatrix} C1 & -S1 & 0 & C1L_1 \\ S1 & C1 & 0 & S1L_1 \\ 0 & 0 & 1 & 0 \\ 0 & 0 & 0 & 1 \end{bmatrix}$$

$$A_2^1(\theta_2) = \begin{bmatrix} C2 & -S2 & 0 & C2L_2 \\ S2 & C2 & 0 & S2L_2 \\ 0 & 0 & 1 & 0 \\ 0 & 0 & 0 & 1 \end{bmatrix}$$

$$A_3^2(\theta_3) = \begin{bmatrix} C3 & -S3 & 0 & C3L_3 \\ S3 & C3 & 0 & S3L_3 \\ 0 & 0 & 1 & 0 \\ 0 & 0 & 0 & 1 \end{bmatrix}$$

.....{5.31}

where $Ci = \cos(\theta_i)$ and $Si = \sin(\theta_i)$.

By evaluating the products of the A matrices, the kinematic equations for the master arm are given by

$$T_2 = A_1^0(\theta_1) * A_2^1(\theta_2)$$

and

$$T_3 = A_1^0(\theta_1) * A_2^1(\theta_2) * A_3^2(\theta_3) = T_2 * A_3^2(\theta_3)$$

when

$$T_2 = \begin{bmatrix} (C1C2-S1S2) & -(C1S2+C2S1) & 0 & (C1C2L_2-S1S2L_2+C1L_1) \\ (S1C2+C1S2) & (C1C2-S1S2) & 0 & (S1C2L_2+C1C2L_2+S1L_1) \\ 0 & 0 & 1 & 0 \\ 0 & 0 & 0 & 1 \end{bmatrix}$$

Using compound angle formulae to simplify the matrix elements ie. where $C1C2 - S1S2 = \cos(\theta_1 + \theta_2)$ is represented by C12 and $C1S2 + S1C2 = \sin(\theta_1 + \theta_2)$ is represented by S12, for parallel joints

$$T_2 = \begin{bmatrix} C12 & -S12 & 0 & (C12L_2 + C1L_1) \\ S12 & C12 & 0 & (S12L_2 + S1L_1) \\ 0 & 0 & 1 & 0 \\ 0 & 0 & 0 & 1 \end{bmatrix}$$

and similarly,

$$T_3 = \begin{bmatrix} C123 & -S123 & 0 & (C123L_3+C12L_2+C1L_1) \\ S123 & C123 & 0 & (S123L_3+S12L_2+S1L_1) \\ 0 & 0 & 1 & 0 \\ 0 & 0 & 0 & 1 \end{bmatrix}$$

.....{5.32}

where $C123 = \cos(\theta_1+\theta_2+\theta_3)$ and $S123 = \sin(\theta_1+\theta_2+\theta_3)$.

In terms of the reference coordinate frame, the position and orientation of the terminal link is given by partitioning the T_3 matrix such that

$$T_3 = \left[\begin{array}{ccc:c} & R & & x_0 \\ & & & y_0 \\ & & & z_0 \\ \hdashline & 0 & & 1 \end{array}\right]$$

where

$$\begin{aligned} x_0 &= C123L_3 + C12L_2 + C1L_1 \\ y_0 &= S123L_3 + C12L_2 + C1L_1 \\ z_0 &= 0 \\ \theta_0 &= \theta_1 + \theta_2 + \theta_3 \end{aligned}$$

.....{5.33}

The 3x3 R sub-matrix is a rotation matrix defining orientation about the x_0, y_0 and z_0 axes using Euler angles. Since rotation about axes x_0 and y_0 are zero then the orientation of the terminal link with respect to z_0 will simply be $\theta_1+\theta_2+\theta_3$.

Kinematic Equations for the RPR slave arm

Figure 5.16 illustrates all joints and coordinate frames for the RPR planar slave arm. Because of the particular planar configuration it becomes necessary to introduce an intermediate coordinate frame in order to maintain the correct relationship between successive frames. The corresponding link parameters are given in Table 5.2 : note that link 2 is defined without any variable - simply allowing the frame of reference to be shifted.

Link No.	α_i	a_i	d_i	θ_i
1	0	0	0	θ_1
2	-90	0	0	-90
3	+90	0	d_2	0
4	0	L_4	0	θ_4

Table 5.2 **Link Parameters for Slave Arm**

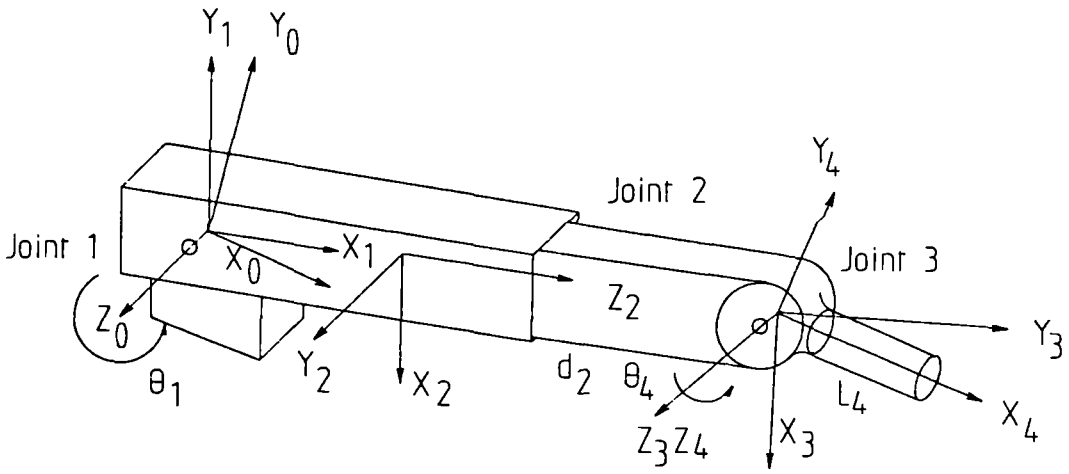

Figure 5.16 *Pantograph coordinate frames*

Substitution of the parameters from Table 5.2 into the 4x4 'A' matrices are as follows

$$A_1^0(\theta_1) = \begin{bmatrix} C1 & -S1 & 0 & 0 \\ S1 & C1 & 0 & 0 \\ 0 & 0 & 1 & 0 \\ 0 & 0 & 0 & 1 \end{bmatrix}$$

$$A_2^1(0) = \begin{bmatrix} 0 & 0 & 1 & 0 \\ -1 & 0 & 0 & 0 \\ 0 & -1 & 0 & 0 \\ 0 & 0 & 0 & 1 \end{bmatrix}$$

$$A_3^2(d_2) = \begin{bmatrix} 1 & 0 & 0 & 0 \\ 0 & 0 & -1 & 0 \\ 0 & 1 & 0 & d_2 \\ 0 & 0 & 0 & 1 \end{bmatrix}$$

$$A_4^3(\theta_4) = \begin{bmatrix} C4 & -S4 & 0 & C4L_4 \\ S4 & C4 & 0 & S4L_4 \\ 0 & 0 & 1 & 0 \\ 0 & 0 & 0 & 1 \end{bmatrix}$$

.....{5.34}

Evaluating the products of the A_i^{i-1} matrices gives the corresponding T_i matrices relating successive coordinate frames to the base coordinate frame, as follows

$$T_3 = A_1^0 * A_2^1 * A_3^2$$

$$T_4 = A_1^0 * A_2^1 * A_3^2 * A_4^3 = T_3 * A_4^3$$

such that

$$T_3 = \begin{bmatrix} S1 & C1 & 0 & C1d_2 \\ -C1 & S1 & 0 & S1d_2 \\ 0 & 0 & 1 & 0 \\ 0 & 0 & 0 & 1 \end{bmatrix}$$

and

$$T_4 = \begin{bmatrix} S14 & C14 & 0 & S14L_4+C1d_2 \\ -C14 & S14 & 0 & -C14L_4+S1d_2 \\ 0 & 0 & 1 & 0 \\ 0 & 0 & 0 & 1 \end{bmatrix}$$

.....{5.35}

using the notation for S14 and C14 defined previously.

The position of the terminal link with respect to the base coordinate frame is obtained from the 4th column of T_4

$$\begin{aligned} x_0 &= S14L_4 + C1d_2 \\ y_0 &= -C14L_4 + S1d_2 \\ z_0 &= 0 \\ \theta_0 &= \theta_1 + \theta_4 + 3\pi/2 \end{aligned}$$

.....{5.36}

Since the pantograph arm is planar, the skeleton structure can be represented as shown in Figure 5.17. The orientation of the end-effector is dictated by the summed angles of θ_1 and θ_4, and including a constant to take into account the different orientation of the two frames of reference.

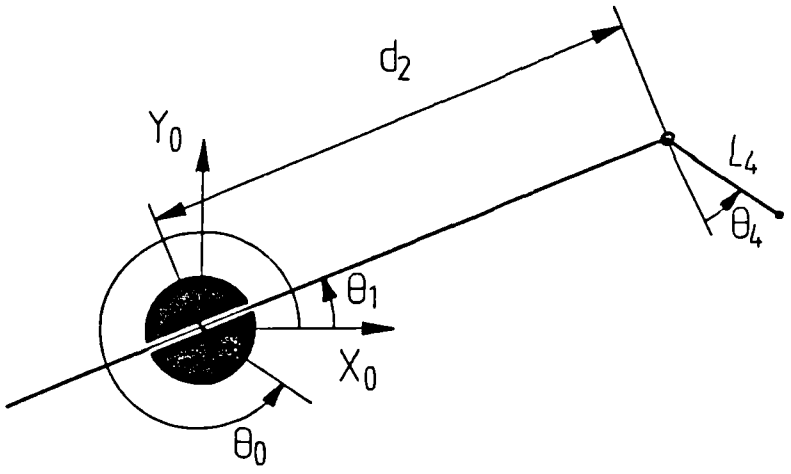

Figure 5.17 *Skeleton of Pantograph slave arm*

5.4.2 Force/torque transformations

Figure 5.18 shows schematically the interaction between task generated forces and the operator's corresponding reaction forces generated at the hand in an 'ideal' generalized control scheme.

The slave arm joint actuator torques induce static forces F_x, F_y and torque T, when the slave arm is in contact with its task environment. Collocated force sensors can be used to measure the resulting joint forces F_{x0}, F_{y0} and torque T_4 which can be computed to generate joint actuator torques τ_1, τ_2 and τ_3 on the master arm so that equivalent reaction forces F_x', F_y' (and torque) T' are exerted on the operator's hand. In reality, the quality of 'feel' is degraded by dynamical forces acting on the master arm, and also by disturbances acting on the slave arm which are superimposed on the task forces measured by the force/torque transducers.

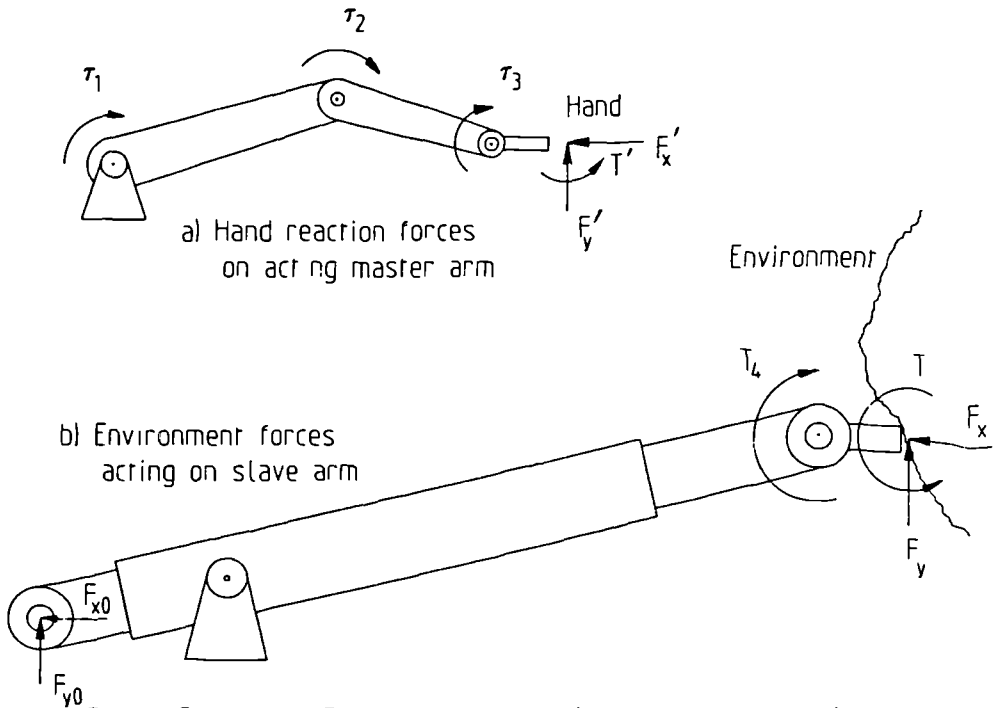

Figure 5.18 *Hand/Environment forces between master & slave*

For the planar system developed here, the force/torque transformation for the master arm was determined from the transpose of the master arm Jacobian using the 4X4 T_3 matrix obtained in the previous section. The procedure outlined allows the joint torques corresponding to the manipulator end-point reaction forces to be computed.

The pantograph mechanism adopted for the design of slave arm is described in the following chapter. A dynamical analysis of the arm is also presented, with the intention of predicting the joint actuator torques corresponding to both dynamically induced and static task/environment forces. The collocated force/torque sensors on this particular design makes the planar force/torque transformations straightforward and have been determined using a classical approach.

Master-arm force transformation using the manipulator Jacobian

The end-effector position and orientation, relative to the base coordinate frame can be defined from the T_3 matrix {5.32}. Using the equations {5.33}, which can be represented as

$$x_0 = \text{Cos}(\theta_1)L1 + \text{Cos}(\theta_1, \theta_2)L2 + \text{Cos}(\theta_1, \theta_2, \theta_3)L3$$
$$y_0 = \text{Sin}(\theta_1)L1 + \text{Sin}(\theta_1, \theta_2)L2 + \text{Sin}(\theta_1, \theta_2, \theta_3)L3$$
and $$\theta_0 = \theta_1 + \theta_2 + \theta_3$$

The Jacobian is computed by finding the partial derivative with respect to each joint, where

$$dx_0 = (\partial x_0/\partial\theta_1)d\theta_1 + (\partial x_0/\partial\theta_2)d\theta_2 + (\partial x_0/\partial\theta_3)d\theta_3$$
$$dy_0 = (\partial y_0/\partial\theta_1)d\theta_1 + (\partial y_0/\partial\theta_2)d\theta_2 + (\partial y_0/\partial\theta_3)d\theta_3$$
and $$d\theta_0 = (\partial\theta_0/\partial\theta_1)d\theta_1 + (\partial\theta_0/\partial\theta_2)d\theta_2 + (\partial\theta_0/\partial\theta_3)d\theta_3$$

which can be expressed in matrix form

$$\begin{bmatrix} dx_0 \\ dy_0 \\ d\theta_0 \end{bmatrix} = J \cdot \begin{bmatrix} d\theta_1 \\ d\theta_2 \\ d\theta_3 \end{bmatrix} \quad \text{.....\{5.37\}}$$

where

$$J = \begin{bmatrix} \partial x_0/\partial\theta_1 & \partial x_0/\partial\theta_2 & \partial x_0/\partial\theta_3 \\ \partial y_0/\partial\theta_1 & \partial y_0/\partial\theta_2 & \partial y_0/\partial\theta_3 \\ \partial\theta_0/\partial\theta_1 & \partial\theta_0/\partial\theta_2 & \partial\theta_0/\partial\theta_3 \end{bmatrix}$$

$$= \begin{bmatrix} -(S1L1+S12L2+S123L3) & -(S12L2+S123L3) & -(S123L3) \\ (C1L1+C12L2+C123L3) & (C12L2+C123L3) & (C123L3) \\ 1 & 1 & 1 \end{bmatrix}$$

.....{5.38}

and hence

$$J^T = \begin{bmatrix} -(S1L1+S12L2+S123L3) & (C1L1+C12L2+C123L3) & 1 \\ -(S12L2+S123L3) & (C12L2+C123L3) & 1 \\ -(S123L3) & (C123L3) & 1 \end{bmatrix}$$

.....{5.39}

The respective joint torques can be represented by the vector $\tau = [\ \tau_1\ \ \tau_2\ \ \tau_3\ ]^T$ and the applied end point force/torque vector $F = [\ F_x + F_y + T\ ]^T$, such that

$$\begin{bmatrix} \tau_1 \\ \tau_2 \\ \tau_3 \end{bmatrix} = J^T \begin{bmatrix} F_x \\ F_y \\ T \end{bmatrix}$$

.....{5.40}

for the particular case where L3 = 0 they reduce to

$$\tau_1 = (C1L1 + C12L2)F_y - (S1L1 + S12L2)F_x + T$$

$$\tau_2 = (C12L2)F_y - (C1L1)F_x + T$$

and

$$\tau_3 = T \qquad \text{.....\{5.41\}}$$

Slave arm force/torque transformations

The external forces exerted on the slave arm at the end-effector by its interaction with the environment are measured using force/torque sensors collocated at each joint. The design of pantograph mechanism incorporates a two-axis load cell located between the X-Y cross-slide and input link. The working principle of the 'pseudo-pantograph' mechanism showing the kinematic relationship between the input and output links, and the location of the force/torque sensors is illustrated in the skeleton diagram of Figure 5.19.

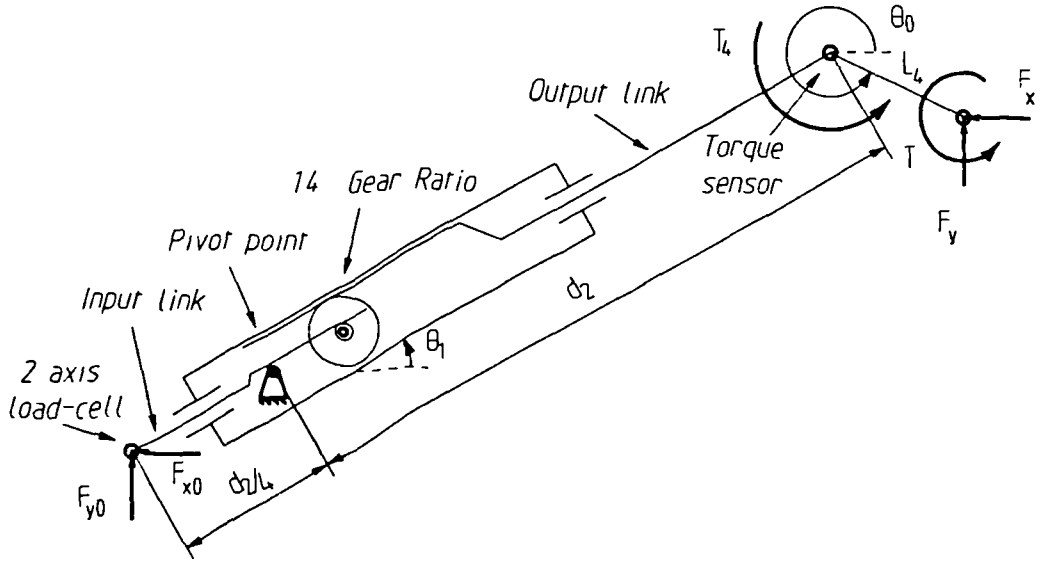

Figure 5.19 *Static forces on pantograph slave arm*

Figure 5.20 gives the free body diagram of the terminal link showing only applied static forces. The external torque T can be estimated from equation {5.37} where F_{x0}, F_{y0} and T_4 are obtained directly from the force/torque sensors, such that

$$T = T_4 - F_{y0}L_4\cos(\theta_o)/4 - F_{x0}L_4\sin(\theta_o)/4$$

$$F_{x4} = F_x$$

$$F_{y4} = F_y \qquad \text{.....\{5.37\}}$$

Note that the reaction torque T_4, acting on the pantograph output link, is sustained by a reaction force at the pivot point. The mechanical advantage of the mechanism is such that the magnitude of the forces sensed at the input point are in the ratio of 4:1 with the forces acting on the output, where

$$F_{x0} = 4 \times F_{x4} = 4 \times F_x$$

$$F_{y0} = 4 \times F_{y4} = 4 \times F_y \qquad \text{.....\{5.38\}}$$

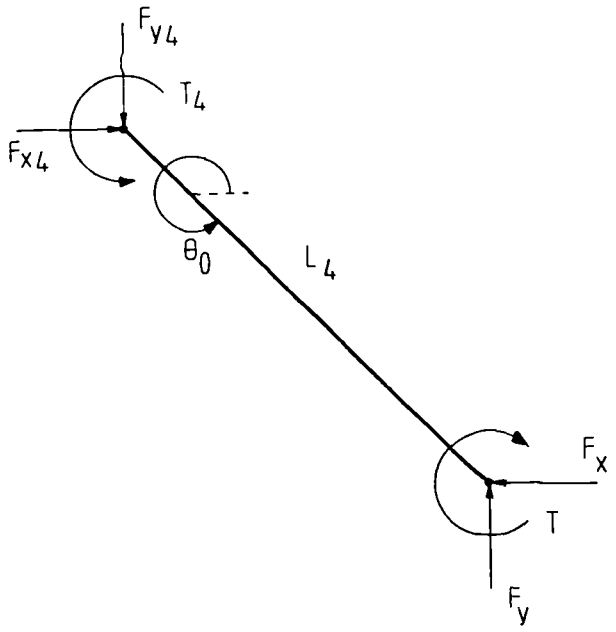

Figure 5.20 *Free body diagram for terminal link*

5.5 Summary

In this chapter, an 'idealized' one degree of freedom model of a master-slave system has been analyzed, based on position/force and position/position bilateral control schemes. The stability and frequency response of the two methods has been assessed for different viscous friction values and force-feedback gains. The effects of disturbances due to noise in the position- feedforward and force-feedback loops has also been discussed.

A one degree of freedom generalized control scheme has been analyzed. For small deviations from a null position the stability of the scheme can be considered the same as that of an equivalent identical master-slave system.

The requirements for multi-degree of freedom generalized control schemes have been addressed, and subsequently applied to a 3 degree of freedom planar system. The implementation of master-slave control and generalized control on a planar experimental rig are fully described in the next chapter.

A comprehensive simulation study of a one degree of freedom master-slave system is presented in Chapter7, which incorporates a 'simple' model of a human operator. The study is based upon joint 2 of identical master and slave arms developed in the experimental facility. The model has been correlated with experimental results obtained on the physical system.

CHAPTER 6

Design of Experimental Facility

A review of commercial robots and manipulator systems that could satisfy the requirements of the research programme and be developed within the budget was carried out in the early stages of the work.

The small industrial robots available at that time would have required extensive modification of their control systems to enable remote operation using a multi-axis master controller. And manufacturers were, in general, reluctant to release confidential information regarding the structure of the robot control system. Recently however, industrial robot control systems have become rather more versatile and now incorporate supervisory and/or adaptive control options, which can facilitate remote operation, ie. Val II Real-Time Path Control [Unimation].

Furthermore, the only force reflecting master-slave manipulator in the UK at that time was sited at the UKAEA Culham Research Laboratory, and the 'Mascot' replica master slave manipulator system [Raimondi,1976] was still undergoing commissioning trials on the JET research programme.

The conversion of a mechanical master slave manipulator system to servoed operation was considered at one stage, although most units of this type are designed for operation in hot cells and have a large telescopic axis. The cost of carrying out the necessary modifications to accomodate servo-motors and placement of feedback transducers was considered to be too prohibitive.

It was therefore decided to design an experimental facility which would incorporate a master controller and slave manipulators to facilitate the force reflecting generalized control scheme proposed by Bejczy [Bejczy,1980]. The equipment which was designed and built consists of three planar 3 degree of freedom manipulator arms, with each joint electrically actuated using a DC servo-motor. A general view of the facility is shown in Figure 6.1.

Figure 6.1 General view of Experimental Rig

An articulated master arm is used to control either of two slave arms at maximum terminal velocities of up to 0.5 metres/second, and apply reaction forces to the hand of up to 100 Newtons. Spatial and dynamical similarity between the identical articulated master and slave arm has permitted the application of direct or continuous control in both unilateral and bilateral operational modes. Control between dissimilar master and slave using a 'pseudo-pantograph' manipulator was achieved by introducing a digital computer to carry out the kinematic transformation, in real time, of the master arm position coordinates to achieve fully resolved position control of the slave arm. In the bilateral mode, simultaneous transformation of slave arm reaction forces is carried out to obtain corresponding joint reaction torques at the master controller.

The Newcastle design of 'pseudo-pantograph' slave arm was based on an original concept patented by Harwell and proposed for the Elite range of servo manipulators [Causer,1981]. The mechanical construction of the prototype mechanism has been simplified without loss of efficiency.

Engineering drawings of the two manipulator arms designed for this study, and associated equipment are given in Appendix VIII, (detail drawings are not included).

At low speeds, independent joint control is normally capable of maintaining the desired trajectory, assuming the actuators are powerful enough and the manipulator configuration does not change significantly. At high speeds however, the dynamic behaviour of the arm can be influenced by variations in the effective moments of inertia, torque coupling between adjacent links, Coriolis and centrifugal forces proportional to velocity cross-products and velocity squared terms respectively. Other disturbances arising from friction, link compliance and backlash in transmission systems pose serious problems when attempting to model the dynamics of the robot.

Control schemes which can compute in real-time the inverse dynamics and implement the necessary feedback control are required to have a sampling frequency of greater than 60Hz if the algorithm is to converge [Luh,Walker & Paul,1980]. With such a restriction it is not surprising that much effort is being directed towards optimising the dynamic formulation. A summary of inverse dynamics and alternative control schemes for high

speed robots has previously been carried out [Tan,1984], and the problem put into perspective.

The original digital controller used in the study was a Z80 based microcomputer. Because of limitations in computational speed it was later replaced by a more powerful digital controller. A detailed desciption of the digital control system is included later in the Chapter.

6.1 Master-arm

The master arm is used to communicate command information between the operator and the slave manipulator. In the bilateral control mode force/torque information generated during the execution of a task by the slave arm is presented to the operators hand in the form of equivalent reaction forces/torques by the master arm.

Several different arrangements for the design of master arm were investigated, and although the configuration adopted was based on an articulated arm with all revolute joints some important issues were raised. The availability of high performance DC servo-motors offering high-torque / low-speed operation constructed using rare earth permanent magnets [Inland] make feasible a design having direct drive. The conventional servo-motor with a high-speed / low-torque capability requires a gearbox to attain adequate torque transmission. However, mounting the drive units directly at the joints imposes increasing inertia loads along the master arm from the hand to shoulder.

The master arm has a semi-circular working envelope of 500mm radius as shown in Figure 6.2. Three revolute joints are used to provide both position and orientation of the control grip within the primary working zone. Each joint is servoed using a conventional high speed DC servo-motor in conjunction with a high reduction gearbox, which incorporates a anti-backlash feature, to provide the torque/speed capability. The master arm is shown in Figure 6.3.

Inertial mass of the master arm is minimised by mounting the motor/gearbox assembly for each joint as close as possible to the shoulder axis. Tension cable provides the transmission to elbow and wrist joint axes, and adjustment is carried out using turnbuckles. The structural link elements are made from

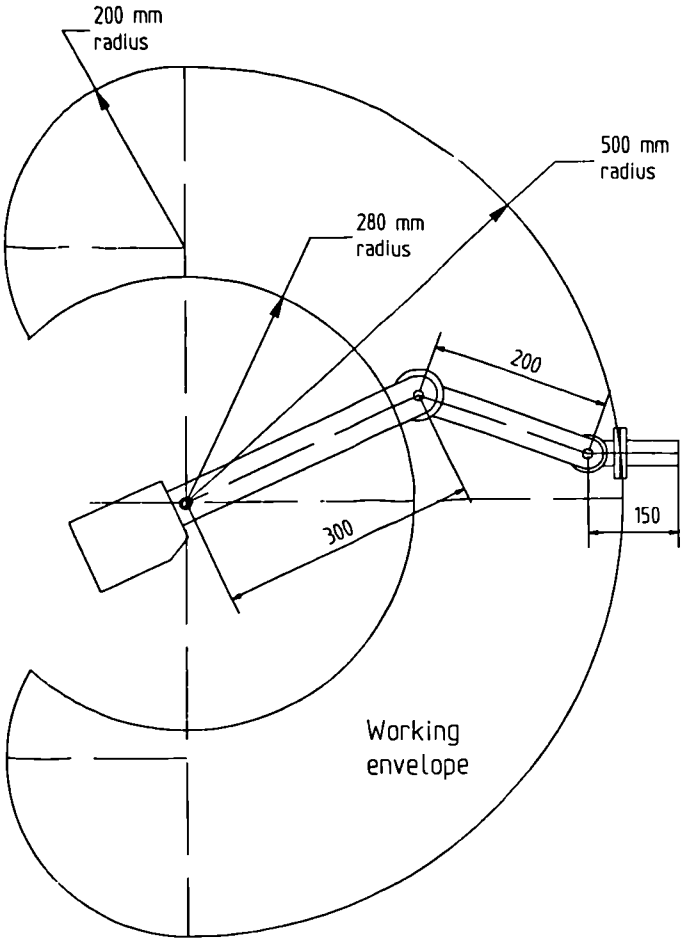

Figure 62 *Articulated arm working envelope*

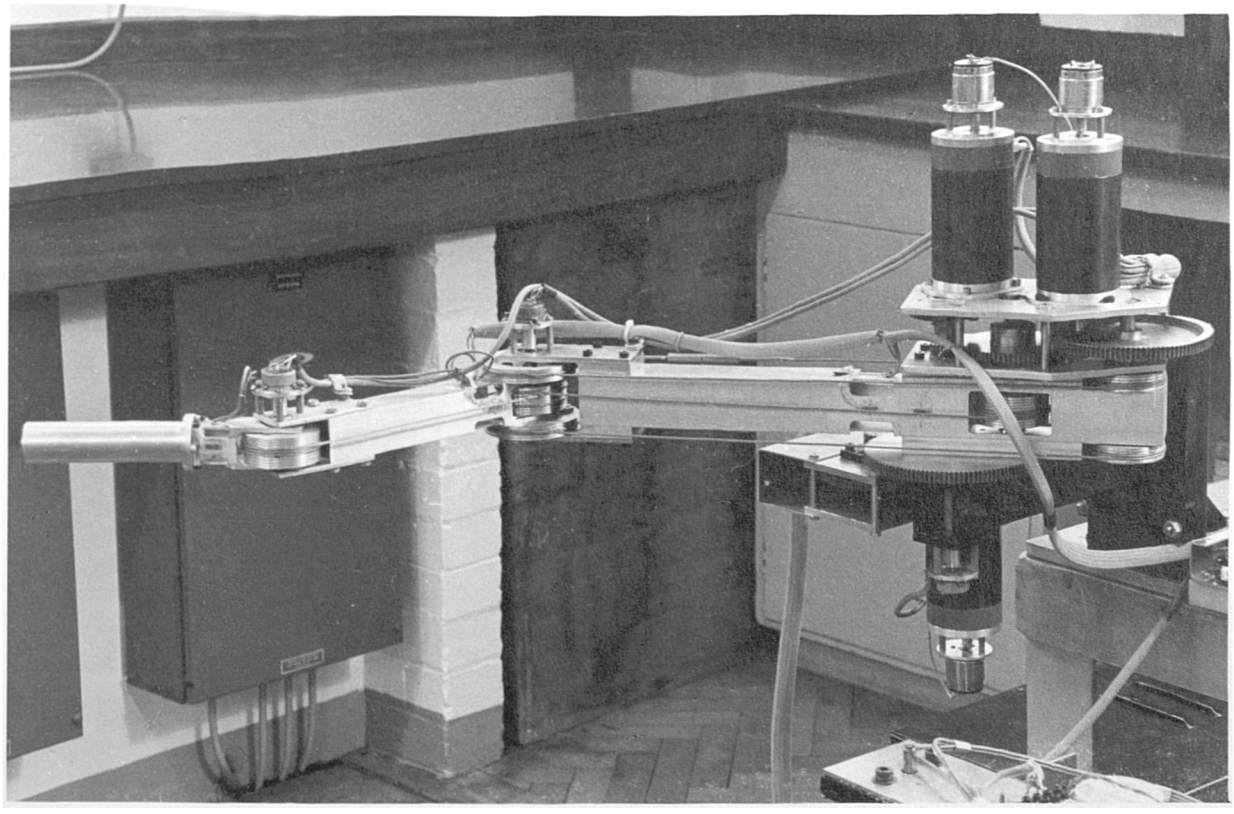

Figure 6.3 Master arm

aluminium box section to give high strength to weight ratio. Precision servo-potentiometers, of the conductive plastic type, are collocated at each joint to measure joint reference position. Joint velocity is measured using a DC tachometer mounted directly on the motor shaft.

The anti-backlash arrangement incorporated in each gearbox influences the ability to backdrive the arm to such an extent that it prohibited the operator from executing fine positioning / fine motion manouvres (discussed later in Chapter 8). The need to minimise backlash reduces considerably the overall transmission efficiency, however, this limitation was overcome by introducing positive torque feedback about each joint.

A strain-gauge bridge was mounted strategically on each of the structural links of the arm, as close as possible to their respective joints so as to enable measurement of joint torque. The amplified signal was then fedback into the servo loop and provided tight torque control about each independent joint. By configuring the torque feedback signal to be positive, and correctly adjusting the gain, the operator was provided with an 'apparent' frictionless mechanism. This novel development yielded not only improved sensitivity but also allowed more precise control of fine motion. Furthermore, velocity feedback damping was used to prevent the operator from attempting to carry out tasks at excessive velocities.

Modularised servo-amplifiers capable of providing 150 Watts continuous output power were also built to drive the master arm. A description of the servo-amplifier design is presented later in the Chapter.

The master arm was designed to provide the operator with continuous reaction forces and torque of 70N and 6Nm respectively at the terminal wrist. A 100% overload capacity can be sustained for short durations. Since speed is not normally a prerequisite for remotely controlled operations it was decided to limit maximum terminal speed to 0.5 metres/second within the defined operating envelope.

aluminium box section to give high strength to weight ratio. Precision servo-potentiometers, of the conductive plastic type, are collocated at each joint to measure joint reference position. Joint velocity is measured using a DC tachometer mounted directly on the motor shaft.

The anti-backlash arrangement incorporated in each gearbox influences the ability to backdrive the arm to such an extent that it prohibited the operator from executing fine positioning / fine motion manouvres (discussed later in Chapter 8). The need to minimise backlash reduces considerably the overall transmission efficiency, however, this limitation was overcome by introducing positive torque feedback about each joint.

A strain-gauge bridge was mounted strategically on each of the structural links of the arm, as close as possible to their respective joints so as to enable measurement of joint torque. The amplified signal was then fedback into the servo loop and provided tight torque control about each independent joint. By configuring the torque feedback signal to be positive, and correctly adjusting the gain, the operator was provided with an 'apparent' frictionless mechanism. This novel development yielded not only improved sensitivity but also allowed more precise control of fine motion. Furthermore, velocity feedback damping was used to prevent the operator from attempting to carry out tasks at excessive velocities.

Modularised servo-amplifiers capable of providing 150 Watts continuous output power were also built to drive the master arm. A description of the servo-amplifier design is presented later in the Chapter.

The master arm was designed to provide the operator with continuous reaction forces and torque of 70N and 6Nm respectively at the terminal wrist. A 100% overload capacity can be sustained for short durations. Since speed is not normally a prerequisite for remotely controlled operations it was decided to limit maximum terminal speed to 0.5 metres/second within the defined operating envelope.

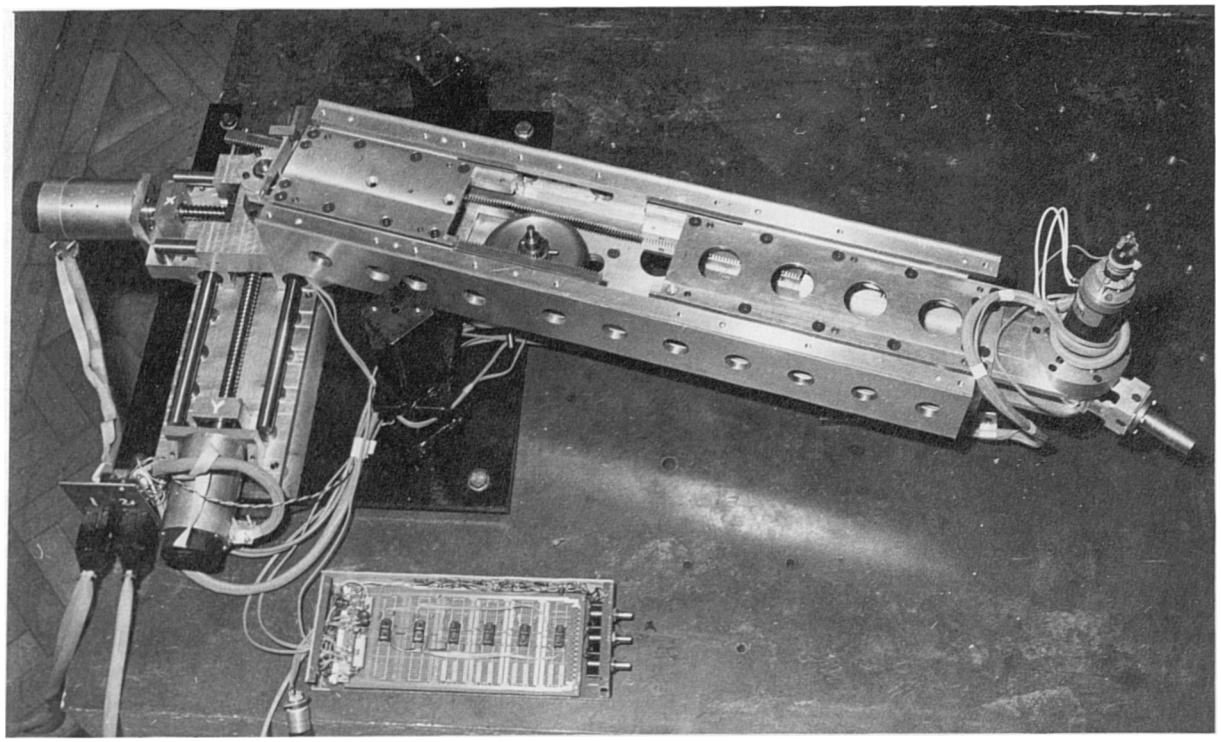

Figure 6.4 Pantograph Mechanism

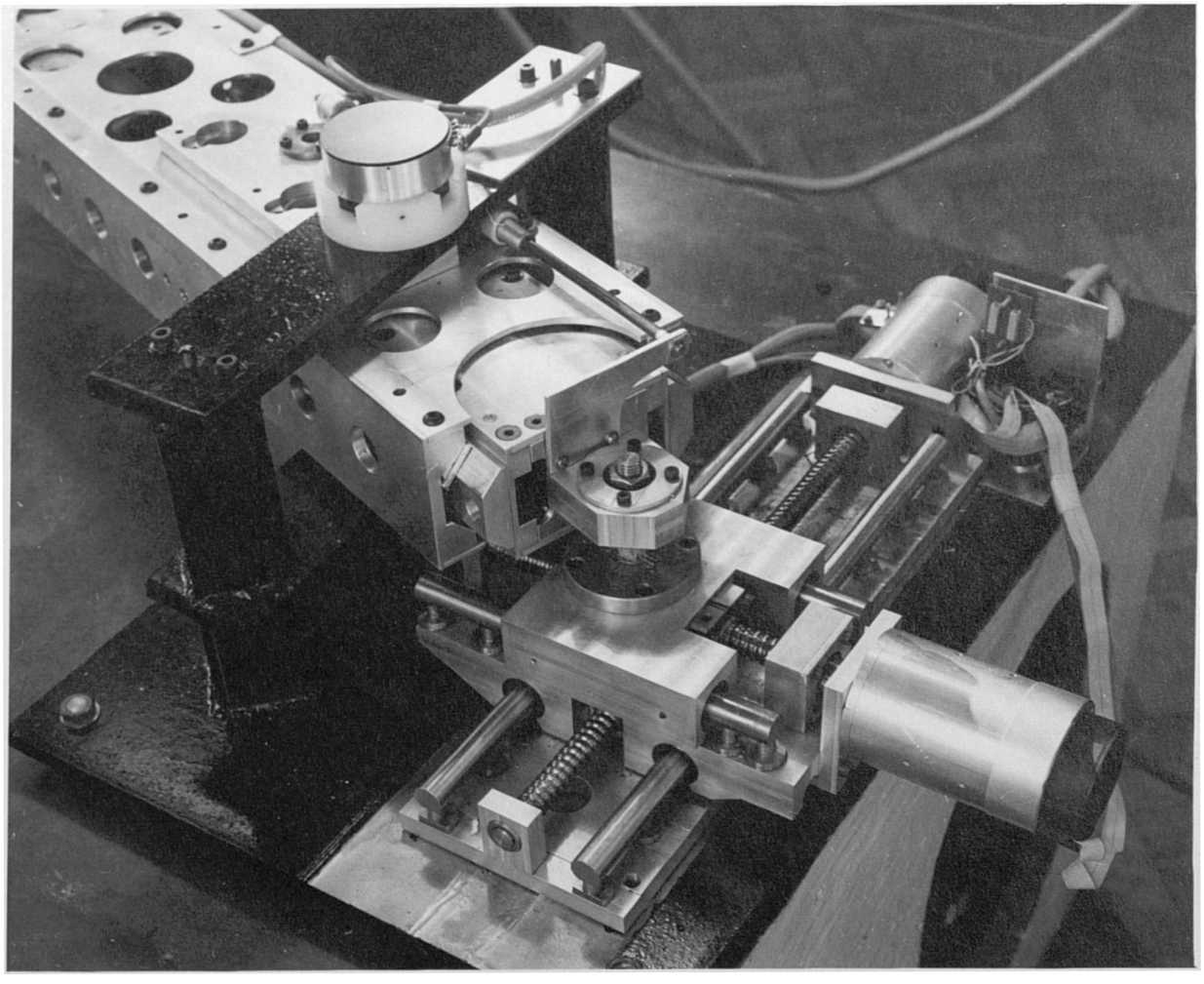

Figure 6.5 X-Y Cross-slide Unit

6.3.1 Synthesis of arm dynamics

In order that the respective motor torques for the three axis pantograph arm could be predicted, a dynamic analysis was carried out, and equations of motion were derived using classical techniques. The relative simplicity of the mechanism makes the analysis reasonably straightforward, and although alternative formulations are available for generating the inverse dynamic equations no significant advantages are to be gained with a 3 degree of freedom planar manipulator arm. The closed form Lagrangian and the recursive Newton-Euler formulations are commonly used for analyzing the inverse dynamic equations of motion of multi-link high speed robots.

Whilst speed of operation is not a prime consideration here, it was felt worthwhile to model the dynamics of the proposed design to ensure that the motor torque-speed characteristics matched the desired performance. The analysis of the relative magnitude of the drive torques was in this case based on a *constrained* trajectory of turning a crank. Successive transformation of velocities and accelerations from the crank to the base of the manipulator were carried out link by link. Similarly input forces/torques were transformed from the crank arm link by link to obtain drive motor torques.

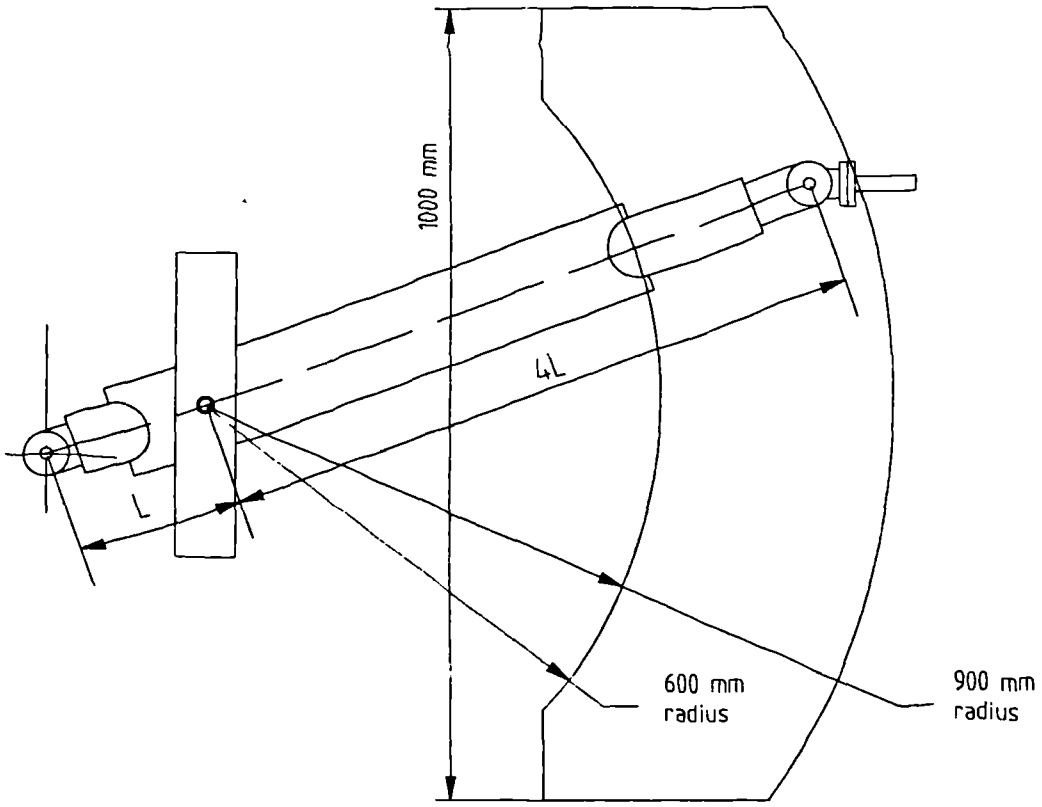

Figure 6.6 Pantograph arm working envelope

An algorithm was written using MS-Pascal [Microsoft] to relate actuator drive torques to crank angle for general input conditions. A schematic arrangement of the crank turning task is shown in Figure 6.7.

6.3.2 Inverse kinematics

The equations of motion for the pantograph arm are summarised below, with reference to Figure 6.7. Derivation of these equations can be found in Appendix I.

In cartesian coordinates,

$$\begin{aligned} X &= X_c - r_3\text{Cos}\,\alpha_3 - r_c\text{Cos}\,\theta \\ Y &= Y_c^{o} - r_3\text{Sin}\,\alpha_3 + r_c\text{Sin}\,\theta \\ r^2 &= X^2 + Y^2 \\ \alpha &= \text{Tan}^{-1}(Y/X) \end{aligned}$$

.....{6.1}

Assuming α_3 is constant,then

$$\begin{aligned} \dot{X} &= \dot{\theta}\, r_c\text{Sin}\,\theta \\ \dot{Y} &= \dot{\theta}\, r_c\text{Cos}\,\theta \end{aligned}$$

and

$$\begin{aligned} \ddot{X} &= \ddot{\theta}\, r_c\text{Sin}\,\theta + \dot{\theta}^2 r_c\text{Cos}\,\theta \\ \ddot{Y} &= \ddot{\theta}\, r_c\text{Cos}\,\theta - \dot{\theta}^2 r_c\text{Sin}\,\theta \end{aligned}$$

.....{6.2}

For constant crank velocity, ie $\ddot{\theta} = 0$, then

$$\begin{aligned} \ddot{X} &= \dot{\theta}^2 r_c\text{Cos}\,\theta \\ \ddot{Y} &= -\dot{\theta}^2 r_c\text{Sin}\,\theta \end{aligned}$$

.....{6.3}

In polar coordinates,

$$\begin{aligned} \dot{\alpha} &= (X\dot{Y} - Y\dot{X})/r^2 \\ \dot{r} &= (X\dot{X} + Y\dot{Y})/r^2 \\ \ddot{\alpha} &= X\ddot{Y}/r^2 - Y\ddot{X}/r^2 - 2\dot{\alpha}\dot{r}/r \\ \ddot{r} &= X\ddot{X}/r + Y\ddot{Y}/r + \dot{\alpha}^2 r \end{aligned}$$

.....{6.4}

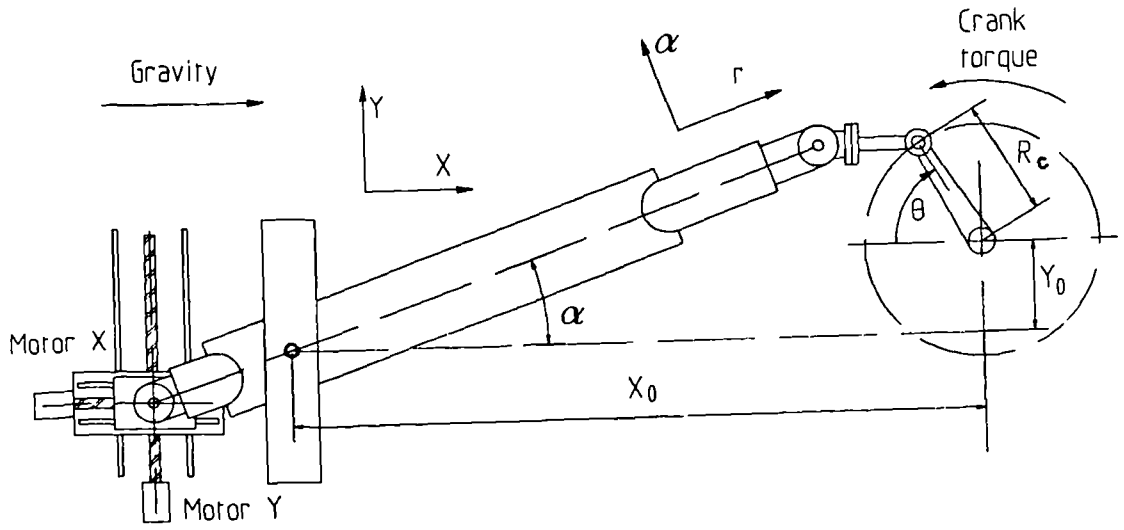

Figure 67 *Schematic of pantograph arm crank test*

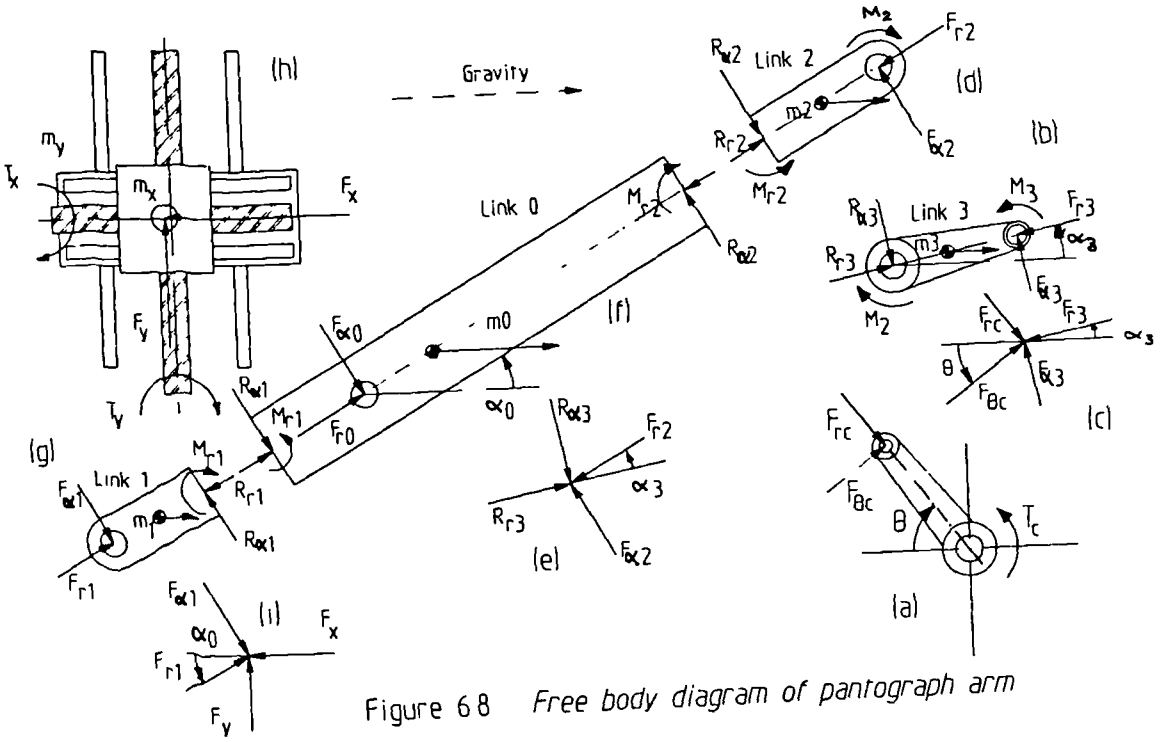

Figure 68 *Free body diagram of pantograph arm*

6.3.3 Inverse dynamics

In general the dynamic equations of motion for the pantograph arm can be obtained by applying D'Alemberts Principle link by link to each element successively from the terminal link to the base. The free-body diagram for each element of the arm is shown in Figure 6.8. The dynamic equations of motion are outlined in Appendix X, and are summarised below for the particular case where $\alpha_3 = \dot{\alpha}_3 = \ddot{\alpha}_3 = 0$, and where gravity acts in the direction shown:

Link 3 - see Figure 6.8.(b)

$$R_{r3} = F_{r3} - m_3[\, g - \ddot{r}_2 \cos\alpha_3 + \dot{\alpha}_3^2(r_2 + r_3 - r_{G3}) \,]$$
$$R_{\alpha 3} = F_{\alpha 3} - m_3 \ddot{\alpha}_3(r_2 + r_3 - r_{G3})$$
$$M_2 = M_3 + F_{\alpha 3}(r_3 - r_{G3}) + R_{\alpha 3} r_{G3} - \ddot{\alpha}_3 I_{G3}$$

where

$$I_{G3} = I_3 - m_3 r_{G3}^2$$

.....{6.5}

Transformation between Link 3 and Link 2 - see Figure 6.8.(e)

$$F_{r2} = R_{r3}\cos(-\alpha_3) - R_{\alpha 3}\sin(-\alpha_3)$$
$$F_{\alpha 2} = R_{r3}\sin(-\alpha_3) + R_{\alpha 3}\cos(-\alpha_3)$$

.....{6.6}

Link 2 - see Figure 6.8.(d)

$$R_{r2} = F_{r2} - m_2[\, g\cos\alpha_2 - \ddot{r}_2 + \dot{\alpha}_2^2(r_2 - r_{G2}) \,]$$
$$R_{\alpha 2} = F_{\alpha 2} - m_2[\, g\sin\alpha_2 + \ddot{\alpha}_2(r_2 - r_{G2}) \,]$$
$$M_{r2} = -F_{\alpha 2} r_{G2} + M_2 + \alpha_2 I_{G2}$$

where

$$I_{G2} = I_2 - m_2 r_{G2}^2$$

.....{6.7}

Link 1 - see Figure 6.8.(g)

$$R_{r1} = F_{r1} + m_1[\, g\cos\alpha_1 + \ddot{r}_1 - \dot{\alpha}_1^2(r_1 - r_{G1}) \,]$$
$$R_{\alpha 1} = F_{\alpha 1} + m_1[\, g\sin\alpha_1 - \ddot{\alpha}_1(r_1 - r_{G1}) \,]$$
$$M_{r1} = F_{\alpha 1} r_{G1} + \ddot{\alpha}_1 I_{G1}$$

where

$$I_{G1} = I_1 - m_1 r_{G1}^2$$

.....{6.8}

Link 0 - see Figure 6.8.(f)

$$F_{r0} = R_{r2} - R_{r1} - m_0(g\text{Cos}\alpha_0 + \dot{\alpha}_0^2 r_{G0})$$
$$F_{\alpha 0} = R_{2} - R_{\alpha 1} + m_0(g\text{Sin}\alpha_0 + \dot{\alpha}_0 r_{g0})$$
$$M_{r1} - M_{r2} + R_{r2}(r_2 - r_{G2}) + R_{r1}(r_1 - r_{G1}) + F_{\alpha 0} = \ddot{\alpha}_0 I_{G0}$$

where

$$I_{G0} = I_0 - m_0 r_{G0}^2$$

.....{6.9}

Transformation between Link 1 and X-Y Table - see Figure 6.8.(i)

$$F_x = F_{\alpha 1}\text{Sin}\alpha_1 + F_{r1}\text{Cos}\alpha_1$$
$$F_y = F_{\alpha 1}\text{Cos}\alpha_1 - F_{r1}\text{Sin}\alpha_1$$

....{6.10}

Equilibrium of X-Y Table - see Figure 6.8.(h)

$$T_x = (F_x - m_x\ddot{X}/k)p/2\pi$$
$$T_y = (F_y - m_y\ddot{Y}/k)p/2\pi$$

....{6.11}

Friction has been neglected in this analysis, which permits simplification of the analysis. The compound gear cluster which provides the necessary transmission between links 1 and 2 has negligible inertia and was omitted from the dynamic equations. However by virtue of the rack and gear connection between links 1 and 2, then

$$R_{r1} = - K.R_{r2}$$

....{6.12}

where

p = 0.005 (leadscrew pitch, m)
K = 4 (pantograph constant)
g = 9.805 (gravitational acceleration, m/s^2)
I_i = Inertia of link 'i' about link axis (kgm_2)

and consequently, $r_2 = K.r_1$.

Link masses and inertias were estimated during the design stage, and on the basis of this data, simulation of the crank turning

task was carried out. The results obtained were used to predict motor torques and hence aided the selection of suitable servo motors. Experimental verification of link masses and inertias was subsequently undertaken, as shown in Table 6.1, and found to be within +/- 10% of previously estimated values. The simulation was then repeated using the physical data to obtain more accurate results.

For the particular case of turning a crank at a constant angular velocity, as shown in Figure 6.8.(a) and (b), assuming the crank has no mass or inertia,

$$F_{\theta c} r_c = T_c$$
$$F_{rc} = 0$$

....{6.13}

Variable	Cross-slide X-axis	Cross-slide Y-axis	Extension arm Link 0	Extension arm Link 1	Extension arm Link 2	Terminal Link 3
Mass (kg)	1.54	5.34	7.73	2.40	3.85	0.8
Inertia(kg/m^2) at mass centre	-	-	0.28	0.02	0.09	0.1
Link centre to mass centre (m)	-	-	0.176	0.126	0.228	0.05

Table 6.1 Parametric details of pantograph arm

Transformation between crank-arm and Link 3

$$F_{r3} = F_{rc}\mathrm{Sin}(\theta - \alpha_3) + F_{\alpha c}\mathrm{Cos}(\theta - \alpha_3)$$
$$F_{\alpha 3} = F_{rc}\mathrm{Cos}(\theta - \alpha_3) - F_{\alpha c}\mathrm{Sin}(\theta - \alpha_3)$$

....{6.14}

6.3.4 Results of analysis

The flow diagram for the simulation is shown in Figure 6.9, and a listing of the program is given in Appendix I. The simulation was carried out using a crank, of radius 100mm, positioned as shown in Figure 6.7. The software developed permitted evaluation of the joint actuator torques in the presence of dynamic constraints, such as gravity, crank torque and crank speed.

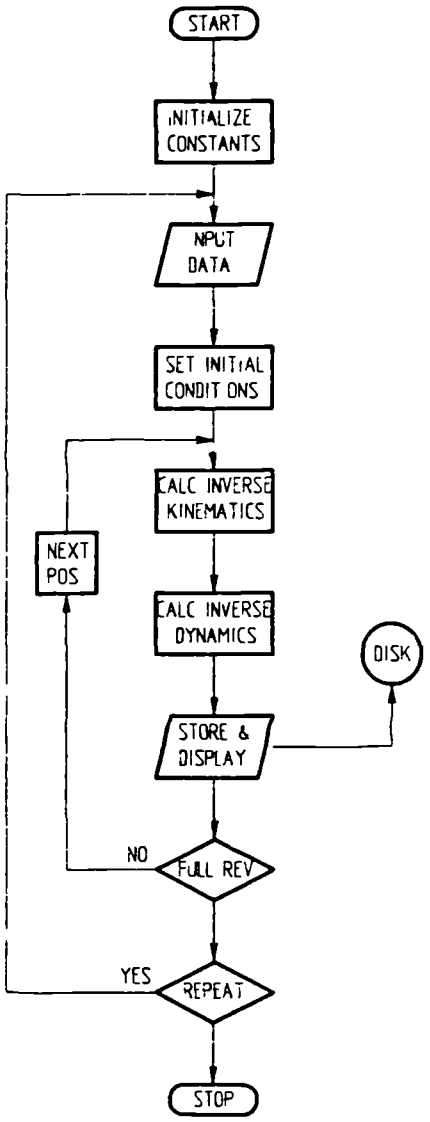

Figure 69 *Flow-diagram for pantograph analysis*

Figure 6.10 illustrates the theoretical actuator torques T_x, T_y and T_3 with a cranking torque of 10Nm, in the absence of any other dynamic loading. The respective torques were plotted as a function of crank angle and, as expected, the joint actuator torques are cyclic. The peak torque of T_y occurred at a maximum reach equivalent to a crank angle of 180^o, and had a magnitude of 0.5Nm.

The influence of cranking speed on the actuator torques is clearly illustrated in Figure 6.11. Two crank speeds were selected, 5 and 20 rads/s, equivalent to terminal speeds of 0.5 and 2.0 m/s. respectively. The theoretical result indicates that at the maximum design speed of 0.5 m/s the dynamic effects on actuator torques are negligible. However, a tip speed of 2.0 m/s does give rise to significant dynamic loading, and under such circumstances it would not be practical to ignore the dynamics of the mechanism in the control scheme.

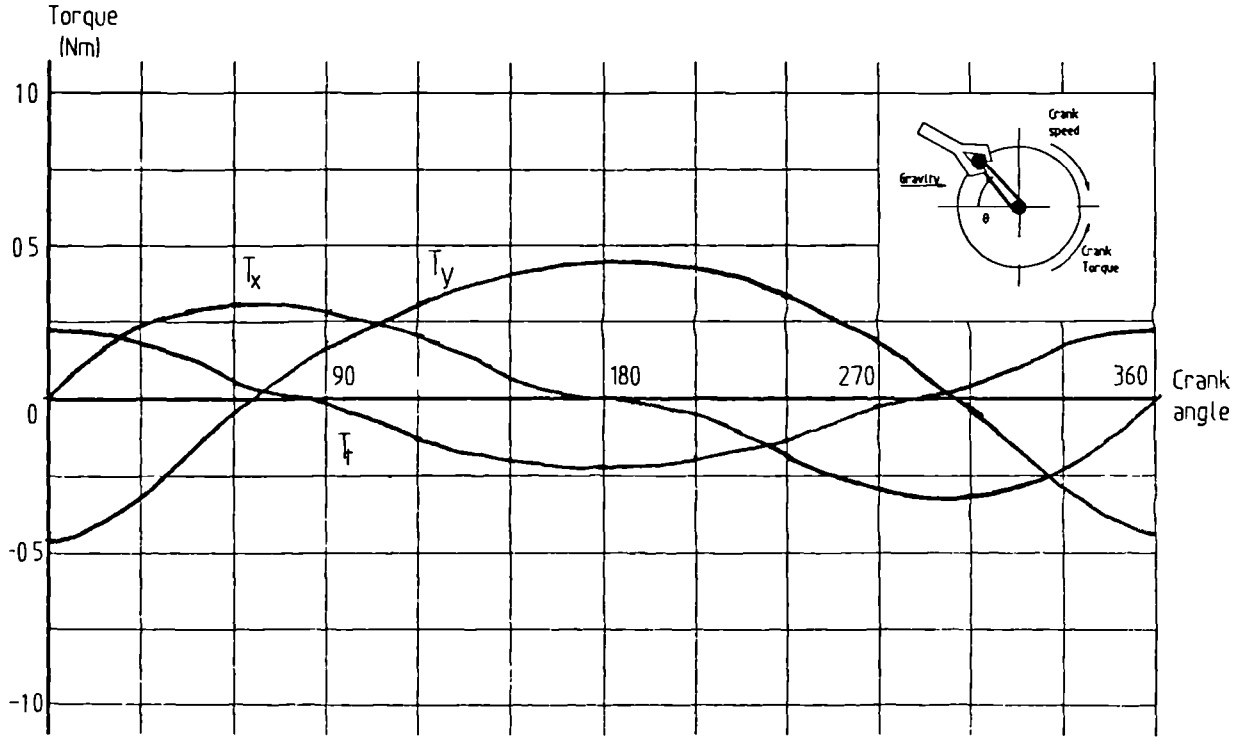

Figure 6.10 *Predicted motor torques when cranking torque 10Nm*

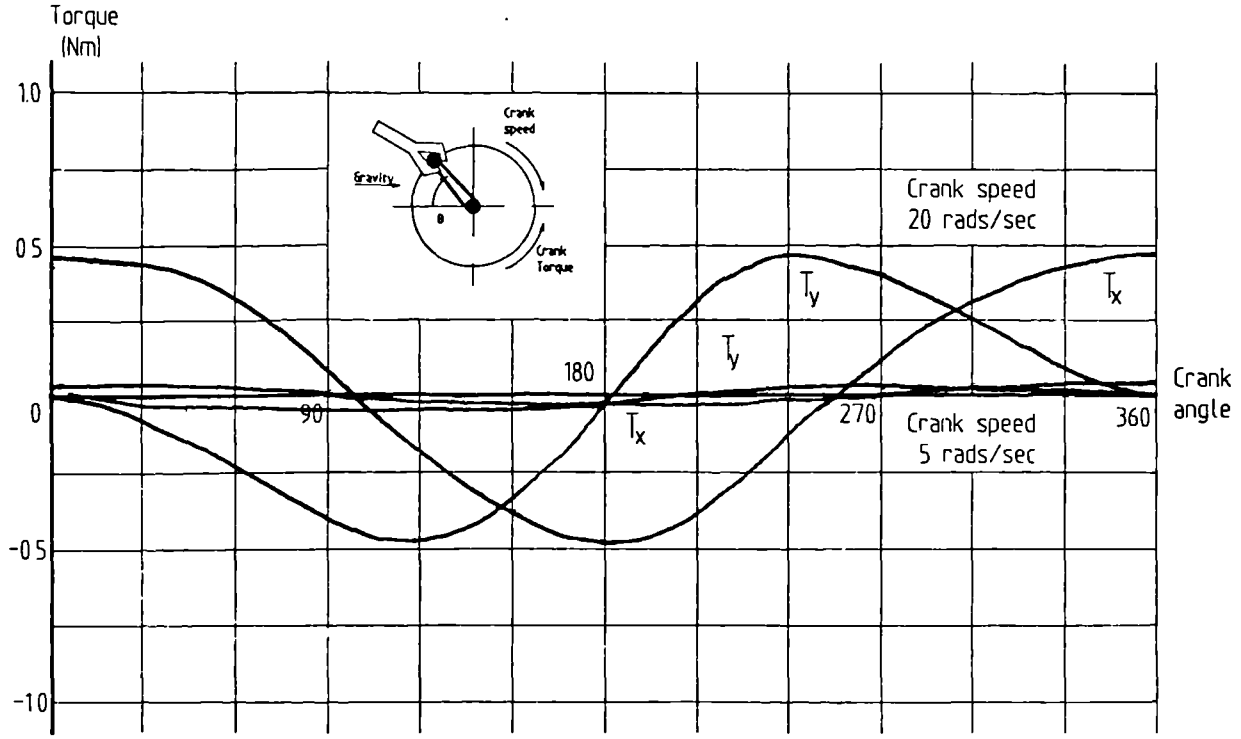

Figure 6.11 Predicted motor torques due to crank speed

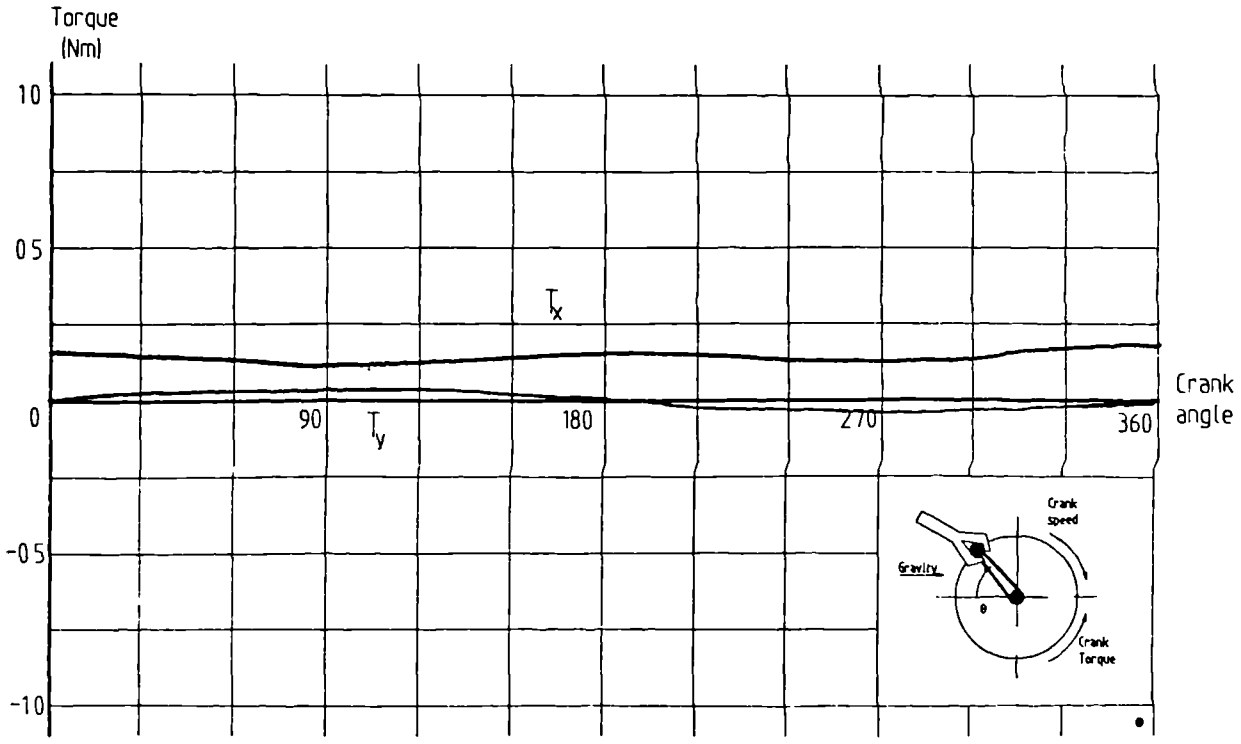

Figure 6.12 *Predicted motor torques due to gravity*

The final simulation run illustrates the influence of gravity on the actuator torques, as shown in Figure 6.12. As expected torque T_x is greater than T_y because of the limited change in angle α_0, the variation in both T_x and T_y is less than +/- 0.05 Nm, however as the crank radius is increased a corresponding increase in amplitude would take place. The peak torque T_x occurred at a maximum reach equivalent to a crank angle of 240^o, and a value of 0.15 Nm.

The dynamic analysis of the pantograph mechanism has permitted the evaluation of joint actuator torques under different constraints. The conclusions drawn from the simulation imply that dynamic disturbances are negligible at the maximum design speed, and that an independent joint control scheme would be adequate. However, since gravitational effects are significant, and are dependent upon positional constraints, it is considered that compensation would be required if the manipulator were to be operated in a gravitational plane.

6.3.5 Selection of servo-motors

Originally the two ballscrews were servoed using three phase brushless DC servo-motors with Sumarium Cobalt permanent magnets which offered high torque capacity coupled with reasonably high speed operation [Inland]. Digital encoders were mounted on the motor shafts, and used with frequency to voltage converters to produce an equivalent analog velocity feedback signal. The X-Y position of the mechanism was achieved using a nonlinear Sine/Cosine potentiometer and rectilinear potentiometer with hardware analog multipliers to yield servo position feedback of both X and Y coordinates.

The brushless motors were selected on the basis of excellent power to weight and torque to weight ratios compared with their conventional counterparts. Elimination of the brushes and commutator make this design particularly attractive in nuclear handling applications because of the elimination of arcing and subsequent detioration of the brushgear in the Argon rich environment of the hot cell. However, what was not forseen was the serious switching transients caused by the brushless motor controllers which corrupted the signal flow information. These transients, occurring at approximately 20 KHz frequency were introducing mains bourne and radiated noise which was being

picked up in the instrumentation and then quantized in the digital controller.

Attempts to reduce the noise by decoupling all input/output signal lines to the servo amplifiers marginally improved noise suppression. Further improvements were made by electrically isolating the offending servo amplifiers and power supplies using precision isolation amplifiers and mains filters. Although these modifications permitted satisfactory implementation of the generalized bilateral control scheme during the preliminary test programme it was decided recently to remove the brushless motors and replace them with conventional servomotors albeit with reduced performance. Conventional DC tachometers were mounted coaxially on the motor shaft. A more detailed assessment of the problems associated with the brushless DC motors can be found in Appendix II.

The rotary terminal joint was servoed using a conventional DC motor and a low-backlash 88:1 harmonic gearbox reduction unit mounted directly on the joint axis. Joint position was measured using a precision servo potentiometer connected to the joint axis via a short belt. A DC tachometer was mounted directly on the motor shaft to measure joint velocity. The terminal joint is illustrated in Figure 6.13.

The capacity of the slave arm at the terminal joint was initially 250N force and 29Nm torque with a 25% overload capability, and maximum operating speed was 0.5 m/second. Because of unforseen problems with the brushless motors on the X and Y axes the maximum force was reduced to only 100N with a corresponding increase in maximum speed up to 0.75 m/second.

Figure 6.14 gives the torque/speed characteristics of the different servo-motors used on the pantograph slave arm. The stall-torque and no-load speed lines for the RBE-1205 brushless DC servo-motors [Inland], and the 42MM014 and 55MM015 conventional servo-motors [Moore-Reed] are shown in relation to the predicted torque/speed curves obtained when turning the crank at a speed of 5 radians/second against a crank torque of 10Nm. The servo-motors were selected on the basis of these envelopes, with servo-motor 42MM014 used to servo the terminal joint. The high-torque/low-speed characteristic of the RBE-1205 servo-motor provided excellent high-torque capability for X and Y axes when

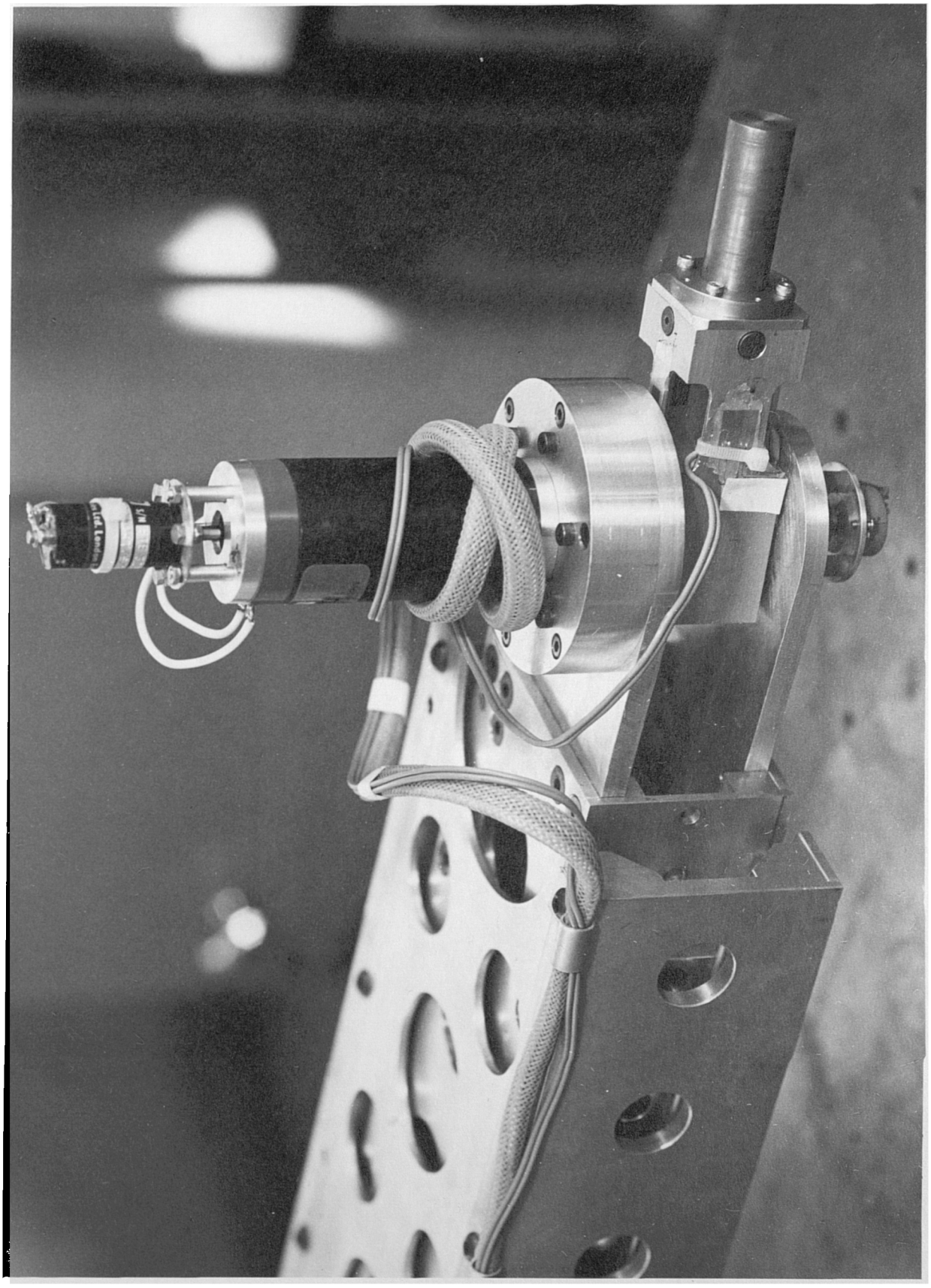

Figure 6.13 Slave Arm Terminal Joint

speed of operation was sacrificed. Note that although the replacement 55MM015 motors do not have the same stall-torque capacity, they nevertheless satisfy the criterion for selection.

6.4 Design of servo-amplifiers

During the design study the 'H' bridge configuration was considered. This type requires only a single power supply and its main disadvantage is that it is not easy to drive in a linear mode, and voltage or current feedback is difficult to achieve since the servo-motor is 'floating' [Electro-craft,1980].

It is also recognised that Pulse Width Modulation (PWM) which is ideally suited to the 'H' bridge configuration can provide high bandwidth performance of the servo amplifier up to 20 kHz. However at the time it was felt that the added complexity and possibility of noise due to the high switching frequencies of the power transistors outweighed any advantages that the 'H' bridge may have.

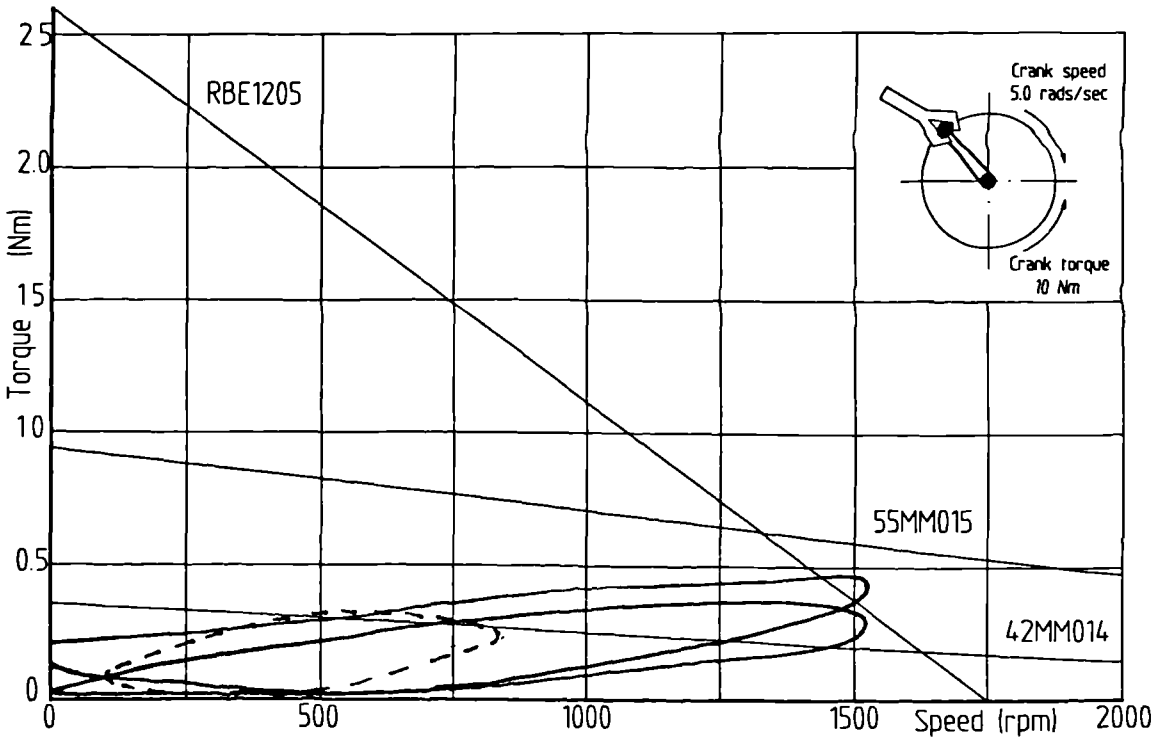

Figure 6.14 *Pantograph arm motor torque-speed characteristics*

Purpose built linear DC servo-amplifiers were designed for driving the conventional DC servo-motors used in the study. A conventional 'T' configuration was used for the output stage. Whilst this type requires dual power supplies and the use of complementary transistors it is easy to drive and voltage and current feedback signals are relatively simple to implement. However the biasing of the two stage output transistors does require some attention since the simultaneous conduction of both power transistors would result in a short circuit between the two power supplies.

The amplifiers are rated at 150 watts, and can sustain a current of 6.5 amperes continuously at 24 volts. A dedicated bi-polar DC power supply provides +/- 28 volts output for each servo-amplifier. A schematic of the circuit is shown in Figure 6.15. Notice that all transducer inputs are buffered and are provided with decoupling capacitors for protection. The velocity feedback input is also provided with an attenuator for gain adjustment. Two additional unbuffered inputs are primarily intended for strain gauge amplifier inputs and for offset balance adjustment. The overall forward gain of the pre-amplifier stage can also be adjusted using a preset potentiometer.

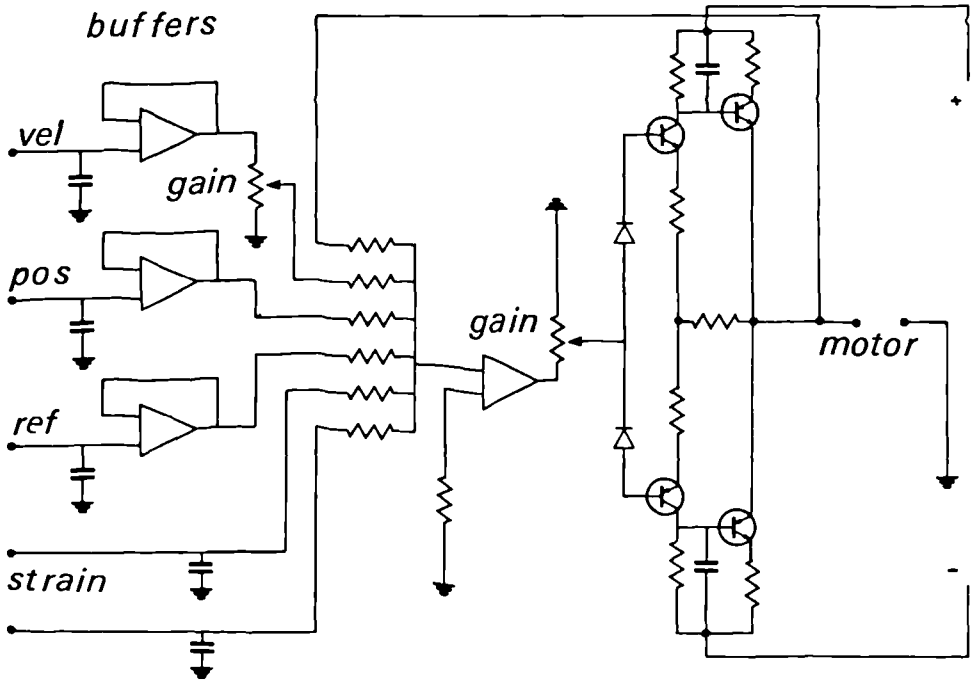

Figure 6.15 Articulated arm servo-amplifiers

6.4.1 Articulated arm servo-amplifiers

During the early stages of the work the replica master-slave control system was fully analog with two way information flow on one-to-one joint correspondence ie. each joint of the master arm was electrically coupled to, and only to, the corresponding joint on the slave manipulator. Thus each master-slave joint pair could track each other in angular position regardless of whether the master or slave arm was being moved.

Figure 6.16 illustrates, diagrammatically the interelationship between corresponding master and slave joint servo-motors. Overall there exists position feedforward control between master and slave, and torque feedback control between slave and master. Perhaps the most significant advantage of the tight torque feedback loop on the master servo is the ability to backdrive the master arm.

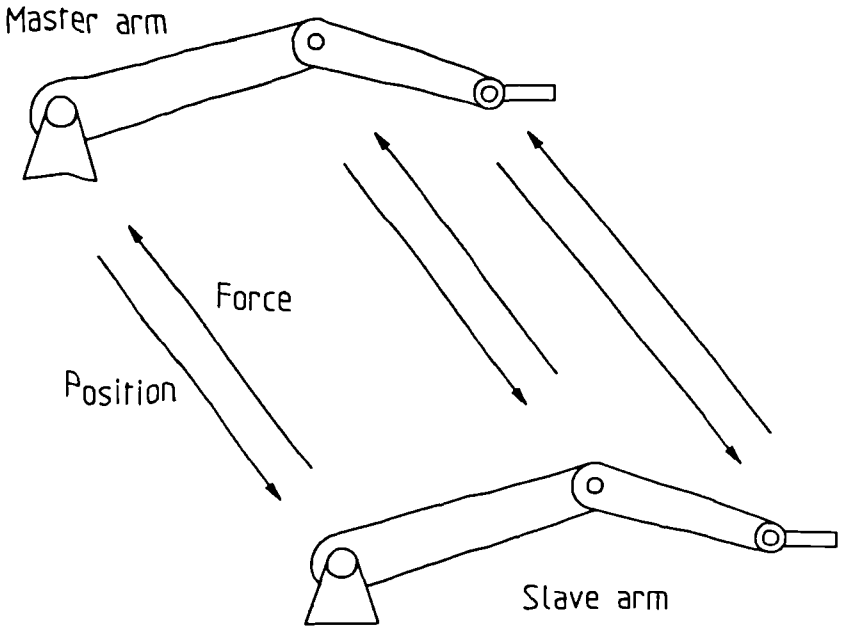

Figure 6.16 *Position/force control of replica MSM*

The friction compensation technique, and its integration into the overall control system has been evaluated using digital simulation. The simulation has been applied to a single degree of freedom, and is based upon parameters appropriate to the elbow joint of the master and slave arms. Stable operation has been verified. The simulation study is fully described in Chapter7.

6.4.2 Pantograph arm servo-amplifiers

The pantograph slave arm was initially designed to incorporate two brushless DC servo-motors for the actuation of the principal X-Y axes. Because of the configuration this required an unconventional approach for the implementation of the closed loop position feedback. Figure 6.5 shows the X-Y cross-slide table. To provide absolute position feedback a non-linear Sine/Cosine potentiometer and a linear potentiometer was used in conjunction with analog multipliers to derive absolute X-Y position information.

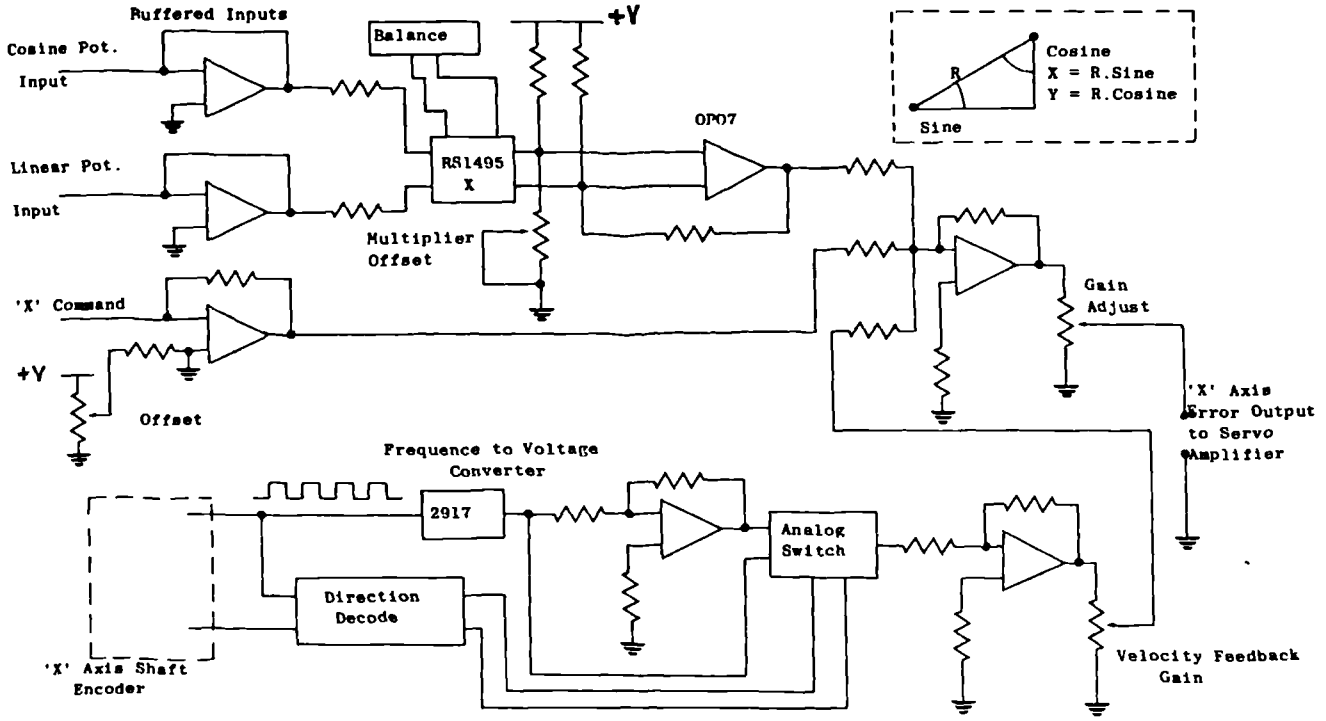

Figure 6.17 Pantograph pre-amplifier circuit

Figure 6.17 shows the schematic design of the pre-amplifier used for the X and Y axes interface. Note that all transducer inputs pass through unity gain buffers. The analog multiplier circuit is used to compute the arm position 'X' coordinate (and 'Y' coordinate) and is an extremely difficult circuit to set up. Sensitive gain and balance control circuits have been incorporated in the design in an attempt to reduce drift.

Optical encoders were used for velocity feedback damping. A frequency to voltage converter incorporating an analog switch for direction decoding was used in conjunction with analog gain control to provide desired velocity feedback. An overall gain adjustment at the output of the pre-amplifier circuit was also included. An additional unbuffered input was provided for strain-gauge inputs.

The brushless motors were servoed using commercial brushless motor controllers. Input power to the controller was provided by a 400 watt, constant voltage (24 volt) unipolar switched mode power supply. The analog output from the individual pre-amplifiers was used to drive the motor controller which was configured in the 'analog duty cycle' control mode. Electronic commutation of the brushless motor was carried out using Hall effect sensors mounted on the motor stator. Control logic within the controller defined the switching sequence for the three phase motor windings.

What was not anticipated with the combination of switching power supply and brushless motor controller was the amount of high-frequency electrical noise generated. Filters were subsequently fitted to all signal inputs in an attempt to limit the noise to an acceptable level. A more detailed description of the brushless motor controller and the techniques used to improve noise immunity are given in Appendix II. Preliminary tests were carried out using the brushless motors, but whilst they provided an excellent torque/speed characteristic the excessive torque ripple resulting from the discrete electronic commutation prevented smooth operation. In the event it was decided to replace them with conventional DC servo-motors which did not match up to the same performance, and consequently the overall specification for the pantograph arm was subsequently lowered.

6.5 Force/torque sensors

Alternative force sensing techniques were assessed to find out whether it was desirable to know individual joint forces or whether it was sufficient to know the exact state of stress and/or loading at several locations on the arm.

Most replica master-slave systems derive joint torque from a knowledge of the torque/current characteristic of the servo motors used. The main limitation of this indirect measurement technique is associated with the effects of friction and backlash in the transmission which can introduce significant noise into the signal content and subsequently reduces the sensitivity of the force feedback. Efficient transmissions using direct drive technology can satisfactorily utilize motor current to estimate joint torque if the expense of high torque servo-motors can be justified [Asada & Kanade, 1983a;1983b].

Researchers have recently attempted to improve the sensitivity of the force reflection by estimating the friction present in the transmission and then incorporating an 'estimator' in the digital loop of the bilateral controller [Suzuki,1983].

Single component force sensors located at each joint can provide a good indication of a particular component of loading. However, for a 6 degree of freedom manipulator having 6 sensors, one associated with each degree of freedom, it will prove difficult to deduce anything other than an approximation of the applied loading at the terminal device. By using a multi-component force/torque sensor located at or near the terminal joint, the resultant reaction forces generated by the task can be relatively well defined. The indeterminate case of loading on all other arm joints, particularly if external loads may be applied to other parts of the arm as in the case of an encounter with an obstacle, must then be defined using alternative sensors arrangements.

In the present study, joint force (or torque) was measured using strain-gauge sensors located on or adjacent to each joint on both slave arms.

The design of strain-gauge amplifier used in the study is shown schematically in Figure 6.18. Originally it was intended to use two active gauges for the bridge and provide temperature compensation using resistors; also the bridge ampifiers were

located inside the control panel. However, because of problems with drift and noise at high gain induced through long lead length and changes in contact resistance through plugs and sockets the design was modified to incorporate a 'head amplifier'. The bridge amplifiers were subsequently moved adjacent to the respective manipulator arm, and compensation resistors replaced by dummy gauges.

Strain-gauge bridges were mounted on both articulated arms as close as possible to the joint axis. To improve sensitivity, the stiffness of the structural members were reduced. This was carried out by machining the box section adjacent to the proposed location for the strain-gauges, as shown in Figure 6.19. Corresponding values of second moment of area I, for both the original and machined box sections are given in Table 6.2, along with calculated bending stiffness for the three sizes of box section used in the design of the manipulator arms.

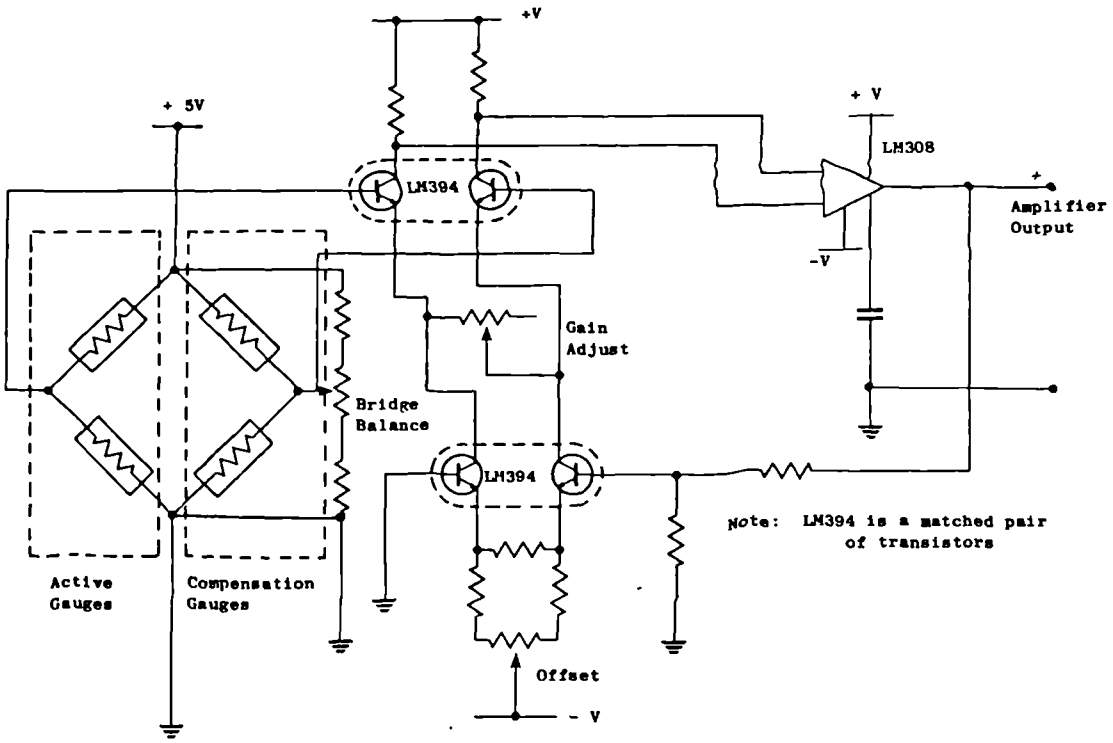

Figure 6.18 Strain-gauge amplifier

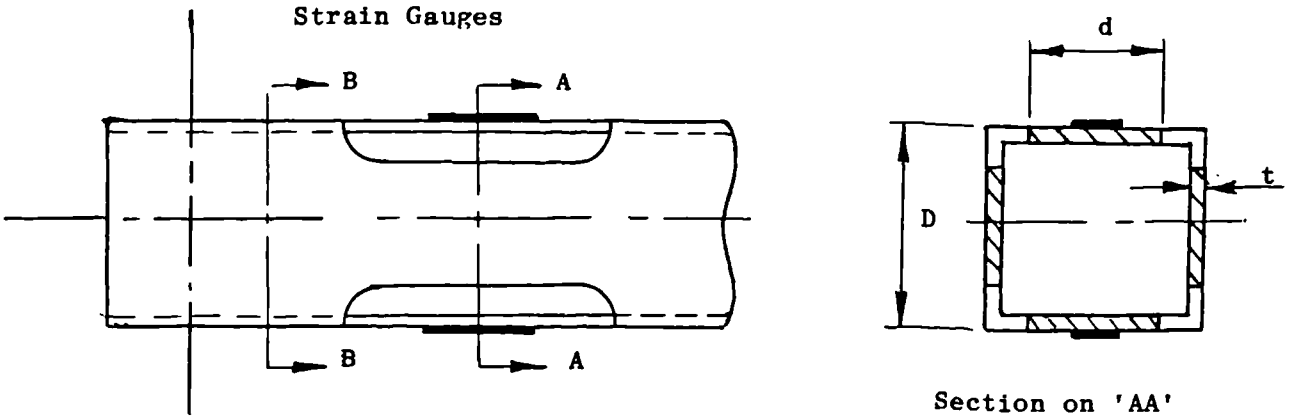

Figure 6.19 Box section modulus reduction

Calculation of Second Moment of Area $I_r = \frac{td^3}{6} + \frac{D^2dt}{2}$ for reduced section.

Second moment of area for Full section $I_c = \frac{2D^3t}{3}$ (mm^4)

Stiffness is defined as $\frac{M}{\epsilon} = \frac{EI}{y}$ E = Youngs Modulus $y = \frac{D}{2}$ (mm^4)

	Section 25 x 25 t=1.8,d=14	Section 30 x 30 t=1.8, d=15	Section 38 x 38 t=1.8, d=18
Full Section $I_c = \frac{2D^3t}{3}$ (mm^4)	18750	32400	65846
Reduced Section $\frac{td^3}{6} + \frac{D^2dt}{2}$ (mm^4)	8698	13972	25142
K_s Stiffness (KNm/Rad)	48.7	61.4	92.6

Table 6.2 Box section - Calculated stiffness

The pantograph slave arm utilised a two axis load cell mounted between the X-Y coordinate table and the input extension arm to measure applied forces. The design of the load cell, and estimated values for section modulus and stiffness are recorded as shown in Figure 6.20. The terminal joint of the pantograph arm was constructed using 38x38 mm square aluminium box section and was also machined to reduce section modulus in accordance with Table 6.2.

Calibration of the strain gauge amplifiers had to be carried out under carefully controlled conditions. In keeping with previous requirements it was necessary to employ decoupling capacitors at strategic positions in the circuit to facilitate the reduction of noise to within acceptable limits.

Because of the relatively high gains necessary to achieve adequate measurement from the bridge amplifiers it was important that the amplifiers were allowed to reach thermal equilibrium, and any drift to have stabilized before attempting to null any offsets. Once this condition had been complied with, normally within several minutes, the control scheme could be tested.

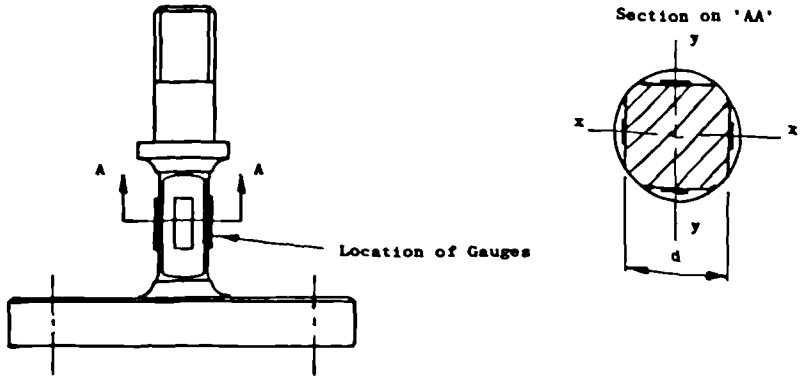

$I_{xx} = I_{yy} = \frac{d^4}{12} = 833\ mm^4$

Material En8, Youngs Modulus $E = 210\ GN\ m^2$

Stiffness $K_s = \frac{M}{\epsilon} = \frac{EI}{y}$

M = Bending Moment

ϵ = Strain

y = d/2

$K_s = 17243\ kNm/Rad$

Figure 6.20 Two axis load-cell

6.6 Digital control system

During the initial stage of the study a Zilog Z80 based microcomputer with a clock speed of 4 MHz was used as a digital controller. The system utilized the S100 backplane which was used to provide additional input/output facilities. A 16 channel, 12 bit data acquisition system with programmable gain amplifier was used for analog to digital conversion. All analog outputs were obtained using a purpose built 6 channel, 12 bit digital to analog converter. Because the S100 bus has only an 8 bit data bus all input/output data translation involved 2 byte transfers.

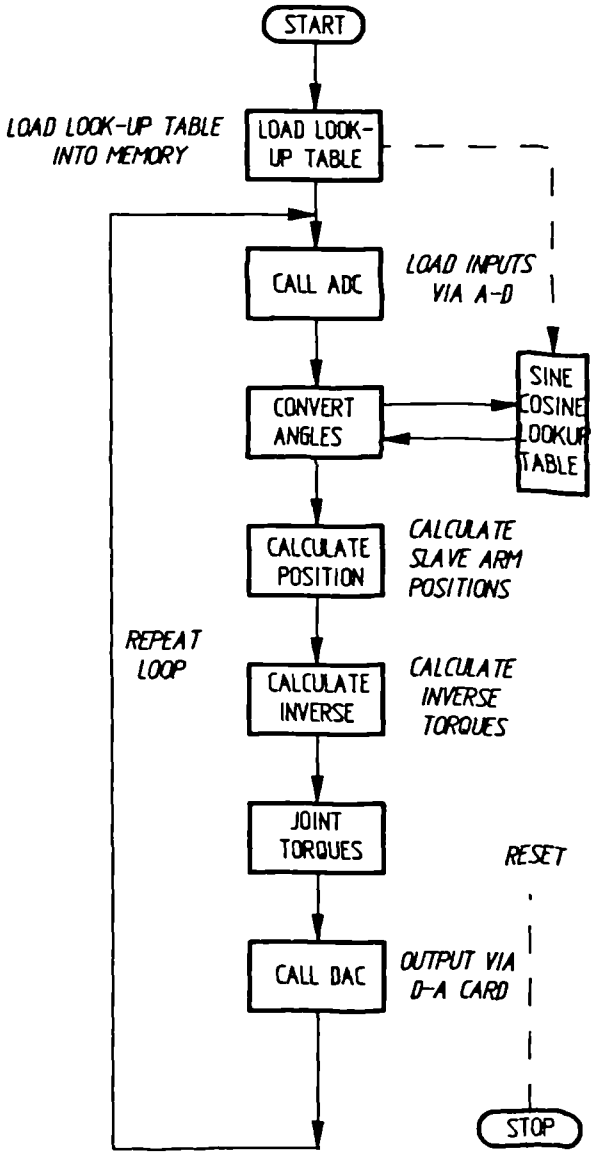

Figure 6.21 Z80 based controller - Flow diagram

The control algorithm was written in Fortran [CPM-Fortran] with the capability of port and memory addressing. The executable code produced using the Fortran compiler was reasonably efficient. However it was not possible to use floating point arithmetic because of the limited computational speed of the microprocessor and all data translation was carried out using integer arithmetic. The additional time penalty involved in trignometic function calls, ie. Sine and Cosine, prohibited their use and it was necessary to develop a 12 bit Sine/Cosine look-up table using 16 KBytes of read-only-memory from a total allocation of 64 KBytes in the memory map.

The flow diagram for the control program is shown in Figure 6.21. The maximum sampling period achieved for the bilateral control algorithm was approximately 24 mS. Whilst the initial tests demonstrated the implementation of the control scheme it was nevertheless considered that the minimum sampling frequency should not be less than 100 Hz, ie. 10 mS sampling period, for adequate stability. Therefore if a more acceptable sampling frequency were to be achieved it would be necessary to employ a faster digital controller. The decision to utilize a Z80 based microcomputer was made principally because at that time the S100 bus was well established and a recognised standard.

However, the rapid developments in microprocessor technology saw the introduction of the IBM personal computer which was soon established as an industry standard. The Intel 8088 microprocessor and 8087 numerical co-processor offered excellent performance with the 'IBM' bus well supported with peripherals. For these reasons it was decided to replace the Z80 machine with an IBM compatible computer.

The present digital controller is based on the Intel 8088 family and has switchable clock speeds up to 8 MHz. Microsoft Fortran (MS-Fortran) and Macro-assembler (MS-Assembler) were used for the control algorithm. A 16 channel (12 bit) analog to digital converter and 3 bidirectional digital input/output ports (8 bit) were available on the data acquisition system for the computer interface. Digital to analog conversion was carried out by a 4 channel (12 bit) peripheral interface board which also incorporated 3 digital I/O ports (8 bits each). Two additional D-A ports (12 bit) were also available on the data acquisition system giving a total of 6 analog output channels, one for each servo-controller input.

MS-Fortran does not support I/O function calls and consequently it was necessary to incorporate assembly language subroutines which were compiled independently of the main Fortran program. The compiled programs are subsequently linked to produce executable code which comprises the main control program.

The improved performance of the PC allowed the use of floating point arithmetic to achieve higher acccuracy, and the supporting numerical co-processor enabled trignometric function calls to be calculated in real-time. A flow diagram of the overall control scheme is shown in Figure 6.22. The implementation of the generalized control scheme, and the practical solution of direct and inverse kinematics and dynamics is descibed in more detail in Appendix III.

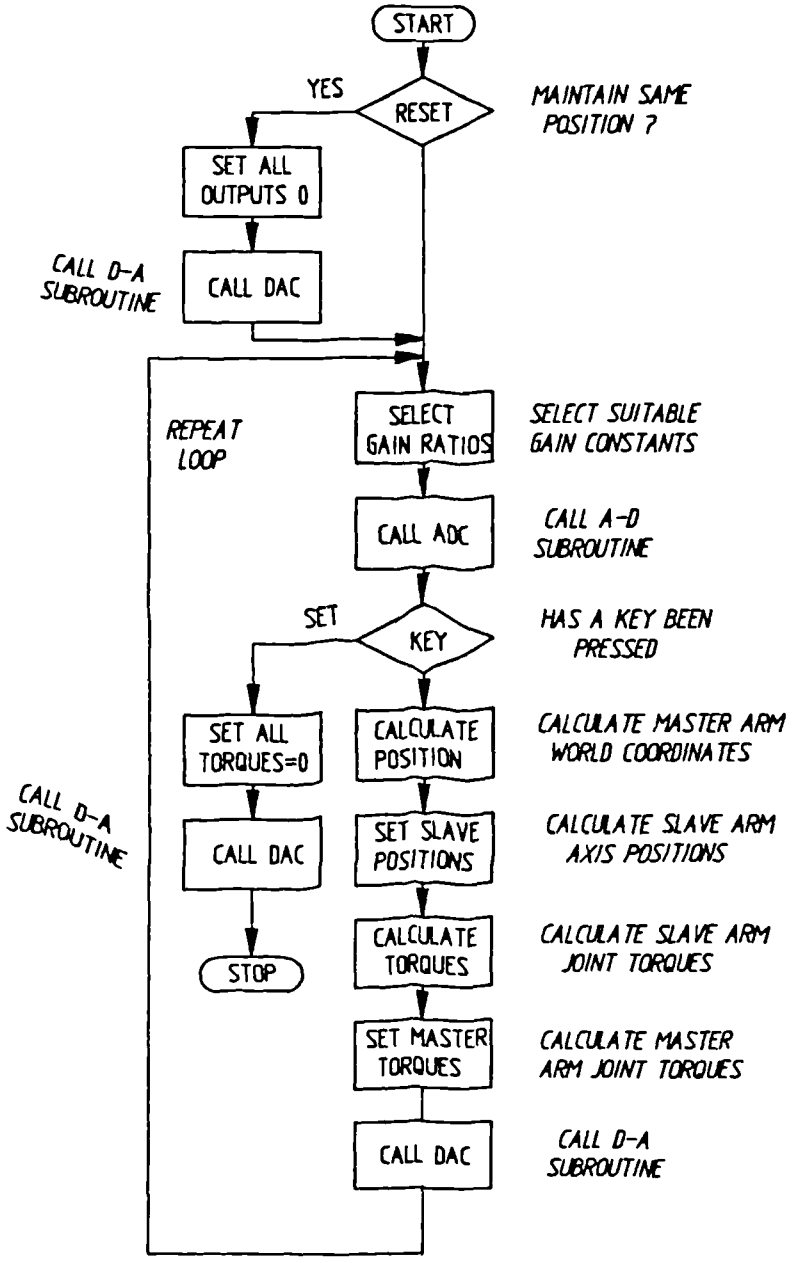

Figure 6.22 Intel 8088 based controller - Flow diagram

A total of 12 analog input channels were sampled using an assembly language subroutine. A-D conversion was carried out with the data acquisition system in the auto-incrementing mode. It was also considered advantageous to manipulate the input data and convert from 12 bit two's complement format to 16 bit signed-binary in preparation for passing back to the main program. In addition the subroutine also tests the status of the keyboard buffer to detect if a key has been depressed. All parameters, including the keyboard status, are passed back to the main calling algorithm which will continue unless a key-interrupt has been detected: in which case a controlled exit back to the computer operating system is carried out.

An assembly language D-A subroutine was used to control the 6 analog outputs. The main program passes parameters to the A-D subroutine which then carries out the conversion. In addition the subroutine is also polling an 8 bit digital input port to determine the status of several control switches and an emergency stop switch. Each analog output is allocated a separate switch which, if activated, is used by the subroutine to inhibit the desired output, and in so doing sets that particular channel output to 0 volts. The emergency stop switch is used to set all analog outputs to 0. The subroutine then returns control back to the main calling program.

Flow diagrams for both A-D and D-A assembly language subroutines are shown in Figure 6.23, and listings are given in Appendix IV. Also included is a listing of a short assembly language program which is automatically executed during computer initialisation to ensure that all analog outputs are set to 0 volts prior to running any control programs.

6.7 Summary

The design of the experimental manipulator arms and their servo-controllers have been described in this chapter. The results of a dynamic analysis carried out on the pantograph slave arm have been presented, from which it was possible to predict the servo-motor torque demands for a crank-turning task under several different conditions. Brushless DC servo-motors were originally selected to drive the main axes of the pantograph arm, however, problems associated with switching transients and torque ripple left no choice but to replace them with conventional DC

servo-motors. Although having a reduced peak-torque rating, the replacement motors satisfied the torque/speed requirements.

Modifications to the digital control system were carried out mid-way through the investigation to achieve a higher sampling frequency. The original digital computer was replaced by a faster machine, and the two different approaches adopted to carry out the generalized control strategy have been discribed.

The implementation of joint torque feedback on the master arm was introduced. The ability to backdrive the transmission is considered particularly useful, and the technique is assessed using digital simulation in the following chapter. Tests to establish the tracking ability and bilateral control are reported in Chapter 8.

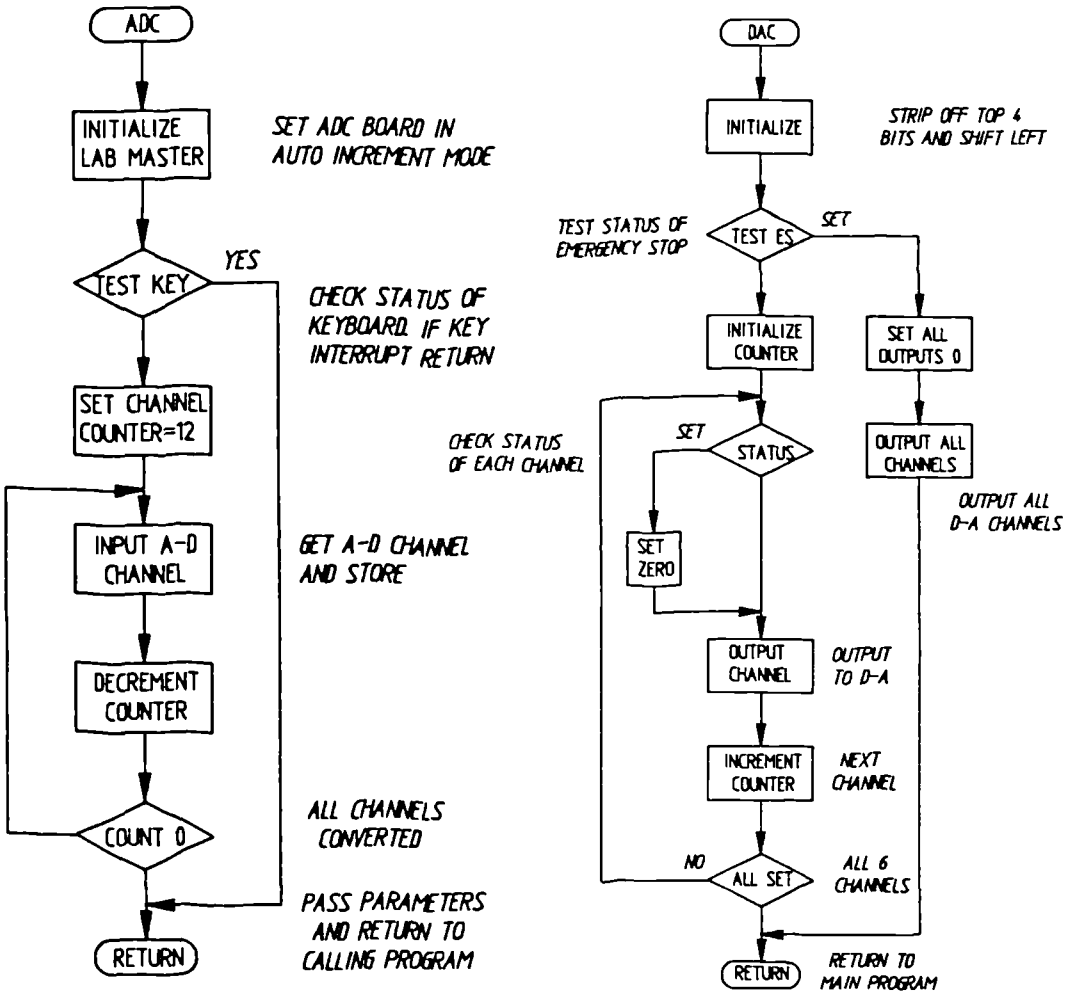

Figure 6.23 Flow diagrams for A-D & D-A subroutines

CHAPTER 7

Modelling of a one degree of freedom master-slave system

Simulation of a remote master-slave manipulator system with a 'man-in-the-loop' could in principle be used to predict both the behaviour of the system and the operator under various conditions when performing typical tasks. Because of the inter-dependency between system and operator it should also be possible to determine the operator's contribution to the overall system performance. However, this is unrealistic in all but very simple systems because the human operator has wide ranging skills and abilities and a highly adaptive nature which makes characterisation using anything other than simple mathematical models extremely difficult.

Modelling of one degree of freedom of a coupled master-slave system enabled the influence of various system parameters on performance to be assessed. It followed that because of dynamic coupling in multiple degree of freedom systems the influence of parametric changes in one axis will influence the overall performance, although it was considered that much valuable information can be obtained by modelling only one axis.

The time domain analysis extends both the position/force and position/position control schemes introduced in Chapter 5, and has been based upon the elbow joint of the articulated master - slave arms described in Chapter 6. As far as possible, the full dynamics associated with the elbow joint have been incorporated in the model, including the servo-amplifier and a simple representation of both human operator and task.

7.1 Digital simulation

The digital simulation language used here is called the Advanced Continuous Simulation Language [ACSL,1986]. An important feature of the language is its free form input with automatic sorting of the model equations, which is in contrast to Fortran where

program execution depends critically on statement order. However, the flexibility of ACSL is considerably extended to include the powerful conditional logic and branching of Fortran which is accomplished using what are called Procedural Blocks, ie. blocks of code within which statement order and execution are governed by Fortran rules.

ACSL provides over fifty special operators, including many non-linear functions ie. QNTZR (Quantization) and BLASH (Backlash), and in addition, all the functions of the standard Fortran library are available. The solution of differential equations requires the use of integration routines, and in this instance the integration algorithm used was the fourth order Runge-Kutta method. Although variable step size algorithms are available it was necessary to ensure adequate accuracy without enduring an excessive run time. An integration step-size ie. integration interval, of 0.0001 seconds was found to be satisfactory.

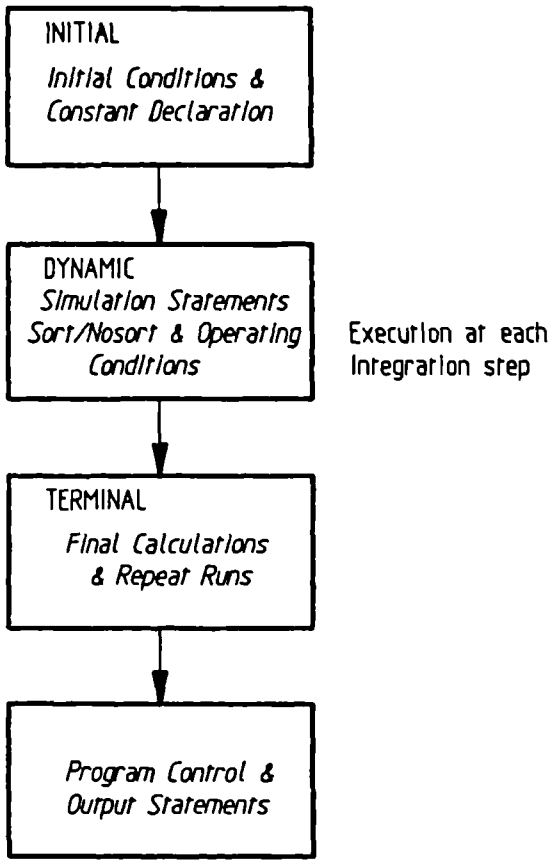

Figure 7.1 *Program structure of ACSL*

The program structure of ACSL is composed of three main segments - Initial, Dynamic and Terminal as shown in Figure 7.1. The Initial segment is used primarily for any one-time calculations. The Dynamic segment contains the structured statements that describe a set of differential equations. The Terminal section is used to carry out final calculations and ordering for any re-runs etc. Additional program control statements are used for subsequent results tabulation and plotting.

Representation of a control system using a block diagram approach is probably the most conventient method of describing the signal flow between the functional elements of a control system. A program called EASE+ [Expert-Ease,1987] provides a convenient graphical input based on block diagrams and utilizes a post-processor to produce ACSL source code. Additional facilities within EASE+ include graphical output of ACSL simulation runs to a plotting device.

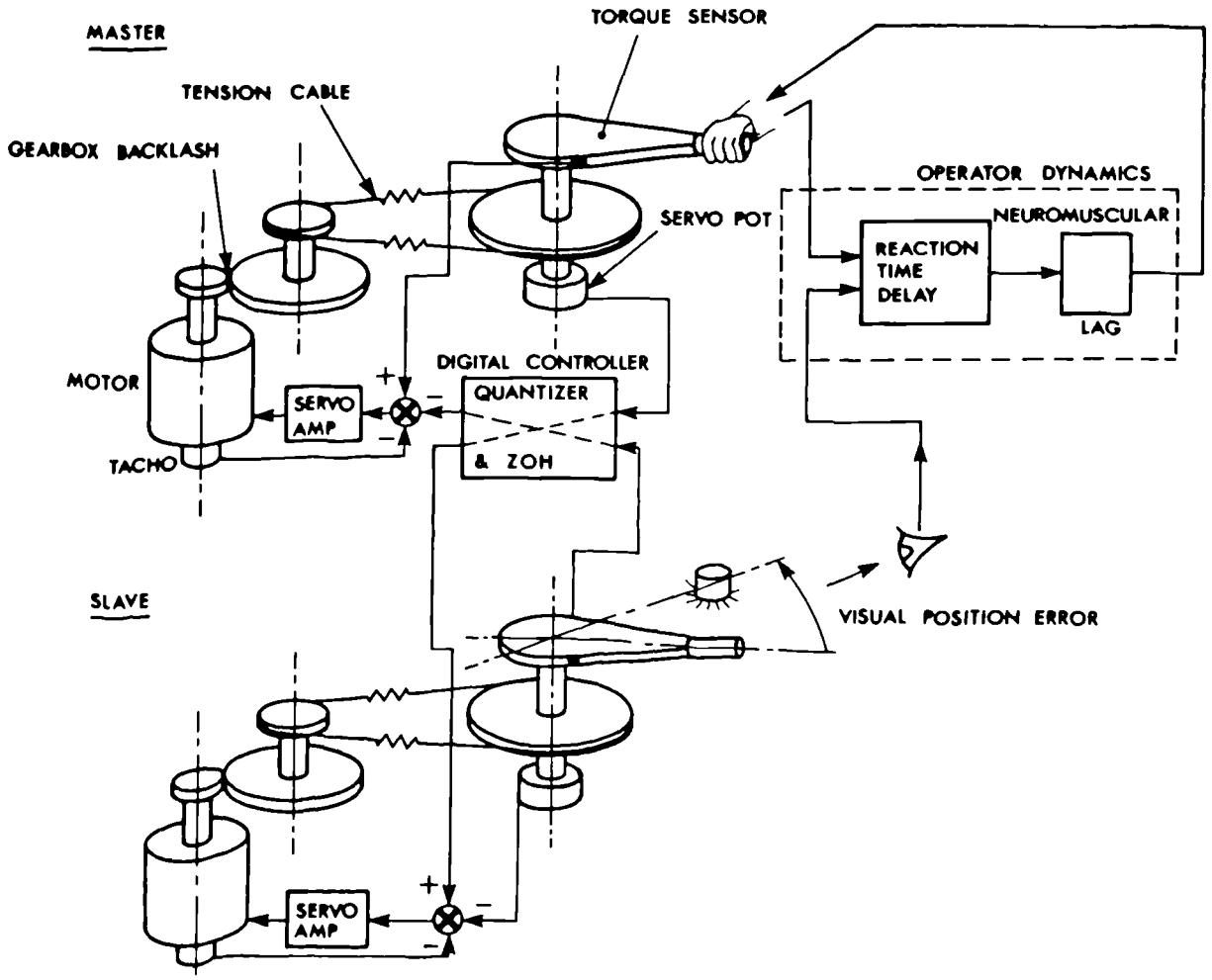

Figure 7.2 Schematic of 1 degree of freedom Master-Slave

7.2 Dynamics of a one degree of freedom master-slave system

The diagram shown in Figure 7.2 illustrates schematically the model, which consists of a pair of interconnected two d.o.f. dynamic systems - connected by virtue of the flexible cable transmission. Verification of system parameters by experiment was used to ensure adequate correlation between experimental and simulation results. Mechanically, both master and slave arms can be considered identical, and are arranged to rotate in the horizontal plane so that gravitational effects can be neglected.

The equations of motion are derived using D'Alemberts method, and for the motor/gearbox assembly (see Appendix V) are written as

$$T_m = \theta'_m(J_m S^2 + C_m S) + (F_a - F_b)r_m/N \qquad \ldots\ldots\{7.1\}$$

where

θ'_m - Angular position of motor shaft (rads)
J_m - Combined inertia of motor/gearbox referred to motor shaft (kgm^2)
C_m - Coefficient of Viscous Damping of motor/ gearbox referred to motor shaft (NmS/rad)
r_m - Radius of gearbox output pulley (mm)
F_a, F_b - Tension force in cable (N)
N - Gearbox reduction ratio
T_m - Motor Torque (Nm)
S - Laplace variable

and similarly for the output link

$$-T_l = \theta_o(J_o S^2 + C_o S) - (F_a - F_b)r_o \qquad \ldots\ldots\{7.2\}$$

where

θ_o - angular position of output link (rads)
J_o - combined inertia of link referred to axis of rotation (kgm^2)
C_o - coefficient of viscous friction of link (NmS/rad)
r_o - radius of link input pulley (m)
T_l - external torque applied to link (Nm)

and

$$(F_a - F_b) = 2k(\theta_m r_m - \theta_o r_o)$$

.....{7.3}

where θ_m - angular position of gearbox output (rads)
k - cable stiffness (N/mm)

Figure 7.3 shows the equivalent block diagram relationship between the dynamic equations {7.1} - {7.3}.

The transfer function for a DC servo-motor can be represented as a first order lag, as follows:

$$I_a(R_a + L_aS) + V_{Bemf} = V_{in}$$

.....{7.4}

where V_{in} - motor terminal voltage (v)
V_{Bemf} - back emf voltage (v)
I_a - armature current (amps)
R_a - armature resistance (ohms)
L_a - armature inductance (henry's)

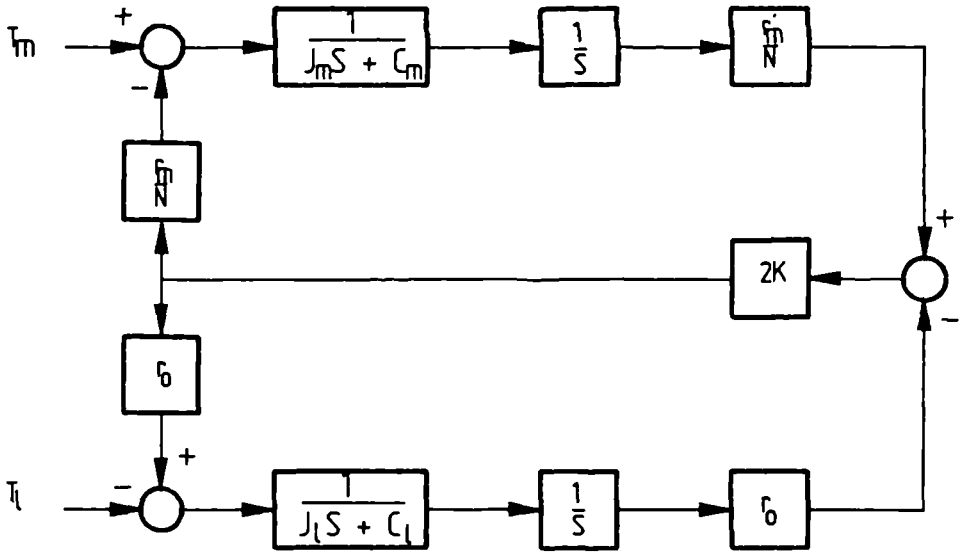

Figure 7.3 *Block diagram of dynamic system*

Schematically, a permanent magnet DC servo-motor can be represented as shown in Figure 7.4(a). The equivalent block diagram is shown in Figure 7.4(b). In general the servo-amplifier time constant is insignificant when compared with the motor time constant and was consequently neglected. The overall block diagram for the master-arm is shown in Figure 7.5 (the block diagram for the slave-arm is identical).

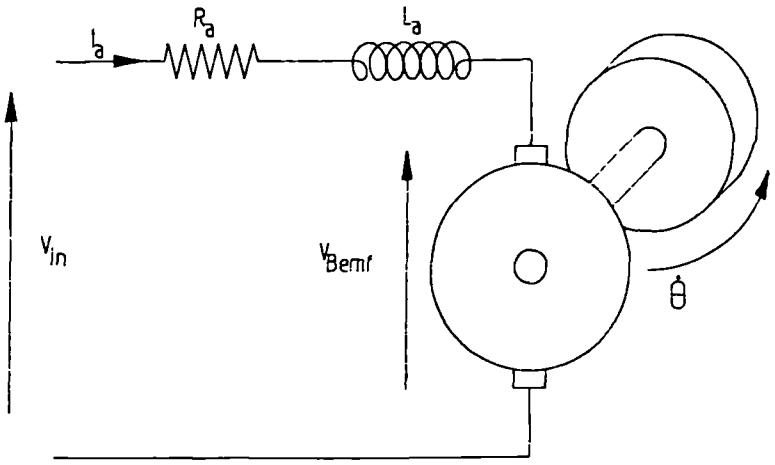

(a)

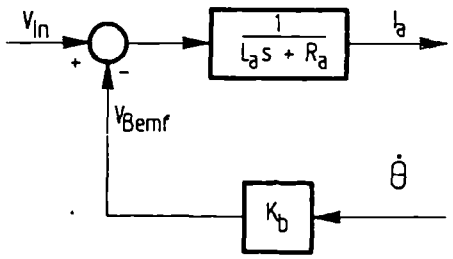

(b)

Figure 7.4 *Electrical analog of DC servo-motor*

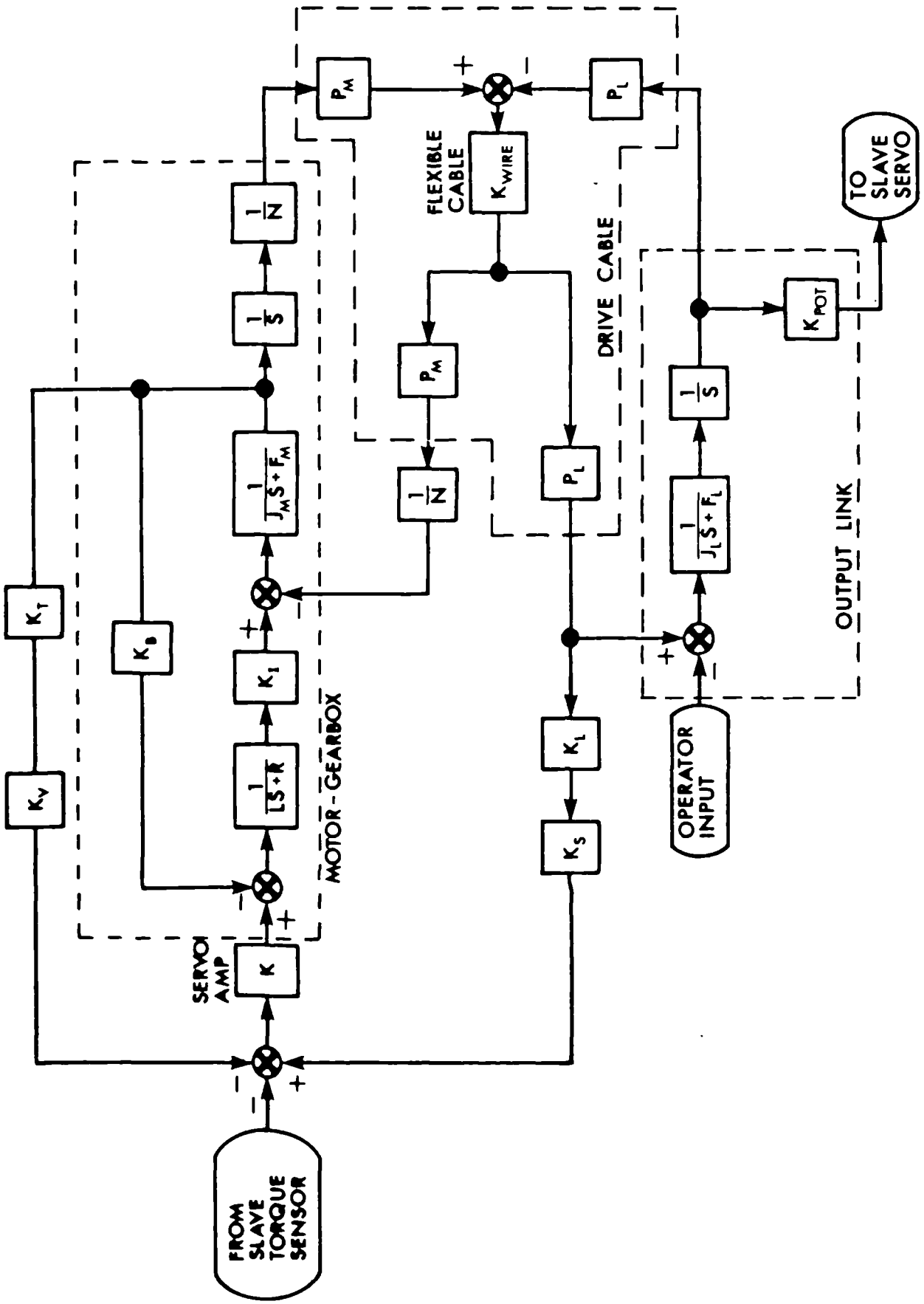

Figure 7.5 Overall block diagram for Master arm

7.2.1 Open-loop step response tests

The servo-amplifier design used in this investigation has been described in Chapter 6, and utilizes a unregulated bipolar power supply to provide a linear +/- DC voltage to drive the output stage of the amplifier. The saturated peak to peak voltages were found to be unsymmetrical, ie. saturation occurred at +11.35 and -12.7 volts. Consequently different open-loop velocities are recorded in clockwise and anticlockwise directions, and a BOUND operator [ACSL,1986] was included in the model to accomodate saturation.

Preliminary open-loop response tests were carried out to verify critical parameters, and the results subsequently correlated against a simulation model. Figure 7.6 represents the actual tachometer voltage, recorded as a function of time, for different dynamic configurations in response to a step change in input voltage. The modulation due to tachometer ripple, occurs at 6 times running frequency and is attributable to the number of poles on the tachometer. The lower frequency cyclic variation is probably due to commutation and/or brush friction.

The equivalent model used for the open-loop system is shown in Figure 7.7, with that part of the model relating to the motor/tachometer/gearbox sub-assembly shown dotted. The equivalent step response of the model for the different configurations is shown in Figure 7.8. Note that the steady state speed of the motor is dictated by the input voltage V_{in} and coefficient of viscous friction C_m. Whilst C_m was selected to achieve an equivalent steady state speed, a comparison of the actual and predicted time constant showed that the model 'inertia' J_m was high. The inertia of motor was checked using a torsional pendulum technique, and was subsequently found to be significantly lower than specified by the manufacturer.

By disconnecting the transmission cable, the open-loop step response of the motor/gearbox assembly was obtained as shown in Figure 7.6(b). Estimation of the overall inertia of the gearbox, referred back to the motor shaft enabled a comparison with the simulation, Figure 7.8(b). Once again C_m had to be adjusted in the model to maintain adequate correlation.

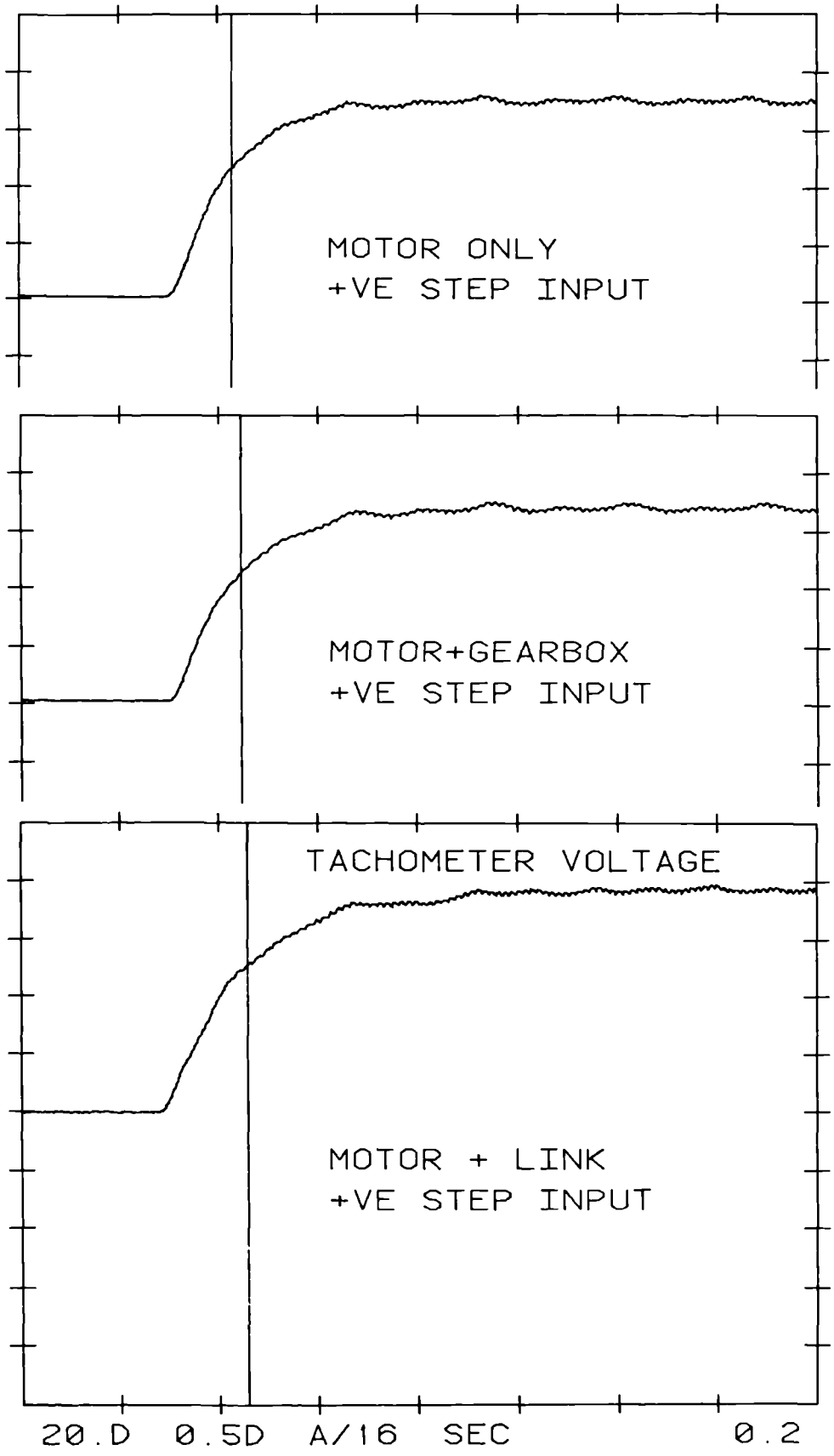

Figure 7.6 Actual open-loop speed response tests

The response of the dynamically coupled master arm, including the output link and the influence of cable compliance was obtained experimentally as shown in Figure 7.6(c), and can be compared with the equivalent model response Figure 7.8(c). The inertia of the output link J_o was obtained experimentally using a compound pendulum technique. Viscous friction coefficient C_o was again selected to maintain good correlation. The influence of cable compliance on both the physical and model responses is particularly noticeable. A list of the parameters used in the simulation, obtained both expimentally and from manufacturers literature is given in Table 8.1.

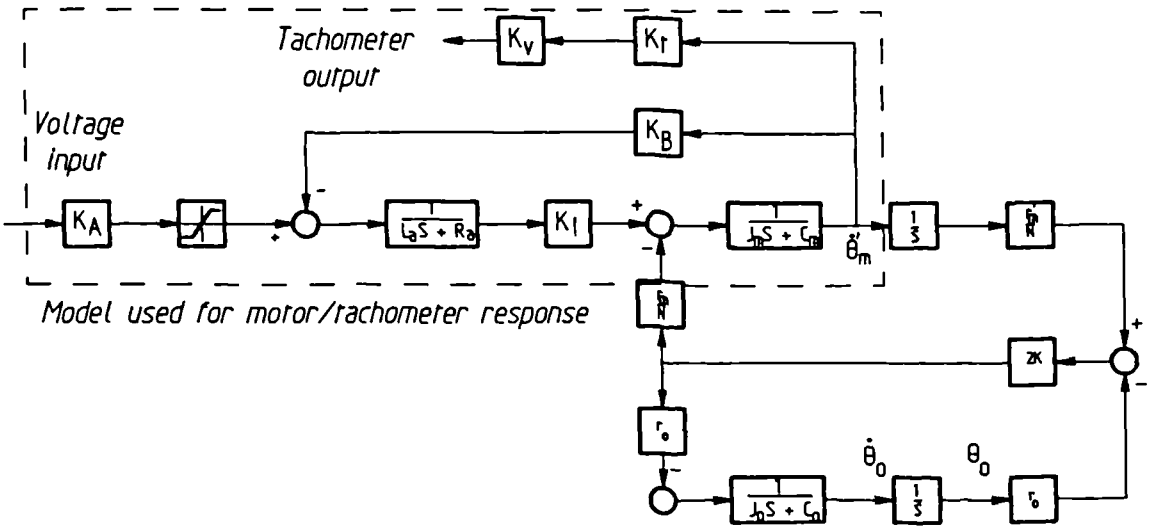

FIGURE 7.7 *Block diagram for open-loop response tests*

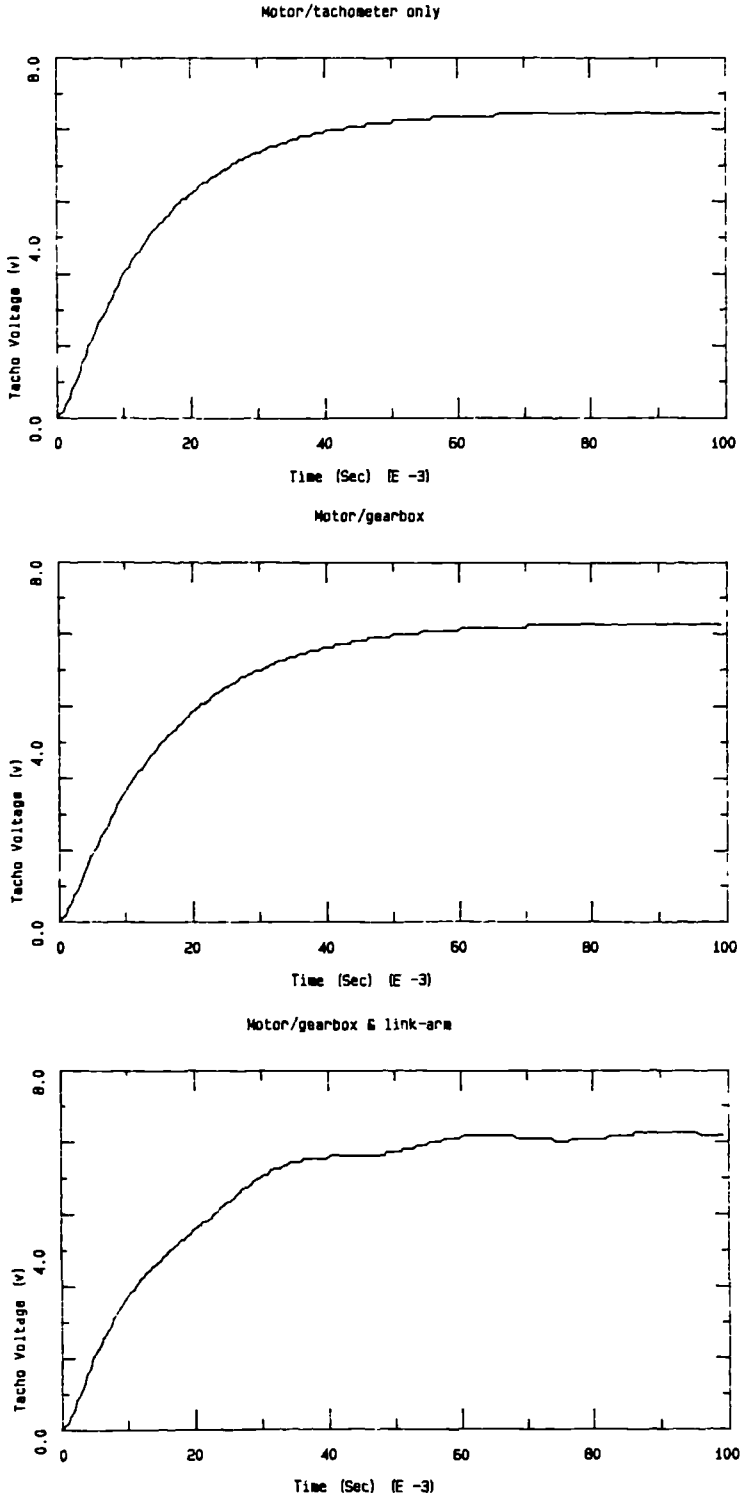

Figure 7.8 Simulated open-loop speed response

Symbol	Definition	Value	Unit
K_A	amplifier voltage gain	40.1	volts/volt
K_T£	tachometer voltage gain	0.0363	volt.sec/rad
K_B£	motor back emf constant	0.057	volt.sec/rad
L_a£	motor armature inductance	0.0012	henrys
R_a£	motor armature resistance	1.2	ohms
K_I£	motor torque constant	0.047	Nm/amp
J_m*	motor/gearbox inertia	4.7E-5	kgm^2
C_m	motor/gearbox viscous friction	2.0E-5	Nm.sec/rad
r_m	gearbox pulley radius	25.0	mm
N	gearbox reduction ratio	48.2	
J_o	output link inertia	0.0147	kgm^2
C_o	output link viscous friction	0.2	Nm.sec/rad
r_o	output link pulley radius	0.35	m
k	cable stiffness	271	N/mm
K_s	link stiffness	61.4	Nm/rad
K_p	potentiometer gain	2.48	volts/rad
K_g	strain gauge amplifier gain	0.0385	volts/unit
K_v	velocity feedback gain	0.02	volts.sec/rad

£ Obtained from manufacturers data sheets.

* Quoted motor inertia 4.48E-5 $kg.m^2$. Value obtained by torsional pendulum experiment 3.7E-5 $kg.m^2$ and adopted.

All other values determined experimentally

Table 7.1 Parametric data used in simulation

Figure 7.9 illustrates the relationship between the different responses of the model for the different configurations discussed, and as expected the system time constant increases with increasing inertia, and the open-loop speed falls with the additional viscous friction introduced at each stage. Table 7.2 illustrates the good correlation between the time constants and peak voltages obtained both experimentally and by simulation.

	Motor/tachometer	Motor/gearbox	All dynamics
Time constant (secs)	0.017 (actual) 0.0172 (model)	0.018 (actual) 0.0186 (model)	0.02 (actual) 0.021 (model)
Peak voltage (volts)	6.87 (actual) 6.83 (model)	6.69 (actual) 6.69 (model)	6.67 (actual) 6.67 (model)

Table 7.2 Comparison between experimental and model results

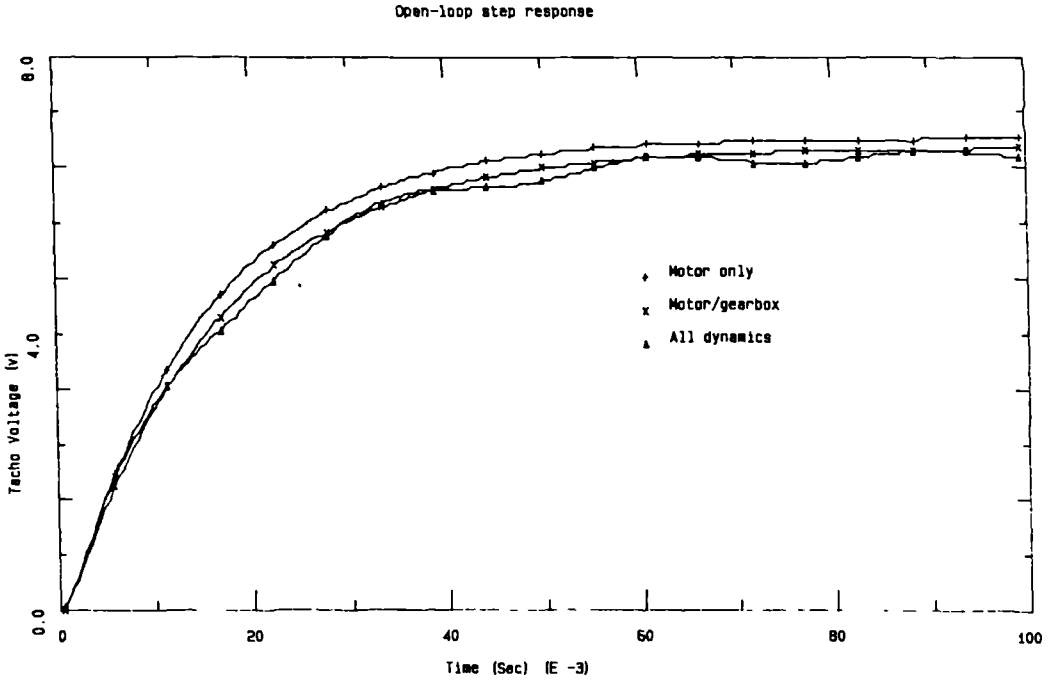

Figure 7.9 Combined simulation open-loop response tests

7.2.2 Closed-loop step response tests

A servo-potentiometer was used to measure the angular position of the link, and proportional plus velocity feedback based on continuous control in the model was achieved as shown in Figure 7.10. Force feedback was introduced in the model, the actual implementation of the 'anti-friction' feedback in hardware and the design of torque sensor have already been described in Chapter 6. The physical location of the torque sensor is particularly important, and strain-gauges mounted on the link assembly, as close as practical to the axis of rotation, were at the time considered to be the best option. In the model, however, the signal flow becomes rather more difficult to interpret and the position at which a signal , considered representative of link strain, could be obtained involved isolating the output link transfer function, in the manner shown in Figure 7.10.

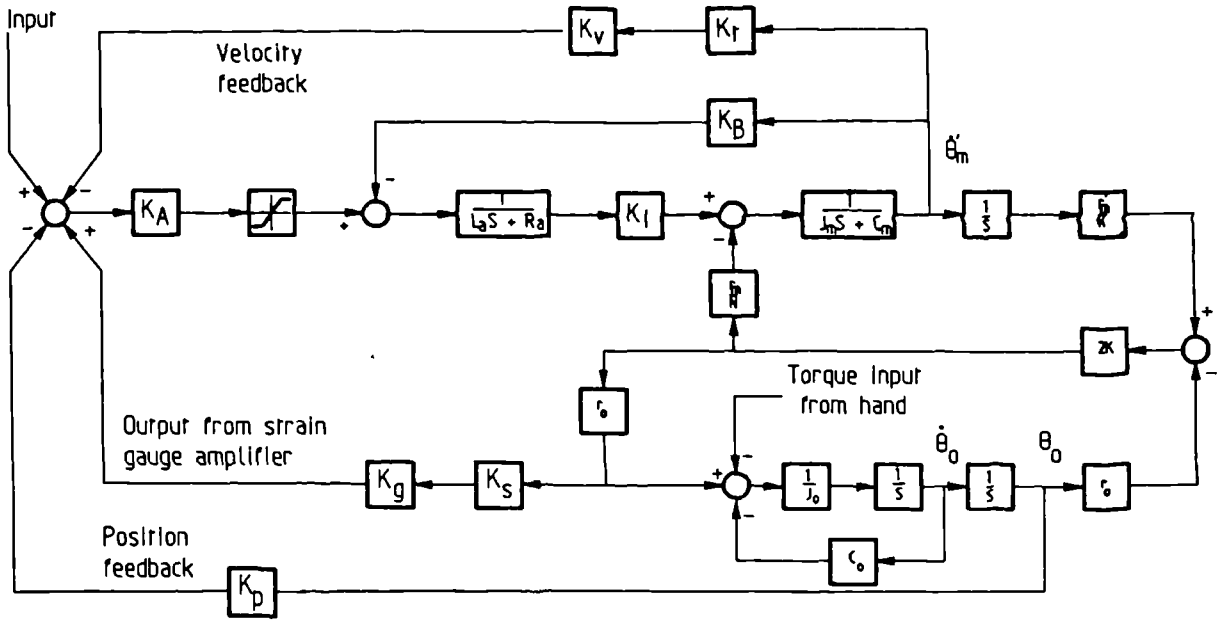

FIGURE 7.10 *Master arm closed-loop servo-system*

The actual step response of the master arm with velocity feedback is shown in 7.11(a) with the corresponding simulated response shown in Figure 7.12(a). The correlation between experimental and simulated results is excellent, with rise times of 0.1 and 0.097 seconds respectively, where rise time is defined as the time taken to reach 90% of the applied step. The introduction of velocity feedback in the model, sufficient to produce a critically damped response was used to set the level of damping in the physical system.

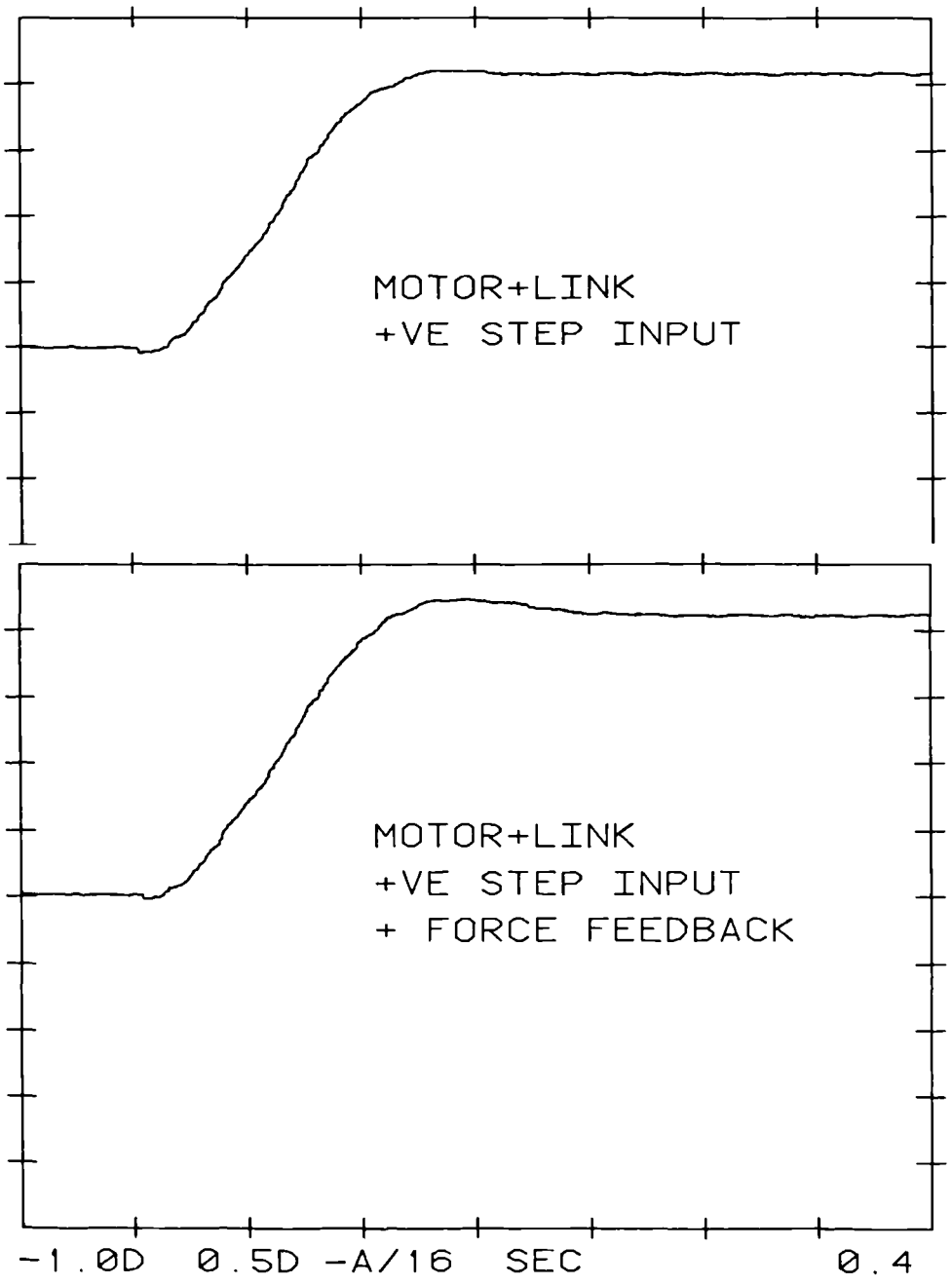

Figure 7.11 Actual closed-loop position response

The closed-loop response of the master arm with force feedback implemented is shown in Figure 7.11(b), and the equivalent model response is shown in Figure 7.12(b), with respective rise times of 0.094 and 0.092 seconds. Velocity feedback gain was pre-set, and the force feedback gain adjusted so that the system could be backdriven. It can be observed that the introduction of the positive feedback loop has a destabilising influence, as expected, however this was compensated for by increasing the velocity feedback gain to eliminate overshoot. The simulated response for the various conditions is shown in Figure 7.13.

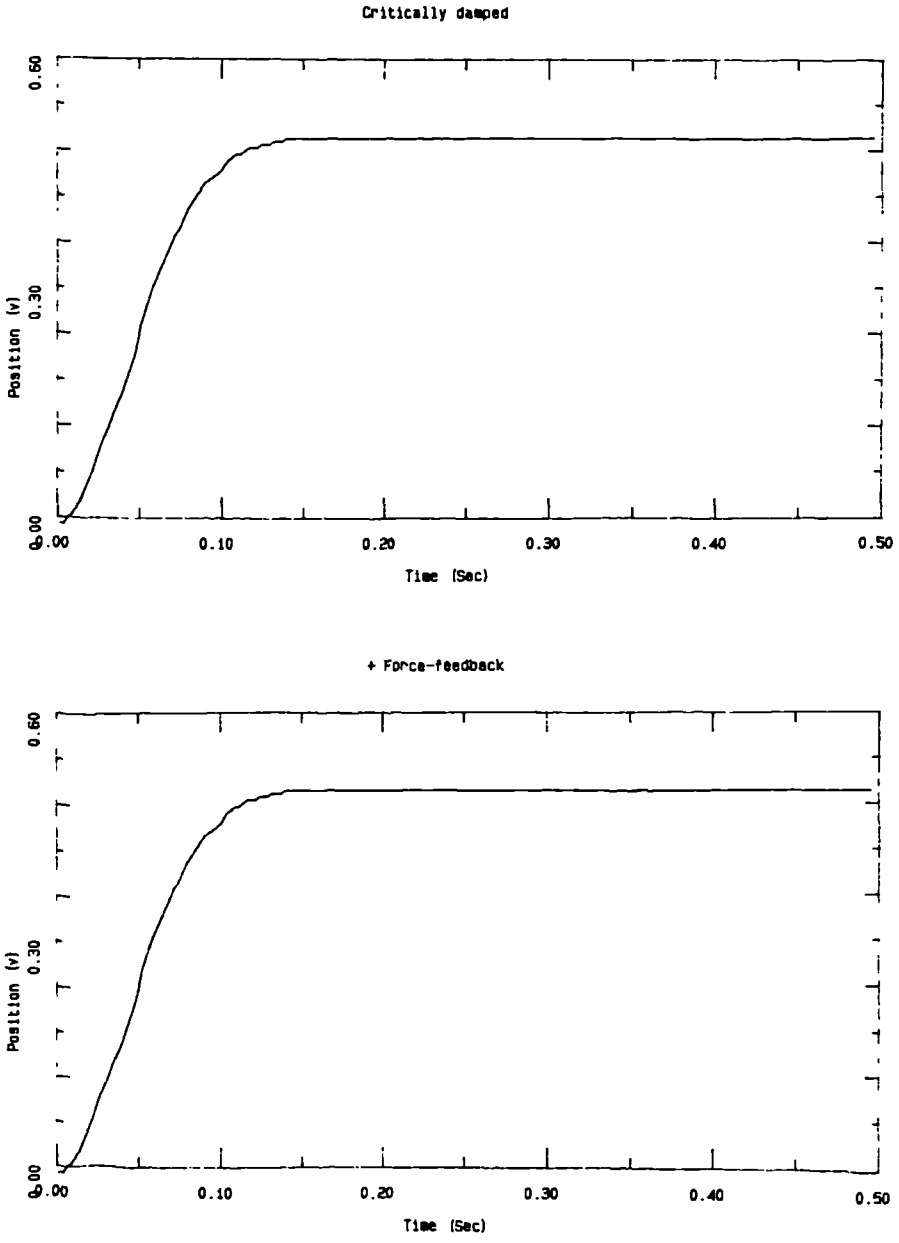

Figure 7.12 Simulated closed-loop position response

7.2.3 Computer controlled master-slave system

Since the generalized control scheme relies heavily on the use of a digital computer for its implementation it was considered relevant to investigate the effects of different sampling frequencies on stability in the master or slave control systems. And to assess the effects of transmission delay between master and slave arms ie. when significant time delays occur as a result of long distance communication between the two sub-systems.

Digital control elements were incorporated into the model to emulate a digital computer. The effects of different sampling periods were simulated using a zero-order hold (ZHOLD) with a 12-bit quantization step (QNTZR), equivalent in this case to 2.44 milli-volts.

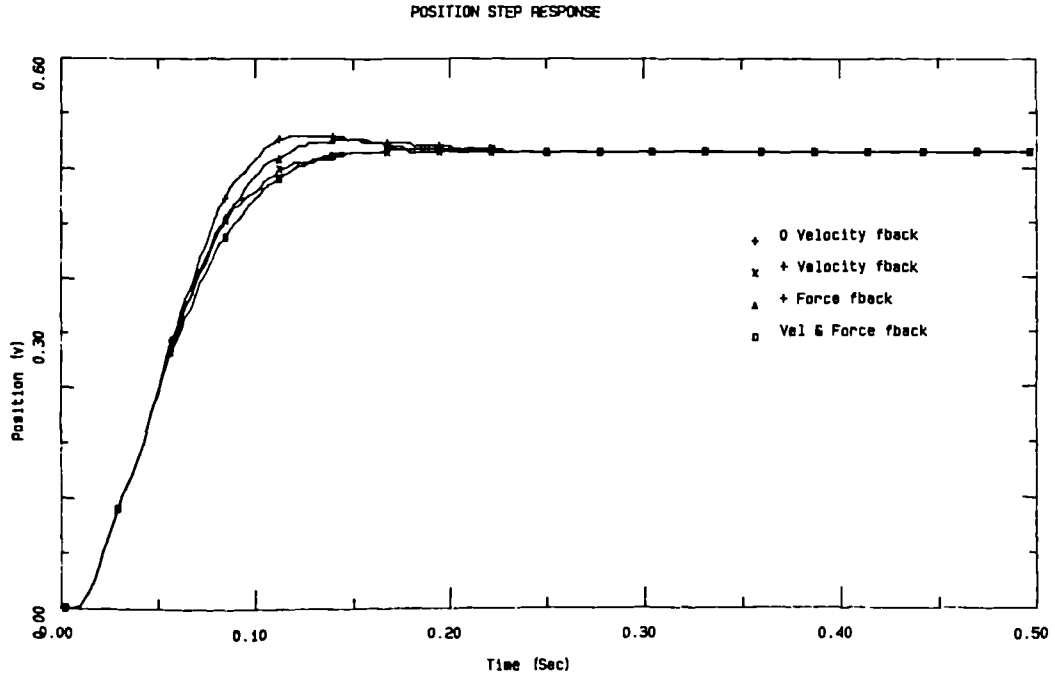

Figure 7.13 Combined simulated closed-loop response

Figure 7.14 presents the closed-loop step response of the model with 'digital' control for a range of sampling frequencies. The 'continuous' step-response has been included for comparison. As expected, an increase in overshoot occurs as the sampling frequency is reduced. Whilst this can be compensated for by increasing the velocity feedback gain, in a physical system the amount of tachometer ripple can limit stable operation.

The model was extended to include an identical one degree of freedom master and slave system. The interconnection between master and slave sub-systems being simulated by discrete ZHOLD and QNTZR transfer functions. The overall master-slave system is shown diagrammatically in Figure 7.15. Communication between master and slave controllers is by position feed-forward, and force feedback, with continuous control being employed in the sub-system feedback loops.

Figure 7.16 shows the effect of increasing transmission delay between master and slave arms when the master arm is commanded to move by a step input. Although not a typical maneuver it nevertheless demonstrates the tracking ability between master and slave in the presence of time delays. The slave arm response is shown for 'continuous' tracking of the master arm, and several different time delays in the 'digital' control mode. The lag between master and slave appears to match the prescribed time delay, when greater than 50 milliseconds. However, when time delays less than 10 milliseconds are introduced the overall lag remains at 40 milliseconds.

The introduction of proportional plus derivative control in the position feedforward loop between master and slave, goes some way to reducing the time lag, but at the expense of stability. Figure 7.17 illustrates the improvement in time lag that can be achieved for several derivative action time constants. The time lag is reduced to 20 milliseconds with P + D control, when the derivative time constant is set at 50 milliseconds. At higher gains the slave arm response tends to become less stable, although this can be to some extent compensated for by use of higher velocity feedback gain.

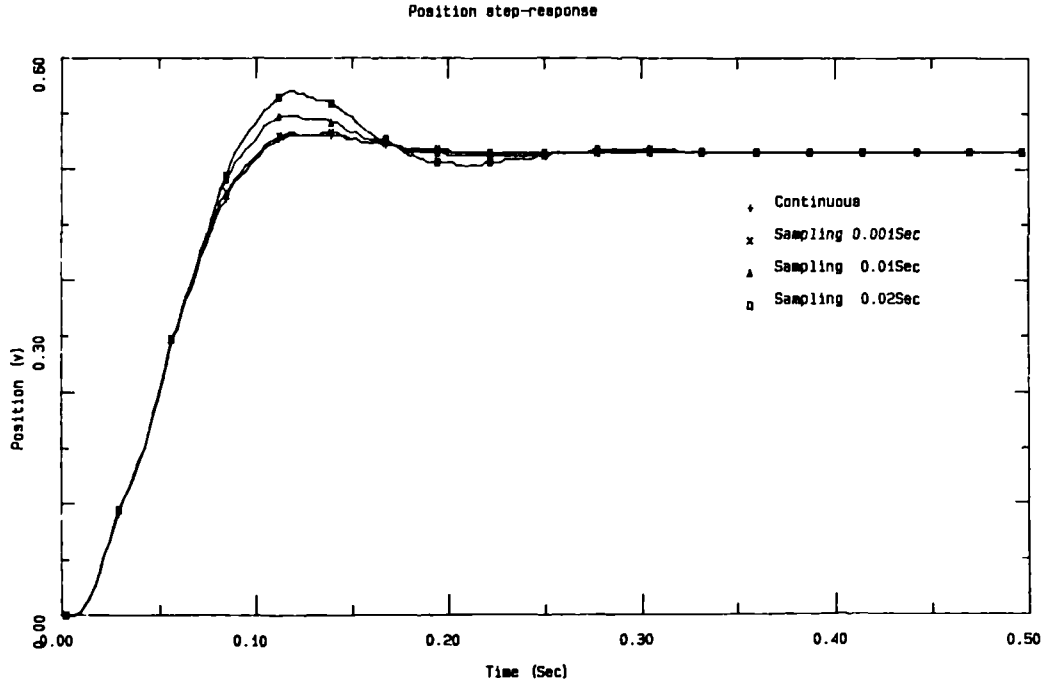

Figure 7.14 Simulated response with 'digitization'

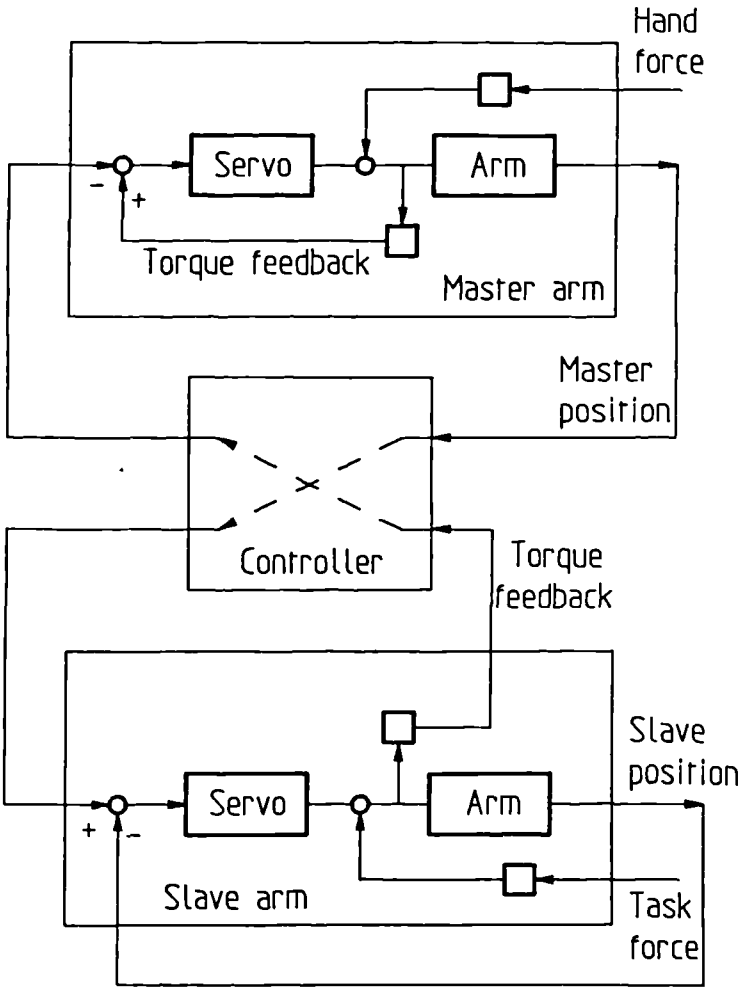

Figure 7.15 *One d.o.f. position/force control*

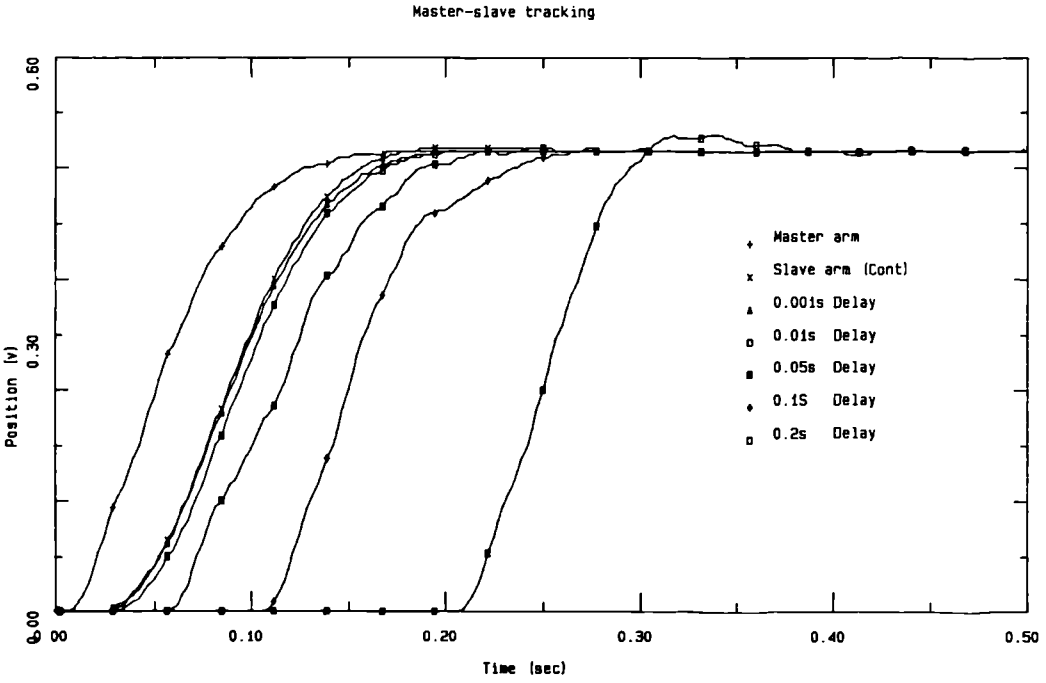

Figure 7.16 Simulated response with transmission delay

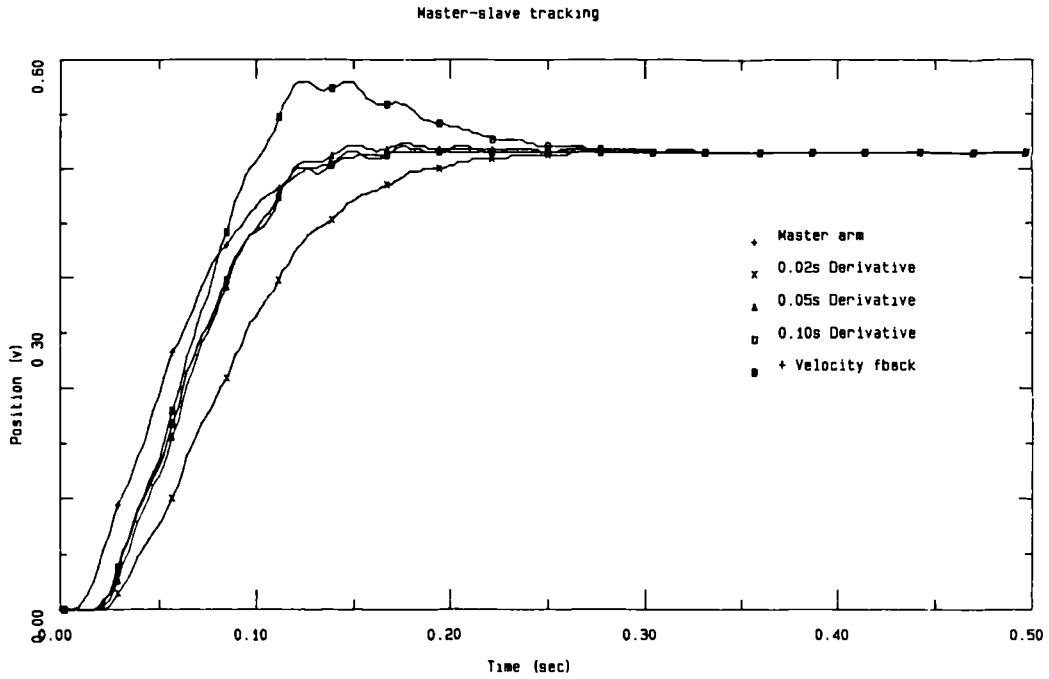

Figure 7.17 Simulated response of slave arm with P+D control

Although the main experimental studies have concentrated on the 'generalized control' scheme using three degree of freedom master and slave arms, it was necessary to provide analog control about each joint servo loop. The time taken to compute necessary position/force transformations between both master and slave controllers using a single microcomputer was approximately 10ms ie. a sampling frequency 100hz. Simulation has shown that frequencies of the order of 1000hz are necessary to minimize the effects of discretization when using digital controllers. Because of the limited sampling frequency (100Hz), the overall gain of the generalized bilateral control scheme had to be reduced with a subsequent compromise in overall performance. To achieve the full potential of the system it would have been necessary to utilize additional computers to provide separate digital control for both master and slave manipulators linked to a supervisory computer to carry out the trajectory planning and force strategy.

7.3 The human operator in the loop

A mathematical model of the human operator in a simulated man-machine system could be used for predicting his behaviour under various conditions when carrying out different tasks, particularly when experimental verification is not possible. The human factors literature includes a wealth of information, stemming mainly from aerospace research, regarding the modelling of the human operator in manual control tasks where it is recognised that the quality of performance of either the human or machine by itself does not determine the quality of system performance [M^{c}Ruer,1980].

However, much of the information regarding the description of the man-machine control interface is complicated by the versatility of the human operator. The human controller can be considered as a combination of sensing, computation and actuating elements, as shown in Figure 7.18 [Allen & M^{c}Ruer, 1979]. Visually sensed inputs communicate via a manipulative output, to a controller element in one of three modes ie. open-loop (precognitive), combined open-loop/closed-loop (pursuit) and closed-loop (compensatory) control interfaces.

Compensatory is the simplest mode of control, where the human acts in response to changes in system input or disturbances with continuous close-loop control exerted over the controlled element. When preview is available eg. when the driver of an automobile can see (and follow) a curved road ahead, the pursuit and compensatory pathways combine, and in principle the quality of control should be much superior than when acting alone. However, previously learned control movements and familiarity with the controlled element dynamics can lead to preprogrammed neuro-muscular commands ie. where the operator employs pre-cognitive control. Pre-cognitive control can also act dually with compensatory actions such that control is initiated by the pre-cognitive action and finished using the compensatory error-driven action.

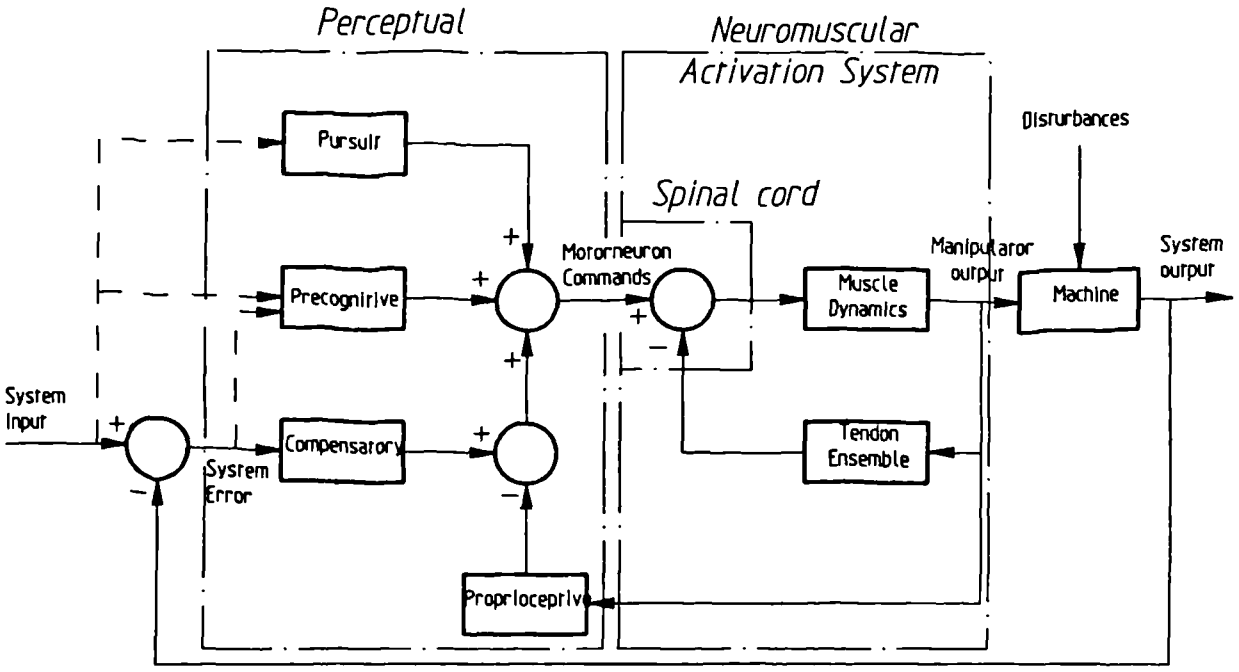

Figure 7.18 *Major human operator pathways [Allen & McRuer,1979]*

Because of the complexity of the human operator control system, only fundamental characteristics have been included in any general theory [McRuer,1980] - some characteristics defy mathematical description and appear random in their nature [Levinson, Baron & Kleinman 1969, Jex & Magdalene 1969].

Simple models based upon early experimental results and frequency response tests of the human operator in one dimensional tracking tasks have been summarised [Sheridan & Ferrell,1974],and are best fitted by a model of the form shown in Figure 7.19, [Rouse,1980]. A quasi-linear equation has been proposed of the form

$$U'(S) = Y_H(S)\, E(S) + N(S)$$

where

$$Y_H(S) = \frac{K_H\, e^{-\tau_d S}(T_L S + 1)}{(T_N S + 1)(T_1 S + 1)}$$

.....{7.5}

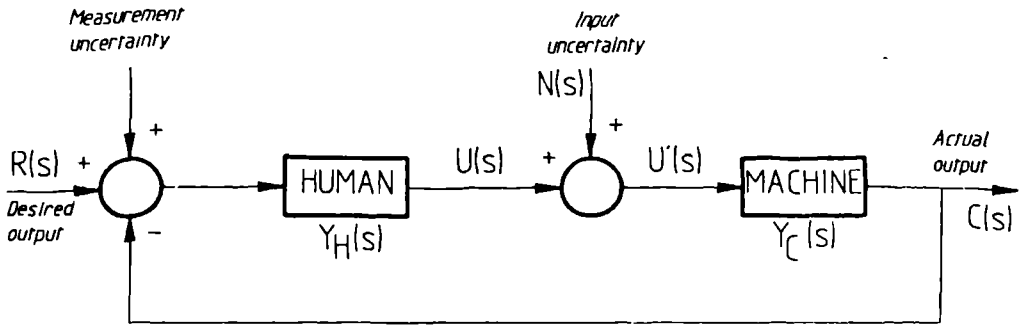

Figure 7.19 *Human-machine control system (Rouse,1980)*

The characteristic response of a non-linear equation to sinusoidal inputs involves the use of describing functions to approximate an input/output description of the human-machine system. The portion of the input/output relationship not accounted for by the describing function is attributed to a random process is termed remnant, and in Figure 7.19 is represented by the term **N**(s). The remnant has three possible different sources ie human non-linear strategies, muscle tremor and variations in the amount of phase lag that can exist between the response and actual command.

The human-operator describing function has five components [M^{c}Ruer & Krendal,1957]. K_H is a loop gain which is adjusted by the operator over a range of 1 - 100 to different tasks. τ_d is a reaction time delay, or residual transmission time lag between 0.12 - 0.2 seconds. T_N is a coefficient of a first order lag inherent in the neuromuscular system, and is approximately equivalent to 0.2 seconds for initiation of muscle displacement. T_L and T_1 are respectively lead and lag coefficients which can be adjusted by the human along with K_H so that the entire closed-loop system conforms to some criterion, whereby on average performance is consistent with good servo control, ie. at low forcing frequencies the open-loop phase lag is very small (much less than 180^{o} or π radians) and there is no tendency to instability - open loop gain is as large as possible to provide good closed-loop tracking. Phase increases with frequency and the gain must be reduced accordingly to prevent instability. In particular, near the cross-over frequency the phase lag must be maintained less than 180^{o} to prevent instability, and preferably should be kept less than 90^{o} for good response.

The main difficulties with the intuitive model is that its parameters vary considerably between tasks, and are also influenced by the characteristics of the input. Since the model incorporates the input/output characteristics of the human plus controlled process whenever a new situation is encountered such as a different task, new experiments are necessary to determine revised model parameters. Under such circumstances a more desirable manual control model would be one whose parameters are not so task sensitive.

The 'crossover' model has been proposed [M^{c}Ruer & Krendel,1957; M^{c}Ruer,1980] to incorporate the idea that the human operator adapts his response so that the overall human-machine system has

'good servo' or good stability and response characteristics. For a particular set of controlled element dynamics defined by Y_c the human will adopt a crossover region transfer characteristic of the form

$$Y_p = \omega_c \, e^{-\tau S}/S \; Y_c \qquad \ldots\ldots\{7.6\}$$

where the crossover frequency ω_c, which is defined as the frequency at which the magnitude of $Y_p Y_c$ is equal to unity, and which tends to be constant for a given set of task variables.

'Extended crossover' models have also been put forward to accomodate a residual phase lag not accounted for in the simple crossover model [McRuer,1980]. The form of the extended crossover model for Y_H alone is

$$Y_H = K_H(T_L S + 1)\, e^{-\tau' S}/(T_1 S + 1)$$

where

$$\tau' = (\omega \tau_d + \alpha/\omega) \qquad \ldots\ldots\{7.7\}$$

The quantity α is a low frequency phase lag coefficient which increases (in the range 0.1 to 0.5 rads/second with the order of Y_c and with increasing forcing frequency.

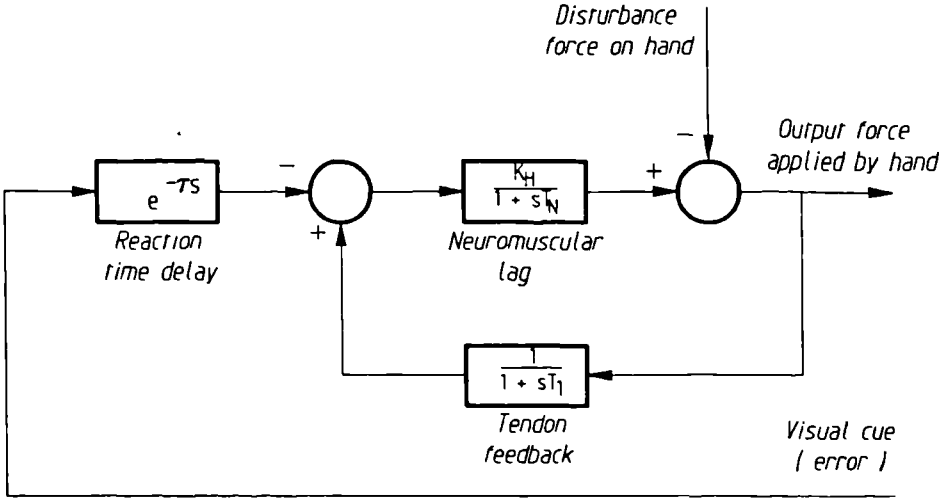

Figure 7.20 *Model of human operator used in simulation*

7.3.1 Application to modelling

The models described previously have assumed the human operator to be observing and controlling using visual cues only. In this application, an outer control loop provides visual feedback to the operator, whilst an additional inner loop provides the necessary tactile or force feedback through the operators hand in response to disturbances arising from interaction at the slave arm. Figure 7.20 shows the model of the human operator adopted for this simulation study.

7.3.2 Response tests

Experimental data from several previous investigations has been summarised [M^{c}Ruer & Krendel,1957] for several different forcing functions. The most relevant experimental tests described refer to a simple tracking task using a spring restrained aircraft control stick [Sheridan & Ferrell,1974]. The operator describing functions for a forcing function having a corner frequency of 2 radians per second were initially adopted for these simulation studies, although some variation in parameters were felt necessary as a result of more recent tests.

In particular, the loop gain $K_H = 40$, reaction time delay $\tau_d = 0.2$ seconds, and neuromuscular lag $T_N = 0.22$ seconds were used to set up the model.

Preliminary tests aimed at measuring the operator reaction time, using a visual indicator to stimulate a reaction at the hand were carried out. A typical response is shown in Figure 7.21. The visual trigger provided the datum from which it was possible to measure the time taken to produce a reaction force, generated using the master arm. From a sample of 20 such tests, an average reaction time and standard deviation of 0.162 and 0.08 seconds respectively were obtained, which was in agreement with previously published data [M^{c}Ruer & Krendal,1957].

A further set of tests were carried out in order to verify the part of the model relating to neuro-muscular control. The tests involved the application of a step input into the master arm servo, to simulate a step change in torque, consistent with the slave arm suddenly coming into contact with an obstacle. The operator response being to brake the master arm whilst

simultaneously applying the necessary reaction force to the master controller.

Figure 7.22 presents the position-force response in the time domain for two successive tests carried out by the same subject. The resulting responses suggest good 'servo' characteristics as the operator attempts to produce an equivalent reaction force. The force responses highlight a distinctive transient during the initial phase associated with the dynamics of the system, and which is subsequently damped out by the operators' hand. However, the variation in the two 'identical' tests illustrates the difficulty in identifying a definitive model of the human operator.

It is conceivable that in such circumstances the operator relies on pro-prioceptive information to null motion, drift etc, without visual feedback,and therefore relies on force/tactile feedback to provide the mechanism for sensing the magnitude of the applied force, and in so doing generate the necessary reaction force, so that motion eventually subsides.

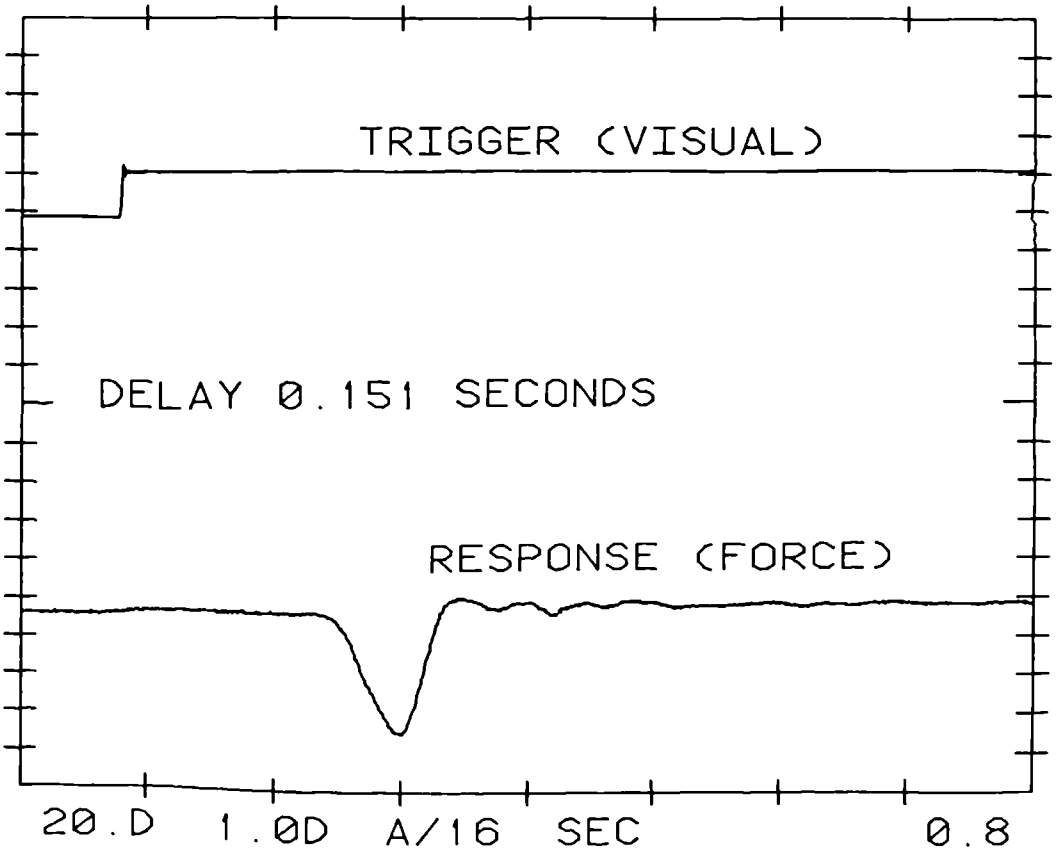

Figure 7.21 Reaction time-delay

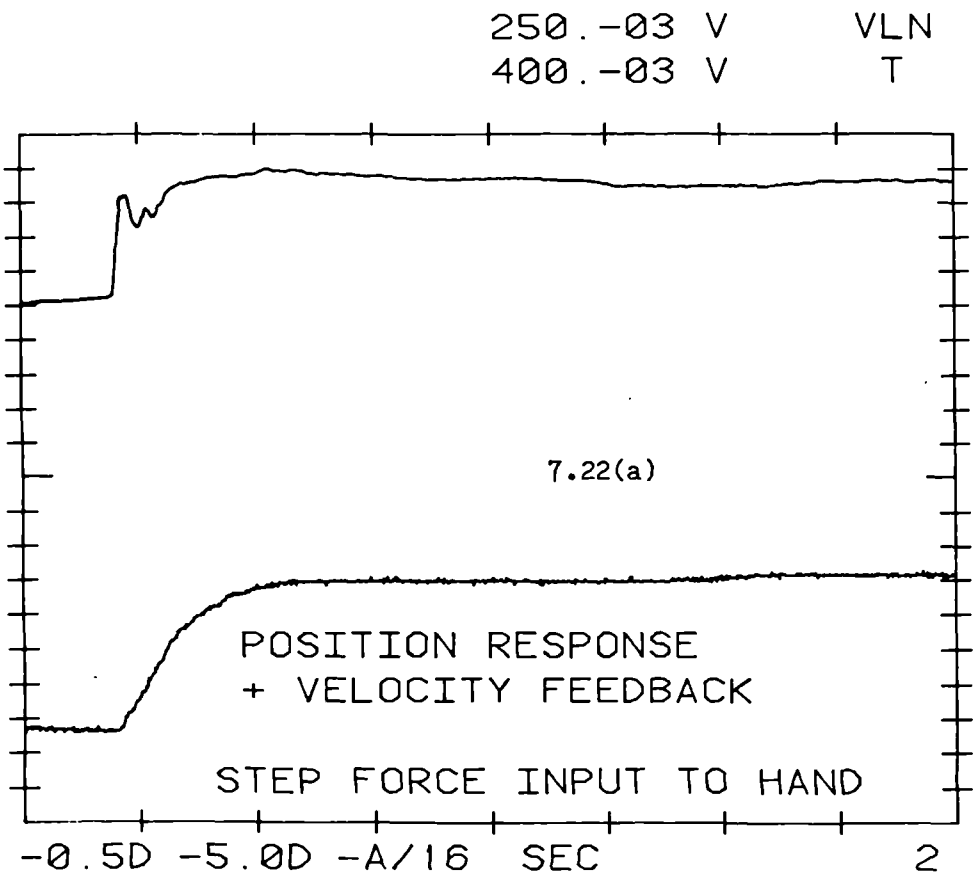

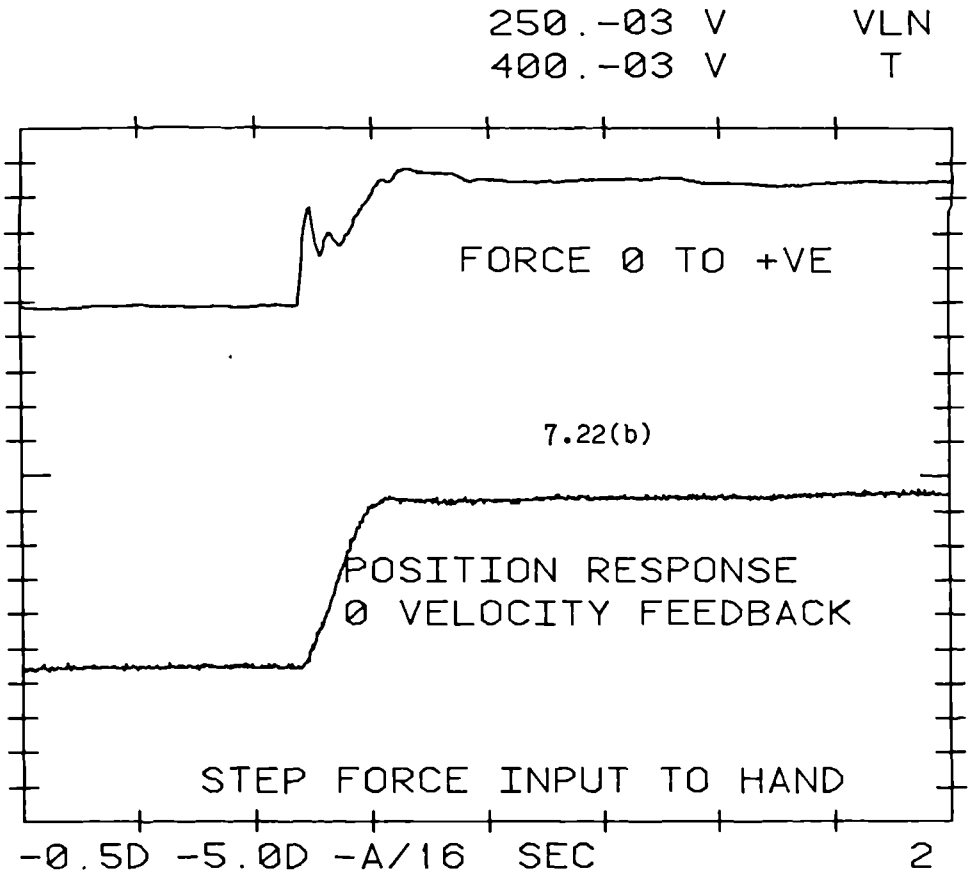

Figure 7.22 Actual position/force response of hand

By incorporating the 'simple' human operator in the model it was possible to assess the effects of a step torque input for different muscle gain and neuro-muscular lag, in the time domain. It can be seen that muscle gain is inversely proportional to the distance moved, and is associated with a faster response, as shown in Figure 7.23(a). The corresponding force response, Figure 7.23(b), illustrates the improvement in response at higher gain, but significantly includes the transient part associated with the machine dynamics. The presence of this particular feature in the simulation gives credibility to the model used.

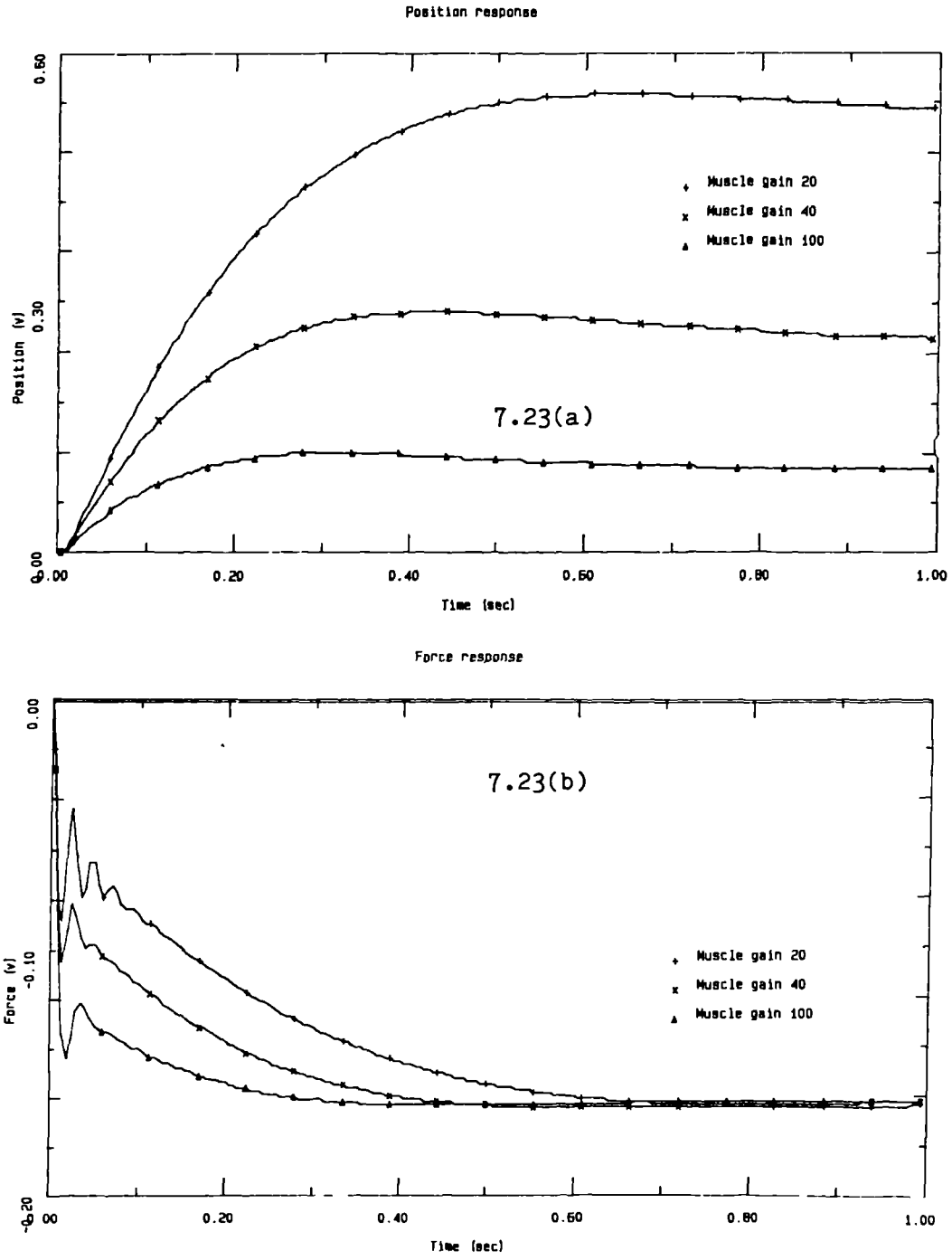

Figure 7.23 Simulated position/force response

Figure 7.24 gives the response in the time domain for different neuro-muscular lags which, as expected, do not infuence the steady state response of the system. A summary of these results is given in Table 7.3, with the experimental data.

Because of the variability of the limited test data, and on the basis of the simulated results, it was reasonable to utilize a muscle gain K_H = 40 and a neuro-muscular lag T_N = 0.15 seconds.

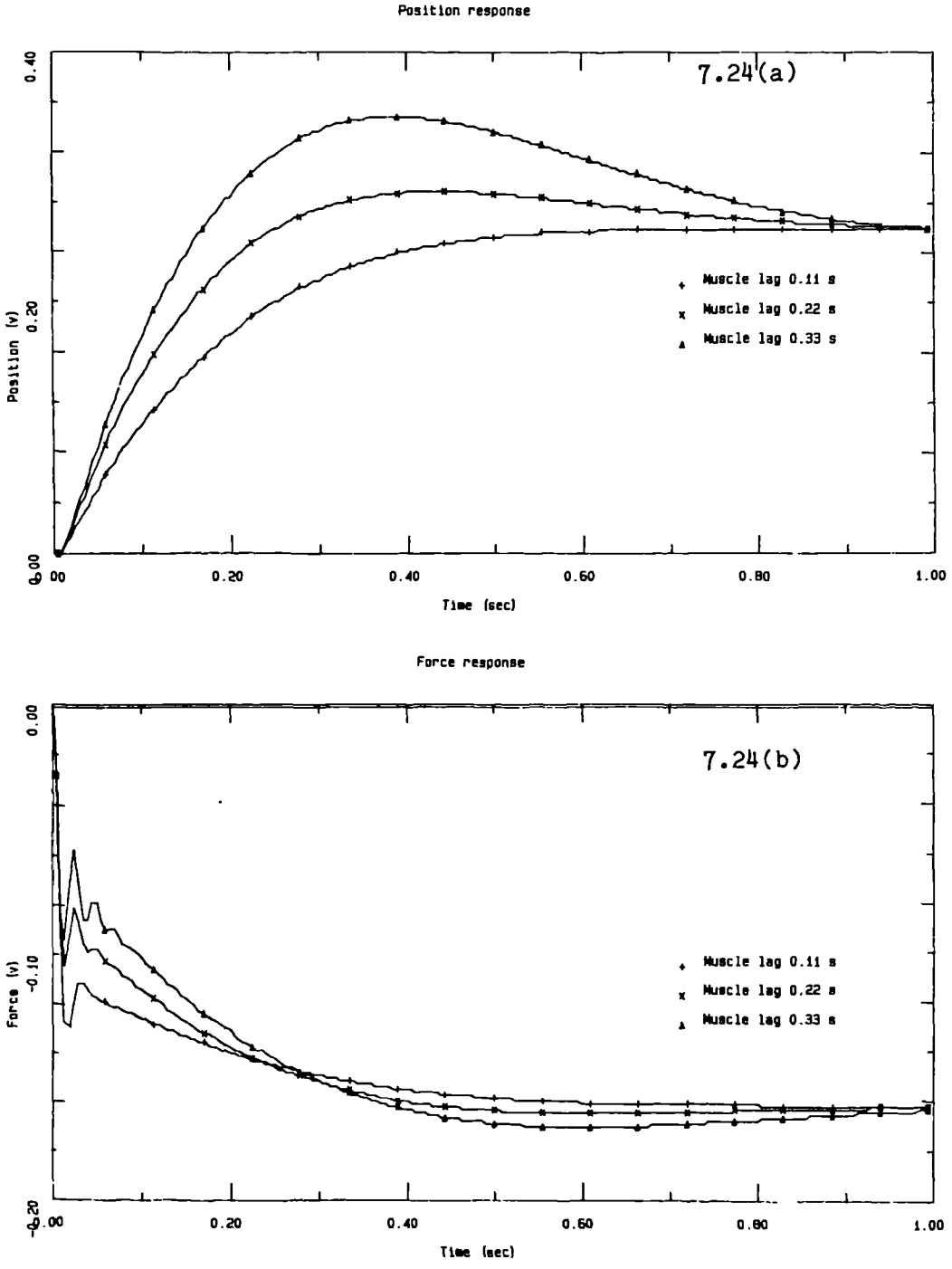

Figure 7.24 Simulated response with varying muscle lag

	Experimental Test		Simulation					
			Muscle gain			Neuromuscular lag		
	(a)	(b)	20	40	100	0.11	0.22	0.33
Steady state position (v)	0.37	0.28	0.53	0.26	0.10	0.26	0.26	0.26
90% Rise time (seconds)	0.26	0.10	0.32	0.20	0.13	0.36	0.20	0.15
% Overshoot ratio	1.00	1.10	1.04	1.10	1.21	1.00	1.10	1.50
Steady state force -ve (v)	0.18	0.18	0.16	0.16	0.16	0.16	0.16	0.16
90% Rise time (seconds)	0.16	0.14	0.40	0.25	0.12	0.25	0.25	0.26
% Ratio of first peak	0.80	0.82	0.55	0.65	0.87	0.81	0.65	0.53

Table 7.3 Comparison between experimental and predicted data

7.3.3 Simulation of a task based on a rigid stop

A 'task' was established, which required the operator to move the master arm, and in so doing drive the slave arm, up to a rigid stop, as shown schematically in Figure 7.2. A visual error is used to force the model until contact is made with the stop. When the slave arm contacts the stop an appreciable torque is exerted on the slave arm output link which is fedback to the operators' hand via the master arm. In the position/force mode this is by direct torque feedback, whilst in the position/position mode as a position error command.

The block diagram for the full model is given in Appendix VI, along with a description of the different transfer functions. It was necessary to include PROCEDURAL blocks where strict order in the model code is essential, using the Easeplus 'CODE' function.

7.3.4 Position/force control

Figure 7.25 shows the simulated response of both master and slave arms with a rigid stop located at 0.5 radians. As the force applied by the operator's hand increases, the master arm is accelerated with the slave arm lagging behind. The visual feedback error is reduced as the slave arm approaches the rigid stop, and the hand force falls progressively, thus decelerating the master arm. The lag that exists between the master and slave arms is sufficient to cause a collision between the slave arm and the rigid stop giving rise to a large force transient which is reflected back, via the the force feedback, to produce a reaction torque in the master arm, as shown in Figure 7.25(b).

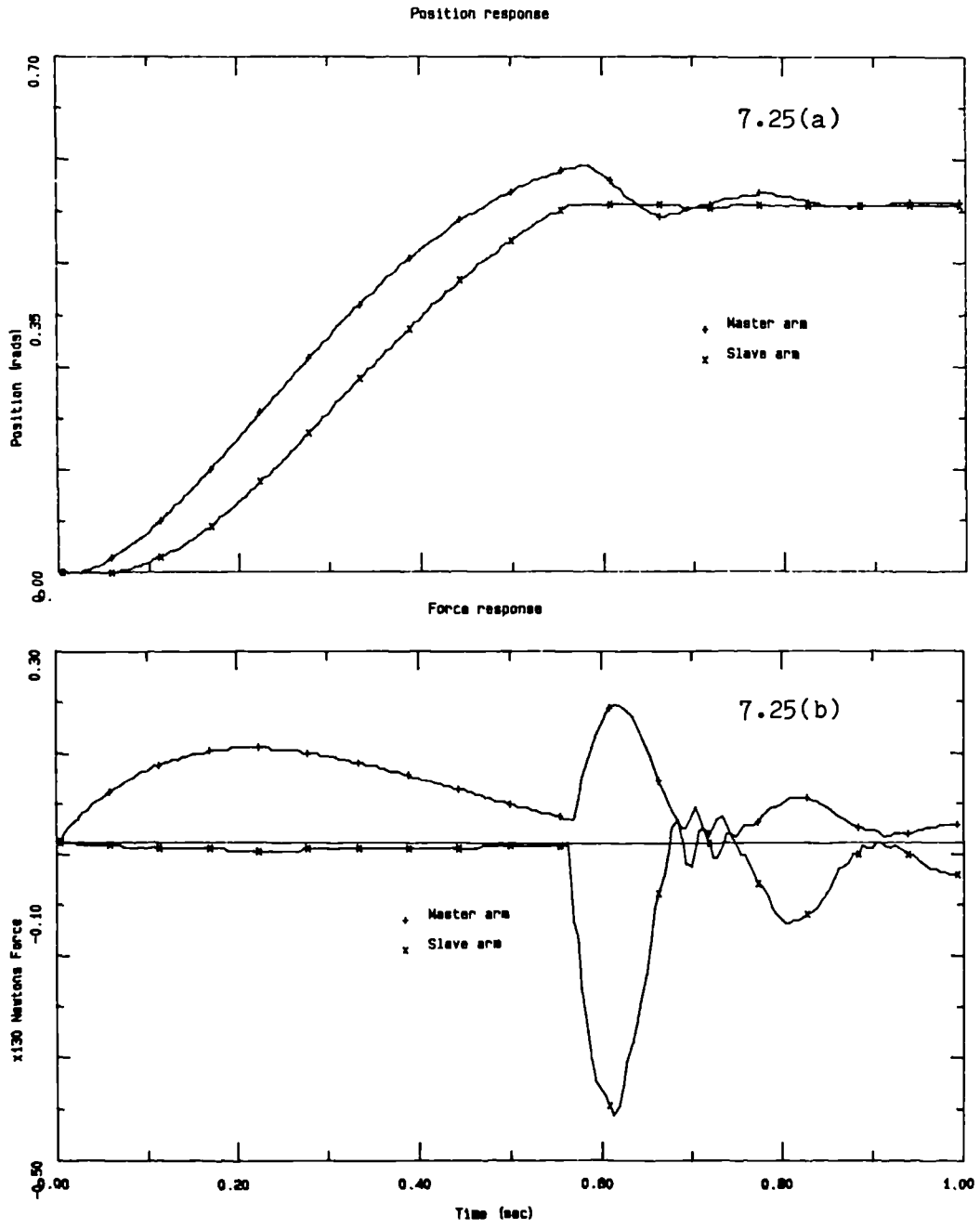

Figure 7.25 Simulated response against fixed stop

However, the model predicts that the first collision is sufficient to cause an interaction between the man-machine system such that the steady state condition is reached only after several subsequent collisions have taken place. Two modes of excitation result, a higher frequency mode attributable to the dynamics of the machine, and a lower frequency mode associated with the coupled man-machine system. Such a transient would not be a desirable feature of a physical master-slave system.

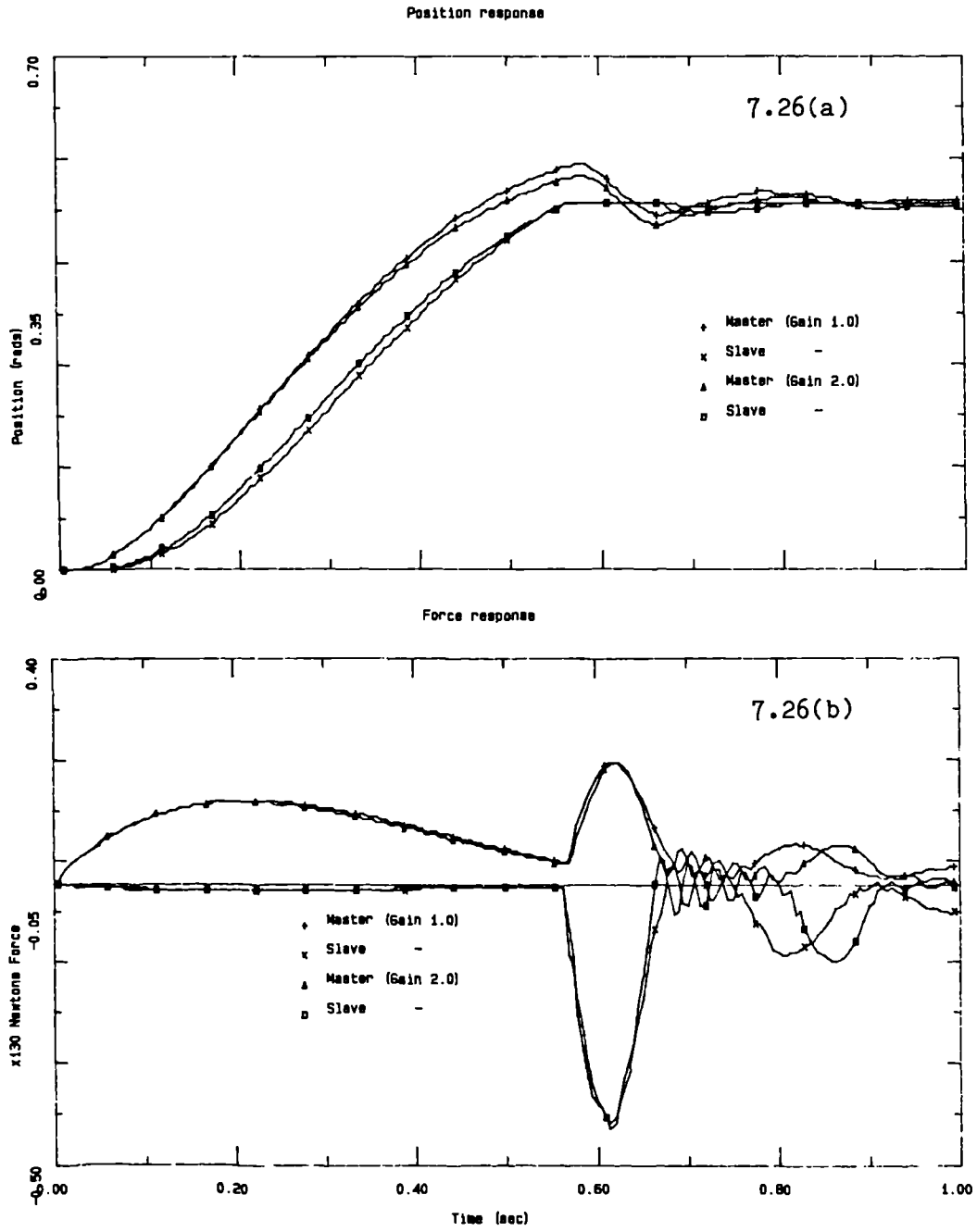

Figure 7.26 Simulated response at different position gain

The design of articulated master slave system adopted in the experimental facility did not lend itself to a single degree of freedom configuration, and it was unfortunately not possible to confirm the predicted results obtained from the task simulation. Evidence to suggest the presence of such force transients in similar situations has been noted during the test programme. In the absence of further experimental data it was nevertheless considered useful to subject the model to further analysis.

Both position feedforward and force feedback gains are of particular interest in assessing the simulated response when driving the slave arm against a rigid stop. Two different proportional gains were used to produce the predicted position-force response shown in Figure 7.26(a) and (b) respectively. It can be observed that when the gain is increased by a factor of 2, the position response changes very little, whereas the corresponding force transient predicts a higher cyclic frequency after the initial collision.

The advantage of using 'anti-friction' force feedback on the master arm is apparent in Figure 7.27. The predicted response in the absence of any +ve force feedback at the master arm is significantly slower when compared with the response achieved when +ve force feedback is used.

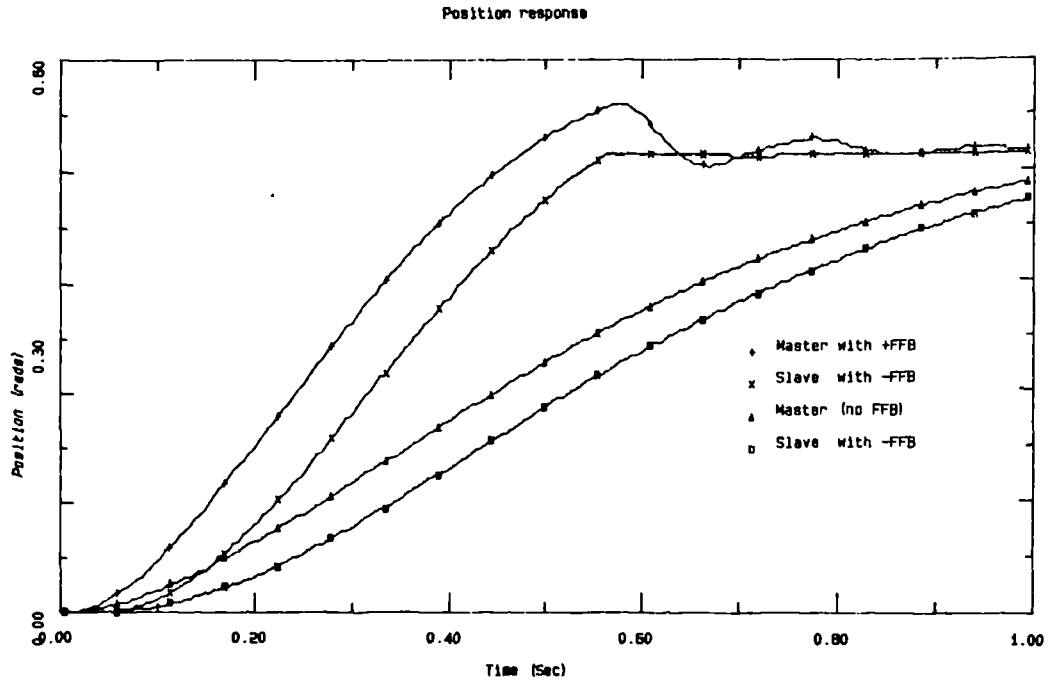

Figure 7.27 Response with no master arm torque feedback

Figure 7.28 illustrates the influence of gain variation in the force feedback loop. As expected, a gain of 20% produces a higher peak force on impact, which is sustained longer because of the operator's impaired reaction. Performance improves at higher gain, bringing about a lowering of the peak force, although at high gain (100-200%) performance is presumably affected as a result of the man-machine interaction between the applied and reaction forces, which introduces a vibratory force response as the system becomes less stable.

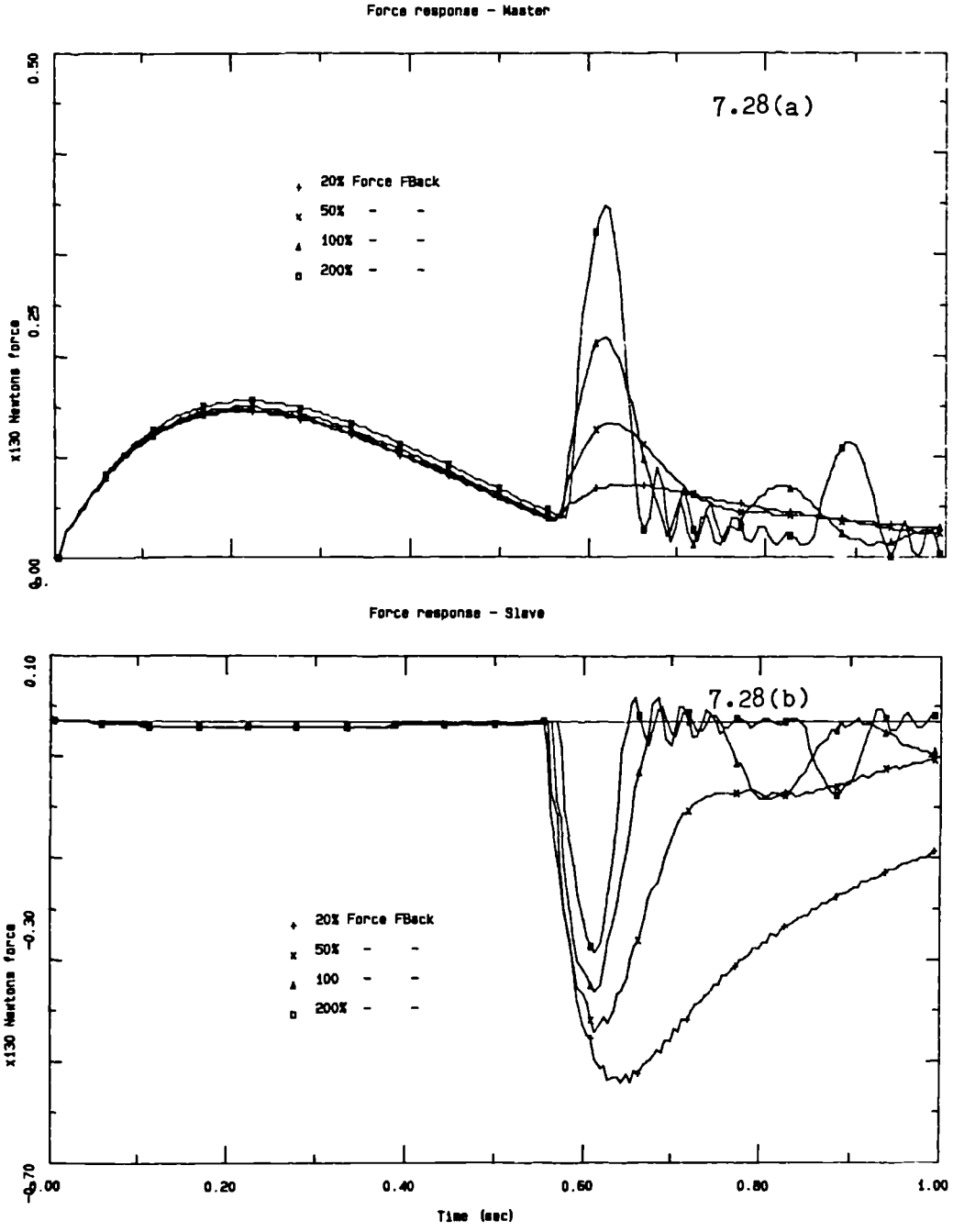

Figure 7.28 Simulated response at different force feedback gain

The introduction of P+D control in the position feedforward loop of the model in a unilateral mode was shown to reduce the amount of lag between master and slave arms with a relatively small derivative time constant (0.02s), albeit with a tendency to de-stabilize the system.

In the bilateral mode however, the model could not tolerate the presence of any derivative action in the feedforward loop, although small amounts of derivative action (0.02s) in the slave-master force feedback loop predicted an improved response as shown in Figure 7.29. Apart from the initial impulse generated as the slave arm impacts the rigid stop, the remainder of the response is free of any cyclic force components which is indicative of good performance.

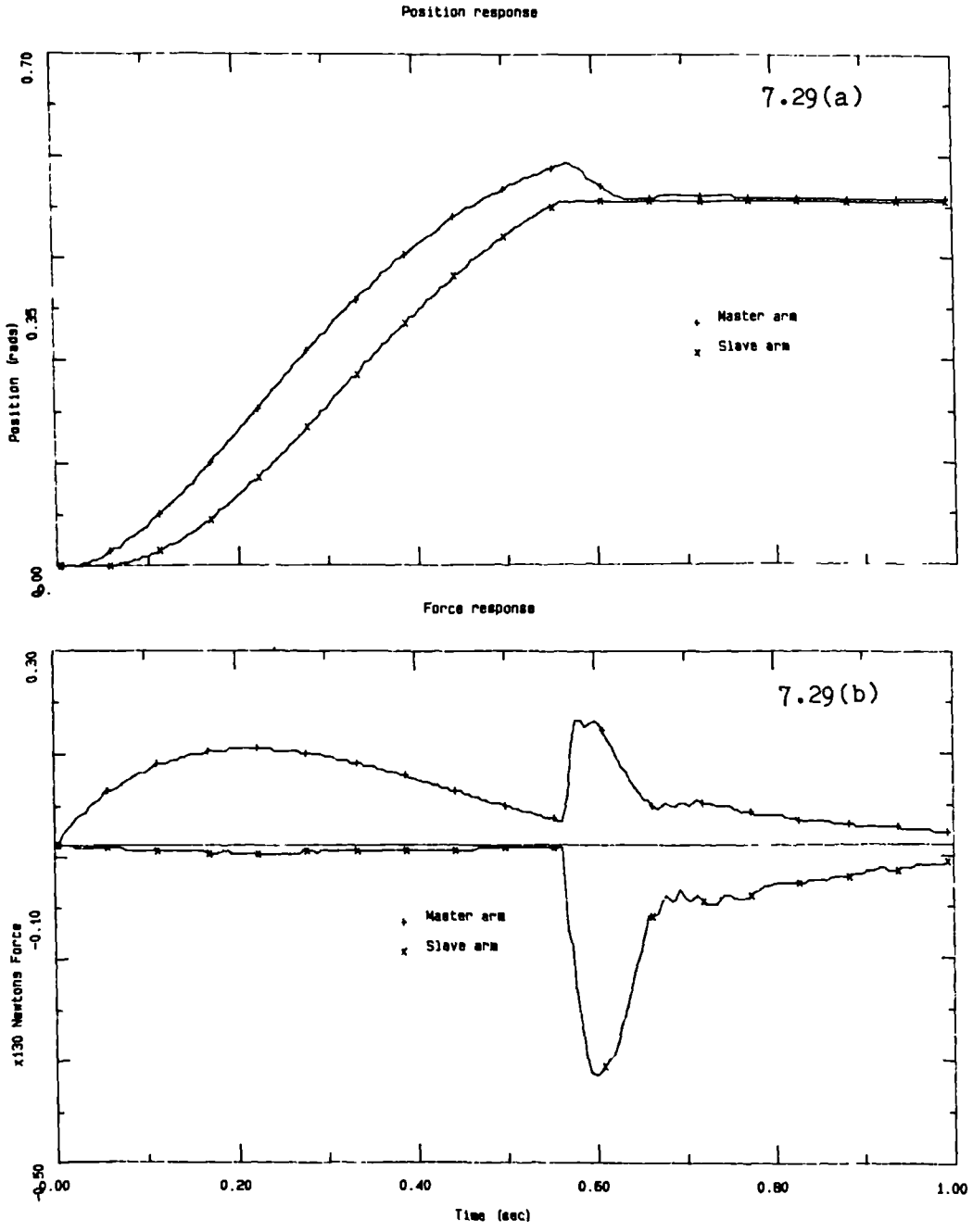

Figure 7.29 Simulated response with P+D in force feedback loop

7.3.5 Position/position control

In the position/position control mode, the torque feedback from the slave arm is replaced by a slave-master position error command which drives the master arm servo. The tight torque feedback loop is retained in the master arm, whilst a negative tight torque loop is added to the slave arm servo, as shown schematically in Figure 7.30.

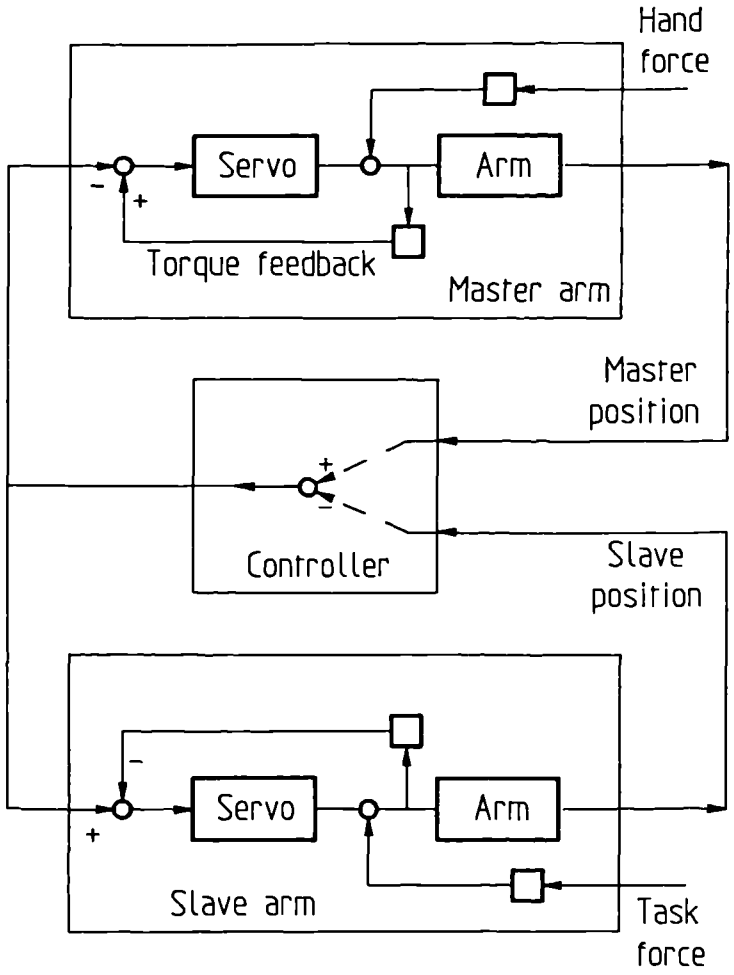

Figure 7.30 *One d.o.f. position/position control*

The advantage of the torque control loop on the slave arm can be seen in Figure 7.31, which shows the force experienced by the slave arm with different feedback gains. Prior to the slave arm coming into contact with the 'hard stop', the simulated response corresponds to that of the equivalent position/force configuration shown in Figure 7.25. However when contact does occur, the response does not show the large force transient predicted in the position/force mode. As the force feedback gain is reduced to zero, so the 'stiffness' of the slave arm servo is increased, and the peak contact force increases. The position response looks extremely stable, once the initial force transient has decayed. Notice that the lag between master and slave is also reduced, although the overall response is somewhat slower.

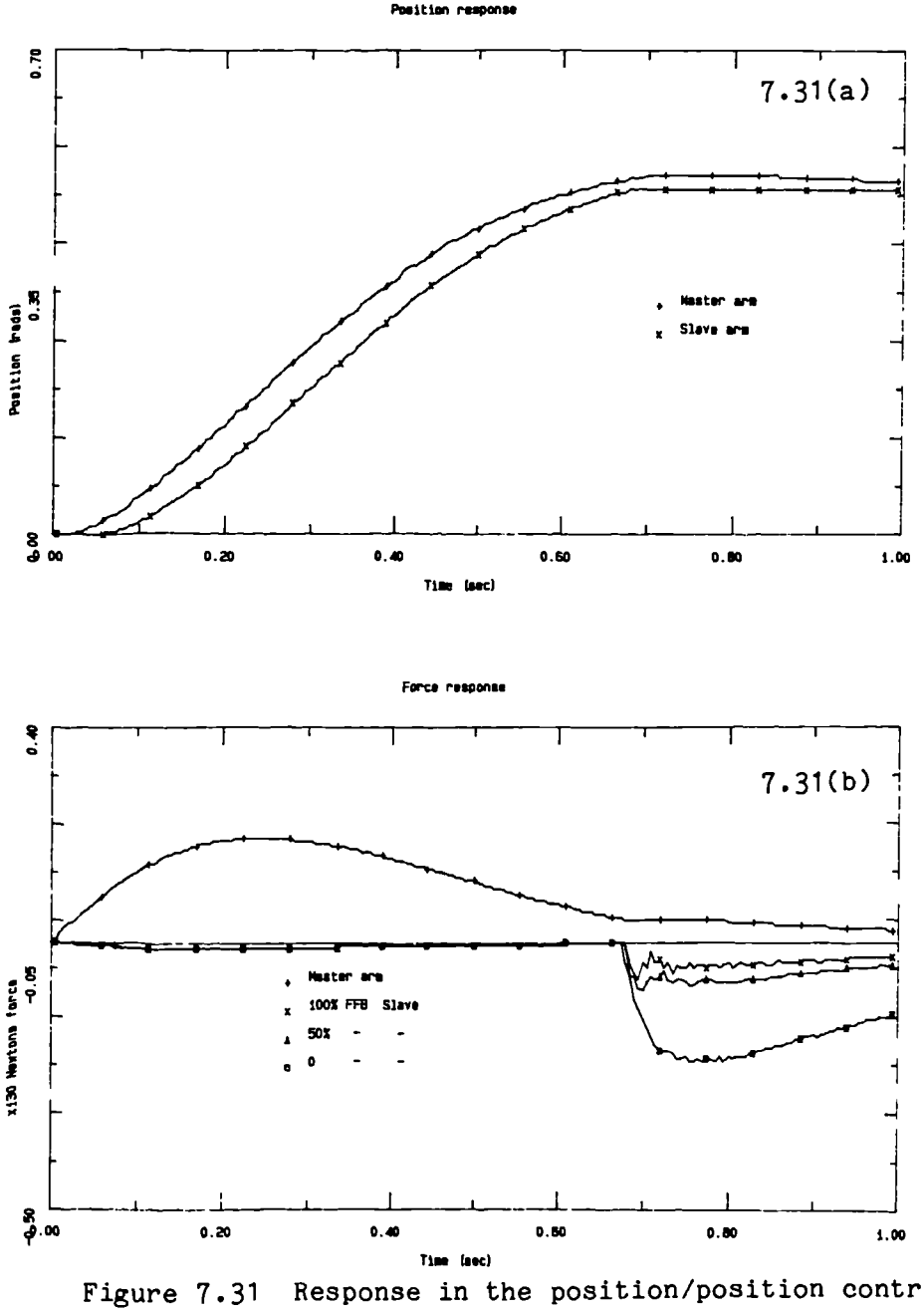

Figure 7.31 Response in the position/position control mode

By increasing the slave arm closed-loop position gain, the lag between master and slave is further reduced, and the speed of response improved as shown in Figure 7.32. The force response predicts that the effort demanded from the operator is also reduced, along with the subsequent reaction force experienced by the operator's hand when contact with the stop is encountered implying about 50% force reflection.

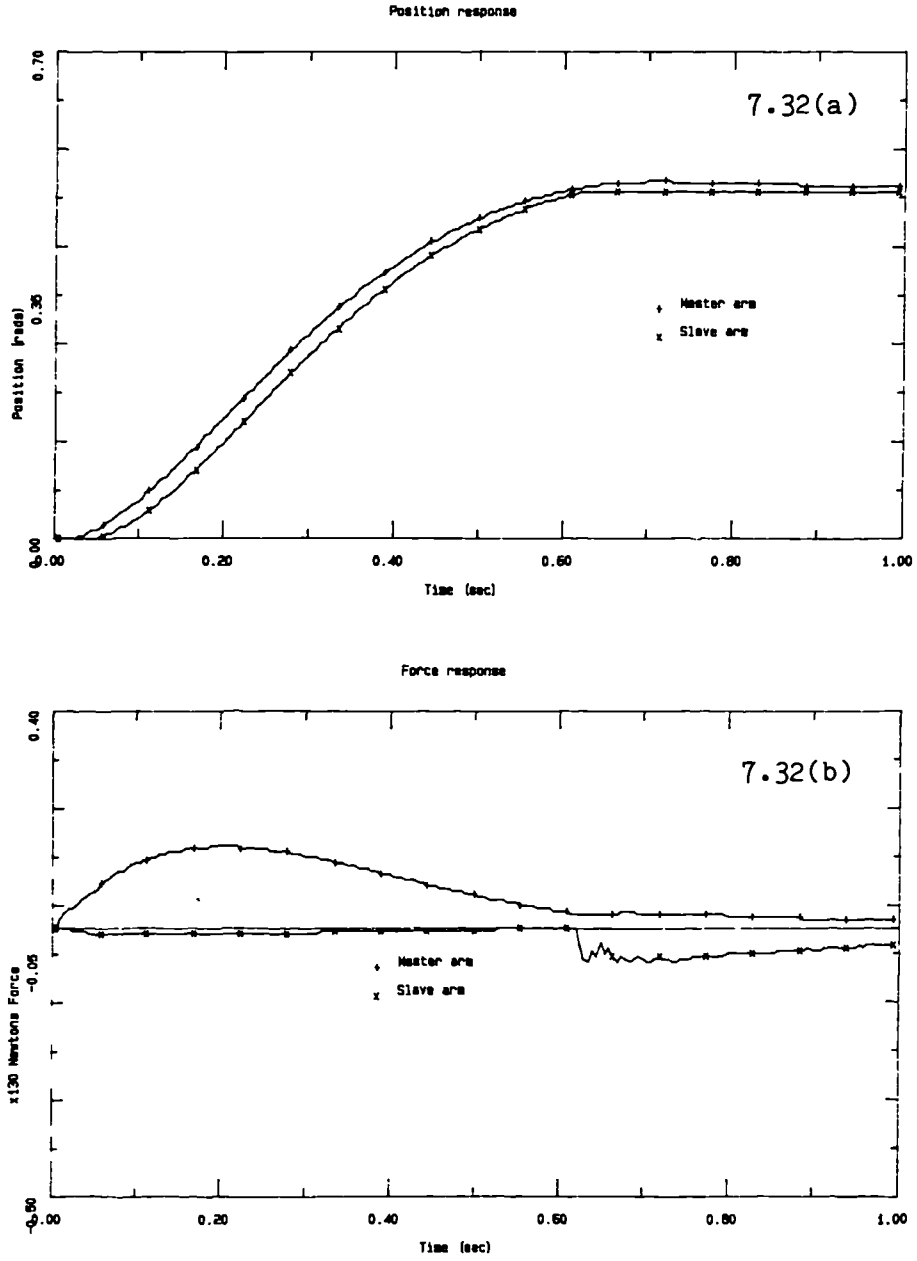

Figure 7.32 Tracking between master & slave

Increasing the gain of the positive torque feedback loop by a factor of 2 does not influence the lag between master and slave arm, however the speed of response is improved. Less effort is also demanded of the operator in accelerating the master arm, but at the expense of reduced force sensitivity when the hard stop is encountered, as shown in Figure 7.33.

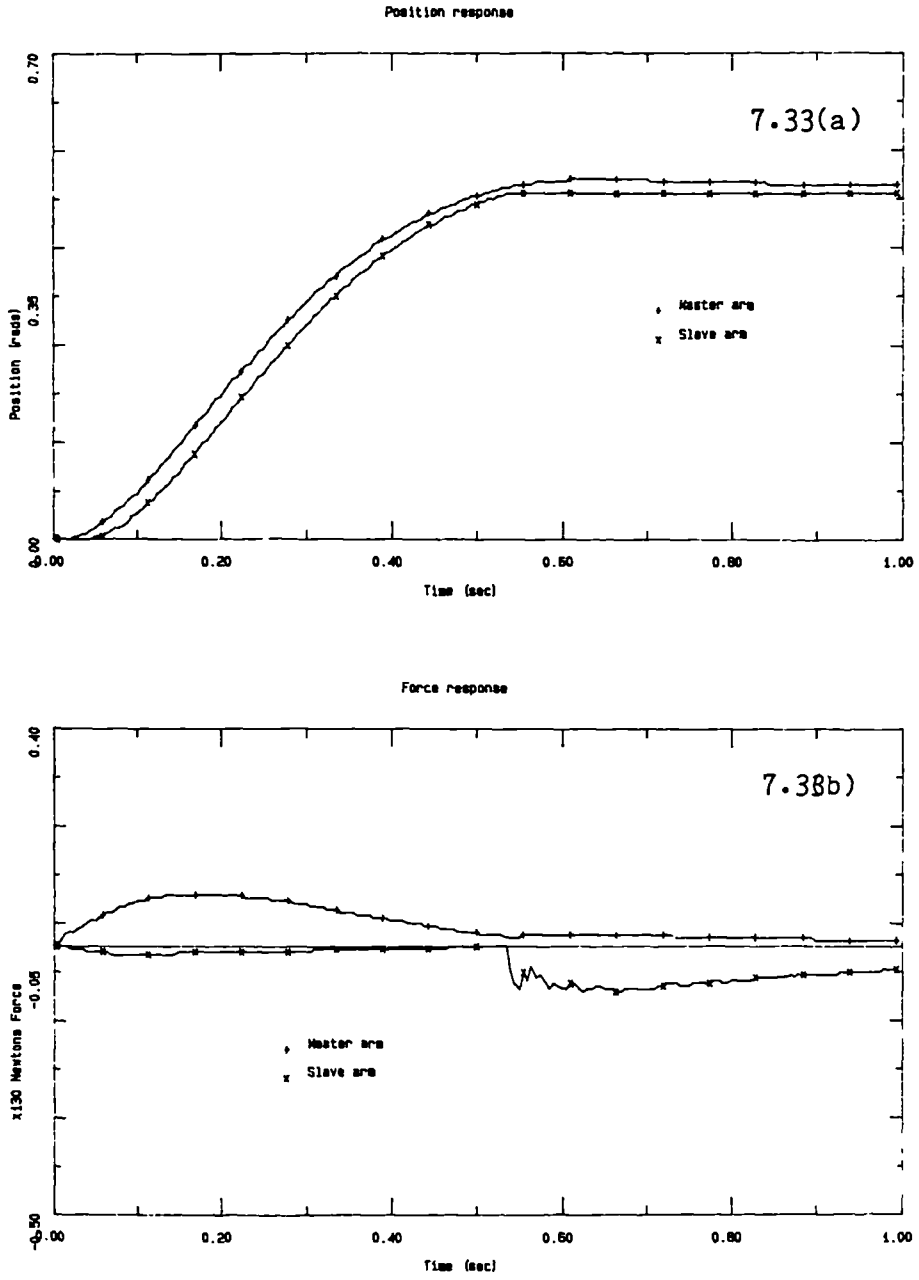

Figure 7.33 Effect of position feedforward gain

7.4 Summary

Parallel studies of one degree of freedom bilateral servo systems has also been reported [Hannaford & Anderson,1988; Tanie et al, 1986]. In particular, the independent work of Hannaford and Anderson on both modelling and experimental investigation of hard contact in a one degree of freedom force reflecting master-slave system is along similar lines to the studies reported here. Their results concentrate on a position/force control scheme, and they also report the presence of a large force transient on initial contact followed by subsequent oscillatory impacts . Tanie has experimented with a technique where the dynamics of the load at the slave arm are reflected back to the master arm controller which then modifies the dynamic of the arm accordingly. The method is claimed to offer improved performance in the presence of time delays.

The 'one' degree of freedom model of a bilateral master-slave system which has been developed in this chapter incorporates, as far as possible, the full dynamics of the identical master and slave arms. By modelling the elbow joint of the articulated arms used in the investigation the performance of the model was validated against that of the experimental system. The simple model of the human operator which was included in the simulation has also allowed the performance of the system to be studied during contact with a hard stop.

Good agreement was achieved between simulated and experimental results when the master arm was subjected to a step increase in torque. The experimental results showed an initial transient, associated with the master arm dynamics, which was quite distinctive. The presence of a similar transient in the simulated results added some confidence to the model.

The tight torque feedback loop employed in the experimental master arm which provided a significant improvement in the ability to backdrive the master arm, was included in the simulation, and the improvement in response demonstrated.

Both position/force and position/position control modes have been studied, and the simulations have shown how difficult it is to achieve satisfactory performance when using position/force control. The rapid build up in the contact force that occurs when the slave manipulator comes into contact with a rigid

obstacle is responsible for exciting the high frequency dynamics of the slave arm, which are extremely difficult to control. The presence of the human operator in the control loop is sufficient to introduce a low frequency oscillation into the system resulting in intermittent contact. Attempts to minimise this oscillation by including a derivative control action have met with some success, although the stability is highly dependent upon its time constant.

Another feature of the position/force control method is the considerable lag that exists when the slave is tracking the master arm. Increasing the forward position gain marginally improves the tracking, but also increases the intermittent contact frequency.

In the position/position mode a tight torque loop about the slave arm servo was also similarly shown to be advantageous in reducing the force transient.

The simulated results obtained in the position/position mode were also considered to be particularly important for several reasons, not least being the absence of the force transient which is characteristic of the position/force mode. Furthermore, improved tracking ability between master and slave has also been predicted. Increased gain in the forward path was consistent with improved response along with an estimated reduction in the operator effort. The torque feedback loop on the slave arm servo was found to reduce the magnitude of the impact force when the slave arm comes into contact with the obstacle by reducing the slave servo stiffness, which obviously compromises the positional accuracy. However, the results appear to be extremely stable, and do not show any tendency towards oscillation.

CHAPTER 8

Experimental Programme

The evaluation of remote manipulator systems has in the past been based upon predefined tasks using a scoring or timing procedure to obtain a qualitative measure of performance. The 'classical' peg-in-hole task has been well documented, and published results from previous investigations are available for comparison. A preliminary test programme based on this task was carried out during the early stages of this work [Bicker,1985]. More recently, efforts have been devoted to the development of a novel crank-turning task in an attempt to introduce a more quantitative assessment of performance than was possible using the peg-in-hole task. Examples of constrained trajectory tasks have been described earlier in Chapter2, and task performance criteria outlined in Chapter 4. The crank -turning and peg-in-hole tasks developed in this study are illustrated in Figures 8.1 and 8.2 respectively. It must be pointed out that the peg-in-hole tests were undertaken with an 8-bit digital system controller, whereas the more recent crank-turning tests were conducted using a 16-bit controller.

8.1 Design of the peg-in-hole experiment

Task variables include hole separation distance and peg-hole diametral clearance, where 'task difficulty' is defined as being inversely proportional to the diametral clearance. The peg was rigidly attached to the terminal post of the slave manipulator and has a nominal diameter of 20 mm. and length 50 mm. A small chamfer was machined on the leading edge of the peg to ease initial insertion. A horizontal plinth was used to support two receptacles and also serves for repositioning and clamping. Five pairs of interchangeable bushes were manufactured with a range of bore diameters toleranced to satisfy the test criteria. Figure 8.3 illustrates the geometric design of the peg and bushes, and the accompanying table indicates the tolerance range adopted for the five sets of bushes. The peg and bushes were manufactured from En8 grade steel and the functional surfaces honed to produce

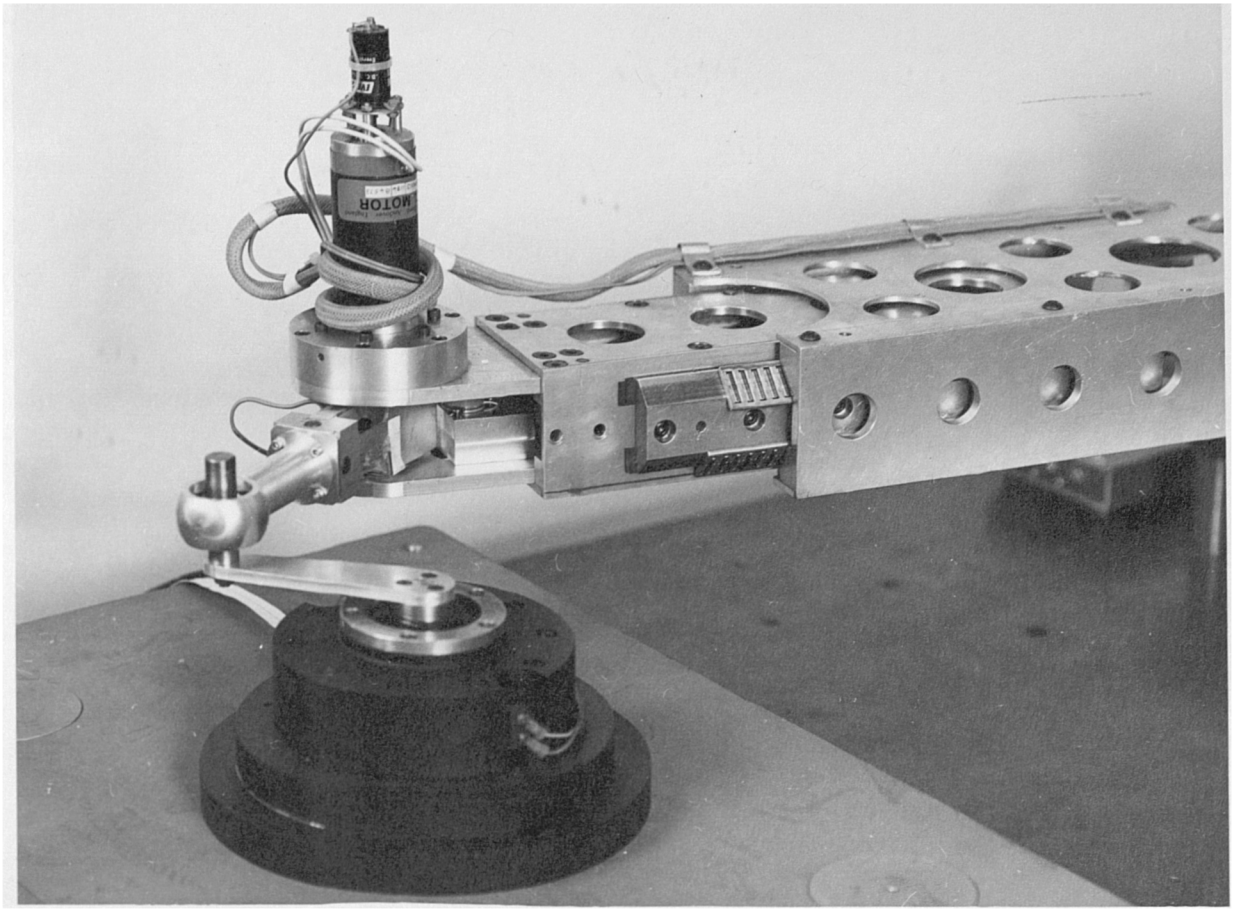

Figure 8.1 Crank turning task

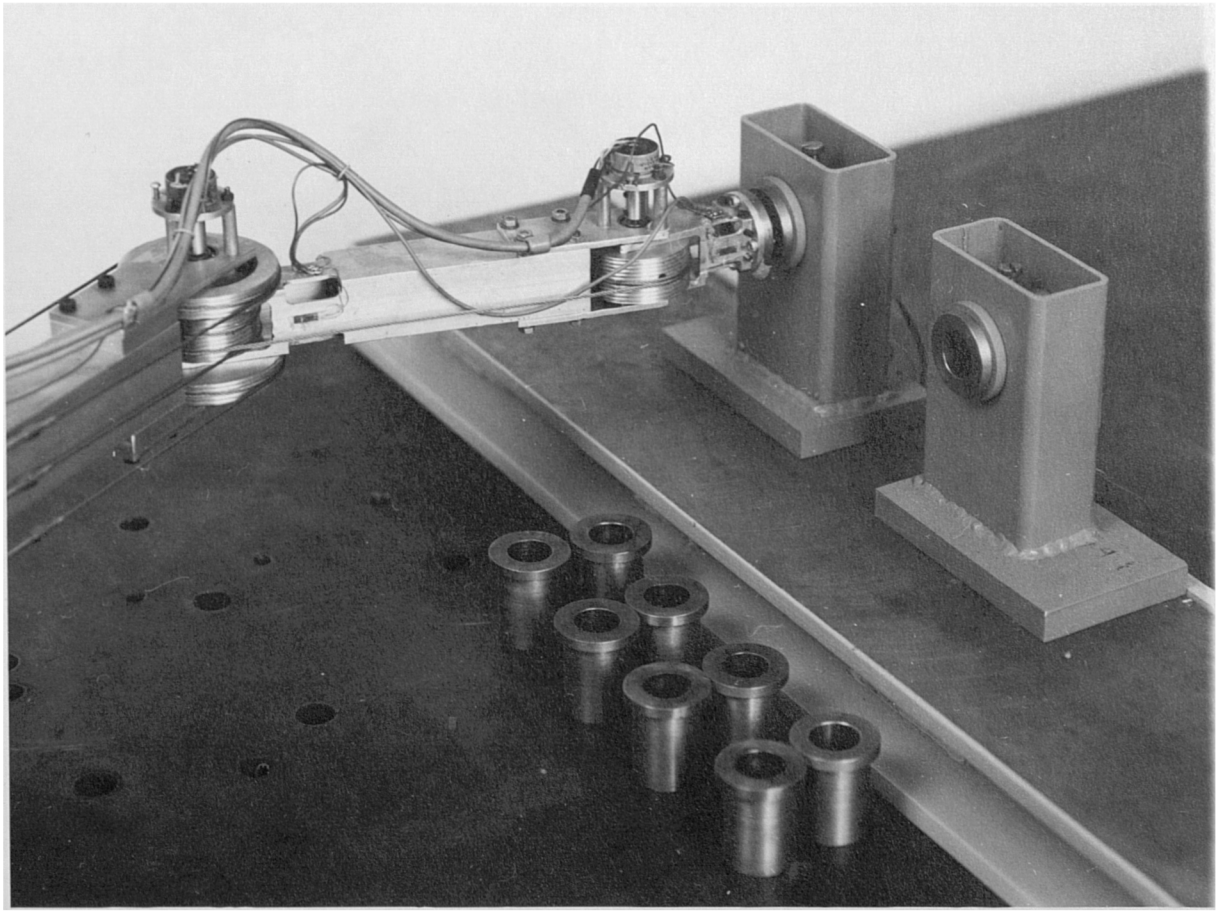

Figure 8.2 Peg in hole task

The peg and bushes were manufactured from En8 grade steel and the functional surfaces honed to produce a surface finish of 0.4 R_a (micrometres). Oil hardening and tempering was carried out to improve wear resistance. The bushes were designed to be located quickly in the receptacles.

Because the manipulator arms are constrained to move in the horizontal plane it was necessary to accurately align the the bushes to ensure that no forces (or torques) are generated out of the plane of operation.

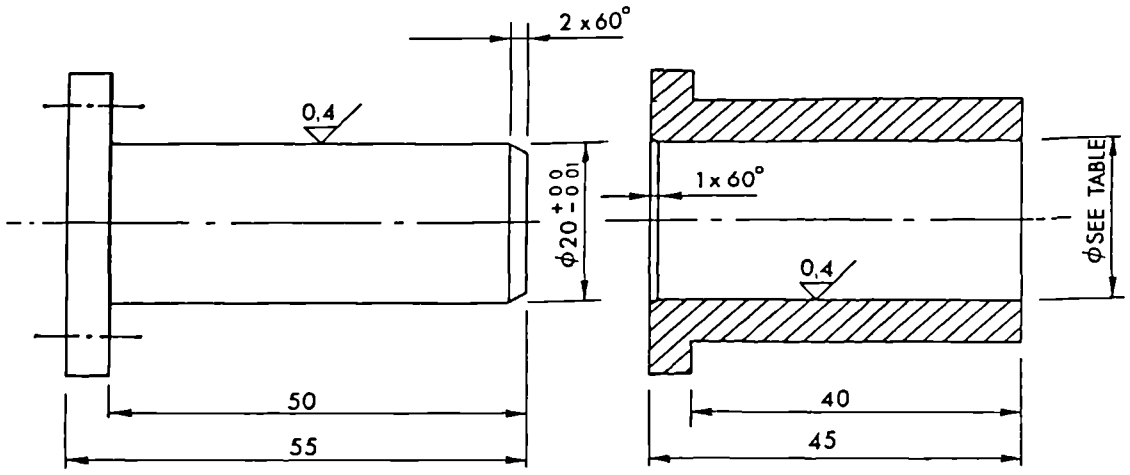

φA	$\phi 20^{+0\,02}_{+0\,01}$
φC	$\phi 20^{+0\,11}_{+0\,01}$
φD	$\phi 20^{+0\,21}_{+0\,20}$
φE	$\phi 20^{+0\,51}_{+0\,50}$
φF	$\phi 20^{+1\,00}_{+0\,99}$

Figure 8.3 Geometric design of peg & bushes

8.1.1 Test sequence

A schematic of the test sequence is shown in Figure 8.4. An electronic timer was used to record the elapsed time through the extraction, transfer and insertion phases of the test cycle. Microswitches were activated by the peg to initiate and stop the timer, a manually operated switch was used to reset the timer after recording task completion time.

Tests were carried out using both the articulated and pantograph slave arms. Prior to beginning a test sequence the operator was allowed a length of time in which to become familiarised with the 'new' test conditions. Each test involved a minimum of 25 repetitions of the test cycle from which it was possible to obtain a statistical mean and standard deviation of the task completion time. Lack of concentration occasionally led to an erroneous result, which was ignored, and the test repeated.

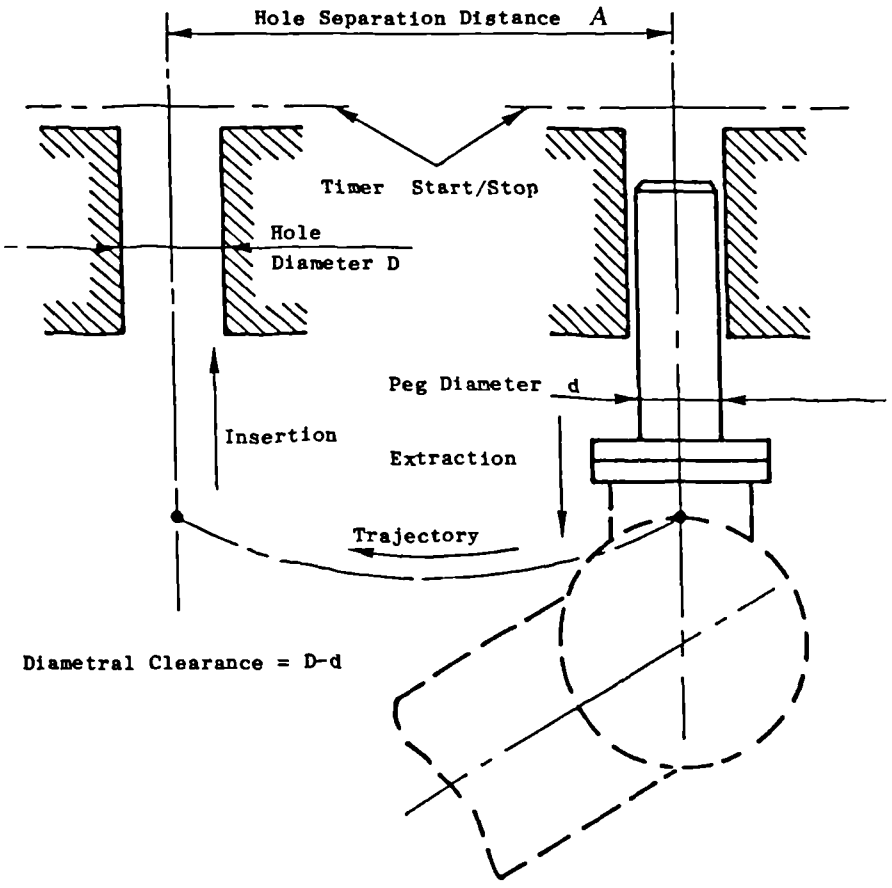

Figure 8.4 Peg-in-hole test sequence

The full test programme was carried out over a period of 12 weeks using only one subject. There was no fixed time for an experimental session, although each session generally lasted for approximately 2 hours, including rest periods. To offset operator learning, parameter changes were as far a practical carried out in a random order.

8.1.2 Analysis of performance

The mean task completion time can be used to provide a qualitative measure of performance. By making changes in system parameters or task variables it is possible to bring about a corresponding change in overall performance.

A task definition based on an index of difficulty I_d [Fitts,1957], and modified for remote manipulative tasks [M^{c}Govern, 1974(a);1974(b)], classifies the peg-in-hole task in terms of its component elements. In this case task difficulty is related to the distance between the two adjacent holes **A**, and the final clearance between peg and hole **(D-d)**, as shown in Figure 8.4, and can be expressed as

$$I_d = \log_2[2A/(D-d)] \qquad .....\{8.1\}$$

Results are presented graphically to show the correlation between the independent variable and mean task completion time.

8.2 Design of crank-turning experiment

The trajectory constraint in the peg-in-hole task is only restricted during the extraction and insertion phases of the test cycle. No constraint exists during the 'transfer' phase, and consequently task completion time is dependent upon transfer speed. The operator will attempt to mimimise the free motion whilst simultaneously trying to achieve high speed to bring about a reduction in task completion time. It is not surprising to find that the variance increases with hole separation distance.

The crank-turning task constrains the trajectory to follow a circular path, which permits criteria, other than task completion

time, to be adopted. In most installations the speed with which a task can be completed is not normally critical. What is desirable however is the ability to successfully accomplish the task without error ie. no ensuing damage to either equipment or environment.

By constraining the trajectory of the slave manipulator arm to rotate around the crank radius, and by analyzing continuously the radial force applied to the crank arm over a full revolution of the crank it is the opinion of the author that the magnitude of the variation in radial force will provide a measure of the performance of the system. The signature will include wide-band 'noise' components as a consequence of the interaction between the slave-arm dynamics and the constraint placed on it by the crank. The amplitude and frequency of the 'noise' will be highly dependent on the performance of the overall control system. In this study only the root-mean-square of the radial force has been considered, although the analysis of vibration in industrial robots [Bicker et al,1989], has shown that the vibration signature contains information which may be particularly important when backlash is present in the gear transmission.

In the experiment presented here the cranking torque was 'pre-set' using a DC powder electro-magnetic clutch, operated through a power amplifier. An IBM-PC AT microcomputer was used to control the crank torque via a 12-bit digital-to-analog converter. The crank arm was integrated with a multi-component dynamic force platform [Kistler], which makes use of four (3 component) piezo-electric force transducers to measure eight components of applied force. In this case only forces in the X and Y directions were required. The crank experiment is shown schematically in Figure 8.5.

The Kistler force platform, which is designed for dynamic force/torque measurement, is extremely rigid. By using high quality charge/voltage amplifiers it is possible to measure the applied forces with minimal drift, although it was necessary to reset the amplifiers at regular intervals to eliminate long term drift using a manually operated remote switch. The outputs from the charge amplifiers were sampled using a multi-channel, 12-bit analog-to-digital data acquisition system.

A 1000 line incremental optical encoder was used in conjunction with a 12-bit up-down counter to measure crank angle. Two 8-bit output latches were used to store position which were then read by the computer. The encoder index pulse was used to reset the counter and provide an absolute position datum.

Crank torque was calibrated over the range of interest, and was found to be linear. A small dead zone and hysterisis band existed which made it necessary to ensure the torque setting was progressively increased during any test sequence.

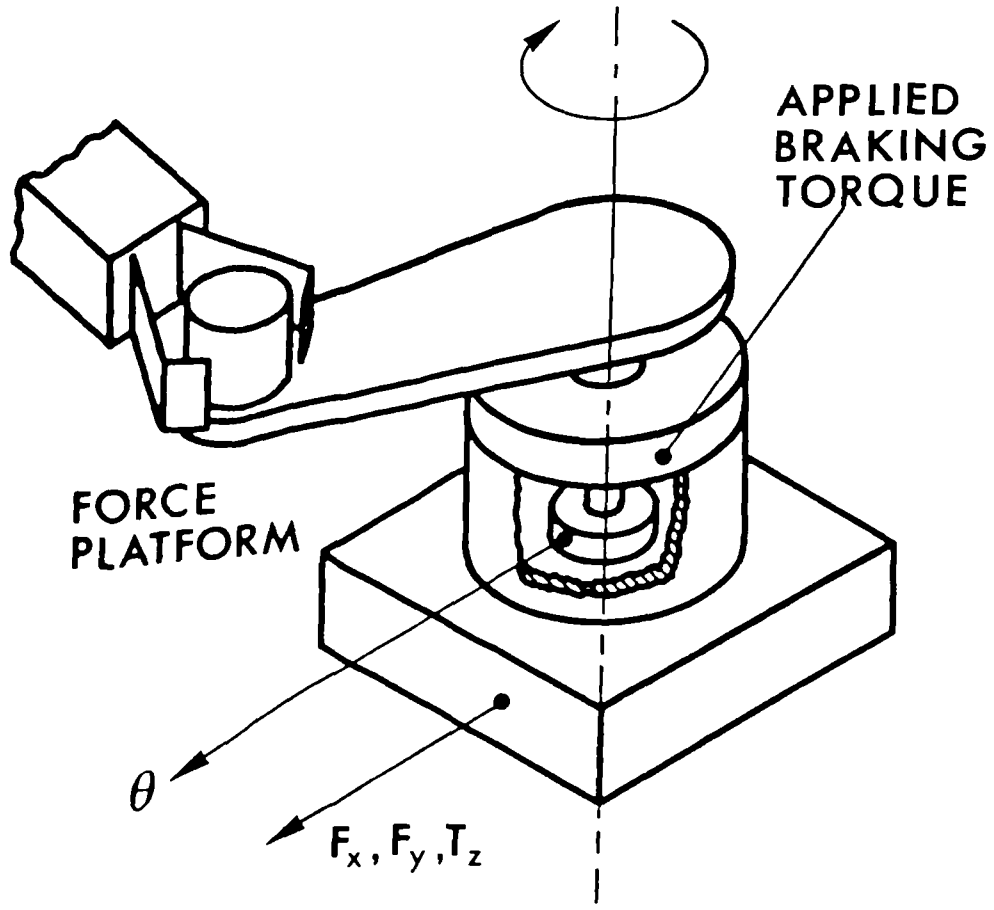

Figure 8.5 Schematic of crank-turning task

8.2.1 Test sequence

Fortran [Microsoft], was used for the data logging routine, with input/output calls written in assembly language. A flow diagram of the storage program is shown in Figure 8.6. After the program is initialised, a file is opened for storage of data, and the desired crank torque is set by calling a D-A subroutine. Data acquisition does not start until the crank has been rotated twice past the reference point, ie. a least two full revolutions. This was considered necessary to ensure that the electromagnetic powder in the clutch was evenly distributed, and perhaps more importantly to give the operator time to adjust to a new situation.

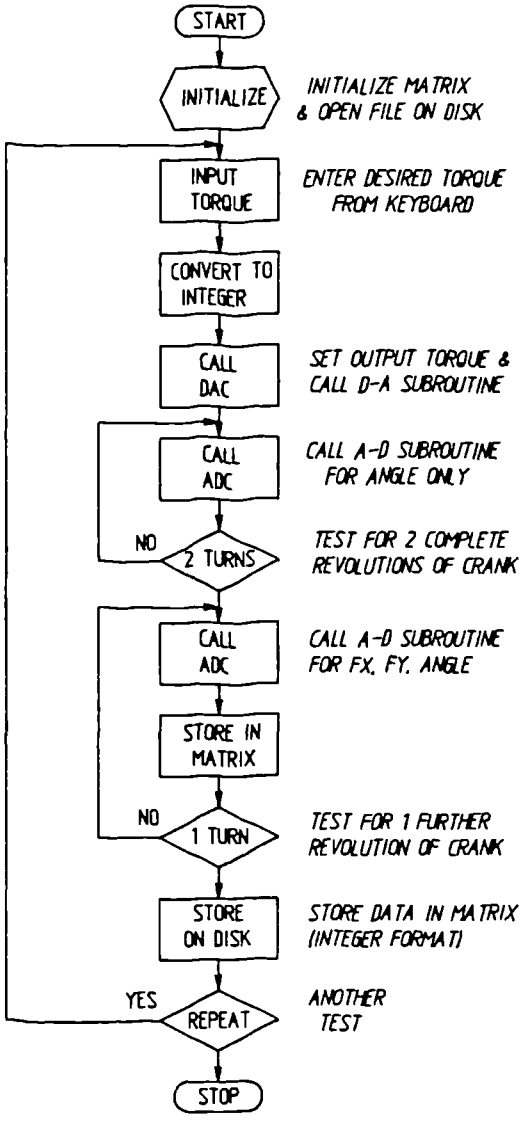

Figure 8.6 Data storage flow diagram

On passing the index position for a third time, reaction forces F_x and F_y, and encoder position N, are logged at each incremental position for a complete revolution of the crank. The stored data is then written to disk so that analysis can be carried out off-line. The test conditions are then modified and the procedure repeated.

8.2.2 Analysis of performance

A two pass algorithm is used to access previously stored data files. In the first pass the equivalent radial and tangential components of the crank forces F_R and F_T respectively, as shown in Figure 8.7(a), are calculated at each position where,

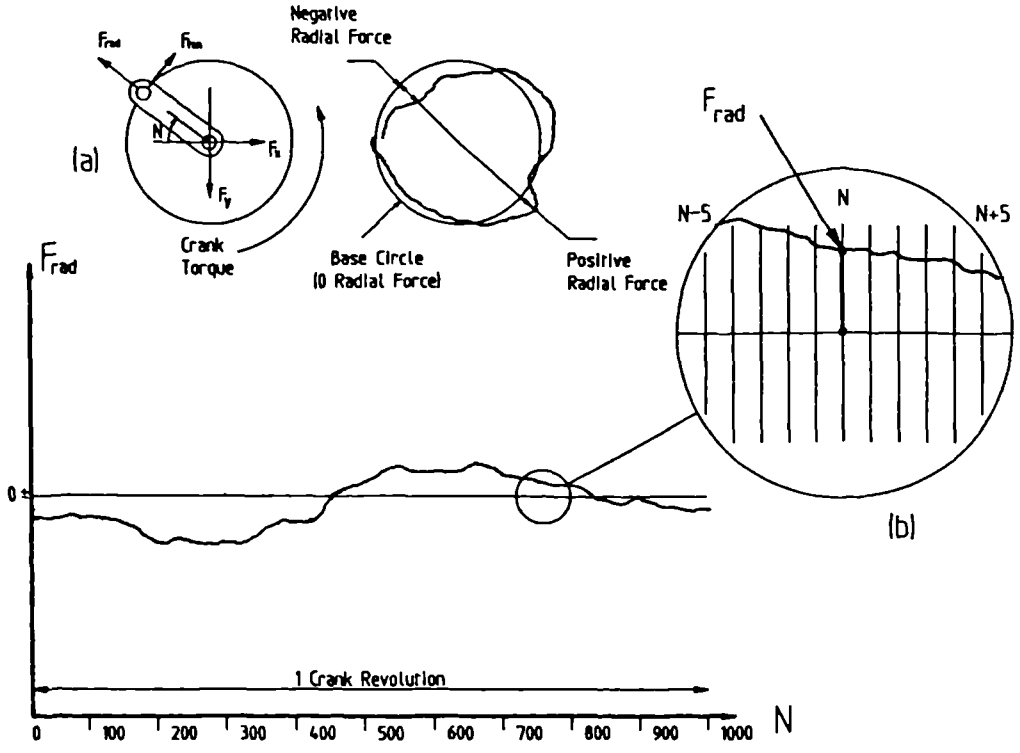

Figure 8.7 *Force analysis of crank-test*

$$F_R = F_X.\cos\theta + F_Y.\sin\theta$$

$$F_T = F_X.\cos\theta - F_Y.\sin\theta \qquad \text{.....\{8.1\}}$$

where $\theta = 2\pi N/1000$ radians

On the second pass, the root-mean-square of both F_R and F_T is summed over a complete crank revolution, (see Figure 8.7(b))

$$F_R = \left(\sum_{N=1}^{1000} F_R[N]^2\right)/1000$$

and

$$F_T = \left(\sum_{N=1}^{1000} F_T[N]^2\right)/1000 \qquad \text{.....\{8.2\}}$$

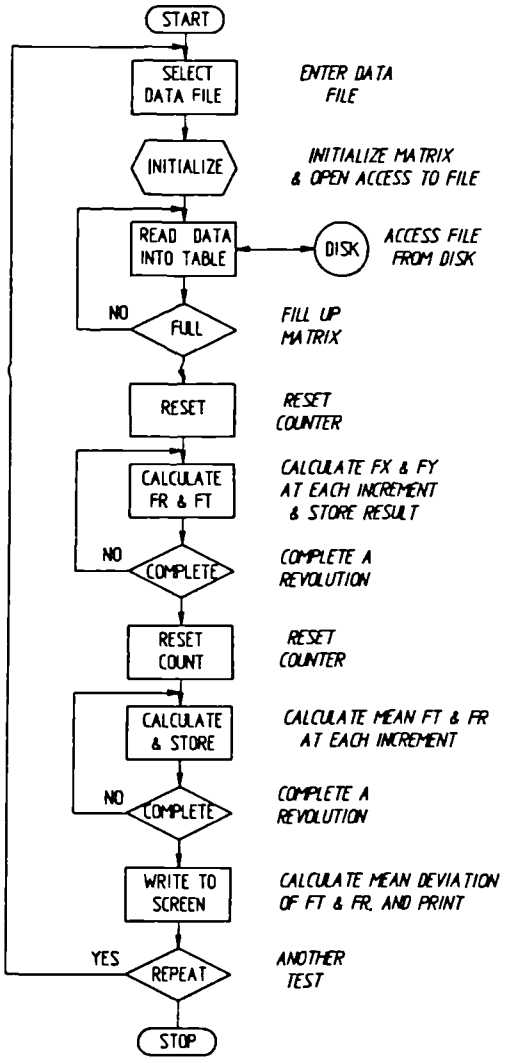

Figure 8.8 Analysis flow diagram

An example of the variation in radial force for a complete crank revolution is illustrated in Figure 8.7(b). The adjacent polar diagram shows the variation in terms of a base circle. The elliptical shape of the force component has been attributed to the position of the operator relative to the input device. The flow diagram for the program used to analyze the data is shown in Figure 8.8.

8.2.3 Performance of the unencumbered hand

Previous investigations have shown that when tasks are undertaken manually, the time to complete the task is shorter and the number of errors made is significantly reduced. It was anticipated that when the crank-turning task is carried out directly, ie by hand, then optimum performance should be achieved by the operator, assuming the test is carried out at approximately the same speed when the manipulator system is interposed.

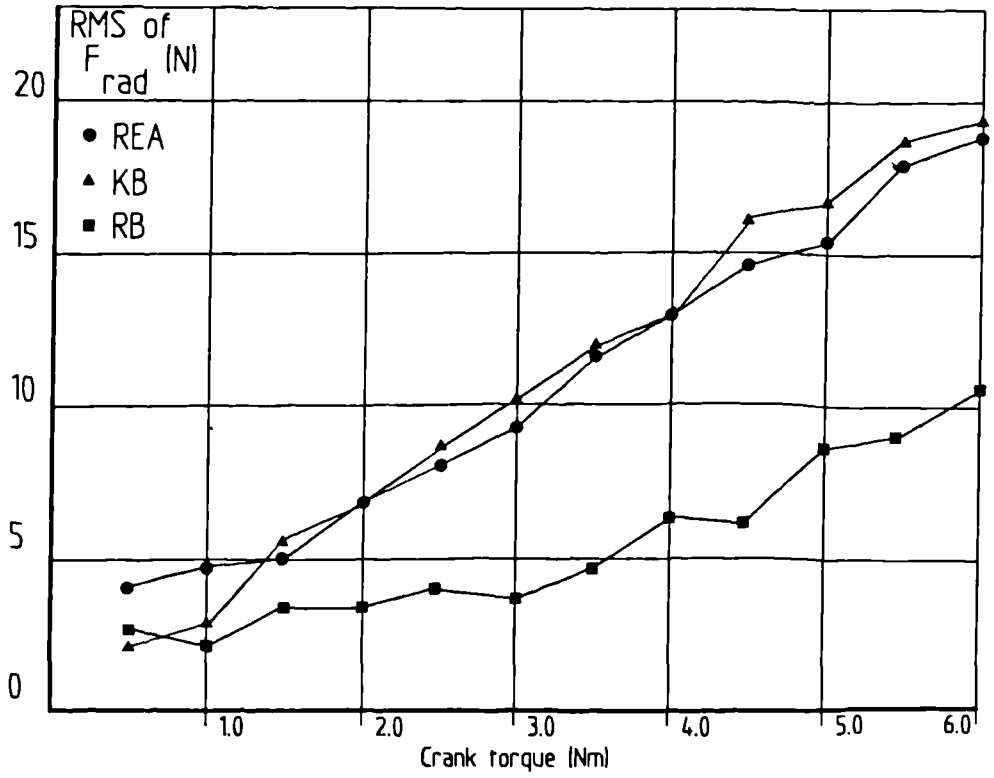

Figure 8.9 *RMS of F_{RAD} against crank torque*

An initial set of tests were carried out to provide a comparative index against which to measure the performance of the manipulator system. The results of these tests are presented in Figure 8.9, and show the relationship between crank-torque and RMS of the radial force. Three subjects, including the author, undertook the tests, and each point on the graph represents only one test sequence. The variation in radial force is very nearly proportional to the crank torque over the range studied, although as the torque is further increased, a physical limit will be reached beyond which the operator will be incapable of rotating the crank. The evidence also suggests that familiarity with the task improves performance, suggested by the effective reduced radial force (RB), when compared with that of 'inexperienced' subjects (REA,KB).

The conclusions drawn from these initial tests suggest that as the task difficulty increases, by virtue of increasing the crank torque, a corresponding increase in variance of the radial force occurs. When the manipulator system is introduced a significant reduction in performance is to be expected.

8.3 Replica master-slave performance tests

An extensive number of tests based on the peg-in-hole task were carried out using the replica master-slave system. The implementation of the bilateral position/force control scheme was achieved by using analog closed-loop control of joint position between the master and slave, and closed loop force control between slave and master, both with adjustable gain.

The initial tests involved carrying out a factorial survey of task variables with unity gain position and force feedback. A further series of tests were designed to assess the influence of force feedback gain on performance.

8.3.1 Initial peg-in-hole factorial survey

A 5x5 parametric survey of task variables, ie. hole separation distance and diametral clearance, versus task completion time was carried out to establish any relevant characteristics of the test. Hole separation distance was varied over the range 100 - 600 mm, and diametral clearance from a mimimum of 0.01 - 1.00 mm.

Table 8.1 presents a summary of the results. The mean time to complete each test is given, along with the standard deviation (in brackets) derived from the 25 repetitions at each test condition. The mean times to carry out the test varied from a mimimum of 2.42 (0.12) seconds, up to a maximum 6.81 (0.71) seconds, which corresponded to maximum-clearance/minimum-distance and minimum-clearance/maximum-distance respectively.

Bush {note 1}	Hole separation distance (mm) {note 2}				
	100	200	300	400	600
A	3.43{3} (0.28)	4.03 (0.28)	4.60 (0.42)	5.98 (0.49)	6.81 (0.71)
C	2.89 (0.18)	3.61 (0.21)	4.39 (0.32)	5.67 (0.28)	6.33 (0.54)
D	2.79 (0.14)	3.49 (0.23)	4.20 (0.22)	4.80 (0.38)	6.41 (0.49)
E	2.57 (0.12	3.34 (0.21)	3.53 (0.32)	4.56 (0.34)	6.18 (0.51)
F	2.42 (0.12)	2.85 (0.11)	3.22 (0.19)	3.65 (0.19)	4.41 (0.27)

Note 1 Bush designation is given in Figure 8.3.
Note 2 Force reflection ratio 1:1.
Note 3 Mean time & standard deviation (brackets) in seconds.

Table 8.1 Results of parametric survey

The relationship between hole separation distance and mean completion time appears to linear, as Figure 8.10 shows. However, as the task difficulty is increased the correlation becomes poorer, which also corresponds to an increase in the variance associated with mean time.

By considering task difficulty I_d, defined by equation {8.1}, versus task completion time, as shown in Figure 8.11, and connecting up the points associated with a particular peg-hole clearance it can be inferred that task completion time tends to zero as task difficulty approaches zero.

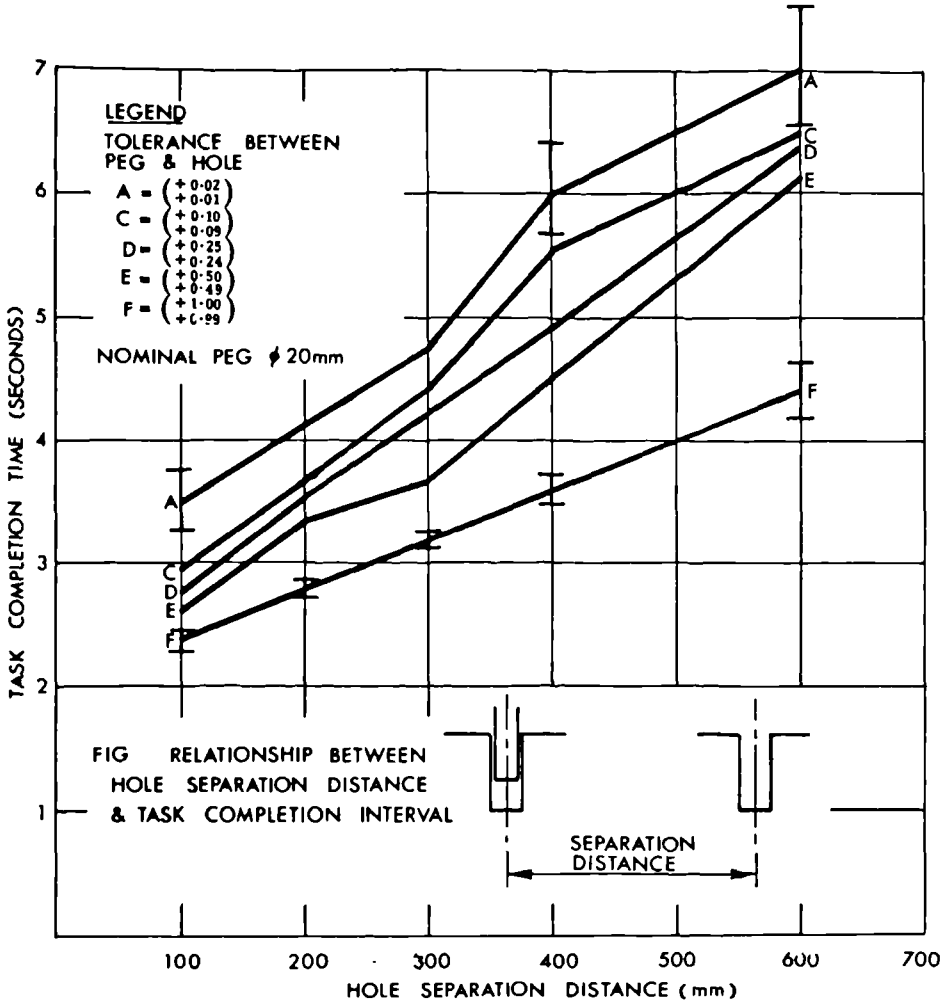

Figure 8.10 Performance versus hole separation

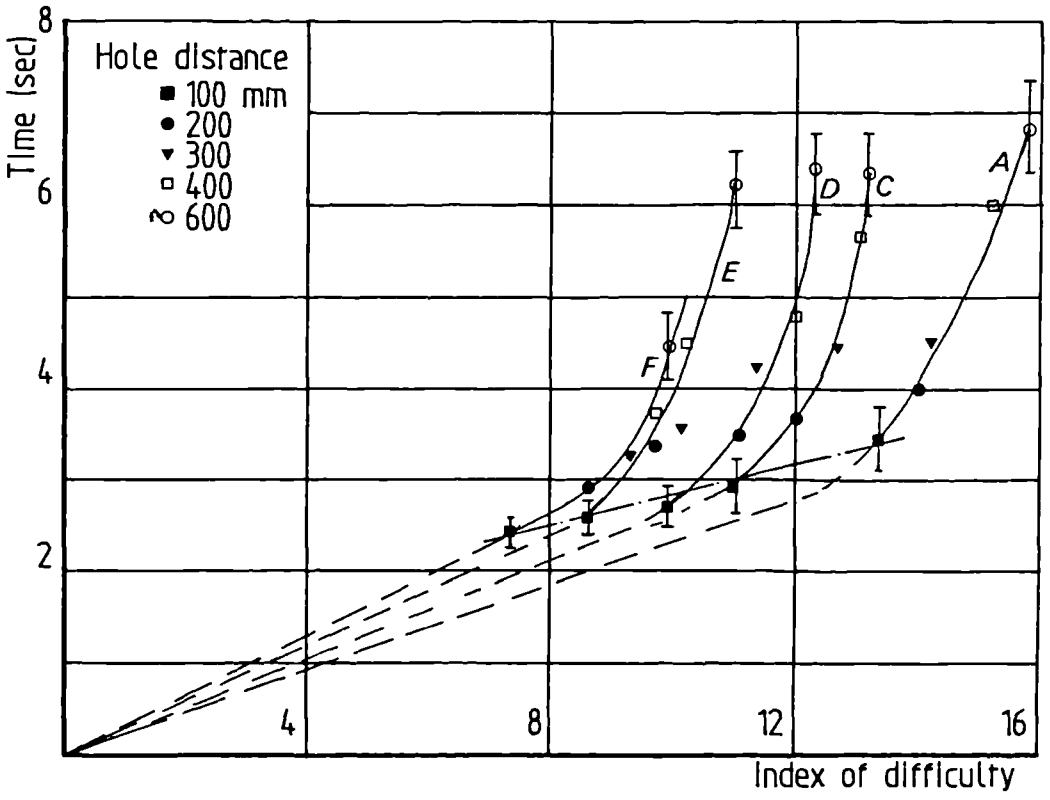

Figure 8.11 *Peg in hole performance vs Index of difficulty*

McGovern has reported that tasks having the same index of difficulty, took approximately the same length of time to complete, although the results presented here suggest otherwise. The 'good' agreement achieved by McGovern was based on tasks having an index of difficulty in the range 5 - 11, compared with 8 - 16 in this study. The convergence that occurs as the task difficulty is reduced may account for the interpretation that no significant difference occurred in the mean completion time.

The points associated with a hole separation distance of 100mm show a linear relationship between I_d and recorded time. A least squares linear regression of these points achieved a correlation of almost one. However, as the separation distance is increased the correlation becomes less significant and the variance increases, which is probably because the operator's performance becomes more erratic when required to traverse greater distances.

The preliminary factorial survey has demonstrated the subjective nature of the peg-in-hole task, although the results were considered more consistent at a hole separation distance of 100mm. On the basis of these findings it was considered acceptable to conduct all further peg-in-hole tests at a hole separation distance of 100mm.

Bush	Force reflection ratio {see note 1}					
	← Unilateral				Full Bilateral →	
	1:32	1:16	1:8	1:4	1:2	1:1
A	3.24{2}	2.03	1.86	2.02	2.20	2.47
	(0.52)	(0.16)	(0.09)	(0.17)	(0.15)	(0.11)
C	3.02	1.97	1.72	1.79	2.01	2.17
	(0.39)	(0.17)	(0.09)	(0.07)	(0.11)	(0.11)
D	2.51	1.73	1.72	1.67	1.77	1.98
	(0.30)	(0.07)	(0.08)	(0.06)	(0.07)	(0.09)
E	2.34	1.65	1.67	1.63	1.71	1.85
	(0.15)	(0.05)	(0.07)	(0.09)	(0.08)	(0.08)
F	2.32	1.58	1.64	1.54	1.64	1.68
	(0.16)	(0.07)	(0.05)	(0.12)	(0.14)	(0.07)

Note 1 Hole separation distance fixed at 100mm.
Note 2 Mean time & standard deviation (brackets) in seconds.

Table 8.2 Results of force reflection ratio on performance

8.3.2 Effect of force reflection ratio on performance

At the time of carrying out these tests no previous studies had sought to qualify the benefits of using force feedback control. It was considered appropriate to carry out a set of tests from which it was subsequently possible to establish a relationship, in terms of task completion time, against force reflection ratio. Recent work has since been published [Draper et al,1987].

Table 8.2 presents the results of a series of tests carried out on the replica master-slave system for a range of force feedback gains from bilateral (1:1) down to almost unilateral (1:32). As previously noted, the variance increases with task difficulty. By presenting the results graphically, as shown in Figure 8.12, the relationship between force reflection ratio and task completion time suggests that optimum performance, was achieved with a force reflection ratio of approximately 1:8.

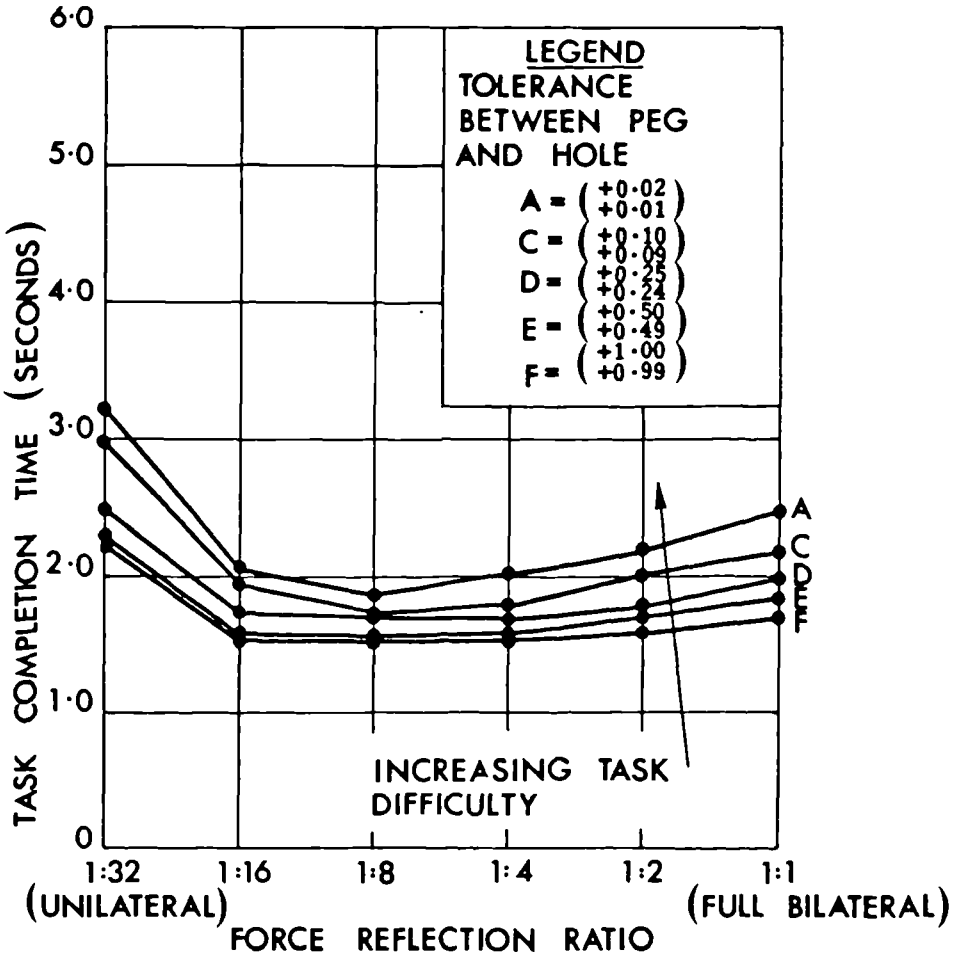

Figure 8.12 Effect on performance of force feedback gain

It has been reported [Goertz,1964] that the human hand is only capable of discriminating between forces in the range 0.07 - 20N, and that above this threshold the sensing mechanism may become saturated. Since the master arm used here can generate about 100N force, there is a possibility that such factors may come into play, and consequently high force feedback gain may have an adverse effect on performance - which may also be responsible for exciting the oscillatory behaviour predicted by simulation. When the peg impacts the edge of the hole on initial contact, the operator reported 'feeling' a force transient.

In unilateral operation there is a tendency for the operator to make mistakes, along with the possibility of jamming or wedging taking place between the peg and hole, particularly when the task difficulty is high.

The results of work going on independently, and in parallel, have recently been published [Draper et al,1987] on the influence of force reflection on performance for a number of different assembly tasks, including peg-in-hole operations. The tests were carried out using commercial master-slave systems, although the range of force reflection ratio's was limited to 1:1, 1:4 and 1 to infinity, ie. unilateral. Improved performance was reported at a ratio of 1:4 compared with the other levels, which supports the results presented here.

The overall evidence suggests that force reflection is beneficial, particularly when the information it provides compliments the operator's other senses. Although vision is considered to be the most important of the human sensory organs, the trajectory constraints imposed on the slave manipulator by the peg-in-hole task demands that force and/or tactile perception be utilized to carry out the force control, whilst the visual perception undertakes the responsibility for controlling position.

When the results are presented isometrically, as shown in Figure 8.13, the combination of tight tolerance and minimal force reflection can be associated with poorer performance, which also indicates an increase in the number of errors and variability of the forces acting at the task/machine interface.

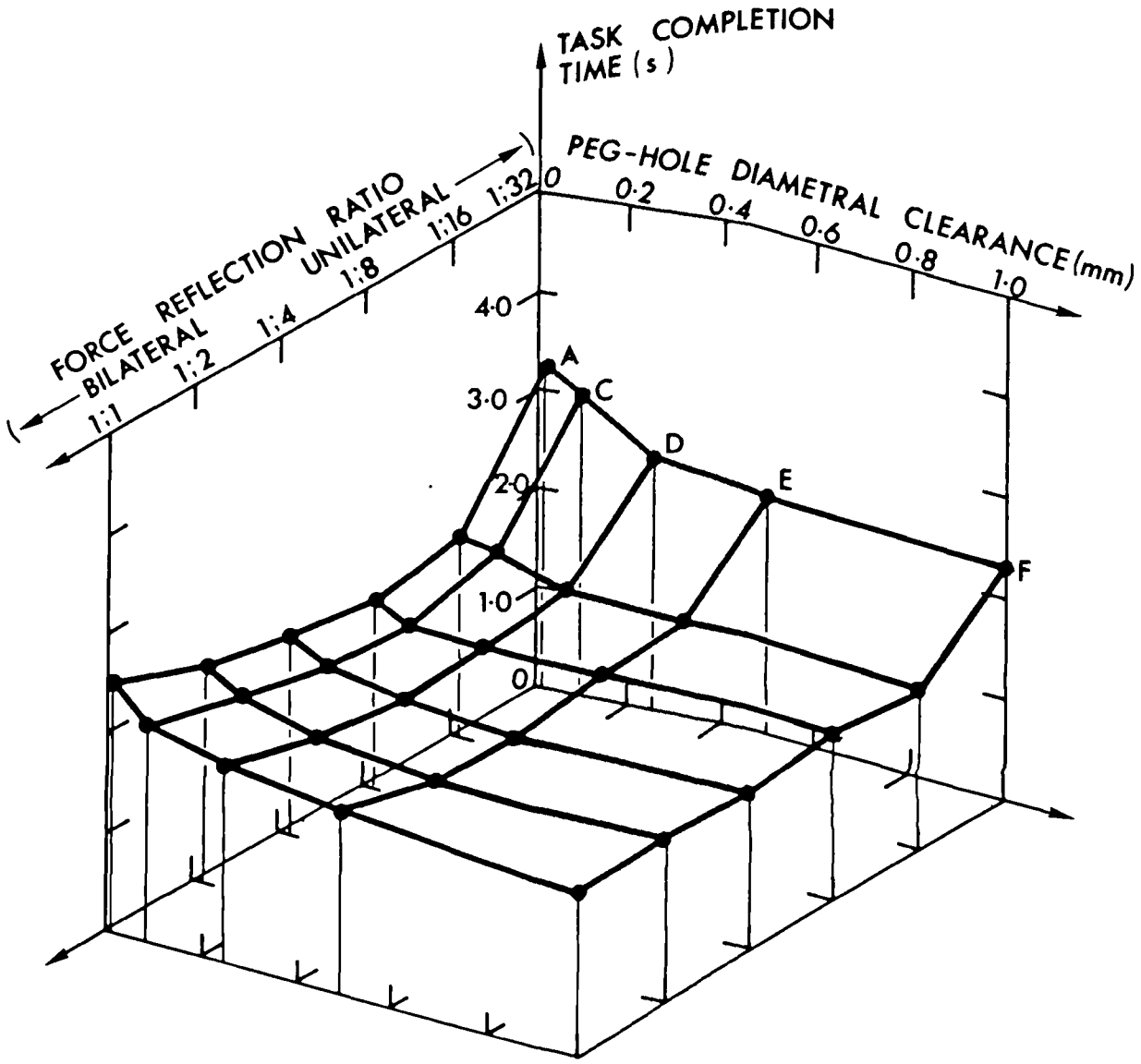

Figure 8.13 Isometric view of factors influencing performance

8.4 Generalized control system performance

Since one of the main advantages of the generalized control technique is to provide fully resolved position control between dissimilar hand controller and slave manipulator, it was considered important to assess the tracking capability of the system in addition to establishing the performance of alternative bilateral control schemes. Figure 8.14 presents an aerial view of the generalized control scheme, which illustrates the relationship between the controller and the slave arm in carrying out peg-in-hole operations.

8.4.1 Tracking ability between hand controller and slave arm

A test was devised to determine the ability of the slave arm to track the movement of the hand controller, which required the operator to describe a circle of approximately 100 mm diameter, using a template placed directly below the hand controller to act as a guide. The digital control software was modified to log the simultaneous positions of both controller and slave arms, in world (X-Y) coordinates, by writing an array of data to file, whilst on-line.

The procedure involved following the circular path in a clockwise direction, starting at approximately the same location each time. Data logging was begun when the shoulder joint torque of the controller exceeded a small threshold value, which occurred when the operator started to move the arm. Data was stored consecutively at each sample interval, ie. approximately every 10mS, for a maximum of 1000 data points. This corresponded to an elapsed time of 10 seconds.

By playing back the stored data through an X-Y recorder, a facsimile of the trajectory of both master and slave arms was obtained. The RMS of the tracking error between both the manipulator arms, summed over all data points, was evaluated as an indicator of performance. Figure 8.15 highlights the tracking ability of the slave arm in following the path of the hand controller.

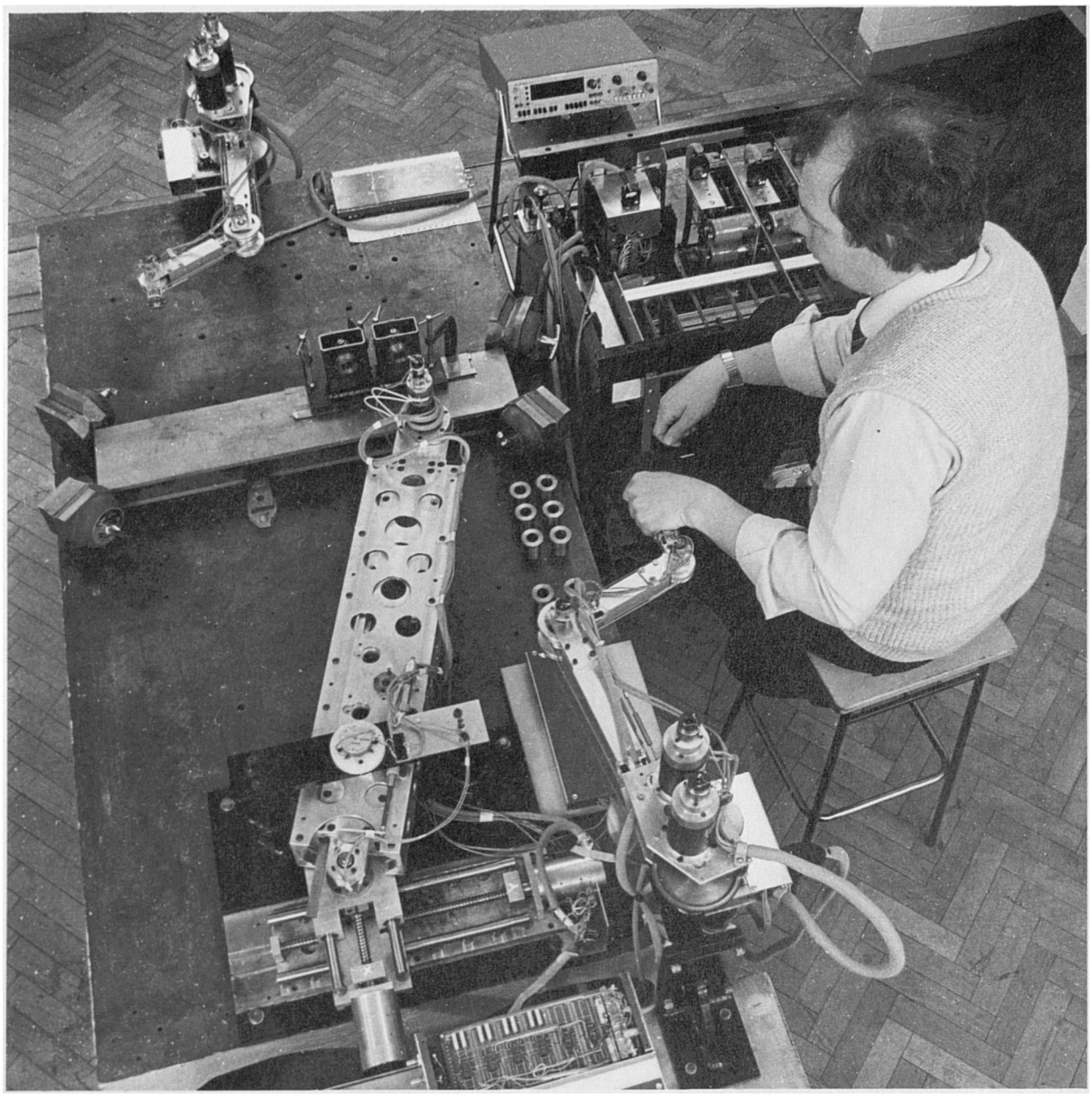

Figure 8.14 Aerial view illustrating Generalized Control

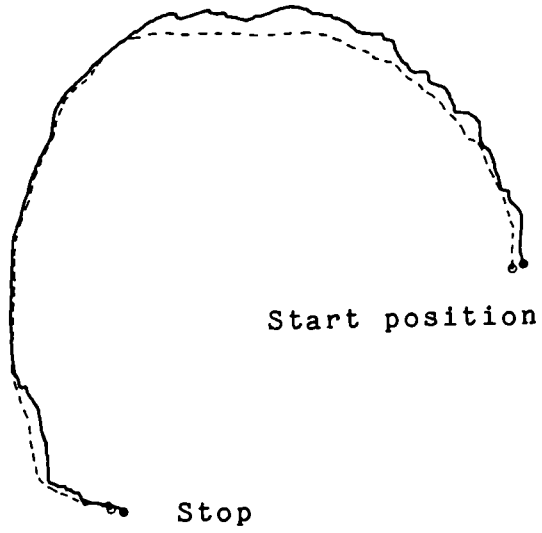

8.15(a) Position fback 50%
+ Torque fback

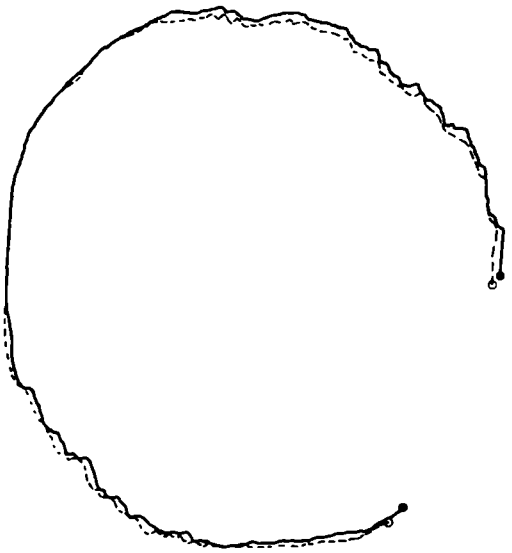

8.15(c) Position fback 250%
+ Torque fback

——— Master arm

– – – – – Slave arm

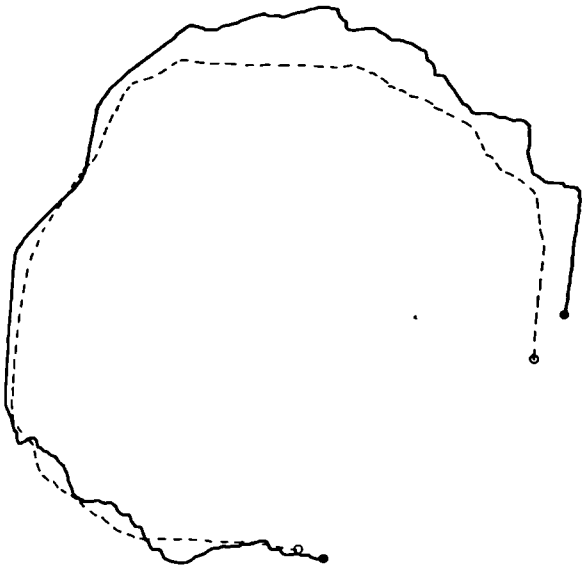

8.15(b) Position fback 50%
0 Torque fback

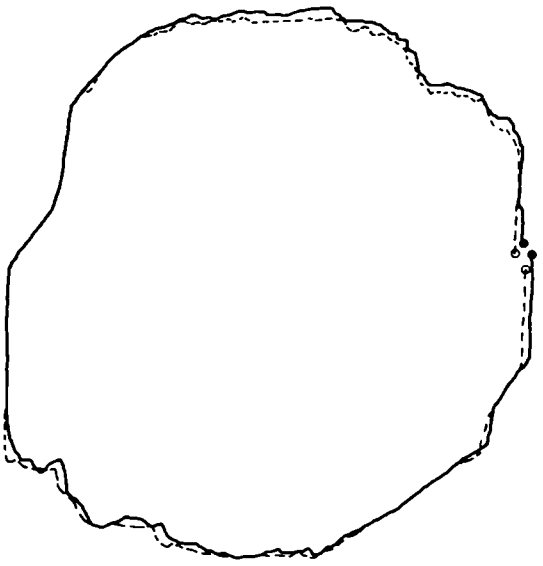

8.15(d) Position fback 250%
0 Torque fback

Since no physical constraints were placed on the manipulator arms, other than the operator attempting to move the end of the master arm through a circular path, unilateral operation was considered adequate. The tight torque feedback loop provided in the servo-controller is intended to assist back-driving of the hand controller, and without which the demands placed on the operator would be higher. Figures 8.15 (a) & (c) illustrate the motion of the master arm achieved with torque feedback, and can be compared with Figures (b) & (d), obtained without torque feedback. More precise tracking of the template by the operator can be observed with the benefit of the 'anti-friction' feature. An increase in position feedforward gain also brings about a marked improvement in the tracking ability of the hand-controller by the slave-arm when a comparison between Figures 8.15 (a) & (b) with (c) & (d) is made, with gains of 1.0 and 2.5 respectively. The improvement in tracking performance is move evident when presented in terms of gain versus RMS tracking error, as shown in Figure 8.16. As expected the relationship is exponential, with improved performance being achieved using torque feedback.

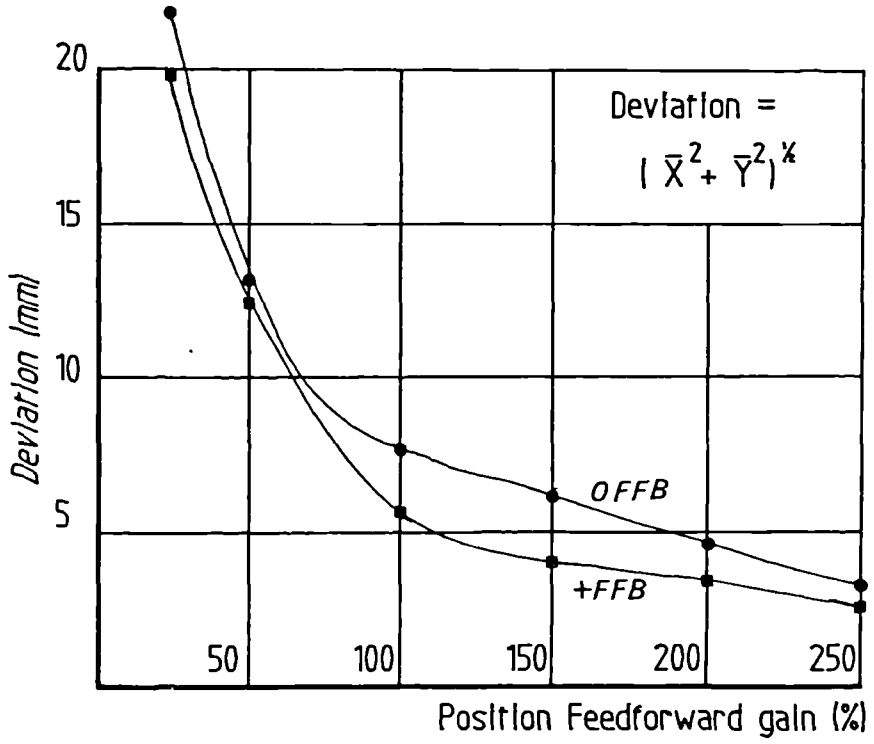

Figure 8.16 *Tracking performance for different position gain*

8.4.2 Peg-in-hole performance tests

The test programme could only be extended to include a limited assessment of generalized control because of the difficulty in maintaining adequate stability when in the bilateral position/force control mode. The effects of low sampling frequency and switching transients associated with the brushless DC servo-motors then in use, combined to produce serious noise problems which corrupted the force sensor outputs. Whilst attempts to minimise noise were moderately successful, it was not practical to undertake the necessary modifications to the hardware at that point in time.

Nevertheless, satisfactory performance was achieved in both unilateral and bilateral mode, albeit with a reduced force feedback gain. By maintaining a hole separation distance of 100 mm., tests were also conducted using a simple design of remote centre compliance [Drake,1977]. The results of these tests are presented in Table 8.3. The relationship between task difficulty and mean task completion time is shown in Figure 8.17.

Bush {note 1}	Test condition {note 2}		
	Unilateral	Unilateral + RCC	1:4 Bilateral
A	4.81{3} (0.74)	3.35 (0.30)	3.39 (0.31)
C	3.42 (0.26)	2.67 (0.23)	2.95 (0.19)
D	3.09 (0.25)	2.54 (0.17)	2.81 (0.14)
E	2.69 (0.16)	2.36 (0.17)	2.58 (0.20)
F	2.65 (0.21)	1.94 (0.21)	2.24 (0.26)

Note 1 Bush designation given in Figure 8.3.
Note 2 Hole separation distance 100mm.
Note 3 Mean time & Standard deviation (brackets) in seconds.

Table 8.3 Peg-in-hole results using generalized control system

As expected, the results associated with the unilateral mode of operation are consistent with reduced performance, and strongly influenced by task difficulty. The large variance that occurred at maximum task difficulty highlighted the incidence of jamming/wedging between peg and hole during initial insertion. In the bilateral mode, the relationship is more linear over the range of task difficulty, and the improvement in completion time become more pronounced with increasing task difficulty. However, the most interesting result is related to those tests conducted using the RCC, which shows improved performance over all other test conditions. The conclusions drawn from such a limited set of test results can only be subjective, and whilst the indications are that bilateral control offers considerable improvement in performance when compared with the unilateral mode, incorporating the RCC device demonstrated its ability to limit the potential for jamming or wedging as the task difficulty is increased. A view of the experimental test incorporating the RCC is shown in Figure 8.18.

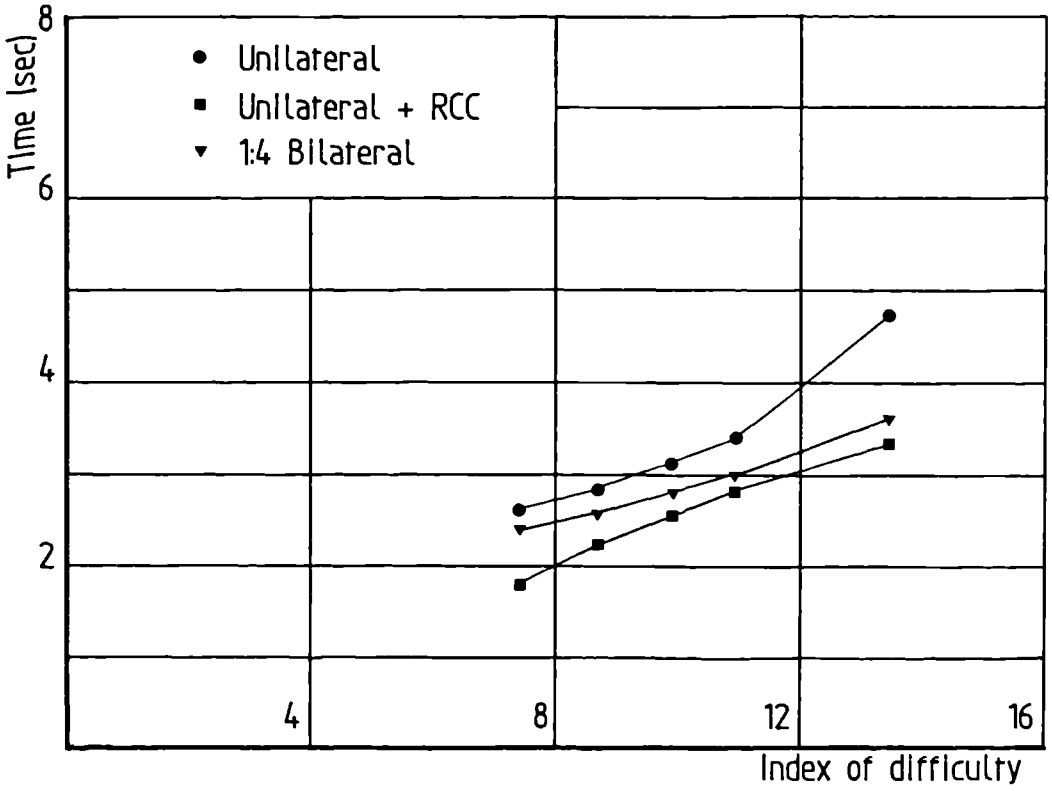

Figure 8.17 *Peg in hole tests using Generalized Control*

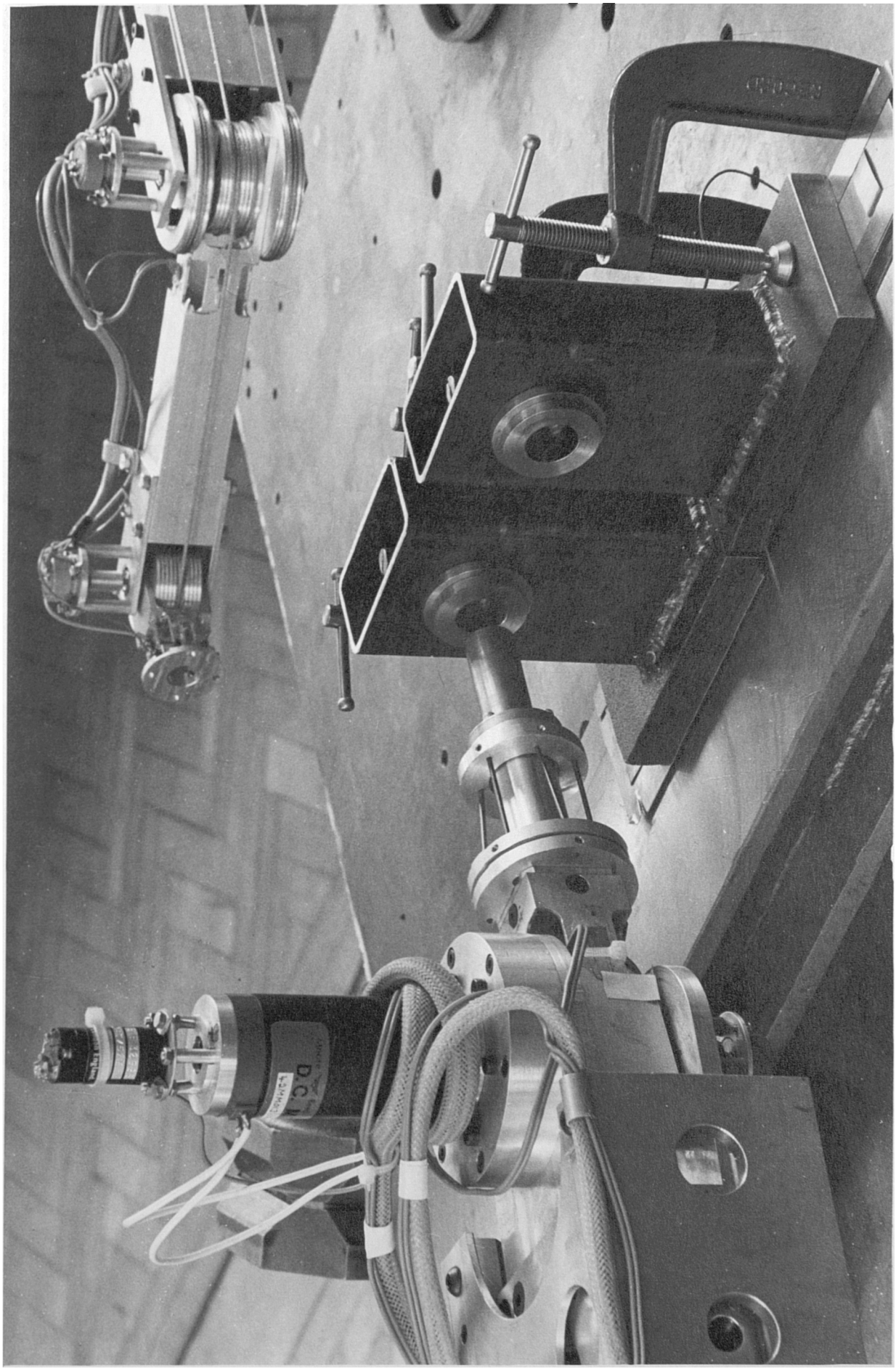

Figure 8.18 View showing peg in hole test carried out using a RCC

8.4.3 Crank performance tests - Position/force control

The crank experiment was designed specifically for assessing the performance of remote manipulator systems when system parameters are modified, and initial tests have been carried out to determine the effect of crank torque on performance. Because of residual magnetism in the electromagnetic clutch, the minimum possible crank torque was found to be 0.7 Nm. When torques greater than 4 Nm were applied to the crank, manipulation of the slave arm was found to be extremely difficult, and it was necessary to limit crank torques accordingly. Further tests were undertaken to establish the influence of position and force feedback gain on the position/force generalized control mode. The experimental arrangement, which has been described previously, is illustrated in Figure 8.1.

Influence of crank torque on performance

Preliminary crank tests were carried out to determine the relationship between the root-mean-square of the radial force, F_{rad}, and the applied crank torque. Table 8.4 presents the results obtained with 0% (unilateral), 50%, and 100% (full bilateral) force feedback gains.

Force feedback gain (%)	Crank torque (Nm)							
	0.7[1]	1.0	1.5	2.0	2.5	3.0	3.5	4.0
0	51.56	52.53	52.42	51.28	51.88	49.10	44.35	41.27
50	14.13	17.38	24.76	31.21	35.30	36.03	37.28	33.11
100	9.02	12.17	18.76	22.08	28.45	31.16	29.25	23.65

Note 1 Minimum possible crank torque

Table 8.4 Crank torque vs RMS of the radial force, F_{rad}

Figure 8.19 illustrates these results in terms of crank torque versus RMS of the radial force, F_{rad}, for each of the three conditions. As expected, the absence of force feedback coincides with large radial forces being exerted on the crank arm, the magnitude of which remains reasonably constant up to a crank torque of 2.5 Nm. At higher crank torques, a noticeable fall in radial force occurs, which has been attributed to the inability of the slave arm to exert sufficient force to rotate the crank effectively. When force feedback is introduced a marked decrease in the radial force occurs, the magnitude of which is evidently related to the crank torque. Again, the radial force 'rolled off' as the crank torque approached the limiting value. With full bilateral control , the radial force was consistently lower over the range of crank-torques, but exhibited the same trend obtained with 50% force feedback. The RMS of the radial force, on the basis of these results, is considered to be a useful measure of system performance.

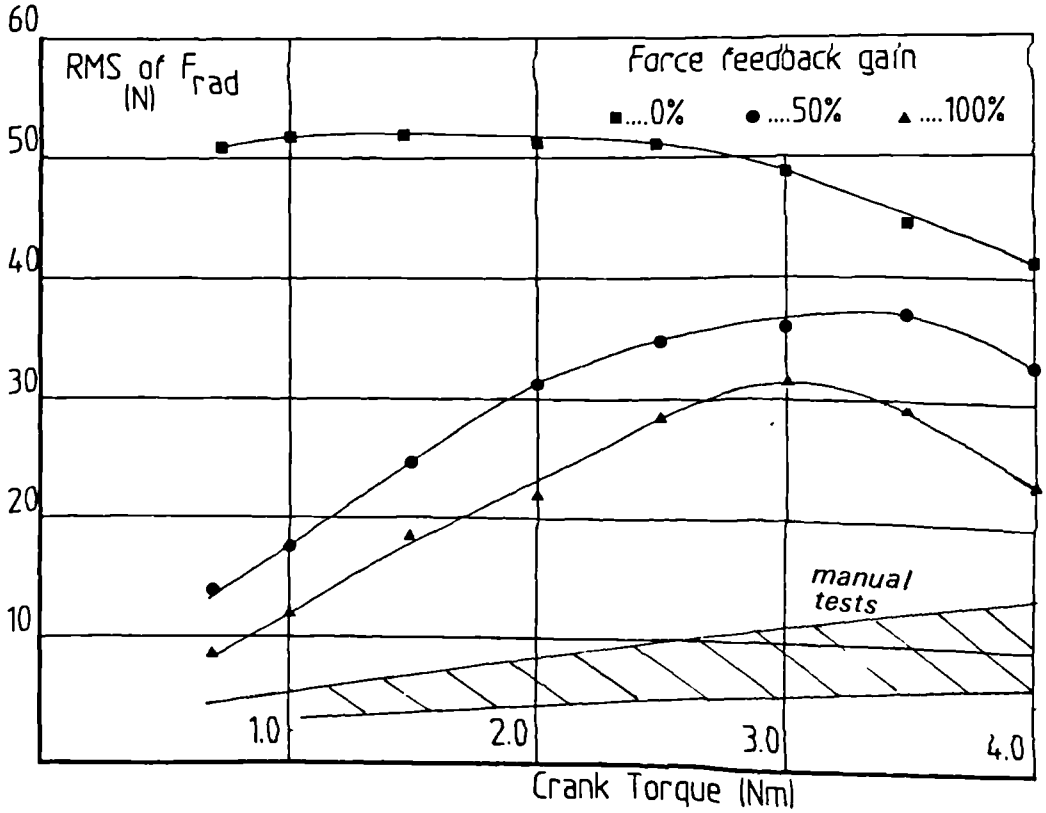

Figure 8.19 *Relationship between $\bar{F}_{rad}$ and crank torque*

The results of the unaided manual tests (see section 8.2.3) have been included. As expected they show an improvement in performance over the manipulator system, even in the full bilateral mode, of approximately 300%. Note also that the manual test results do not 'roll off' at the higher torques, which indicates the improved capability of the operators in when performing the same task.

On the basis of these preliminary results it was decided to carry out all further crank turning tests using only nominal crank torques to avoid possible interaction with performance as a consequence of operating near the physical limits of the slave arm.

Influence of force feedback gain on performance

Using a position feedforward gain of 1.0, and with crank torque pre-set to 1.0 Nm, a set of tests were carried out to establish the effect of force feedback gain on performance. The results are presented in Table 8.5.

Force feedback gain (%)	Unilateral ←			Bilateral →		
	0	20	40	60	80	100
Mean radial force F_{rad} (N)	53.88	31.67	20.07	12.55	11.25	15.19

Note Crank torque set at 1 Nm

Table 8.5 Results of force feedback gain vs. RMS of radial force

Figure 8.20 illustrates the relationship, which suggests that an optimum performance exists between the limits of unilateral and full bilateral control. By plotting the radial force component as a function of crank angle, as shown in Figure 8.21, an explanation can be put forward as to why this should be so. With no force feedback, (see Figure 8.21a), peak radial forces greater than 100 N have been recorded. The variation of the radial force over the full cycle suggests that the constraints imposed by the crank geometry give rise to significant tracking errors between

the master and slave. Since the operator can only rely on visual information to maintain adequate control over position, he can only attempt to move the master arm through a similar trajectory. When force feedback is introduced the tracking error is reduced, and the magnitude of the radial force decreases as the master arm is 'forced' to follow the crank trajectory. However, at high gain the high frequency dynamics associated with the slave-arm/task interaction excite uncontrollable modes which result in an increase in the amplitude of oscillation of the radial force. The operator , in attempting to carry out the task is faced with the additional burden of damping out these low frequency disturbances in order to maintain stability.

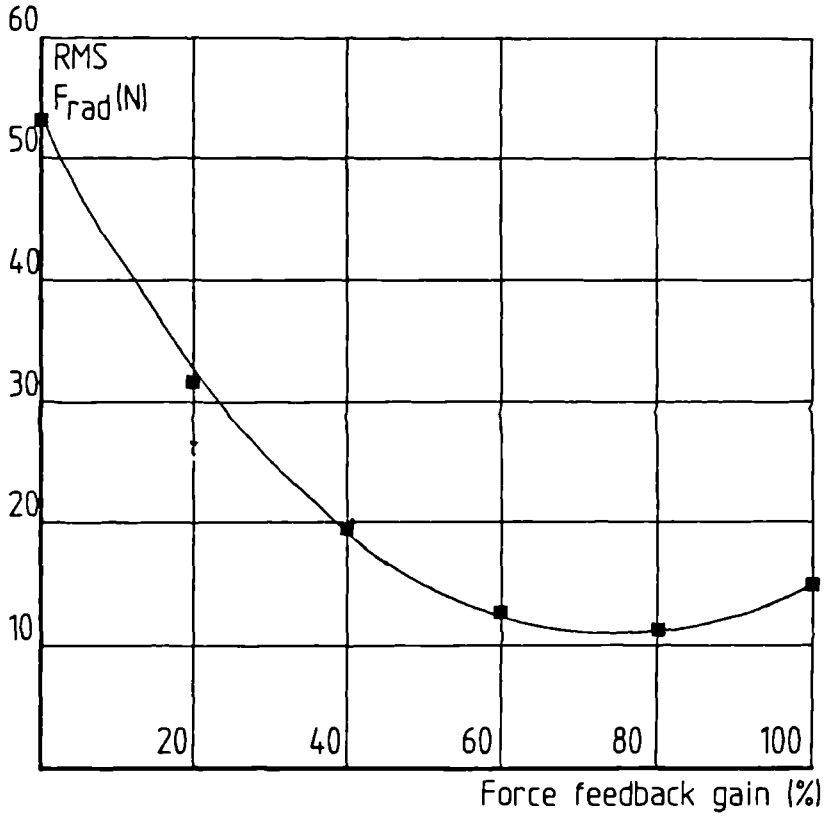

Figure 8.20 *Relationship between* $\bar{F}_{rad}$ *and force feedback gain*

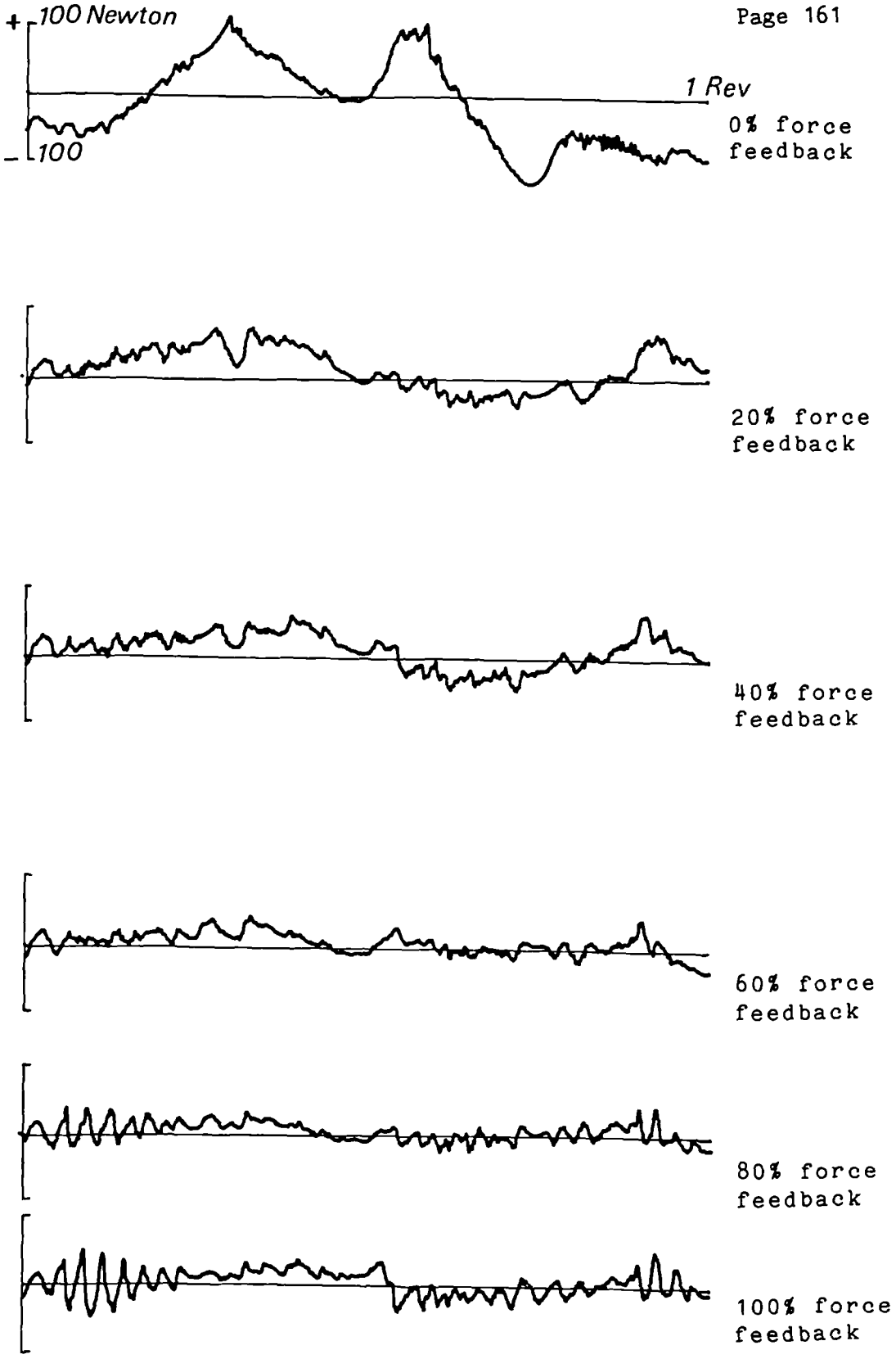

Figure 8.21 Influence of force feedback gain on radial force

Influence of position gain on performance

The significance of force feedback gain has been demonstrated in the previous section. To establish the influence on performance of position gain another set of tests were conducted in the bilateral position/force mode, on this occasion using 80% force feedback gain, but with variable position feedback gains in the range 50 - 175%. Table 8.6 presents the results of these tests, and Figure 8.22 illustrates the performance relationship.

Position gain (%)	50	75	100	125	150	175
RMS Radial force (N)	13.37	12.08	13.13	13.94	14.88	16.57

Note Crank torque pre-set to 1 Nm

Table 8.6 Results of position feedforward gain on performance

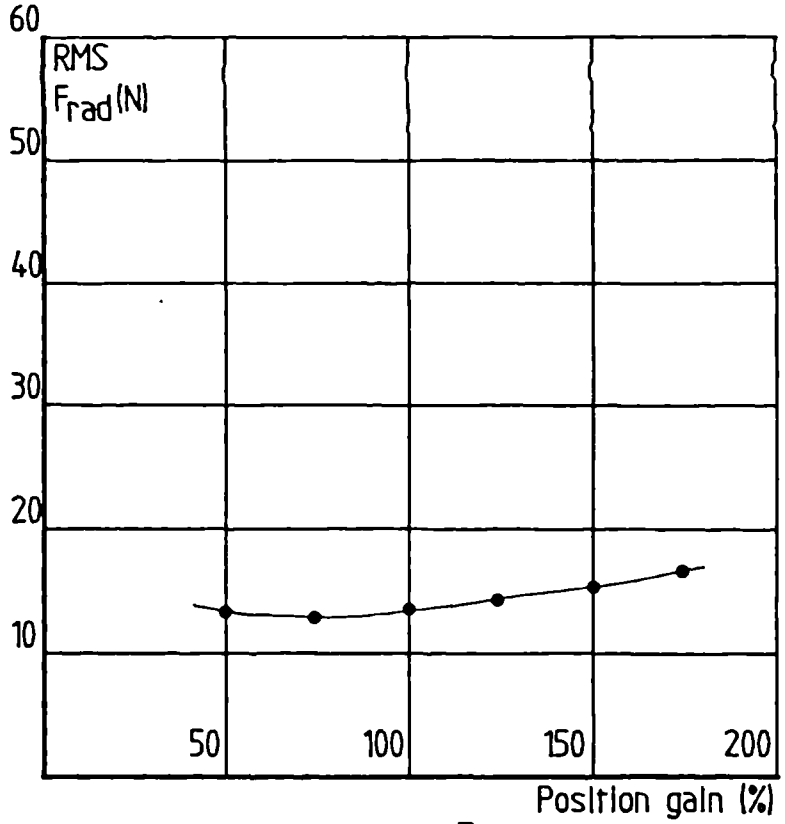

Figure 8.22 *Relationship between* $\bar{F}_{rad}$ *and position gain*

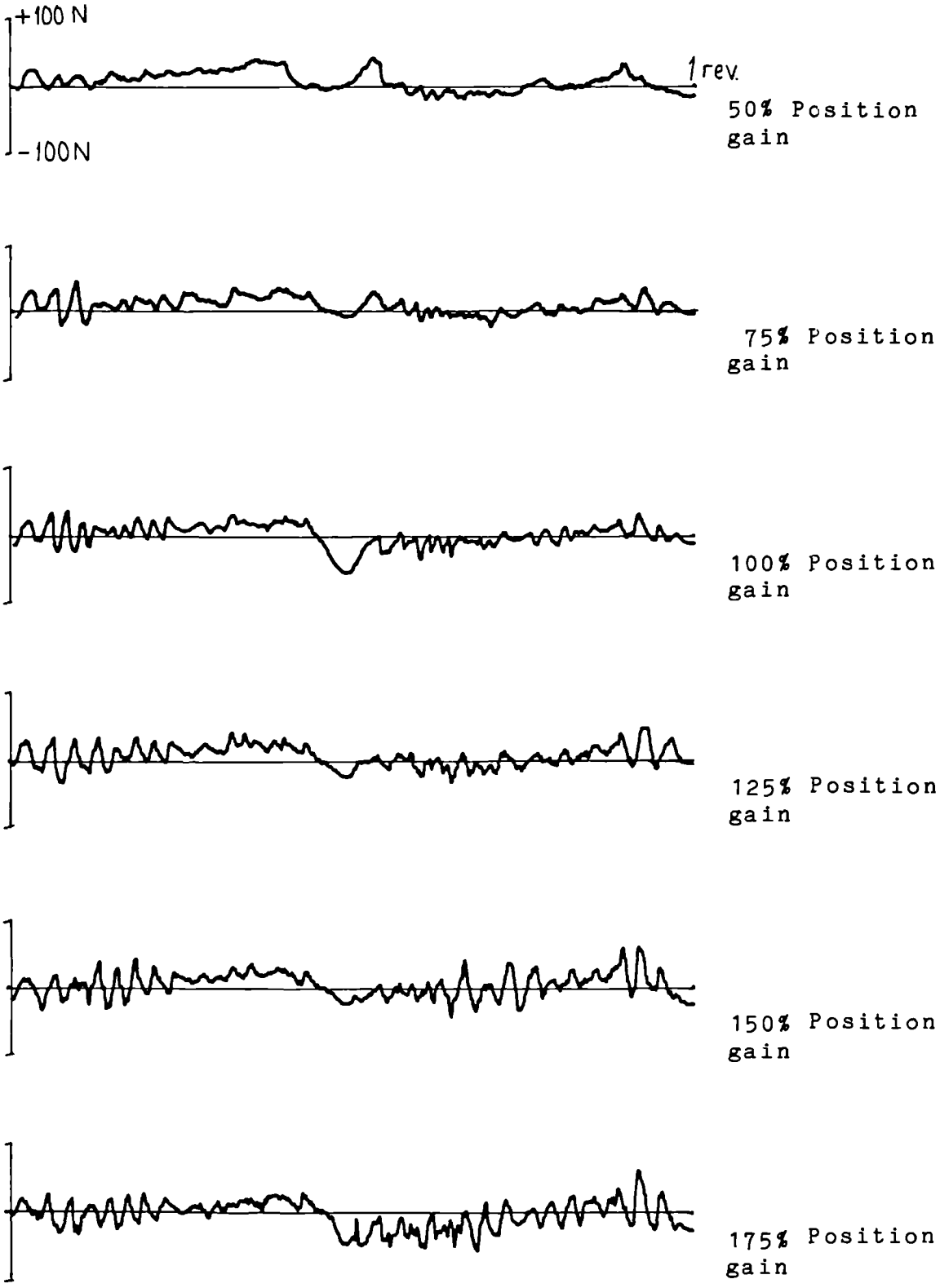

Figure 8.23 Influence of position feedforward gain on radial force

At low gains, the mean radial force remains relatively constant at about 12 N. However, as the gain is increased a corresponding increase in mean radial force occurs. From the derived plots of radial force versus crank angle shown in Figure 8.23, the oscillatory nature of the radial force increases in amplitude with increasing gain. The stability of the system at a gain of 175% could only be maintained by the operator actively damping out this resonant behaviour using his hand.

The excitation of the higher frequency dynamics is a characteristic of using a stiff force sensor. By employing local joint torque feedback it was possible to adjust the servo loop compliance, and in so doing reduce excitation. Table 8.7 lists the results obtained with different levels of joint torque feedback gain, conducted using a position gain of 100% and a force feedback gain of 80%.

From Table 8.7 it can be observed that mean radial force does not vary significantly over the range of results, however, the corresponding plots of radial force against crank angle, reproduced in Figure 8.24 clearly demonstrates the attenuation of the resonant modes even at moderate gains. It should be pointed out that the introduction of local joint torque control reduces the overall 'stiffness' of the associated servo loop. Positional accuracy depends upon the forces acting on the slave manipulator, and when in the gravitational field the mass of the manipulator arm, and its payload, will cause an offset which will depend on the configuration. The magnitude of gravitational forces acting on the pantograph arm have been analyzed in Chapter 6, although active compensation could be included in the digital control software to null its effect.

Joint torque gain (%)	0	20	40	60	80	100
RMS Radial force (N)	13.72	11.42	14.49	14.15	16.97	15.40

Note Crank torque pre-set to 1 Nm

Table 8.7 Results of local joint torque control on performance

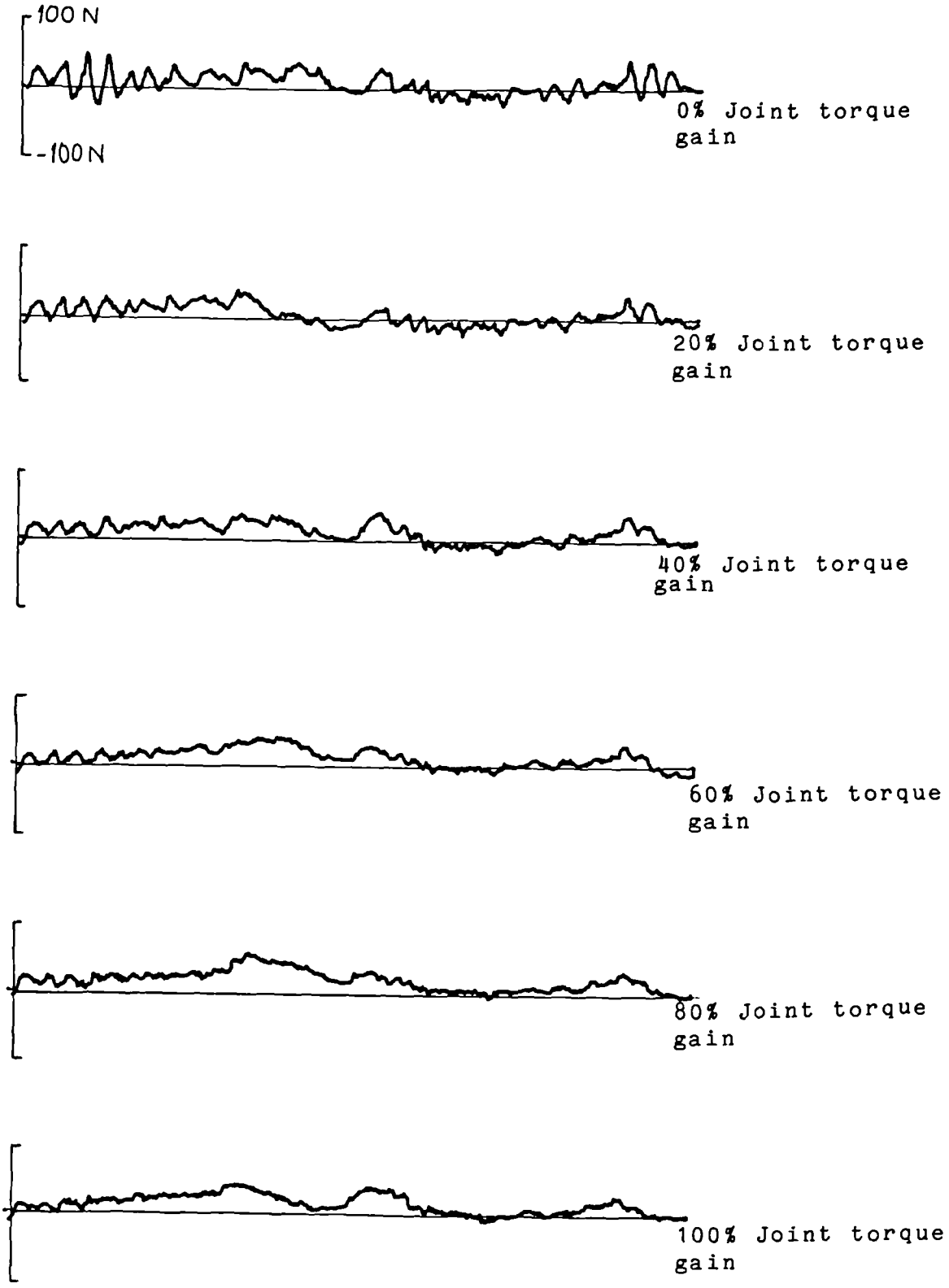

Figure 8.24 Influence of joint torque feedback gain on radial force

8.4.4 Crank performance tests - Position/position control

Fully resolved 'bilateral' position/position control between dissimilar master and slave arms has recently been demonstrated. A preliminary assessment of performance has been carried out to establish the merits, if any, of the control scheme.

Influence of slave-master position gain on performance

Table 8.8 presents the results of initial tests to establish the relationship between position feedback gain, ie. slave-master position gain, for a range of crank torques.

Feedback gain (%)	Crank Torque (Nm) 0.7	1.0	2.0	3.0	4.0
0	51.34	52.67	51.21	49.83	40.61
50	34.31	40.62	47.67	48.03	38.11
100	27.59	31.66	42.37	38.18	33.04
150	25.12	29.65	39.44	36.97	29.81

Table 8.8 Results of position feedback gain on performance

Figure 8.25 presents the results in terms of performance as a function of crank torque for the different feedback gains. The improvement in performance is consistent with increasing gain. However, when compared with similar tests carried out in the position/force mode (see Figure 8.19), performance is substantially reduced at lower crank torques. At higher torques, only a marginal difference in performance is evident. When compared with the manual tests the overall performance is poorer.

Plots of F_{rad} versus crank angle were reproduced for the 1.0 Nm crank torques, as shown in Figure 8.26. With increasing feedback gain, the radial force falls progressively. Also at peak gain there is no indication of the tendency to excite the vibration which was a characteristic of the position/force control mode.

Influence of master-slave position gain on performance

The results of performance tests on the system for different position feedforward gains, ie. master-slave position gain, are given in Table 8.9. A position feedback gain of 100% was selected, and feedforward gains in the range 50 - 200% were evaluated. Servo-compliance was also introduced about each joint, and results from these tests have been included.

Torque feedback (%)	Feedforward gain (%)			
	50	100	150	200
0	43.16	57.98	62.91	55.61
50	27.61	37.04	45.39	42.02

Table 8.9 Results of feedforward gain on performance

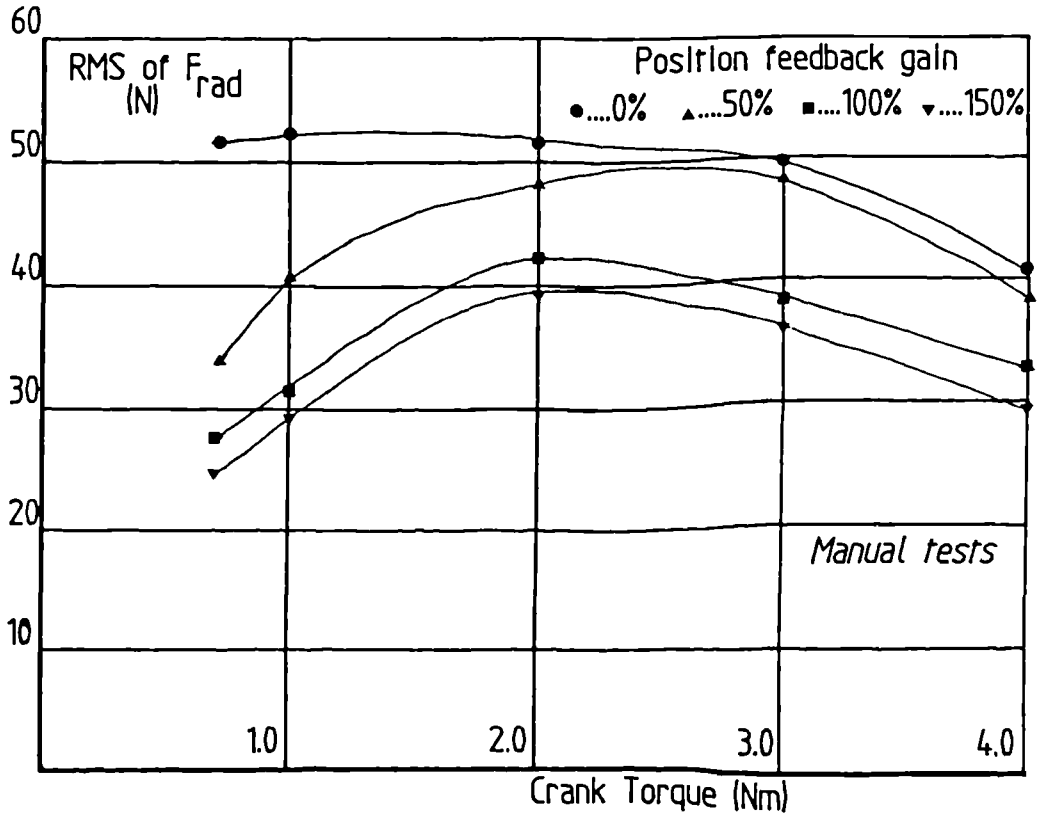

Figure 8.25 *Relationship between F_{rad} and crank torque*

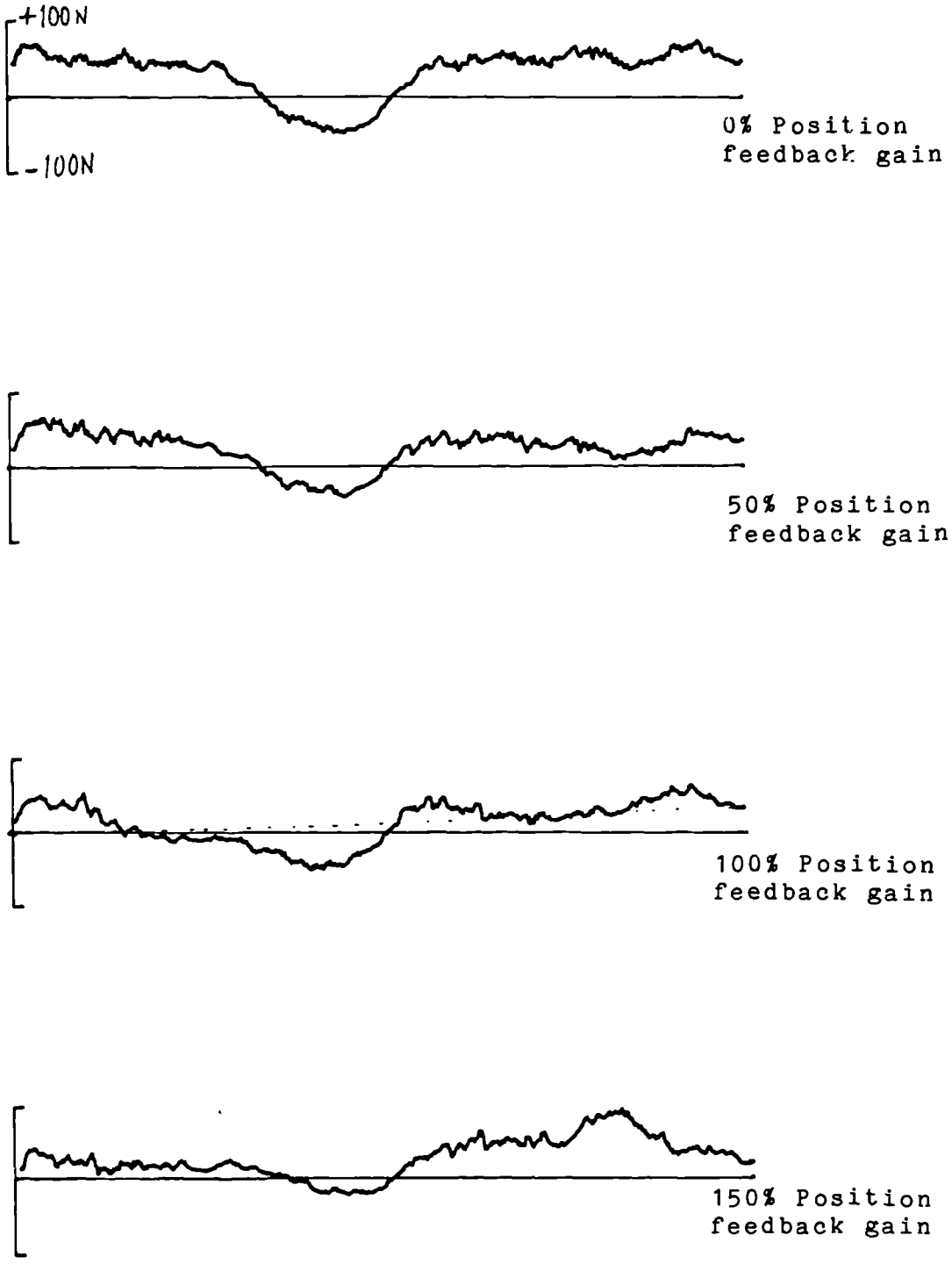

Figure 8.26 Influence of position feedback gain on radial force

Figure 8.27 illustrates the relationship between feedforward gain and performance. The addition of torque feedback brings about a distinct improvement, although when compared with the equivalent position/force strategy performance is considered to be inferior. The benefits of the local joint torque feedback are more noticeable when the plots of radial force versus crank angle are compared, (Figures 8.28 & 8.29). A marked decrease in peak radial force is recorded with joint compliance, although a tendency to excite higher modes is evident at high gain. However, the operator reported that the overall stability of the system was considerably better than that achieved in the position/force scheme, although plots of radial force indicate that higher frequency dynamics are beginning to get excited, and which may be related to the sampling frequency.

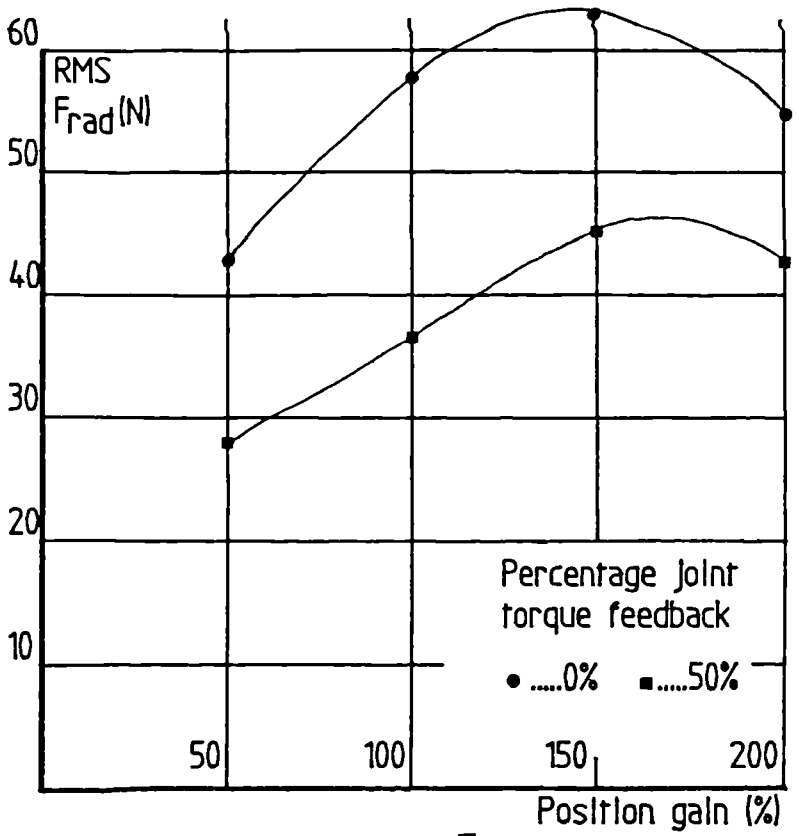

Figure 8.27 *Relationship between* $\bar{F}_{rad}$ *and position gain*

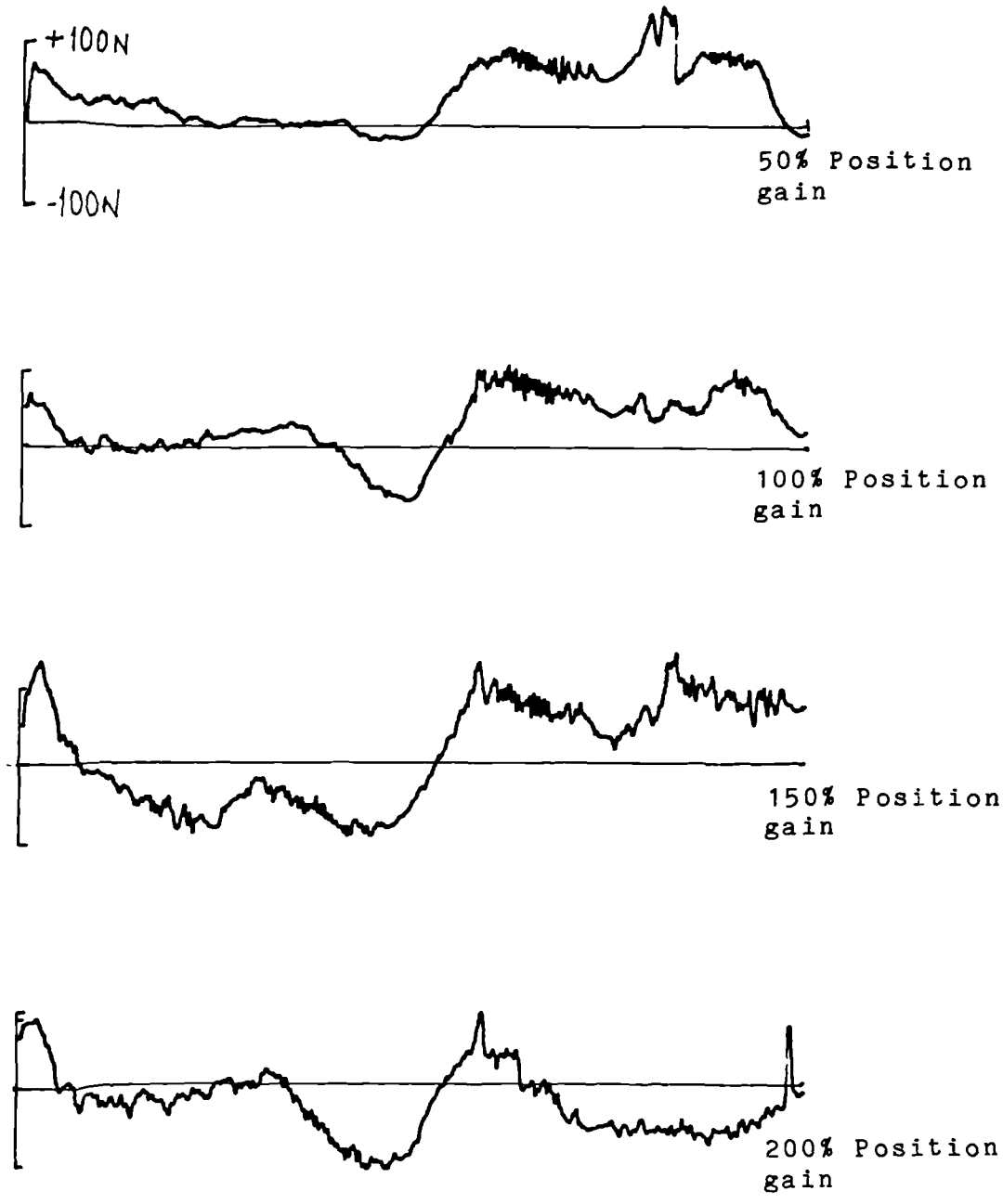

Figure 8.28 Influence of position feedforward gain on radial force - 0% torque feedback

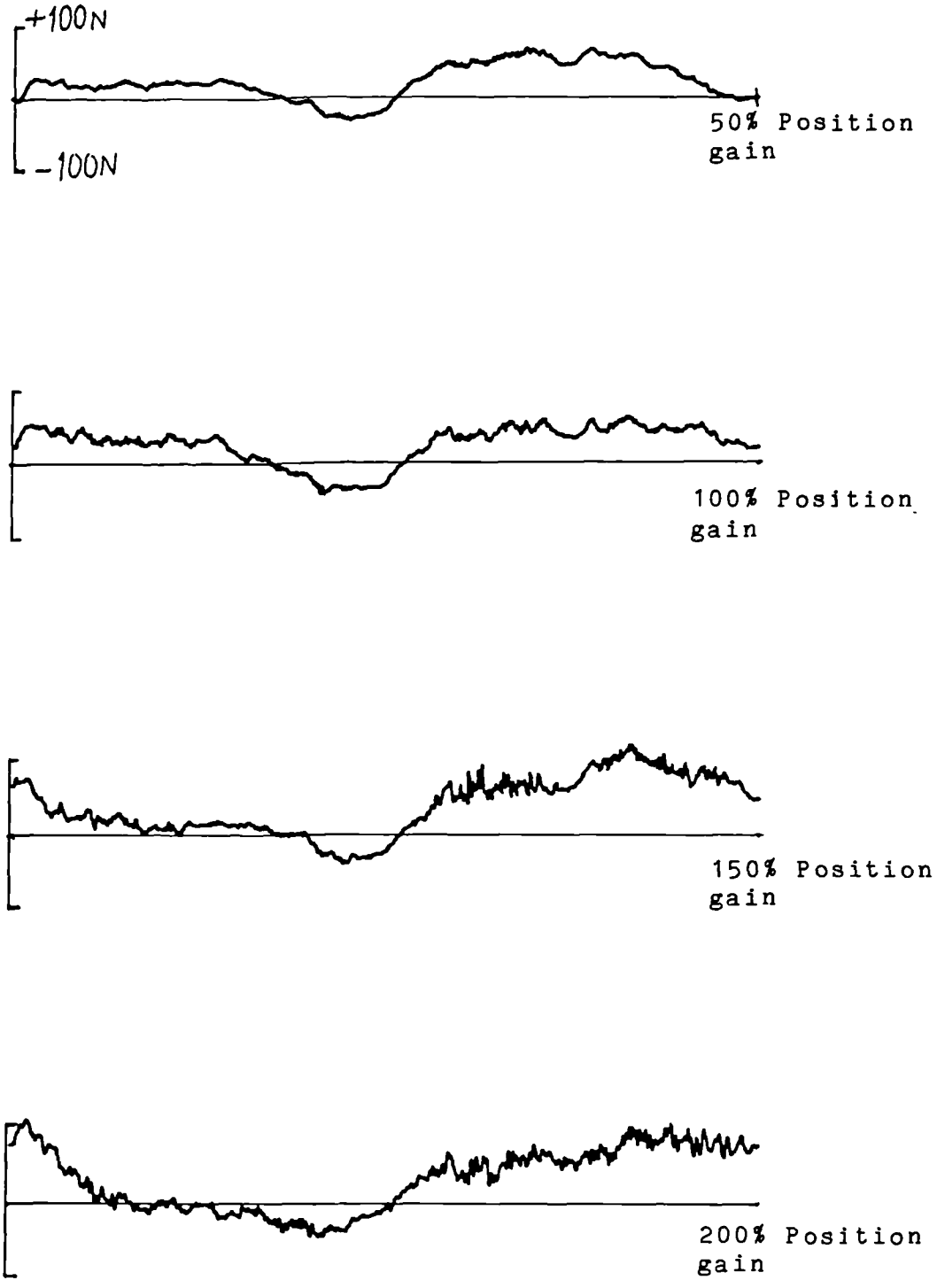

Figure 8.29 Influence of position feedforward gain on radial force - 50% Torque feedback

8.5 Summary of results

The initial peg in hole tests carried out on the replica master-slave system provided qualitative information regarding the performance of the system. The results of a factorial survey have been analyzed using the Fitts index I_d, in terms of task completion time. However, in contrast to earlier work, the correlation between task difficulty and performance was not very good. Evaluation of the influence of force feedback gain has identified an optimum performance between the limits of unilateral and full-bilateral control.

The results of similar tests carried using the generalized position/force control scheme once again demonstrated the advantages of bilateral control, although problems with the control system limited the scope of the test programme. The results obtained using a simple passive compliance (RCC) demonstrated the anti-jamming features off the device and resulted in an improvement in performance.

A novel crank turning test has been developed which makes use of the constrained geometry of the task, and a new performance criteria has been adopted based on the variation in radial crank force which is automatically logged during the test cycle.

Generalized position/force control has been successfully implemented, although some problems with stability were encountered. The tracking between dissimilar master and slave arms has been evaluated, and the advantage of using tight torque control about each joint of the master arm to improve back driving has been demonstrated.

In the bilateral mode, with high force sensitivity there is a tendency to excite forced oscillation at the slave/task interface which in turn affects the stability of the overall man-machine system, and gives rise to severe disturbances at the operators hand. The results obtained from crank tests confirm that optimum performance occurs between the limits of unilateral and bilateral control.

Generalized position/position control has, it is believed been demonstrated for the first time. Although the quality of 'force' feedback was considered inferior to the sensitivity achieved with position/force control, the overall stability was significantly

better. However there may be applications where the lack of force sensitivity is not considered to be a disadvantage, particularly when using high gain hydraulic systems.

Chapter 9

Conclusions and Recommendations for Further Work

A versatile, experimental remote tele-manipulator system has been developed during the course of this investigation. The planar manipulator system can be configured in one of several modes, including replica master-slave control and generalized control between dissimilar master and slave arms. Digital simulation has been used extensively to model elements of the system, and the results obtained have compared favourably with experimental data.

9.1 Conclusions

The investigation has addressed several aspects of tele-manipulation, the most important being the potential advantage of incorporating force feedback to the operator. Whilst the benefits of force reflection have been recognised for some time, little has been done to quantify its contribution.

To gain an understanding of the the behaviour of a force reflecting tele-manipulator system, a planar manipulator system was designed and built to study alternative control schemes.

A number of novel developments have resulted from the investigation, notably, the use of local torque feedback about each joint of the master arm. This feature has enabled improved manipulation of the master arm by allowing it to be easily backdriven by 'reducing' the effective friction in the master arm transmission system.

Generalized control between the articulated master arm and a 'pseudo-pantograph slave arm has also been successfully implemented. The feasability of carrying out fully resolved position/force control relies heavily on a computer to calculate, in real-time, the direct and inverse kinematic transformations between joint and world coordinate frames for master and slave arms. Although problems were experienced with the stability of the system adequate control was eventually achieved, with a

sampling frequency of approximately 100 Hz. Recently the concept has been extended to include fully resolved position/position control between master and slave arms.

The problems associated with the stability of force feedback have been highlighted when attempting to carry out tasks which constrain the motion of the slave manipulator. To establish the reasons behind this a single axis dynamic model of a master-slave system was developed, and digital simulation carried out. The dynamic model was based upon the elbow joint of the articulated manipulator arms, and was considered as a pair of coupled two degree of of freedom systems. A simple representation of the human operator has been included, and good agreement achieved between actual response tests and simulation. A task based on a rigid stop has been used to evaluate the overall response of the man-machine model, and the study has provided a firm foundation on which to develop alternative control schemes.

The response of the system when contact with the rigid stop occurred has highlighted the rapid force transients associated with position/force control, which suggested that structural resonances were being excited giving rise to an oscillatory contact, similar to that experiencied by operators of the rig when the slave manipulator arm contacts the environment. The model was shown to be very sensitive to gain changes, and again evidence from experimental tests supports these findings. Using the model, simulation of a position/position control scheme was also carried out. The results indicated that the characteristic force transient associated with initial contact was not as dominant in this mode, although the overall response of the system was considered somewhat slower. Whilst the scheme was more tolerant of changes in parameters, and as such more robust than the equivalent position/force control scheme, it was considered worthwhile to implement the generalized control scheme in this mode, and to compare its performance with that of conventional position/force control.

This investigation has also tried to establish, by experiment, a quantitative criteria against which the performance of remote tele-manipulator systems can be evaluated. A review of previous work in this field has been carried out, which revealed that the tests normally adopted measure qualitative performance. These are usually based on the time to complete a specific task, or set of tasks, then compared with the same task carried out manually.

Two tasks were adopted to evaluate the performance of the different configurations. Early tests were based on a peg-in-hole task, and task completion time was used as a measure of performance. Whilst the results of these tests are considered to be subjective, a previously unreported relationship between system performance and force feedback gain suggested that optimum operator performance lies somewhere between the limits of unilateral and bilateral control.

A new performance criteria which is based on force information derived from a crank turning task has been developed, and the results of preliminary tests suggest that it may have the potential for providing quantitative information regarding the performance of the system.

Preliminary crank turning tests were carried out using the rig to assess the influence of parameter changes on performance. The constrained trajectory of the crank turning task suggested that the variation in the radial force acting on the crank arm at any time could be considered a valuable indicator of performance. When the task is carried out manually, the operator will attempt to maintain radial forces as small as possible, whilst simultaneously rotating the crank arm around its trajectory as smoothly as possible. When the manipulator system is interposed, the resulting loss in dexterity can be attributed to system gain changes, and in particular to the sensitivity of force feedback gain.

9.2 Recommendations for further work

The facility has potential for further work, however, it would be beneficial to improve the digital control system to allow operation at a higher sampling frequency. This could be achieved by employing independent digital controllers for each manipulator arm, with communication between master and slave being coordinated by a supervisory computer carrying out the necessary kinematic and dynamic transformations.

The problems of high frequency noise encountered when using the DC brushless motors has prevented the pantograph slave arm from being used to its full potential. An alternative method of providing electronic commutation, using optical encoders should help to reduce the cogging action, and if used in conjunction

with the isolation amplifiers should improve noise immunity. It is also suggested that the present analog position transducers be replaced by digital encoders to give better resolution and faster conversion rates, and perhaps implementing a table look-up scheme rather than carrying out trignometric calculations in real-time, which are very time consuming.

The location of the joint mounted force sensors used in the investigation are particularly sensitive to the disturbances associated with the dynamics of the arm, as well as those from the task. Consequently when using high gain force feedback this can be troublesome. Under the circumstances it would be worthwhile to consider the use of multi-component wrist force sensors mounted on both master and slave arms. It will then be possible to compute the inverse force/torque transformation and present the estimated joint torques to the master arm, allowing it to be backdriven. This concept could also be extended to a tele-robotic installation where in principle, a small industrial robot could be used as a 'master' driving a 'slave' robot. The potential of supervisory and real-time path control options, now available on commercial robot manipulators, integrated with high speed microcomputers may make this an attractive solution.

Simulation becomes a valuable tool if used correctly, and the results obtained in this investigation suggest that much information is to be obtained from studying single axis implementation. It is possible to carry out modifications to the existing facility to achieve single axis operation. Thus different dynamics models of the human operator can be assessed, and verification by experiment will prove very interesting, perhaps paving the way for more extensive modelling of multi-degree of freedom remote tele-manipulator systems.

The preliminary results obtained from the crank test indicates that the force information, if correctly interpreted will lead to a quantitative measure of performance, not only for remote manipulator systems, but may also prove to be of use to the medical profession in the diagnosis of muscular and motor-neuron diseases in humans.

Judging by the nature of the force information which has been obtained from the crank tests, it should be possible to carry out a spectral analysis of the frequency and amplitude variation of radial force to identify possible structural and resonant

frequencies in the manipulator and closed-loop man-machine system. This approach will make possible an assessment of the influence of dynamic factors such as compliance, backlash and friction in the manipulator transmission system and to factors associated with servo controllers and control laws, such as sampling frequency and quantization effects.

It is intended, in the near future to carry out a programme of tests, using the crank task, on a prototype 6 degree of freedom hydraulic master-slave system. The tests will be conducted with the multi-component force platform, and the additional degrees of freedom that are constrained by the task should provide valuable information regarding the performance of the system, and in so doing demonstrate the significance of this type of test.

REFERENCES

Abel E, Brown MH, Fischer PJ, Garlick DR & Hanna TT (1987), "The Harwell robotics programme - Telerobotics plus industrial standards", Proc of Int Workshop on Nuclear Robotic Technologies and Applications: Present & Future, Lancaster, Vol 1, Paper 7.

ACSL (1986), Advanced Continuous Simulation Language, Mitchell & Gauthier Associates, Concord, Massachusetts.

Allen RW & M^{c}Ruer D (1979), "The man machine interface - Pursuit control", Automatica, Vol 15, pp 683-686.

Asada H & Kanade T (1983), "Design of direct drive mechanical arms", Trans ASME, J of Vibration Acoustics Stress & Reliability in Design, Vol 105, pp 312-316.

Asada H, Kanade T & Takeyama I (1983), "Control of direct drive arm", J of Dynamic Systems Measurement & Control,Trans ASME, Vol 105, pp 136-142.

Asada H & Slotine JJ (1986), Robot Analysis and Control, Wiley Interscience.

Asea (1982), IRB 6/2 Industrial Robot - Programming Manual, ASEA Industrial Robot Systems, Vasteras, Sweden.

Bejczy AK (1980), "Sensors, controls and man-machine interface for advanced teleoperation", Science, Vol 208, Part 4450, pp 1327-1335.

Bejczy AK & Brooks TL (1980), "Advanced control techniques for tele-operation in earth orbit", Proc of 7th Annual Symp of Assoc of Unmanned Vehicle Systems, Dayton Ohio, pp 59-74.

Bejczy AK & Salisbury JK (1980), "Kinesthetic coupling between operator and remote manipulator", Proc of ASME Int Conf on Computer Technology, San Fransisco, pp 197-211.

Bejczy AK & Handlykken M (1980), "Generalization of bilateral force-reflecting control of manipulators", CISM-IFToMM, Proc of 4th Symposium on Theory & Practice of Robots & Manipulators, Warsaw, Sept 1981, pp 300-312.

Bertsche WR, Pesch AJ & Winget CL (1977), "Operator performance in undersea manipulator systems", Woods Hole Oceanographic Inst, Report No WHOI-77-6.

Bicker R (1985), "Application of force feedback in remote telemanipulation", Final Report, University of Newcastle upon Tyne, May 1985.

Bicker R & Maunder L (1985), "Some developments in tele-manipulators", Int Summer School on the Practice of Robots, October 1985.

Bicker R & Maunder L (1986),"Force feedback in tele-manipulators" CISM-IFToMM, Proc of 6th Int Symp on Theory and Practice of Robots and Manipulators, Cracow, pp 211-218.

Bicker R & Maunder L (1987a), "Force control in remote teleoperation", Proc of Int Workshop on Nuclear Robotic Technologies, Lancaster, Vol 3, Paper 19.

Bicker R & Maunder L (1987b), "The development of performance criteria for telemanipulators", CISM-IFToMM, Proc of 7th Int Conf on Theory of Machines & Mechanisms, Seville, pp 1191-1194.

Bicker R, Tsakalotos OI & Pittaris (1987),"Advances in the design and control of flexible manipulators", SME, Proc of Robots 11 / 17th ISIR, Chicago, Paper MS87-426.

Bicker R, Burn K & Maunder L (1988), "The man-machine interface in remote manipulation", Ergonomics Society, Proc of Int Symp on Teleoperation and Control, pp 151-158.

Bicker R, Daadbin A & Rosinski Y (1989), "Monitoring of vibration in industrial robots", ASME, 12th Biennial Conf on Mechanical Vibration & Noise, Montreal, Sept 1989, (to be presented)

Bicker R (1989), "Simulation of a one degree of freedom remote manipulator", United Kingdom Simulation Council, 3rd European Simulation Congress, Edinburgh, Sept 1989, (to be presented).

Book WJ & Field W (1980),"Experiments relating task & manipulator characteristics", Proc of Int Conf on Cybernetics & Society, pp 225-226.

Book WJ & Hannema DP (1981),"Master slave manipulator performance for various dynamic characteristics and positioning task parameters", Trans IEEE, J of Systems Man & Cybernetics, Vol SMC-10, Part 11, pp 764-771.

Booker RA & Smith GW (1973), "X- Reference bilateral control for the shuttle attached manipulator", Proc of Intercon Int Conf & Exposition, IEEE, Vol 4,Part 40, pp 1-12.

Brown JW (1976), "Shuttle remote manipulator system workstation -- Man-machine engineering", Human Factors Society, Proc of 6th Congress of Int Ergonomics Assoc, Santa Monica, CA, pp 149-153.

Burn K (1979), "The man-machine interface", Ph D Thesis, Newcastle upon Tyne, (to be published).

Causer R (1981), Micro-manipulator, UK Patent No. 7931801.

Cole GV (1986), "A hydraulic powered manipulator for the nuclear industry", BHRA, Proc of the 7th Int Fluid Power Conf, Bath England, Sept 1986, pp 231-236.

Cole GV & M^{c}Pherson G (1988), "Hydraulic manipulator offers reliability and easy maintenance", Nuclear Engineering International, April 1988, pp 39-42.

CPM (1980), Digital Research, Pacific Grove, California.

Denavit J & Hartenberg RS (1955), "Kinematic notation for lower pair mechanisms based upon matrices", Trans ASME, J of Applied Mechanics, June 1955, pp 215-221.

Doetsch KH (1977), "The remote manipulator system for the space shuttle orbiter", Proc of Deutsche Gesellschraft fur Luft und Raumfahrt (DGLR), Berlin, Sept 1977, pp 261-269.

Drake SH (1977), "Using compliance in lieu of sensory feedback for automatic assembly", Report NSF/RA-770846, Charles Stark Draper Lab, Cambridge, Massachusetts.

Draper JV, Herndon N, Weil BS & Moore WE (1987),"Effects of force reflection on servomanipulator task performance", American Nuclear Society, Proc of ANS 1987 Int Topical Meeting on Remote Systems & Robotics in Hostile Environments, Washington, pp 654-660.

Ease+ACSL (1987), Ease+Acsl User Application Manual, Expert-Ease Systems Inc, Concord, Massachusetts.

Electro-Craft (1980), DC Motors Speed Controls & Servo Systems, Electro-Craft Corporation, Hopkins, Minnesota.

Ferrell WR (1965), "Remote manipulation with transmission delay", Trans IEEE, J of Human Factors in Electronics,Vol HFE-6,pp 24-32.

Ferrell WR (1966),"Delayed force feedback", Trans IEEE, J of Human Factors in Electronics, Vol-HFE8, pp 449-455.

Ferrell WR & Sheridan TB (1967), "Supervisory control of remote manipulation", Trans IEEE, Spectrum, October 1967, pp 81-88.

Ferrell WR (1972), "Command language for supervisory control of remote manipulation", NASA, Proc of 1st Int Conf on Remotely Manned Systems, Sept 1972, Pasadena, pp 369-373.

Ferrell WR (1977), "Adaptive supervisory control of remote manipulation", IEEE, Proc of 1977 Int Conf on Decision and Control, pp 549-552.

Fitts P (1954), "Information capacity of the human motor system in controlling the amplitude of movement", J of Experimental Psychology, Vol 47, Part 6, pp 381-391.

Flatau CR, Vertut J, Giulbaud J-P, Germond J-C, Glachet C (1972), "MA22 - A compact bilateral servo master-slave manipulator", American Nuclear Society, Proc of 20th Conf on Remote Systems Technology, pp296-302.

Flatau CR, Greeb FJ & Booker RA (1972), "Preliminary correlations between control modes of manipulator systems and their performance indices", NASA, Proc of 1st Int Conf on Remotely Manned Systems, Pasadena, pp 189-198.

Flatau CR (1973), "The manipulator as a means of extending our dexterous capabilities to larger and smaller scales", American Nuclear Society, Proc of 21st Conf on Remote Systems Technology, pp 47-50.

Flatau CR (1977), "SM 229 - A new compact servo master slave manipulator", American Nuclear Society, Proc of 25th Int Conf on Remote Systems Technology, pp 169-173.

Freedy A & Weltman G (1977), "Performance improvement in remote manipulation with time delay by means of a learning system", NASA, Proc of 1st Int Conf on Remotely Manned Systems, Pasadena, pp 397-407.

Galbiati L, Mancini C & Raimondi T, (1964), "A compact and flexible servo system for master slave electric manipulators", American Nuclear Society, Proc of 12th Int Conf on Remote Systems Technology, pp 73-87.

Goertz RC (1952a), "Fundamentals of general purpose remote manipulators", Nucleonics, Vol 10, Part 11, pp 36-42.

Goertz RC (1952b), "A force reflecting positional servo mechanism", Nucleonics, Vol 10, Part 11, pp 43-45.

Goertz RC et al (1954), "General purpose manipulators", Nucleonics, Vol 12, Part 11, pp 45-49.

Goertz RC (1964), "Manipulator systems development at Argonne Nat Lab. (ANL)", American Nuclear Society, Proc of 12th Int Conf on Remote Systems Technology, pp 117-136.

Handlykken M & Turner T (1980), "Control system analysis and synthesis of a 6 dof hand controller", IEEE, Proc of 19th Conf on Decision and Control, pp 1197-1205.

Hannaford B & Anderson (1988), "Experimental and simulation studies of hard contact in force reflecting teleoperation", IEEE, Proc of Int Conf on Robotics and Automation, pp 584-589.

Hill JW (1979), "Study of modelling and evaluation of remote manipulation tasks with force feedback", Stanford Research Institute, Jet Propulsion Lab Final Report No. 95-5178.

Inland, Direct Drive DC Servo-Motors, Kollmorgen Corporation, Sierra Vista, Arizona

Jelatis DG (1976), "Characteristics and evaluation of master slave manipulators", National Bureau of Standards, Workshop on Performance and Evaluation of Programmable Robotas and Manipulators, Washington, Report No SP-459, pp 141-146.

Jex HR & Magdaleno RE (1969), "Corroborative data on normalization of human operator remnant",Trans IEEE,Vol 10,p 137.

Kumar P, Truss P & Wagner-Bartak CG (1979), "System design features of the space shuttle remote manipulator", ASME-IFToMM, Proc of 5th World Congress on Theory of Machines & Mechanisms, Montreal, pp 839-842.

Levison WH, Baron S & Klienman DL (1969), "A model for controller remnant", Trans IEEE, J on Man-Machine Systems, Vol 10, p 101.

Luh JYS, Walker MW & Paul RP (1980), "On-line computational scheme for mechanical manipulators", Trans ASME, J of Dynamic Systems Measurement & Control, Vol 102, pp 66-76.

M^{c}Ruer D & Krendel ES (1974), " Mathematical models of human pilot behaviour", AGARDograph 188.

M^{c}Ruer D (1980), "Human dynamics in man-machine systems", Automatica, Vol 16, pp 237-253.

M^{c}Govern DE (1974a), "Comparison of two manipulators using a standard task of varying difficulty", ASME, Proc of ASME Annual Meeting, New York, Paper No. 74-WA-BIO.4, pp 106-110.

M^{c}Govern DE (1974b), "Task analysis scheme with implications for supervisory control of remote manipulators", IEEE, Proc of Int Conf on Systems Man and Cybernetics, pp 462-466.

M^{c}Govern DE (1977), "Investigation of supervisory control of remote manipulation", IFToMM, J of Mechanism and Machine Theory, Vol 12, pp 3-9.

Martin HL, Satterlee PE & Bolfing BJ (1982), "Distributed digital processing for servo manipulator control", American Nuclear Society, Proc of 30th Conf on Remote Systems Technology, Washington, pp 117-123.

Mason MT (1981), "Compliance and force control for computer controlled manipulators", Trans IEEE, J on Systems, Man & Cybernetics, Vol SMC-11, No 6, pp 418-432.

Matsushima K & Nagai A (1981), "On the Remote Mini Manipulator 'Tiny Mini' Control - Its arm and gripper", Proc of 11th Int Symp on Industrial Robots, Part 11A-6, pp 645-653.

Matsushima K (1984), "Development of servo manipulators", Proc of Int Computer Symposium, Taipei Tiawan.

Microsoft (1985), Microsoft Corporation, Bellevue, California.

Moore-Reed, Permanent Magnet DC Motors, Andover, England.

Mosher RS (1967), "Hardiman to Handyman", Society of Automotive Engineers, Proc of Automotive Engineering Congress, Paper 670088, Detroit, Michigan, Jan 1967.

Paine G (1979), "Microprocessors for real time displays and control of space teleoperators", IEEE, Proc of 1st Int Symp on Mini and Micro Computers in Control, San Diego, pp 144-151.

PAR Systems, 'TRU-Motion' master-slave manipulator, Programmed & Remote Systems Corporation, St Paul, Minnesota, October 1974.

Paul RP (1972), "Modelling, trajectory calculation and servoing of a computer controlled arm", Stanford Research Institute, Technical Memo AIM-177 (STAN-SC-72-311).

Paul RP, Shimano B & Mayer GE (1981a),"Kinematic control equations for simple manipulators", Trans IEEE, J of Systems Man & Cybernetics, Vol SMC-11, Part 6, pp 449-455.

Paul RP, Shimano B & Mayer GE (1981b), "Differential kinematic equations for simple manipulators", *Trans IEEE, J of Systems Man* & Cybernetics, Vol SMC-11, Part 6, pp 456-460.

Paul RP (1981), Robot Manipulators: Mathematics, Programming, & Control,MIT Press.

Perratt D (1987), "The CEGB advanced robotics system developments for in-reactor inspection and repair", Proc of Int Workshop on Nuclear Robotic Technologies and Applications : Present & Future, Lancaster, Paper 3.

Raibert MH & Craig JJ (1981), "Hybrid position force control of manipulators", Trans ASME, J of Dynamics Systems Measurement & Control, Vol 102, pp 126-133.

Raimondi T (1976), "Remote handling in the Joint European Torus (JET) Fusion Experiment", American Nuclear Society, Proc of 24th Conf on Remote Systems Technology, Washington, pp 188-195.

Rouse WB (1980), Systems Engineering Models of Human-Machine Interaction,System Science & Engineering, Series Volume 6, North Holland.

Saenger EL & Pegden CD (1972), "Terminal pointer hand controller and other recent teleoperator controller concepts", NASA, Proc of 1st Int Conf on Remotely Manned Systems, Pasadena, pp 327-336.

Salisbury JK & Craig JJ (1982),"Articulated hands - force control and kinematic issues", Int J of Robotics Research, Vol 1, Part 1, pp 4-17.

Sanders BC, Abel E, Brown MH, Cole GV & White LJ (1987), "An overview of the UKAEA active handling and robotics programme", American Nuclear Society, Proc of ANS 1987 Int Topical Meeting on Remote Systems and Robotics in Hostile Environments, Washington, pp 14-21.

Sheridan TB & Ferrell WR (1963), "Remote manipulative control with transmission delay", Trans IEEE, J on Human Factors in Electronics, Vol HFE-4, pp 25-29.

Sheridan TB & Ferrell WR (1974),Man-Machine Systems: Information, Control & Decision Models of Human Performance, MIT Press, Cambridge, Massachusetts.

Sheridan TB (1976a), "Towards a general model of supervisory control", Proc of Int Symp on Monitoring Behaviour and Supervisory Control", Berchtesgaden, pp 271-280.

Sheridan TB (1976b), "Modelling supervisory control of robots", CISM-IFToMM, Proc of 2nd Symp on Theory & Practice of Robots & Manipulators, Warsaw, pp 421-434.

Sheridan TB (1976c), "Evaluation of tools and tasks : reflections on the problem of specifying robot manipulator performance", National Bureau of Standards, Workshop on Performance and Evaluation of Programmable Robots and Manipulators, Report SP-459, pp 27-38.

Simbol (1987), *Cambirdge Control ltd, Cambridge, England.*

Starr GP (1979), "A comparison of control modes for time-delayed remote manipulation", Trans IEEE, J on Systems, Man & Cybernetics, Vol SMC-9, No 4, pp 241-246.

Stone RJ (1988), "Future trends in man-machine interface design for telerobotics in hazardous environments", CERT, Workshop on Designing the Human-Machine Loop, Toulouse, June 1988.

Suzuki M, Ozaki N, chikawa Y, asai M, Kato K & Uno T (1982), "A bilateral servo manipulator for remote maintenance in nuclear facilities", American Nuclear Society, Proc of 25th Conf on Remote Systems Technology, pp 138-145.

Tan N (1984), "The dynamics of articulated mechanisms", PhD Thesis, University of Newcastle, September 1984.

Tanie K, Komoriya K, Kaneko M, Ohno T & Fukuda T (1986), "Dynamics reflection bilateral remote control", CISM-IFToMM, Proc of 6th Int Symp on Theory and Practice of Robots and Manipulators, Warsaw, Sept 1986.

Unimation, Programming Manual - Users Guide to VAL II : 398T1, Unimation Incorporated, Danbury Connecticut, May 1985.

Verplank WL (1976), "Research on remote manipulators at NASA Ames research centre", National Bureau of Standards, Workshop on the Performance and Evaluation of Programmable Robots and Manipulators, Report No SP-459, pp 259-231.

Vertut J et al (1981), "Short transmission delay on a force reflective bilateral manipulator", CISM-IFToMM, Proc of 4th Int Symp on Theory and Practice of Robots and Manipulators, pp 0-20.

Vertut J (1981),"Prospects for robotics in the nuclear industry", Revue Generale Nucleaire, Part 1, pp 6-12. (translation)

Vertut J, Papot L, ossignol C & Tiret A (1973), "Contribution to define a dexterity factor for manipulators", American Nuclear Society, Proc of 21st Int Conf on Remote Systems Technology, pp 38-46.

Watson PC & Drake SH (1975), "Pedestal wrist force sensors for automatic assembly", Proc of 5th International Symposium on Industrial Robots, Chicago, pp 501-511.

Whitney DE (1969), "Resolved Motion Rate Control (RMRC) of manipulators and human prostheses", Trans IEEE, J of Man Machine Systems, Vol MMS-10, Part 2, pp 47-53.

Whitney DE, Book WJ & Lynch PM (1974), "Design and control considerations for industrial and space manipulators", Proc of Joint Conf on Automatic Control, Austin, pp 591-598.

Whitney DE (1982),"Quasi-static assembly of compliantly supported rigid parts", Trans ASME, J of Dynamics Systems Measurement & Control, Vol 104, pp 65-77.

Wilt DR, Pieper DL, Frank AS & Glenn GG (1977),"An evaluation of control modes in high gain manipulator systems", CISM-IFToMM, J of Mechanism and Machine Theory, Vol 12, pp 373-386.

Yamamoto M, Inada E, Maeda M, Tosha K, Kawai S & Takahashi J (1982),"Remote maintenance equipment for hot cell facilities", American Nuclear Society, Proc of 30th Conf on Remote Systems Technolgy, Washington, Vol 2, pp 132-137.

APPENDIX I

PANTOGRAPH SIMULATION PROGRAM

Appendix I.1 - Equations of Motion

Appendix I.2 - Pascal Program Source Code

Appendix I.1 - Equations of Motion

The kinematic relationship between the pantograph arm input / output links and the crank is shown in Figure I.1.

The following nomenclature has been used :

X,Y	-	Position of pantograph output link
X_c,Y_c	-	Position of crank centre of rotation
r_c	-	Crank radius (m)
r_1	-	Radius of input link (m)
r	-	Radius of terminal link from main axis (m)
r_3	-	Terminal link length (m)
α	-	Main body angle (rads)
α_3	-	Terminal link absolute angle (rads)
θ	-	Crank angle (rads)
k	-	Kinematic pantograph ratio

First derivative is denoted dx/dt, and second derivative d^2x/dt^2, or can be expressed using dot notation.

The following kinematic relationships exist

$$X_c = X + r_3.\text{Cos}\,\alpha_3 + r_c.\text{Cos}\,\theta$$

$$Y_c = Y + r_3.\text{Sin}\,\alpha_3 - r_c.\text{Sin}\,\theta$$

.....{I.1}

$$r^2 = X^2 + Y^2$$

$$r = k.r_1$$

and

$$\text{Tan}\,\alpha = Y/X \quad \text{or} \quad \alpha = \text{Tan}^{-1}\,Y/X$$

.....{I.2}

Assuming $\alpha_3 = 0$, then since {I.1} are functions of θ only,

Rearranging {I.1} gives

$$X = X_c - r_3 + r_c.\text{Cos}\,\theta$$

$$Y = Y_c + r_c.\text{Sin}\,\theta$$

Equations of motion - Obtained using partial derivatives.

The velocities $\dot{X}$ and $\dot{Y}$ are given by

$$\dot{X} = \dot{\theta}\, r_c.\mathrm{Sin}\,\theta$$

$$\dot{Y} = \dot{\theta}\, r_c.\mathrm{Cos}\,\theta \qquad \text{.....\{I.3\}}$$

and the accelerations $\ddot{X}$ and $\ddot{Y}$ from

$$\ddot{X} = \ddot{\theta}\, r_c.\mathrm{Sin}\,\theta + \dot{\theta}^2 r_c.\mathrm{Cos}\,\theta$$

$$\ddot{Y} = \ddot{\theta}\, r_c.\mathrm{Cos}\,\theta - \dot{\theta}^2 r_c.\mathrm{Sin}\,\theta$$

for constant crank velocity, ie. $\ddot{\theta} = 0$, then

$$\ddot{X} = \dot{\theta}^2 r_c.\mathrm{Cos}\,\theta$$

$$\ddot{Y} = -\dot{\theta}^2 r_c.\mathrm{Sin}\,\theta \qquad \text{.....\{I.4\}}$$

To find angular and radial components of velocity and acceleration it is required to transform into the approporiate coordinate frames. Therefore,

$$\frac{dr}{dt} = \frac{\partial r}{\partial X}.\frac{dX}{dt} + \frac{\partial r}{\partial Y}.\frac{dY}{dt}$$

and

$$\frac{d^2r}{dt^2} \quad \frac{\partial^2 r}{\partial x^2}.\frac{dX}{dt}^2 + \frac{\partial r}{\partial X}.\frac{d^2X}{dt^2} + 2\frac{\partial^2 r}{\partial Y \partial X}.\frac{dX}{dt}.\frac{dY}{dt} + \frac{\partial r}{\partial Y}.\frac{d^2Y}{dt^2} + \frac{\partial^2 r}{\partial Y^2}.\frac{dY}{dt}^2$$

where

$$\partial r/\partial X = X/r\,, \qquad \partial r/\partial Y = Y/r\,,$$

$$\partial^2 r/\partial X^2 = Y^2/r^3\,, \quad \partial^2 r/\partial Y^2 = X^2/r^3\,,$$

and

$$\partial^2 r/(\partial X\, \partial Y) = -XY/r^3$$

Using dot notation can be expressed,

$$\dot{r} = X\dot{X}/r + Y\dot{Y}/r$$

and

$$\ddot{r} = X\ddot{X}/r + Y\ddot{Y}/r + \dot{\alpha}^2 r$$

.....{I.5}

Similarily,

$$\alpha = \mathrm{Tan}^{-1}(Y/X)$$

then

$$\frac{d\alpha}{dt} = \frac{\partial\alpha}{\partial X}\frac{dX}{dt} + \frac{\partial\alpha}{\partial Y}\frac{dY}{dt}$$

and

$$\frac{d^2\alpha}{dt^2} = \frac{\partial^2\alpha}{\partial X^2}\frac{dX}{dt}^2 + \frac{\partial\alpha}{\partial X}\frac{d^2X}{dt^2} + 2\frac{\partial^2\alpha}{\partial X\partial Y}\frac{dX}{dt}\frac{dY}{dt} + \frac{\partial^2\alpha}{\partial Y^2}\frac{dY}{dt}^2 + \frac{\partial\alpha}{\partial Y}\frac{d^2Y}{dt^2}$$

where

$$\partial\alpha/\partial X = -Y/r^2, \qquad \partial\alpha/\partial Y = X/r^2$$

$$\partial^2\alpha/\partial X^2 = 2XY/r^4, \quad \partial^2\alpha/\partial Y^2 = -2XY/r^4$$

and

$$\partial^2\alpha/(\partial X\,\partial Y) = (Y^2 - X^2)/r^4$$

Using dot notation, can be expressed as

$$\dot{\alpha} = (X\dot{Y} - Y\dot{X})/r^2$$

and

$$\ddot{\alpha} = X\ddot{Y}/r^2 - 2\dot{\alpha}\dot{r}/r - Y\ddot{X}/r^2$$

.....{I.6}

Denotes centre of Mass of Link

Note Crank Radius = 100 mm
Crank Angular Velocity ω (Rads/Sec)
Crank Torque, Tc (Nm)
Predicted joint torques Tx, Ty, Tø

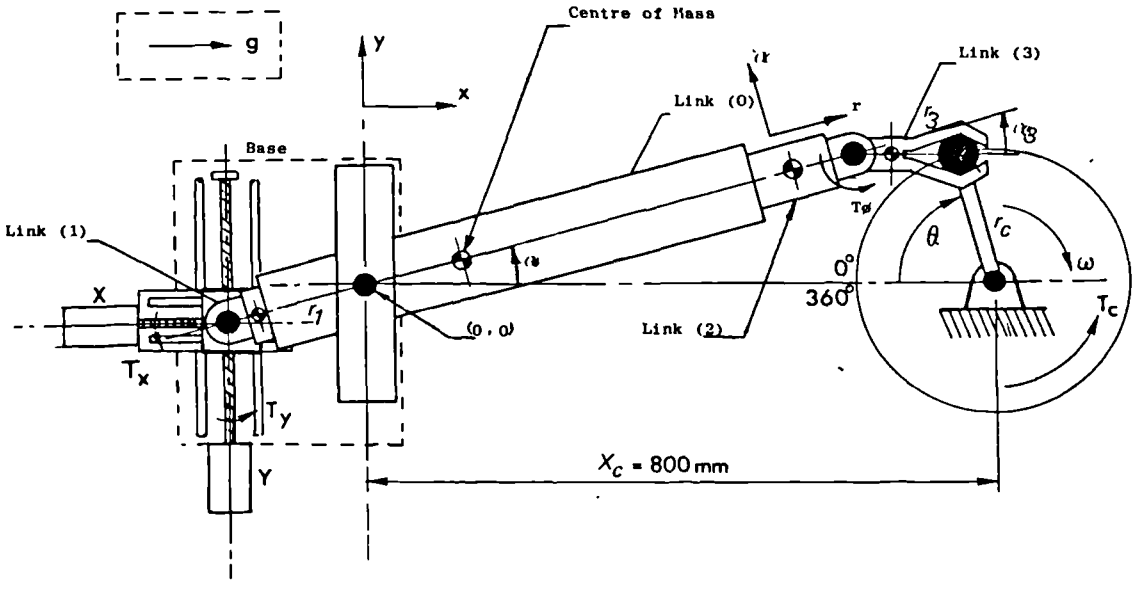

Figure I.1 Kinematics of a simulated crank turning test

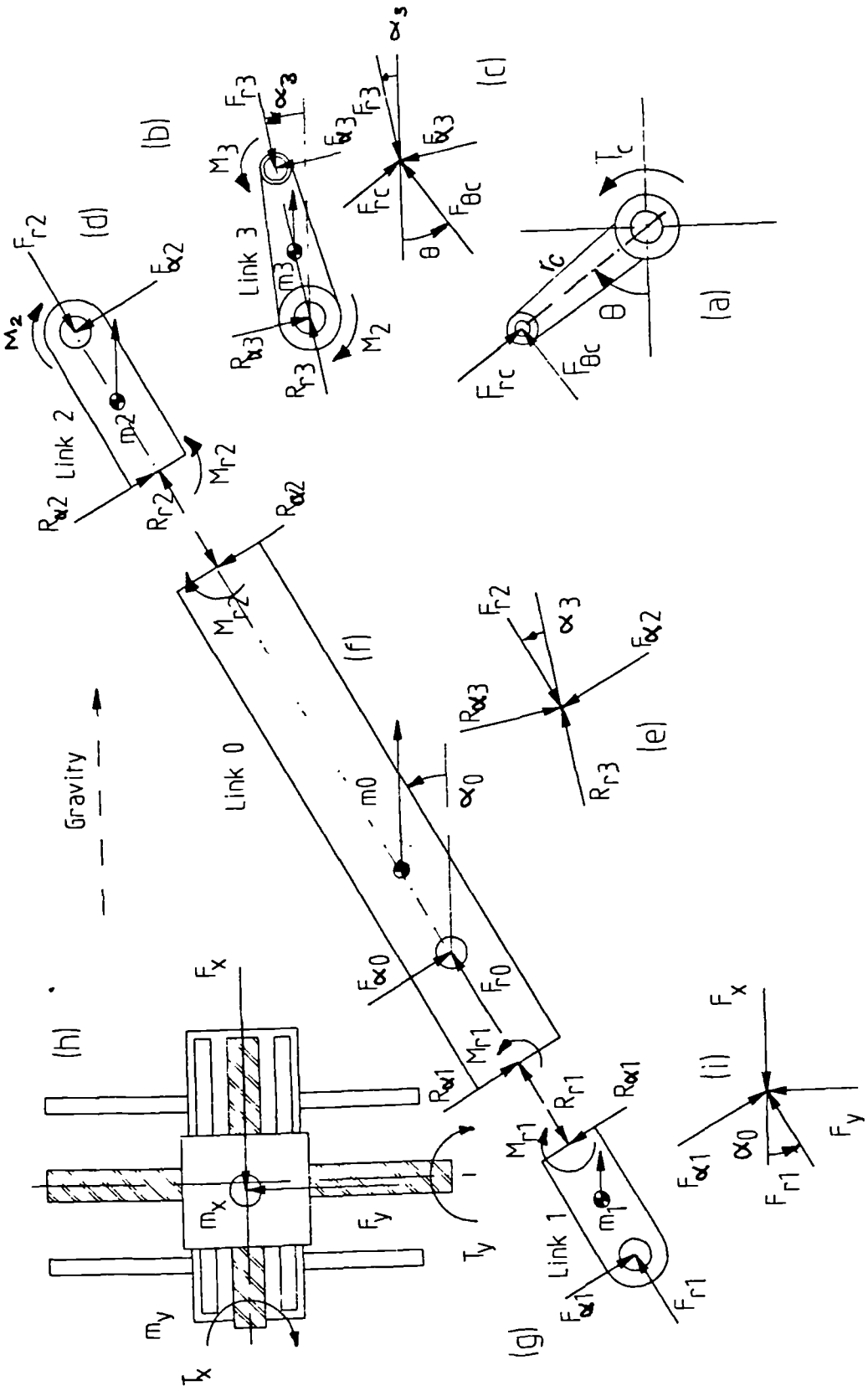

Figure I.2 Free body diagrams of pantograph arm elements

Listing of Pantograph simulation program - SIMULATE.PAS

```
PROGRAM ANALYSIS( INPUT, OUTPUT);

                  {FORCE/INERTIAL ANALYSIS OF 3 D.O.F. SLAVE ARM }
                  {BASED ON HARWELL 'PSEUDO-PANTOGRAPH' MECHANISM}

        {***THIS PROGRAM INCLUDES DYNAMIC / INERTIAL FORCES***}


CONST MASS0=7.73 ; MASS1=2.40 ; MASS2=3.85 ; MASS3=0.40 ;
         INERTIA0=0.277 ; INERTIA1=0.020 ; INERTIA2=0.090 ;INERTIA3=0.0;
         RADIUSG0=0.176 ;RADIUSG1= 0.126 ;RADIUSG2=0.228 ;RADIUSG3=0.050;
         {RADIUSG*=RELATIVE TO LINK PIVOT POINT}
          K=4;C1=0; C2=0; C3=0; RADIUS3=0.200;

VAR THETA, THETADOT, THETA2DOT, RADIUS, RADIUSDOT, RADIUS2DOT,
         PHIDOT, PHI2DOT, FRAD3,FPHI3,MOMENT3,FRAD2, FTHETA2,MOMENT2,
         FRAD1,FTHETA1,FRAD0,FTHETA0, FORCEX, FORCEY,THETACOS,THETASIN,
         PHICOS,PHISIN,GRAVITY,X,Y,X1,Y1,R,OMEGA,OMEGADOT,DEGREES,
         ROMEGACOS,ROMEGASIN,XDOT,YDOT,X2DOT,Y2DOT,FX3,FY3,
         TORQUEFORCE,EXFX3,EXFY3:REAL;

         INDEX:INTEGER;


PROCEDURE TORQUE;

        CONST PITCH=0.005; PI=3.14159; FRICTX=0.0;FRICTY=0.0;
              MASSX=1.54; MASSY=5.34;

        VAR   TORQUEX, TORQUEY, MSPEEDX, MSPEEDY, TORQUET, MSPEEDT : REAL;

        BEGIN

                TORQUEX:=(MASSX*X2DOT+FORCEX+MASSX*GRAVITY+FRICTX*XDOT)
                         *PITCH/(2*PI);

                TORQUEY:=(MASSY*Y2DOT+FORCEY+FRICTY*YDOT)*PITCH/(2*PI);

    MSPEEDX:=XDOT*60/PITCH;

    MSPEEDY:=YDOT*60/PITCH;

TORQUET:=MOMENT2/88;

    MSPEEDT:=PHIDOT*88*60/(2*PI);

WRITELN(TORQUEX,' ',TORQUEY,' ',TORQUET,' ',MSPEEDX,' ',MSPEEDY,
' ',MSPEEDT);
        END;
```

Listing continued - SIMULATE.PAS

```
{DISPLAY USER INPUT DATA}


BEGIN

INDEX:=0;
FOR INDEX:= 1 TO 10 DO

BEGIN
WRITELN;
WRITELN;
WRITE('   ','INPUT GRAVITATIONAL ACCELERATION (M/S2)=  ');
READ(GRAVITY);
WRITELN;

{SET KINEMATIC CONDITIONS}

WRITE('   ','ENTER CRANK X-POSITION CENTRE (M)=  ');
READ(X1);
WRITELN;

WRITE('   ','ENTER CRANK Y-POSITION CENTRE (M)=  ');
READ(Y1);
WRITELN;

WRITE('   ','ENTER CRANK PIVOT RADIUS (M)=  ');
READ(R);
WRITELN;

WRITE('   ','INPUT CRANK SPEED (RAD/SEC)=  ');
READ(OMEGADOT);
WRITELN;

{ENTER EXTERNAL FORCE/MOMENTS AT TERMINAL}

WRITE('   ','ENTER EXTERNAL FORCE X-DIRECTION (N)=  ');
READ(EXFX3);
WRITELN;

WRITE('   ','ENTER EXTERNAL FORCE Y-DIRECTION (N)=  ');
READ(EXFY3);
WRITELN;

WRITE('   ','ENTER MOMENT TORQUE AT TERMINAL DEVICE (NM)=  ');

READ(MOMENT3);
WRITELN;

WRITE('   ','ENTER CRANKING TORQUE (NM)=  ');
READ(TORQUEFORCE);
TORQUEFORCE:=TORQUEFORCE/R;
```

Listing continued - SIMULATE.PAS

```
WRITELN;
WRITELN;

WRITELN('TORQUE-X':11,'TORQUE -Y':17,'TORQUE-T':17,'MSPEEDX':17,
'MSPEEDY':17,'MSPEEDT':17);
WRITELN('  (NM)  ':11,'  (NM)   ':17,'  (NM)  ':17,'  (RPM)  '
  :17,'  (RPM)  ':17,'  (RPM)  ':17);
WRITELN;

DEGREES:=0.0;

WHILE DEGREES <=360 DO

        BEGIN

        OMEGA:=DEGREES*2*3.14159/360;
        ROMEGACOS:=R*COS(OMEGA);
        ROMEGASIN:=R*SIN(OMEGA);

        X:=(X1-ROMEGACOS-RADIUS3)/K;
        Y:=(Y1+ROMEGASIN)/K;
        XDOT:=-OMEGADOT*ROMEGASIN/K;
        YDOT:=OMEGADOT*ROMEGACOS/K;
        X2DOT:=-SQR(OMEGADOT)*ROMEGACOS/K;
        Y2DOT:=-SQR(OMEGADOT)*ROMEGASIN/K;

        RADIUS:=SQRT(SQR(X)+SQR(Y));
        THETACOS:=X/RADIUS;
        THETASIN:=Y/RADIUS;
        PHICOS:=-THETACOS;
        PHISIN:=THETASIN;

        RADIUSDOT:=XDOT*THETACOS+YDOT*THETASIN;
        THETADOT:=(YDOT*THETACOS-XDOT*THETASIN)/RADIUS;
        PHIDOT:=-THETADOT;
        RADIUS2DOT:=X2DOT*THETACOS+Y2DOT*THETASIN+SQR(THETADOT)*RADIUS;
        THETA2DOT:=(Y2DOT*THETACOS-X2DOT*THETASIN-2*THETADOT*RADIUSDOT)/RADIUS;
        PHI2DOT:=-THETA2DOT;

 {CRANKING TORQUE}

 FX3:=TORQUEFORCE*SIN(OMEGA)+EXFX3;
 FY3:=TORQUEFORCE*COS(OMEGA)+EXFY3;

 {EXTERNAL FORCE TRANSFORMATION}

 FRAD3:=-(FX3*THETACOS+FY3*THETASIN);
 FPHI3:=-FY3*THETACOS+FX3*THETASIN;
```

Listing continued

```
{TERMINAL LINK FORCE TRANSFORMATION}

MOMENT2:=(INERTIA3+MASS3*SQR(RADIUSG3))*PHI2DOT+MOMENT3-C3*PHIDOT
         -FPHI3*RADIUS3;

FRAD2:=FRAD3*PHICOS-FPHI3*PHISIN+PHI2DOT*RADIUSG3*MASS3*PHISIN
       +SQR(PHIDOT)*RADIUSG3*MASS3*PHICOS;

FTHETA2:=FRAD3*PHISIN+FPHI3*PHICOS+SQR(PHIDOT)*RADIUSG3*MASS3*PHISIN;

{EXTENSION ARM FORCE EQUATIONS}

FRAD1:=K*FRAD2+GRAVITY*THETACOS*(MASS1+K*MASS2)+RADIUSDOT*(C1-SQR(K)*C2)
       +MASS1*(RADIUS2DOT-SQR(THETADOT)*(RADIUS-RADIUSG1))
       -K*MASS2*(K*RADIUS2DOT-SQR(THETADOT)*(K*RADIUS-RADIUSG2));

FTHETA1:=(THETA2DOT/RADIUS)*(MASS0*SQR(RADIUSG0)+MASS1*SQR(RADIUS-RADIUSG1)
         +MASS2*SQR(K*RADIUS-RADIUSG2))-MOMENT2/RADIUS
         +(INERTIA0+INERTIA1+INERTIA2)*THETA2DOT/RADIUS
         -FTHETA2*K+GRAVITY*THETASIN*(MASS0*RADIUSG0-MASS1*(RADIUS-RADIUSG1)
         +MASS2*(RADIUS*K-RADIUSG2))/RADIUS;

FRAD0:=FRAD1-FRAD2-GRAVITY*THETACOS*(MASS0+MASS1+MASS2)
       -MASS0*SQR(THETADOT)*RADIUSG0
       +MASS1*(SQR(THETADOT)*(RADIUS-RADIUSG1)-RADIUS2DOT)
       -MASS2*(SQR(THETADOT)*(K*RADIUS-RADIUSG2)-K*RADIUS2DOT);

FTHETA0:=FTHETA1-FTHETA2+GRAVITY*THETASIN*(MASS0+MASS1+MASS2)
         -MASS0*THETA2DOT*RADIUSG0
         +MASS1*(THETA2DOT*(RADIUS-RADIUSG1)+2*THETADOT*RADIUSDOT)
         +MASS2*(THETA2DOT*(K*RADIUS-RADIUSG2)+2*K*THETADOT*RADIUSDOT);

{FORCE TRANSFORMATIONS TO X-Y CO-ORDINATE FRAME}

FORCEX:=FRAD1*THETACOS-FTHETA1*THETASIN;

FORCEY:=FRAD1*THETASIN+FTHETA1*THETACOS;

{TRANSFORMATION TO MOTOR DRIVE TORQUES}
{REQUIRE TO DETERMINE MASS OF CROSSSLIDE TABLES}

THETA:=360*ARCTAN(Y/X)/(2*3.14159);
TORQUE;
DEGREES:=DEGREES+30;

END;
WRITELN;
WRITELN('   ','END OF COMPUTATION');
WRITELN;
END;
END.
```

APPENDIX II

NOISE REDUCTION TECHNIQUES

Appendix II.1 - Brushless Motors

Appendix II.2 - Low-pass Filters

Brushless Motors

The brushless motors selected to drive the pantograph slave arm were chosen principally because of their excellent power to weight ratio. Hall effect sensors are used to generate the electronic commutation via commercial three phase brushless motor controllers, which are shown schematically in Figure II.1. Input power was provided by 400 Watt constant voltage (24V) switched mode power supplies.

Disturbances arising from induced noise into the control system was eventually traced to the switching logic of the motor controllers. The switching transients had an adverse effect on analog inputs, particularly force and position sensor signals. Frequencies up to 20 kHz, generated by a pulse width modulation circuit were introducing mains bourne and radiated noise into the sensitive circuits. Attempts to reduce the noise by decoupling all input/output circuits gave only a marginal improvement to noise immunity.

It was eventually decided to electrically isolate all power supplies and brushless motor controller inputs using precision isolation amplifiers, as shown in Figure II.2. The units were eventually housed in a separate enclosure and mains filters incorporated. The overall reduction in noise was substantial and at the time reasonable control of the pantograph arm was achieved.

More recently, because of the significant torque ripple generated by the brushless motors it was necessary to replace them with conventional DC servo-motors having a smaller torque ripple, and unfortunately a lower overall torque rating.

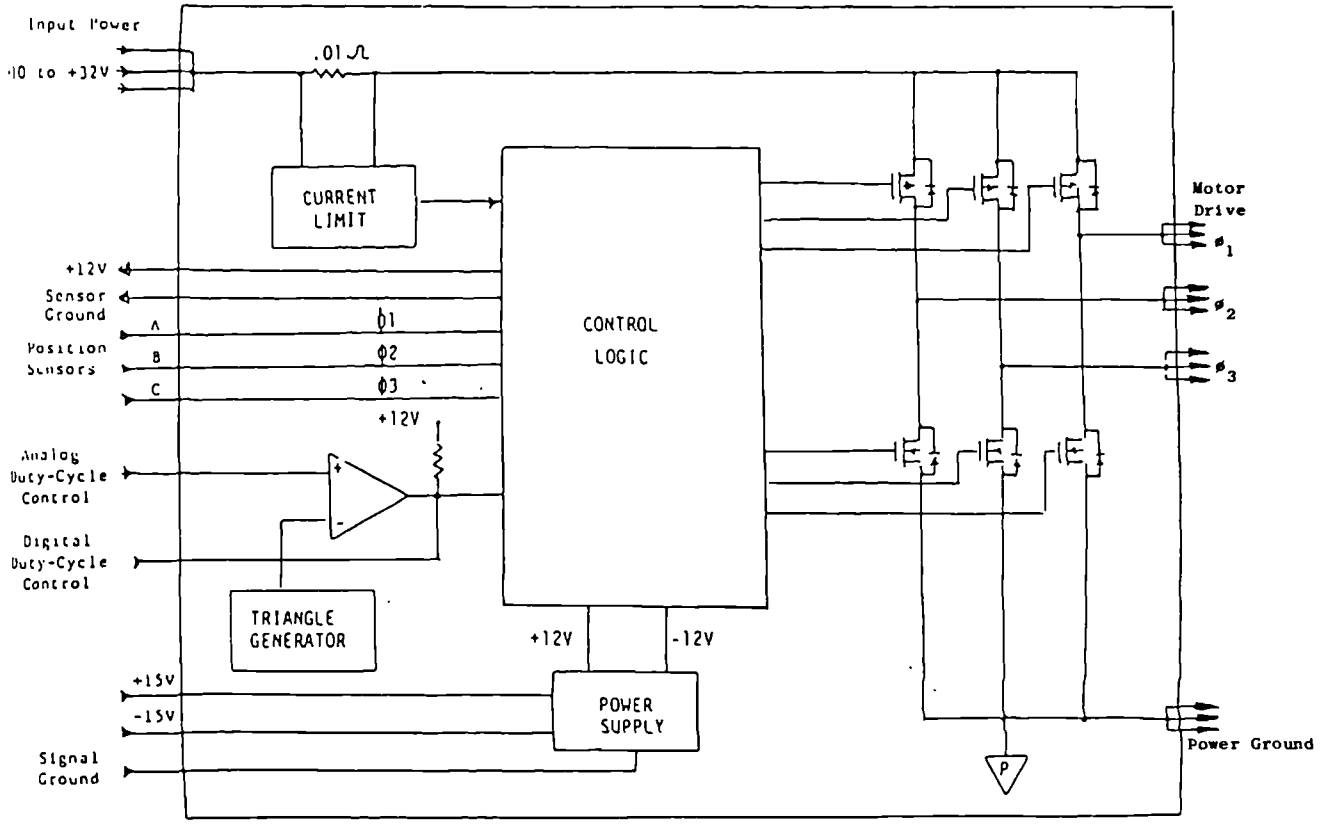

Figure II.1 Brushless motor controller

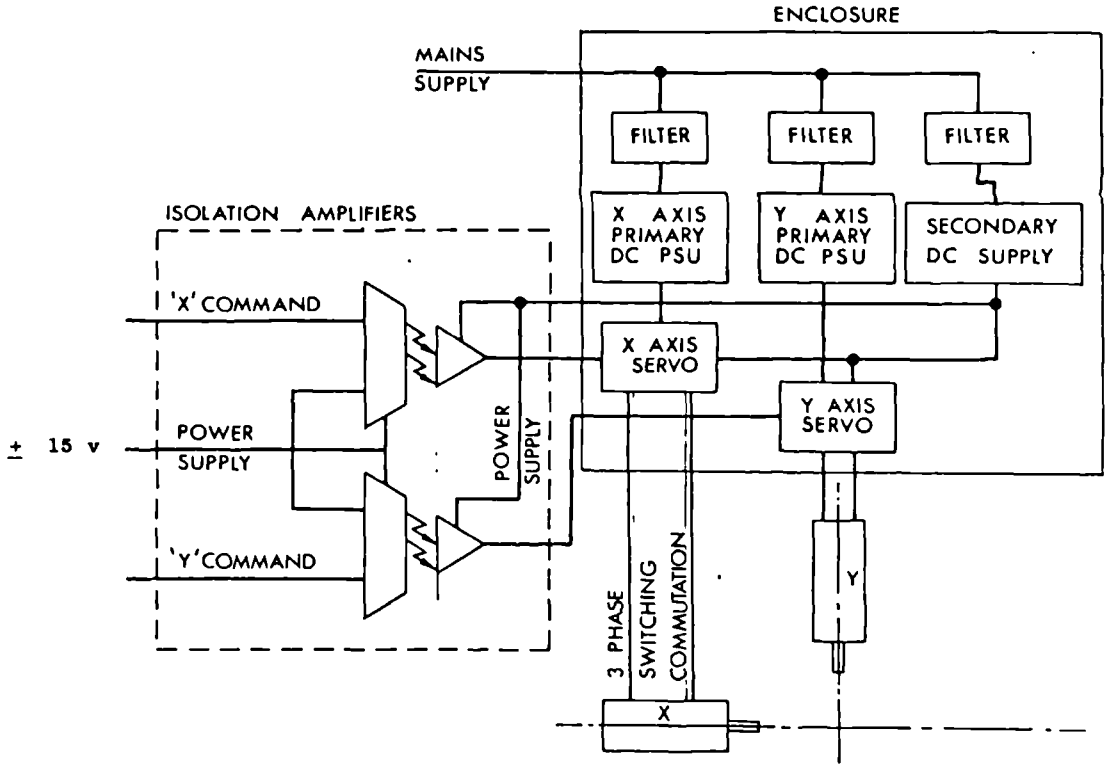

Figure II.2 Isolation circuit for brushless motors

Design of Low-pass filters

When a continuous signal is sampled, using a digital computer operating in discrete time, some signal information may be lost. There is also the possibility that spurious information, not present in the original signal is created. The sampling process can produce harmonics, usually called aliases which can interfere with the signal content. To avoid this problem, the sampling frequency must be at least twice as high as the highest frequency present in the signal (Shannon's theorem). However in practice it is often necessary to sample at up to 5-10 times the highest frequency if aliasing problems are to be avoided. Under such circumstances it is considered more appropriate to filter the signal before it is sampled. Obviously high frequency noise will also be troublesome, which can be filtered out using an 'anti-alising' low-pass filter.

Simple resistance-capacitance (RC) filters were used initially in an attempt to overcome the problems described in the previous section, however noise is only reduced in proportion to its frequency. If there is not a wide frequency band separating the signal from the noise, it is necassary to use active filters which can also provide a sharp cut-off frequency to eliminate aliases.

Two pole low-pass filters were incorporated in the sensitive circuits of all force sensors outputs prior to being sampled by the computer. A Butterworth filter having a cut-off frequency of 25 Hz (160 Rads/sec) and an attenuation rate of -6dB per octave to give the flattest amplitude response over the bandpass frequency range was selected. The basic second order transfer function describing the output is given by

$$T_{LP} = \frac{A_{LP}\omega_o^2}{S^2 + (\omega_o/Q)S + \omega_o^2}$$

where the cut-off frequency $\omega_o = 2\pi f_o$, and Q is called the Q-factor.

A universal active filter, UAF21 (Burr-Brown) was used in the non-inverting mode as shown in Figure II.3.

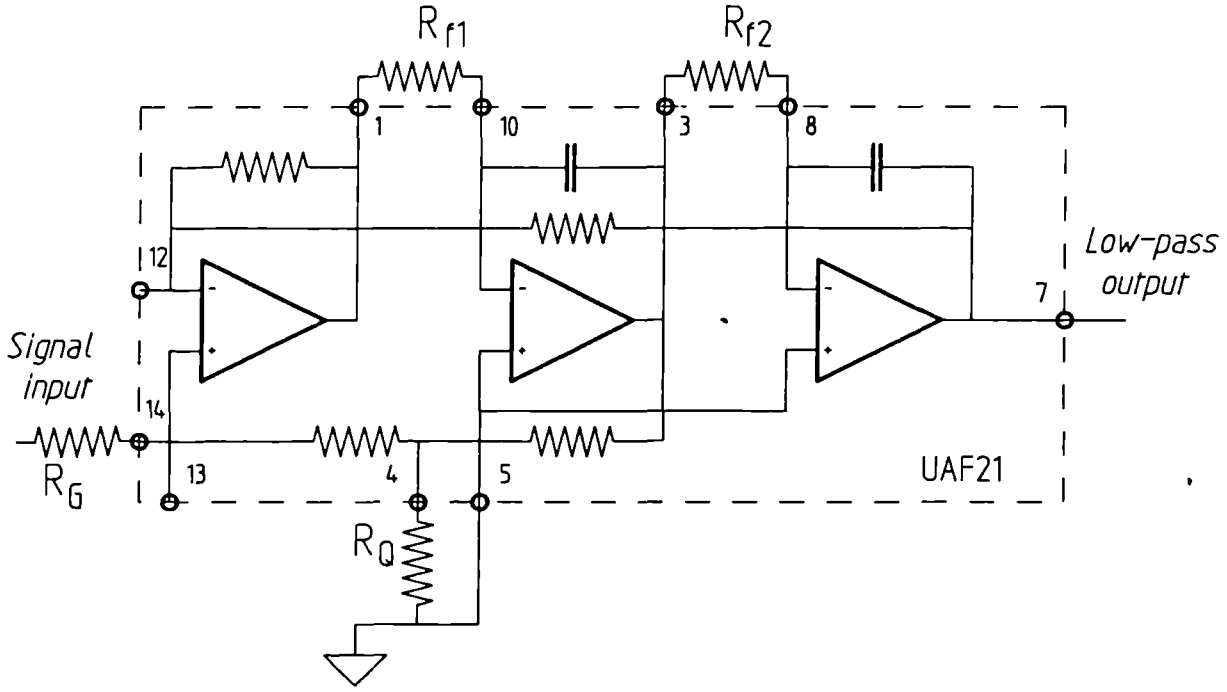

Figure 11.3 *Circuit for 2 Pole Butterworth Filter*

APPENDIX III

GENERALIZED CONTROL

Appendix III.1 - Master Arm Kinematics

Appendix III.2 - Pantograph Arm Kinematics

Appendix III.3 - Position/Force Fortran Program

Appendix III.4 - Position/Position Fortran Program

Appendix III.1 - Master arm kinematics

The direct and inverse kinematics for both articulated master arm and pantograph slave arm can be determined with relative ease. Figure III.1 illustrates the kinematic relationships between master and slave arms.

Master arm direct kinematics

$$X_M = L_1\text{Cos}(\theta_1) + L_2\text{Cos}(\theta_1 + \theta_2)$$

$$Y_M = L_1\text{Sin}(\theta_1) + L_2\text{Sin}(\theta_1 + \theta_2)$$

$$\theta = \theta_1 + \theta_2 + \theta_3$$

.....{III.1}

Master arm inverse kinematics

$$R = R_1 + R_2$$

Using Cosine Rule,

$$L_2^2 = L_1^2 + R^2 - 2L_1R\ \text{Cos}\,\alpha_1$$

In this case L_1 = 3 Units, and L_2 = 2 Units long, thus

$$\alpha_1 = \text{Cos}^{-1}[(R + 5/R)/6]$$

and

$$\alpha_2 = \text{Cos}^{-1}[(R - 5/R)/4]$$

Therefore

$$\theta_1 = \text{Cos}^{-1}(R/X_m) - \alpha_1$$

$$\theta_2 = \alpha_1 + \alpha_2$$

and

$$\theta_3 = \theta - \alpha_1 - \alpha_2$$

.....{III.2}

Appendix III.2 - Pantograph arm kinematics

$$X_S = R_S \text{ Cos } \Omega_1$$

$$Y_S = R_S \text{ Sin } \Omega_1$$

and

$$\Phi_S = \Omega_1 + \Omega_2$$

.....{III.3}

Slave arm inverse kinematics

$$R_S = (X_S^2 + Y_S^2)^{1/2}$$

$$\Omega_1 = \text{Cos}^{-1} (X_S/R_S)$$

and

$$\Omega_2 = \Phi_S - \Omega_1$$

.....{III.4}

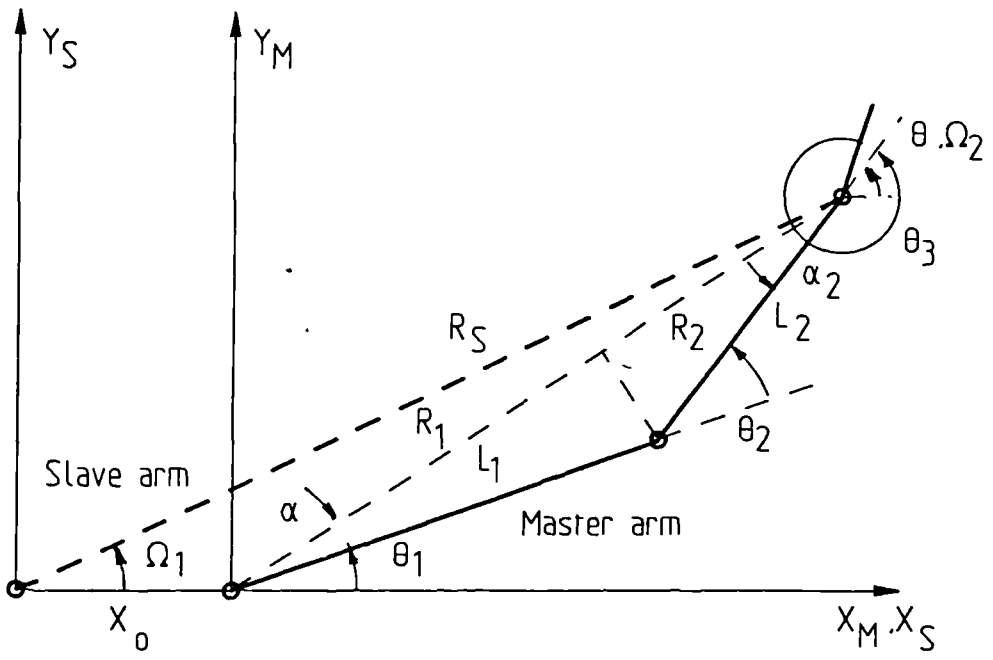

Figure III.1 *Kinematic relationship between master and slave arms*

Appendix III.3 Position / Force Control Fortran Program

Program name - POSFOR.FOR

```
C       ****                    FILE POSFOR.FOR                    ****
C
C       **      PROGRAM TO CARRY OUT MASTER SLAVE CONTROL            **
C       **      USING PANTOGRAPH SLAVE ARM - BILATERALLY             **
C
C       **      THIS PROGRAM CALLS THE FOLLOWING ASSEMBLY            **
C       **      LANGUAGE SUBROUTINES :                               **
C       **      (1)    ADC.ASM - 12 BIT A/D  12 CHANNEL + KEY       **
C       **                                     INTERRUPT             **
C       **      (2)    DAC.ASM - 12 BIT D/A   6 CHANNEL             **
C
C       *       INTEGER VARIABLES   AD1-AD12 ANALOG INPUTS           *
C       *       INTEGER VARIABLES   DA1-DA6  ANALOG OUTPUTS          *
C
C       ***     KEY INTERRUPT ROUTINE BASED ON KEY INTEGER          ***
C
        INTEGER*2  KEY,AD1,AD2,AD3,AD4,AD5,AD6,
     1             AD7,AD8,AD9,AD10,AD11,AD12,
     2             DA1,DA2,DA3,DA4,DA5,DA6
C
        REAL*8     COS1,COS2,SIN1,SIN2,THETA1,THETA2,THETA3,
     1             MXREF,MYREF,THETAREF,OMEGA1,OMEGA2,RADIUS,
     2             SINOMEGA,COSOMEGA,SXREF,SYREF,SOMEGA,MXOFFSET,
     3             XERROR,YERROR,OMEGAERR,OMEGAGAIN,XGAIN,YGAIN,
     4             PHI1GAIN,PHI2GAIN,PHI3GAIN,SCALEX,SCALEY,
     5             SCALES,FFBGAIN,GAIN1,GAIN2,GAIN3,L1SIN1,
     6             L2SIN2,L1COS1,L2COS2,FORCEX,FORCEY,TORQUS,
     7             TORQU1,TORQU2,FFWGAIN

C
C       *       AD1  = MASTER ARM SHOULDER POSITION                  *
C       *       AD2  =    "    "  ELBOW       "                      *
C       *       AD3  =    "    "  WRIST       "                      *
C       *                                                            *
C       *       AD4  =    "    "  SHOULDER  TORQUE                   *
C       *       AD5  =    "    "  ELBOW       "                      *
C       *       AD6  =    "    "  WRIST       "                      *
C       *                                                            *
C       *       AD7  =  SLAVE ARM BASE     POSITION                  *
C       *       AD8  =    "    "  RADIAL      "                      *
C       *       AD9  =    "    "  WRIST       "                      *
C       *                                                            *
C       *       AD10 =  SLAVE ARM Y-AXIS    FORCE                   *
C       *       AD11 =    "    " X-AXIS      "                       *
C       *       AD12 =    "    "  WRIST     TORQUE                   *
```

Listing continued - POSFOR.FOR

```
C
C
C       *       DA1   =  MASTER ARM SHOULDER COMMAND            *
C       *       DA2   =    "     "  ELBOW       "               *
C       *       DA3   =    "     "  WRIST       "               *
C       *                                                       *
C       *       DA4   =  SLAVE  ARM  X-AXIS  COMMAND            *
C       *       DA5   =    "     "   Y-AXIS     "               *
C       *       DA6   =    "     "   WRIST      "               *


C       *               SET GAIN CONSTANTS                      *


C       ***     FORCE FEEDBACK GAIN  IS  FFBGAIN=0.2    ***

2       WRITE(*,3)
3       FORMAT(' INPUT FORWARD GAIN -  ',\)
        READ (*,4) FFWGAIN
4       FORMAT(F6.2)
        IF (FFWGAIN.GT.3.0) GOTO 2
        IF (FFWGAIN.LT.0) GOTO 2

5       WRITE(*,6)
6       FORMAT(' INPUT FORCE FEEDBACK GAIN -  ',\)
        READ(*,4) FFBGAIN
        IF (FFBGAIN.GT.1.0) GOTO 5
        IF (FFBGAIN.LT.0) GOTO 5

        GAIN1 = 1.18577*FFBGAIN
        GAIN2 = 1.18577*FFBGAIN
        GAIN3 = 1.923*FFBGAIN

        XGAIN      =   1123.541*FFWGAIN
        SXOFFSET   =   3.0
        YGAIN      =  -814.53*FFWGAIN
        OMEGAGAIN  =   1375
        GAINOMEGA  =   1375*FFWGAIN
        PHI1GAIN   =   995
        PHI2GAIN   =   1020
        PHI3GAIN   =   931
        SCALEX     =   0.5
        SCALEY     =   0.4
        SCALES     =   1.595745

C       *       CALL ANALOG INPUT SUBROUTINE ADC                *

100     CALL ADC(KEY,AD12,AD11,AD10,AD9,AD8,AD7,AD6,AD5,AD4,AD3,AD2,AD1)
        IF (KEY.EQ.0) GOTO 1000
```

Listing continued - POSFOR.FOR

```
        THETA1 = AD1
        THETA2 = AD2
        THETA3 = AD3

        THETA1 = THETA1/PHI1GAIN
        THETA2 = THETA2/PHI2GAIN + THETA1
        THETA3 = THETA3/PHI3GAIN + THETA2

        OMEGA1 = -AD7
        RADIUS =  AD8
        OMEGA2 =  AD9

        OMEGA1 = OMEGA1/OMEGAGAIN
        OMEGA2 = OMEGA2/1380
        RADIUS = 7.76 - RADIUS/835.82


C       *               RESOLVE JOINT ANGLES                    *

        SIN1 = SIN(THETA1)
        COS1 = SQRT(1-SIN1*SIN1)
        SIN2 = SIN(THETA2)
        COS2 = SQRT(1-SIN2*SIN2)

        L1SIN1 = 3*SIN1
        L2SIN2 = 2*SIN2
        L1COS1 = 3*COS1
        L2COS2 = 2*COS2

C       *       CALCULATE WORLD COORDINATES - MASTER ARM        *

        MXREF     =  (L1COS1 + L2COS2)
        MYREF     =  (L1SIN1 + L2SIN2)

C       *               SLAVE ARM POSITION                      *

C       *               RESOLVE JOINT ANGLES                    *

        SINOMEGA = SIN(OMEGA1)
        COSOMEGA = SQRT(1-SINOMEGA*SINOMEGA)

C       *       CALCULATE SLAVE ARM WORLD COORDINATES           *

        SXREF     = COSOMEGA*RADIUS - SXOFFSET
        SYREF     = SINOMEGA*RADIUS
        SOMEGA    = OMEGA1-OMEGA2
```

Listing continued - POSFOR.FOR

```
C       *           CALCULATE POSITION ERROR COMMANDS           *

        XERROR   = (MXREF - SXREF)*XGAIN
        YERROR   = (MYREF - SYREF)*YGAIN
        OMEGAERR =  -(SOMEGA)*GAINOMEGA
        IF (XERROR.GT.2048) XERROR=2048
        IF (XERROR.LT.-2047) XERROR=-2047
        IF (YERROR.GT.2048) YERROR=2048
        IF (YERROR.LT.-2047) YERROR=-2047
        IF (OMEGAERR.GT.2048) OMEGAERR = 2048
        IF (OMEGAERR.LT.-2047) OMEGAERR = -2047

C       *       CALCULATE FORCE COMMANDS

        FORCEX = AD11
        FORCEY = AD10
        TORQUS = AD12
        FORCEX = FORCEX*SCALEX
        FORCEY = FORCEY*SCALEY
        TORQUS = TORQUS*SCALES

        TORQU1 = FORCEX*MYREF  - FORCEY*MXREF
        TORQU2 = FORCEX*L2SIN2 - FORCEY*L2COS2

        DA1 =  NINT(TORQU1*GAIN1)
        DA2 =  NINT(TORQU2*GAIN2)
        DA3 =  NINT(THETA3*PHI3GAIN)

C       *       RESOLVE INTEGER VALUES FOR DAC ROUTINE      *

        DA6 = NINT(OMEGAERR)
        DA5 = NINT(YERROR)
        DA4 = NINT(XERROR)

        CALL DAC(DA1,DA2,DA3,DA4,DA5,DA6)

C       WRITE(*,200) COSOMEGA,RADIUS,SXREF

        GOTO 100

200     FORMAT(3F10.5)

1000    CALL DAC(0,0,0,0,0,0)
        WRITE (*,1100)
1100    FORMAT(' KEYBOARD INTERRUPT RECIEVED : PROGRAM ABORTED')
        STOP
        END
```

Appendix III.4 Position / Position Control Fortran Program

Program name - POSPOS.FOR

```
C       ****                    FILE POSPOS.FOR                    ****
C
C       **      PROGRAM TO CARRY OUT MASTER-SLAVE POSITION          **
C       **              /POSITION CONTROL                           **
C
C       **      CALLS ASSEMBLY LANGUAGE SUBROUTINES :               **
C       **      (1)    ADC.ASM - 12 BIT A/D  12 CHANNEL + KEY       **
C       **                                     INTERRUPT            **
C       **      (2)    DAC.ASM - 12 BIT D/A   6 CHANNEL             **
C
C       *       INTEGER VARIABLES   AD1-AD12 ANALOG INPUTS           *
C       *       INTEGER VARIABLES   DA1-DA6  ANALOG OUTPUTS          *
C
C       ***     KEY INTERRUPT ROUTINE BASED ON KEY INTEGER          ***
C
        INTEGER*2  KEY,AD1,AD2,AD3,AD4,AD5,AD6,
     1             AD7,AD8,AD9,AD10,AD11,AD12,
     2             DA1,DA2,DA3,DA4,DA5,DA6
C
        REAL*8     COS1,COS2,SIN1,SIN2,THETA1,THETA2,THETA3,
     1             MXREF,MYREF,THETAREF,OMEGA1,OMEGA2,RADIUS,
     2             SINOMEGA,COSOMEGA,SXREF,SYREF,SOMEGA,MXOFFSET,
     3             XERROR,YERROR,OMEGAERR,OMEGAGAIN,XGAIN,YGAIN,
     4             PHI1GAIN,PHI2GAIN,PHI3GAIN,ALPHA1,ALPHA2,
     5             L1SIN1,L2SIN2,L1COS1,L2COS2,FFWGAIN,FFBGAIN,
     6             PHI1ERR,PHI2ERR,PHI3ERR,RADI,T1,T2

C
C       *       AD1  = MASTER ARM SHOULDER POSITION                  *
C       *       AD2  =    "    "  ELBOW      "                       *
C       *       AD3  =    "    "  WRIST      "                       *
C       *                                                            *
C       *       AD4  =    "    "  SHOULDER  TORQUE                   *
C       *       AD5  =    "    "  ELBOW      "                       *
C       *       AD6  =    "    "  WRIST      "                       *
C       *                                                            *
C       *       AD7  =  SLAVE ARM BASE     POSITION                  *
C       *       AD8  =    "    "  RADIAL     "                       *
C       *       AD9  =    "    "  WRIST      "                       *
C       *                                                            *
C       *       AD10 =  SLAVE ARM Y-AXIS    FORCE                   *
C       *       AD11 =    "    " X-AXIS      "                       *
C       *       AD12 =    "    "  WRIST     TORQUE                   *
C
C
```

Listing continued - POSPOS.FOR

```
C
C       *       DA1  =  MASTER ARM SHOULDER COMMAND             *
C       *       DA2  =    "     "  ELBOW       "                *
C       *       DA3  =    "     "  WRIST       "                *
C       *                                                       *
C       *       DA4  =  SLAVE  ARM  X-AXIS  COMMAND             *
C       *       DA5  =    "     "   Y-AXIS     "                *
C       *       DA6  =    "     "   WRIST      "                *


C       *              PRE-SET GAIN CONSTANTS                   *


2       WRITE(*,3)
3       FORMAT(' INPUT FORWARD GAIN -  ',\)
        READ (*,4) FFWGAIN
4       FORMAT(F6.2)
        IF (FFWGAIN.GT.3.0) GOTO 2
        IF (FFWGAIN.LT.0) GOTO 2

5       WRITE(*,6)
6       FORMAT(' INPUT FEEDBACK GAIN -  ',\)
        READ(*,4) FFBGAIN
        IF (FFBGAIN.GT.3.0) GOTO 5
        IF (FFBGAIN.LT.0) GOTO 5


        XGAIN      =   1123.541*FFWGAIN
        SXOFFSET   =   3.0
        YGAIN      =  -814.53*FFWGAIN
        OMEGAGAIN  =   1375
        GAINOMEGA  =   1375*FFWGAIN
        PHI1GAIN   =   995*FFBGAIN
        PHI2GAIN   =   1020*FFBGAIN
        PHI3GAIN   =   931*FFBGAIN

C       *       CALL ANALOG INPUT SUBROUTINE ADC        *

100     CALL ADC(KEY,AD12,AD11,AD10,AD9,AD8,AD7,AD6,AD5,AD4,AD3,AD2,AD1)
        IF (KEY.EQ.0) GOTO 1000

        THETA1 = AD1
        THETA2 = AD2
        THETA3 = AD3

        THETA1 = THETA1/995
        T1     = THETA1
        T2     = THETA2/1020
        THETA2 = T2 + THETA1
        THETA3 = THETA3/931 + THETA2
```

Listing continued - POSPOS.FOR

```
        OMEGA1 = -AD7
        RADIUS =  AD8
        OMEGA2 =  AD9

        OMEGA1 = OMEGA1/OMEGAGAIN
        OMEGA2 = OMEGA2/1380
        RADIUS = 7.76 - RADIUS/835.82


C       *               RESOLVE JOINT ANGLES - MASTER ARM       *

        SIN1 = SIN(THETA1)
        COS1 = SQRT(1-SIN1*SIN1)
        SIN2 = SIN(THETA2)
        COS2 = SQRT(1-SIN2*SIN2)

        L1SIN1 = 3*SIN1
        L2SIN2 = 2*SIN2
        L1COS1 = 3*COS1
        L2COS2 = 2*COS2

C       *       CALCULATE WORLD COORDINATES - MASTER ARM        *

        MXREF     =  (L1COS1 + L2COS2)
        MYREF     =  (L1SIN1 + L2SIN2)

C       *       RESOLVE JOINT ANGLES - SLAVE ARM                *

        SINOMEGA = SIN(OMEGA1)
        COSOMEGA = SQRT(1-SINOMEGA*SINOMEGA)

C       *       CALCULATE WORLD COORDINATES - SLAVE ARM         *

        SXREF     = COSOMEGA*RADIUS - SXOFFSET
        SYREF     = SINOMEGA*RADIUS
        SOMEGA    = OMEGA1-OMEGA2

C       *       CALCULATE INVERSE KINEMATICS FOR MASTER ARM     *
C       *               SEE NOTEBOOK (DATE 4-9-87)              *

        RADI     =  SQRT(SXREF**2 + SYREF**2)
        IF (RADI.GE.5) RADI = 5
        ALPHA1   =  ACOS((5/RADI+RADI)/6)
        ALPHA2   =  ACOS((RADI-5/RADI)/4)
        IF (SXREF.GE.5) SXREF = 5
        PHI1     =  (ASIN(SYREF/RADI)-ALPHA1)
        PHI2     =  (ALPHA1+ALPHA2)
C       PHI3     =  SOMEGA
```

Listing continued - POSPOS.FOR

```
C       *           CALCULATE POSITION ERROR COMMANDS           *

        PHI1ERR  = (T1 - PHI1)*PHI1GAIN
        PHI2ERR  = (T2 - PHI2)*PHI2GAIN
        PHI3ERR  = (THETA3)*PHI3GAIN
C       PHI3ERR  = (THETA3 + THETA2 + THETA1 - PHI3)*PHI3GAIN

        IF (PHI1ERR.GT.2047)  PHI1ERR =  2047
        IF (PHI2ERR.GT.2047)  PHI2ERR =  2047
        IF (PHI3ERR.GT.2047)  PHI2ERR =  2047
        IF (PHI1ERR.LT.-2048) PHI1ERR = -2048
        IF (PHI2ERR.LT.-2048) PHI2ERR = -2048
        IF (PHI3ERR.LT.-2048) PHI3ERR = -2048

        XERROR   = (MXREF - SXREF)*XGAIN
        YERROR   = (MYREF - SYREF)*YGAIN
        OMEGAERR =  -(SOMEGA)*GAINOMEGA

        IF (XERROR.GT.2048)      XERROR =  2048
        IF (YERROR.GT.2048)      YERROR =  2048
        IF (OMEGAERR.GT.2048)  OMEGAERR =  2048
        IF (XERROR.LT.-2047)     XERROR = -2047
        IF (YERROR.LT.-2047)     YERROR = -2047
        IF (OMEGAERR.LT.-2047) OMEGAERR = -2047


C       *       RESOLVE INTEGER VALUES FOR DAC ROUTINE          *

        DA6 = NINT(OMEGAERR)
        DA5 = NINT(YERROR)
        DA4 = NINT(XERROR)
        DA3 = NINT(PHI3ERR)
        DA2 = NINT(PHI2ERR)
        DA1 = NINT(PHI1ERR)

        CALL DAC(DA1,DA2,DA3,DA4,DA5,DA6)

C       WRITE(*,200) COSOMEGA,RADIUS,SXREF

        GOTO 100

200     FORMAT(3F10.5)

1000    CALL DAC(0,0,0,0,0,0)
        WRITE (*,1100)
1100    FORMAT(' KEYBOARD INTERRUPT RECIEVED : PROGRAM ABORTED')
        STOP
        END
```

APPENDIX IV

ASSEMBLY LANGUAGE SUBROUTINES - SOURCE CODE

Appendix IV.1 - Analog to Digital Conversion

Appendix IV.2 - Digital to Analog Conversion

Analog to Digital Assembly Language Subroutine - ADC.ASM

```
;       FILE ADC.ASM  ASSEMBLY LANGUAGE SUBROUTINE
;
;       *       ANALOG TO DIGITAL CONVERSION : 12 CHANNELS      *
;       *       IN AUTO-INCREMENT MODE                          *
;       *                                                       *
;       *               PLUS KEY INTERRUPT                      *
;       *       BASE ADDRESS SET AT 1808 (0710H)                *
;
STACK   SEGMENT PARA STACK 'STACK'
        DB      256 DUP (0)             ; 256 BYTES STACK SPACE
STACK   ENDS
;
DATA    SEGMENT PARA PUBLIC 'DATA'
        DB      256 DUP (0)
DATA    ENDS
;
CODE    SEGMENT PARA    PUBLIC 'CODE'
;
ASSUME  CS:CODE         ; ESTABLISH NORMAL CODE SEGMENT ADDRESSABILITY
ASSUME  DS:DATA         ; ESTABLISH NORMAL DATA SEGMENT ADDRESSABILITY
ASSUME  ES:DATA         ; ESTABLISH EXTRA SEGMENT ADDRESSABILITY
;
;
PUBLIC  ADC
ADC     PROC    FAR
;
        PUSH    BP      ; SAVE FRAMEPOINTER ON STACK
        MOV     BP,SP
;
        MOV     DX,1812 ; CONTROL REGISTER : BASE + 4
;
        MOV     AL,128  ; CONTROL BYTE VALUE : DISABLE AUTO-INCREMENT (BIT7)
        OUT     DX,AL   ; & ALL INTERRUPTS, BITS 0 & 1 IGNORED
;
        INC     DX      ; BASE + 5
        MOV     AL,255  ; A/D CHANNEL SELECT BYTE : IN AUTO INCREMENT MODE
        OUT     DX,AL   ; MUST BE 1 LESS THAN FIRST CHANNEL SELECTED (0)
;
        INC     DX      ; BASE + 6
        OUT     DX,AL   ; START CONVERSION : OUTPUT ANYTHING
;
        SUB     DX,2    ; BASE + 4
WAIT:   IN      AL,DX   ; INPUT STATUS BYTE
```

ADC.ASM (Continued)

```
                        ; RESET WHEN HIGH DATA BYTE READ IN.
        JZ      WAIT    ; WAIT IF AL<128
;
        ADD     DX,2    ; BASE + 6
        IN      AL,DX   ; RESET BIT 7 BY READING HIGH BYTE : A/D DONE
;
        SUB     DX,2    ; BASE + 4
        MOV     AL,0    ; CONTROL BYTE : ENABLE AUTO-INCREMENT (BIT7 = 0) &
        OUT     DX,AL   ; DISABLE ALL INTERRUPTS, BITS 0 & 1 IGNORED.
;
        INC     DX      ; BASE + 5
        OUT     DX,AL   ; A/D CHANNEL SELECT BYTE : STARTING CHANNEL NUMBER ((
;
        PUSH    SI      ; SAVE SEGMENT INDEX REGISTER ON STACK
        MOV     SI,2    ; 'SI' IS USED IN BASE + INDEX CALCULATION BELOW
;
        MOV     CH,12   ; STORE NUMBER OF CHANNELS IN 'CH'
;
        INC     DX      ; BASE + 6
ADLOOP: OUT     DX,AL   ; START CONVERSION : WRITE ANYTHING
;
        SUB     DX,2    ; BASE + 4
ADWAIT: IN      AL,DX   ;
        TEST    AL,128  ; WAIT IF <128 INPUT AT 'AL'
        JZ      ADWAIT  ; JUMP IF ZERO FLAG SET TO ADWAIT:
;
        INC     DX      ; BASE + 5
        IN      AL,DX   ; INPUT LOW BYTE IN 'AL'
        MOV     CL,AL   ; STORE LOW BYTE IN 'CL'
;
        INC     DX      ; BASE + 6
        IN      AL,DX   ; INPUT HIGH BYTE IN 'AL'
        MOV     AH,AL   ; STORE HIGH BYTE IN 'AH'
;
        MOV     AL,CL   ; RESTORE LOW BYTE IN 'AL'
;
        ADD     SI,4    ; 'SI' IS USED IN THE INDIRECT MODE [BP+SI]
        MOV     BX,[BP+SI]      ; STACK ADDRESS
        MOV     [BX],AX ; MOVE CONTENTS OF AX ONTO STACK
                        ; NOTE:   DS:[BX] = [BX]
;
        DEC     CH      ; NEXT CHANNEL
        JNZ     ADLOOP  ; JUMP TO ADLOOP: IF ZERO FLAG NOT SET
;
        MOV     AH,1
        INT     16H
        JZ      TEST
        MOV     AX,0
        ADD     SI,4
        MOV     BX,[BP+SI]
        MOV     [BX],AX
```

ADC.ASM (Continued)

```
        JMP     CONT
;
TEST:   MOV     AX,1
        ADD     SI,4
        MOV     BX,[BP+SI]
        MOV     [BX],AX
;
CONT:   POP     SI          ; RESTORE 'SI'
        POP     BP          ; RESTORE FRAMEPOINTER
        RET     52          ; RETURN 48 BYTES
;
ADC     ENDP
CODE    ENDS
        END
```

Digital to Analog Assembly Language Subroutine - DAC.ASM

```
;               *****                FILE  DAC.ASM                  *****
;
;               *       DIGITAL TO ANALOG CONVERSION : 6 CHANNEL        *
;
;               *       [1]  DADIO BOARD : IN DOUBLE BUFFERED MODE      *
;               *       4 CHANNELS - BASE ADDRESS SET AT 0730H (1840D)  *
;               *       OUTPUT IS SET TO TWO'S COMPLEMENT IN THIS PROG  *
;               *       & THE OUTPUT WORD WRITTEN TO DADIO PORT MUST    *
;               *       BE +/- 2047/48 IN 12 BIT  FORMAT  - THE PROGRAM *
;               *       SUBTRACTS 2048 FROM THE PASSED PARAMETER THEN   *
;               *       SHIFTS THE RESULT 4 BITS TO THE LEFT, VIS       *
;               *       HHHHHHHH:LLLLXXXX                               *
;
;               *       [2]  LABMASTER BOARD - 2 CHANNELS - BASE        *
;               *       ADDRESS IS SET TO 0710H (1808D).                *
;               *       OUTPUT WORD WRITTEN TO LABMASTER IN SAME        *
;               *       FORMAT AS ABOVE, HOWEVER NO CONVERSION IS       *
;               *       REQUIRED FOR OUTPUT.                            *
;
;
;               *       [3] LABMASTER BOARD - 8255 PARALLEL PORT 'A'    *
;               *       USED IN MODE 0 TO TEST STATUS OF CONTROL BOX    *
;               *       AS FOLLOWS :                                    *
;               *                                                       *
;               *       BIT 0 -
;               *       BIT 1 -
;               *       BIT 2 -
;               *       BIT 3 -
;               *       BIT 4 -
;               *       BIT 5 -
;               *       BIT 6 - EMERGENCY STOP : NULL ALL OUTPUTS
;               *       BIT 7 - NOT USED
;
;
STACK   SEGMENT   PARA STACK 'STACK'
        DB        256 DUP (0)        ;  256 BYTES STACK SPACE
STACK   ENDS
;
DATA    SEGMENT   PARA  PUBLIC 'DATA'
        DB        256 DUP (0)
DATA    ENDS
;
CODE    SEGMENT   PARA PUBLIC 'CODE'
;
        ASSUME    CS:CODE    ; ESTABLISH NORMAL CODE SEG. ADDRESSABILITY
        ASSUME    DS:DATA    ; ESTABLISH NORMAL DATA SEG. ADDRESSABILITY
        ASSUME    ES:DATA    ; ESTABLISH EXTRA SEG. ADDRESSABILITY
;
;
```

DAC.ASM (Continued)

```
PUBLIC  DAC
DAC     PROC      FAR
;
        PUSH      BP
        MOV       BP,SP
;
;               *       START STATUS TEST       *
;
        MOV     DX,1823 ;   PARALLEL PORT CONTROL BYTE LOCATION
        MOV     AL,144  ;   SET MODE 0, PORT 'A' AS INPUTS ON 8255
        OUT     DX,AL
;
        CALL    SUBR1   ;   SUBROUTINE TO GET VALUE IN DIGITAL PORT
        TEST    AL,64   ;   IS EMERGENCY STOP ACTIVE !
        JZ      DODAC   ;   JUMP IF ZERO FLAG NOT SET
;
;       *       'NULL' ROUTINE SETS ALL OUTPUTS TO ZERO *
;
        MOV     DX,1811 ; BASE ADDRESS + 3 - LABMASTER BOARD
        MOV     AL,0    ; OUTPUT A '0'
        OUT     DX,AL   ; OUTPUT ZERO TO HIGH BYTE
;
        DEC     DX      ; BASE ADDRESS + 2
        OUT     DX,AL   ; OUTPUT ZERO TO LOW BYTE & CONVERT
;
        DEC     DX      ; BASE ADDRESS + 1
        OUT     DX,AL   ; OUTPUT ZERO TO HIGH BYTE
;
        DEC     DX      ; BASE ADDRESS
        OUT     DX,AL   ; OUTPUT ZERO TO LOW BYTE & CONVERT
;
;
;       *       DADIO BOARD - 4 CHANNELS        *
;
        MOV     CL,0H   ; VALUE OF LOW BYTE TO BE WRITTEN TO PORT
        MOV     CH,80H  ; VALUE OF HIGH BYTE TO BE WRITTEN TO PORT
;
        MOV     DX,1841 ; BASE ADDRESS + 1 - DADIO BOARD
;
        MOV     AL,CH
        OUT     DX,AL
;
        DEC     DX
        MOV     AL,CL
        OUT     DX,AL
;
        ADD     DX,3
        MOV     AL,CH
        OUT     DX,AL
;
        DEC     DX
```

DAC.ASM (Continued)

```
        MOV     AL,CL
        OUT     DX,AL
;
        ADD     DX,3
        MOV     AL,CH
        OUT     DX,AL
;
        DEC     DX
        MOV     AL,CL
        OUT     DX,AL
;
        ADD     DX,3
        MOV     AL,CH
        OUT     DX,AL
;
        DEC     DX
        MOV     AL,CL
        OUT     DX,AL   ; DOUBLE BUFFERED MODE SELECTED - ALL OUTPUT HERE
        JMP     CONT
;
;       *       END OF NULL ROUTINE     *
;
;
;       *       NORMAL DAC OPERATION    *
;
;               *       LABMASTER               *
;
DODAC:  CALL    SUBR1
        TEST    AL,1
        JZ      HERE1
        MOV     AX,0
        JMP     CONT1
HERE1:  MOV     BX,[BP+26]      ; GET VOLTAGE [1]
        MOV     AX,DS:[BX]      ;
;
CONT1:  MOV     DX,1809 ; BASE ADDRESS + 1
        MOV     CL,AL   ;
        MOV     AL,AH   ;
        OUT     DX,AL   ; OUTPUT HIGH BYTE
;
        DEC     DX      ; BASE ADDRESS + 0
        MOV     AL,CL   ;
        OUT     DX,AL   ; OUTPUT LOW BYTE
;
;
        CALL    SUBR1
        TEST    AL,4
        JZ      HERE2
        MOV     AX,0
        JMP     CONT2
```

DAC.ASM (Continued)

```
HERE2:  MOV     BX,[BP+22]      ; GET VOLTAGE [2]
        MOV     AX,DS:[BX]      ;
;
CONT2:  MOV     DX,1811 ; BASE ADDRESS + 3
        MOV     CL,AL   ;
        MOV     AL,AH   ;
        OUT     DX,AL   ; OUTPUT HIGH BYTE
;
        DEC     DX      ; BASE ADDRESS + 2
        MOV     AL,CL   ;
        OUT     DX,AL   ; OUTPUT LOW BYTE
;
;               *       END OF LABMASTER ROUTINE        *
;
;
;               *       START OF DADIO BOARD ROUTINE    *
;
          MOV       CL,4
;
        CALL    SUBR1
        TEST    AL,16
        JZ      HERE3
        MOV     AX,0
        JMP     CONT3
HERE3:    MOV       BX,[BP+18]    ;
          MOV       AX,DS:[BX]    ; GET VOLTAGE [3]
CONT3:    SUB       AX,800H       ; SUBTRACT 2047 FROM PASSED PARAMETER
          SHL       AX,CL         ;
;
          MOV       DX,1841       ; BASE ADDRESS + 1   ;  BASE ADDR. = 1840D
          MOV       CH,AL         ;
          MOV       AL,AH         ;
          OUT       DX,AL         ; output HIGH byte to ADDRESS+1
;
          DEC       DX            ;  ADDRESS
          MOV       AL,CH         ;
          OUT       DX,AL         ; output LOW byte to ADDRESS
;
;
        CALL    SUBR1
        TEST    AL,2
        JZ      HERE4
        MOV     AX,0
        JMP     CONT4
HERE4:    MOV       BX,[BP+14]     ;
          MOV       AX,DS:[BX]    ; GET  VOLTAGE [4]
CONT4:    SUB       AX,800H
          SHL       AX,CL         ;
;
```

DAC.ASM (Continued)

```
            MOV       DX,1843       ; BASE ADDRESS + 3
            MOV       CH,AL         ;
            MOV       AL,AH         ;
            OUT       DX,AL         ; output HIGH byte to ADDRESS+3
;
            DEC       DX            ;
            MOV       AL,CH         ;
            OUT       DX,AL         ; output LOW byte to ADDRESS+2
;
;
          CALL    SUBR1
          TEST    AL,8
          JZ      HERE5
          MOV     AX,0
          JMP     CONT5
HERE5:    MOV     BX,[BP+10]        ;
          MOV     AX,DS:[BX]        ; GET VOLTAGE [5]
CONT5:    SUB     AX,800H
          SHL     AX,CL             ;
;
          MOV     DX,1845           ; BASE ADDRESS +5
          MOV     CH,AL    ;
          MOV     AL,AH    ;
          OUT     DX,AL    ; OUTPUT HIGH BYTE TO ADDRESS+5
;
          DEC     DX       ;
          MOV     AL,CH    ;
          OUT     DX,AL    ; OUTPUT LOW BYTE TO ADDRESS+4
;
;
          CALL    SUBR1
          TEST    AL,32
          JZ      HERE6
          MOV     AX,0
          JMP     CONT6
HERE6:    MOV     BX,[BP+6]         ;
          MOV     AX,DS:[BX]        ; GET VOLTAGE [6]
CONT6:    SUB     AX,800H
          SHL     AX,CL             ;
;
          MOV     DX,1847           ; BASE ADDRESS+7
          MOV     CH,AL    ;
          MOV     AL,AH    ;
          OUT     DX,AL    ; OUTPUT HIGH BYTE TO ADDRESS+7
;
          DEC     DX       ;
          MOV     AL,CH    ;
          OUT     DX,AL    ; OUTPUT LOW BYTE TO ADDRESS+6 &
;                          ; SET ALL OUTPUTS (NB: DOUBLE BUFFERED)
          JMP     CONT
```

DAC.ASM (Continued)

```
;
;
;
CONT:       POP         BP              ; RESTORE FRAMEPOINTER
            RET         24              ; RETURN 16 BYTES
SUBR1    PROC     NEAR
         MOV      DX,1820
         IN       AL,DX
         RET
SUBR1    ENDP
;
;
DAC       ENDP
CODE      ENDS
          END
```

APPENDIX V

Dynamic Simulation Model for One Degree of Freedom Master Arm

Appendix V.1 - Dynamic Model of 1 Dof Master-Slave

Appendix V.2 - Experimentally Determined Data

Appendix V.1 - Dynamic Model of 1 Dof Master Arm

The dynamic model used to represent the motor/gearbox and output link is shown in Figure V.1. The system consists of two dynamically coupled second order systems - connected by a flexible cable of stiffness K.

The following nomenclature is used :

T_m - Motor Torque (Nm)
T_L - Applied load torque (Nm)
J_m' - Inertia of motor/pinion gear G_1 ($kg.m^2$)
J_{23} - Combined Inertia of Gears G2 & G3 ($kg.m^2$)
J_{4M} - - - - Gear G4 & Pulley ($kg.m^2$)
J_O - - - - Output link & Pulley ($kg.m^2$)
C_m' - Viscous friction coefficient (N.m.rad/sec)
C_O - - - - -
F_1 - Contact force between gears G1 & G2 (N)
F_2 - - - - - G3 & G4 (N)
F_a - Tension force in cable (N)
F_b - - - - - -
r_{G1} - Radius of gear G1 (m)
r_{G2} - - - - G2 -
r_{G3} - - - - G3 -
r_{G4} - - - - G4 -
θ_m' - Motor position (rads)
θ_O - Link output position (rads)

The equations of motion for the system are as follows:

Servo-motor and pinion gear G1

$$T_m - J_m'.\ddot{\theta}_m' - C_m'.\dot{\theta}_m' - F_1.r_{G1} = 0$$

Intermediate gear cluster - G2 & G3

$$F_1.r_{G2} - J_{23}. \quad - F_2.r_{G3} = 0$$

Output gear and pulley

$$F_2.r_{G4} - J_{4M}.\ddot{\theta}_m - (F_a - F_b)r_m = 0$$

Output Link and pulley

$$(F_a - F_b)r_o - T_L - J_o.\ddot{\theta}_o - C_o.\dot{\theta}_o = 0$$

Relationship between cable compliance and input/output pulleys

$$(F_a - F_b) = 2K(\theta_m.r_m - \theta_o.r_o)$$

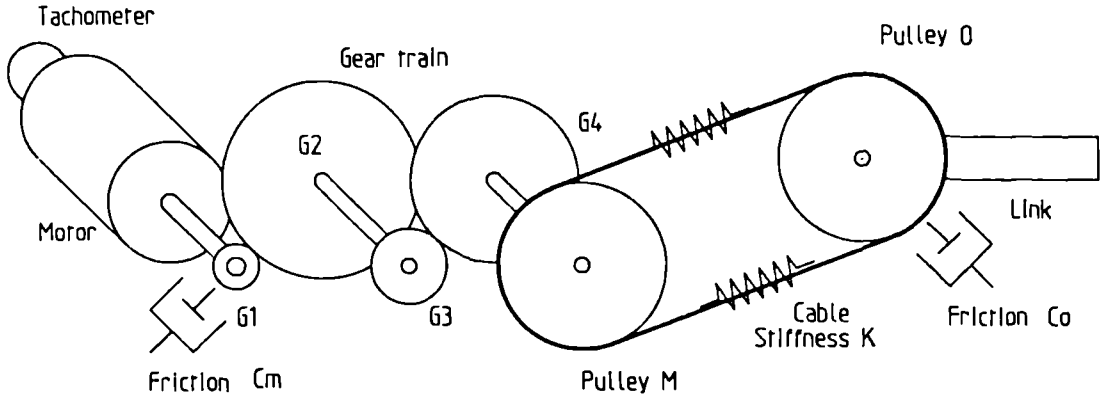

Figure V.1 *Dynamic Model of 1 d.o.f Master arm*

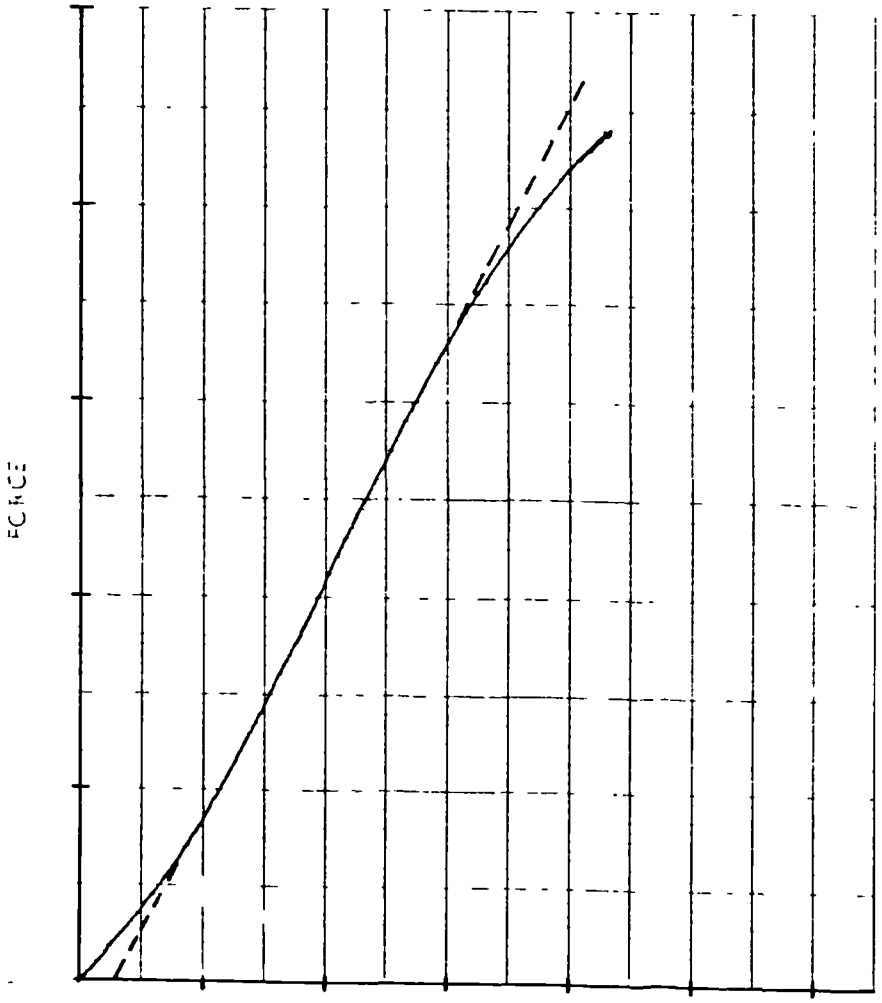

Figure V.2 Load - Extension graph for tesnion cable

Appendix V.2 - Experimental Data

Cable Stiffness

Figure V.2 shows the results of a load-extension experiment on a sample of the stainless steel cable used to provide the transmission to the elbow and wrist joints of the articulated arms used in the study.

Specification (as supplied)

Construction - 7 x 19 ,
Diameter - 1.7 mm ,
Breaking Load - 1910 Newtons.

Test Results

Stiffness - 271 N/mm
Breaking Load - 2200 Newtons.

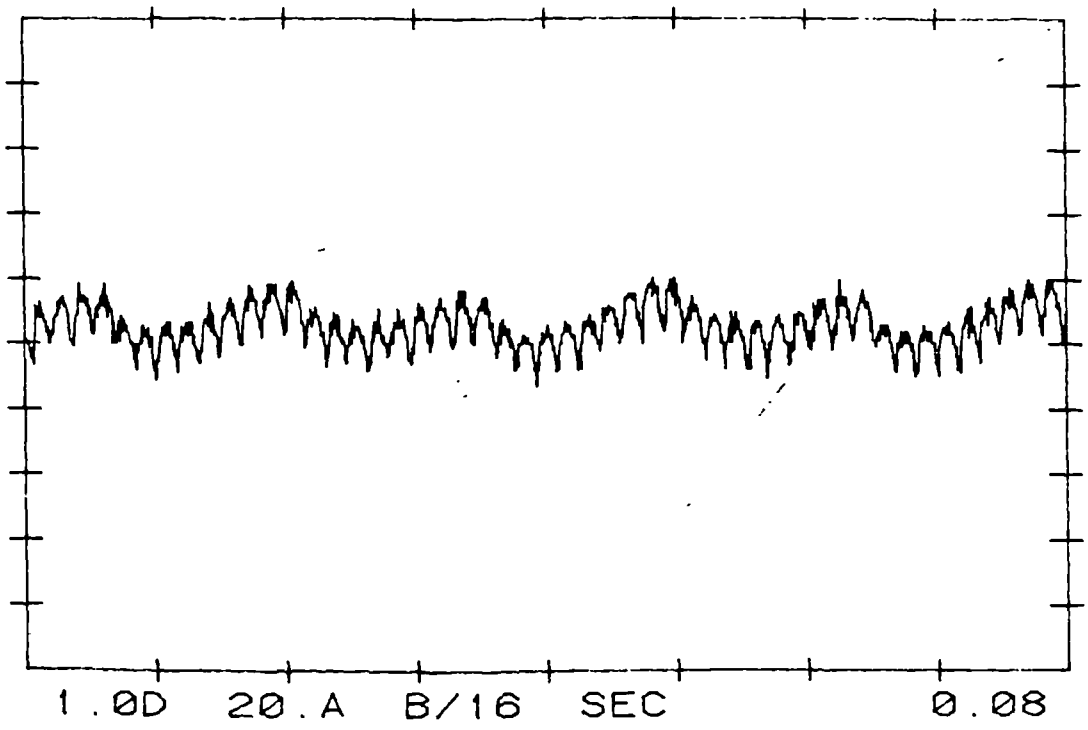

Figure V.3 Tachometer ripple

Tachometer Ripple

Figure V.3 illustrates the cyclic nature of the signal obtained from the DC tachometers used in the investigation. The ripple frequency occurs at 6 times running frequency, and is characterised by an additional low-frequency component occurring at running frequency. Ripple amplitude is dependent upon tachometer speed.

Frequency Response

Figure V.4 presents the results of a transfer function analysis carried out on the master arm elbow joint. A Fast Fourier Transform (FFT) analyser was used to introduce a swept sine wave signal into the closed-loop servo system, and the transform was obtained by averaging over fifty cycles. With closed-loop position control implemented the phase and amplitude response was obtained over the frequency range 0 - 20Hz. The -90° phase cross-over frequency coincides with a natural frequency of 5.2 Hz, which is in good agreement with the model. The heavily damped response, if approximated to a damped second order system, has a damping factor of approximately 0.9.

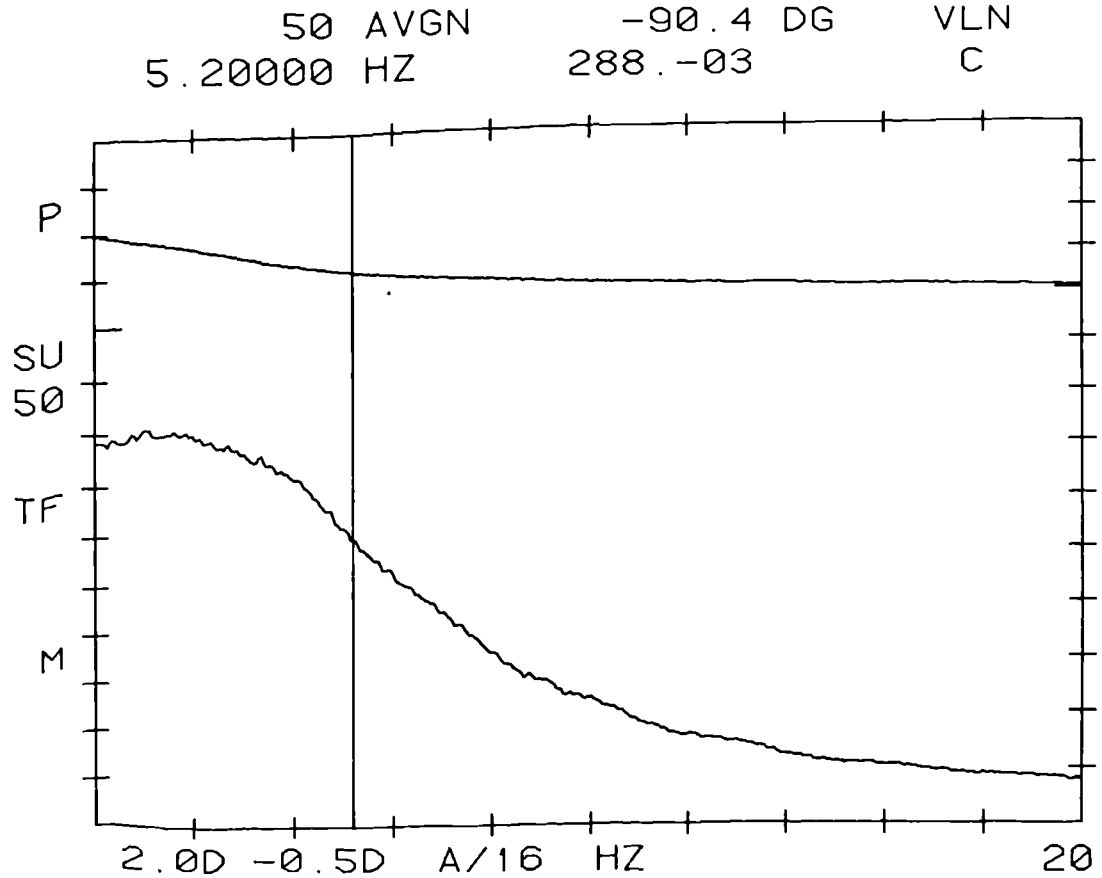

Figure V.4 Frequency response of elbow joint

APPENDIX VI

ACSL SIMULATION MODEL - ONEDOFMS.CSL

Appendix VI.1 - Block Diagram of Full Simulation Model

Appendix VI.2 - Ease+ACSL Graphics Pages of Model

Appendix VI.3 - Listing of ACSL Model Source Code

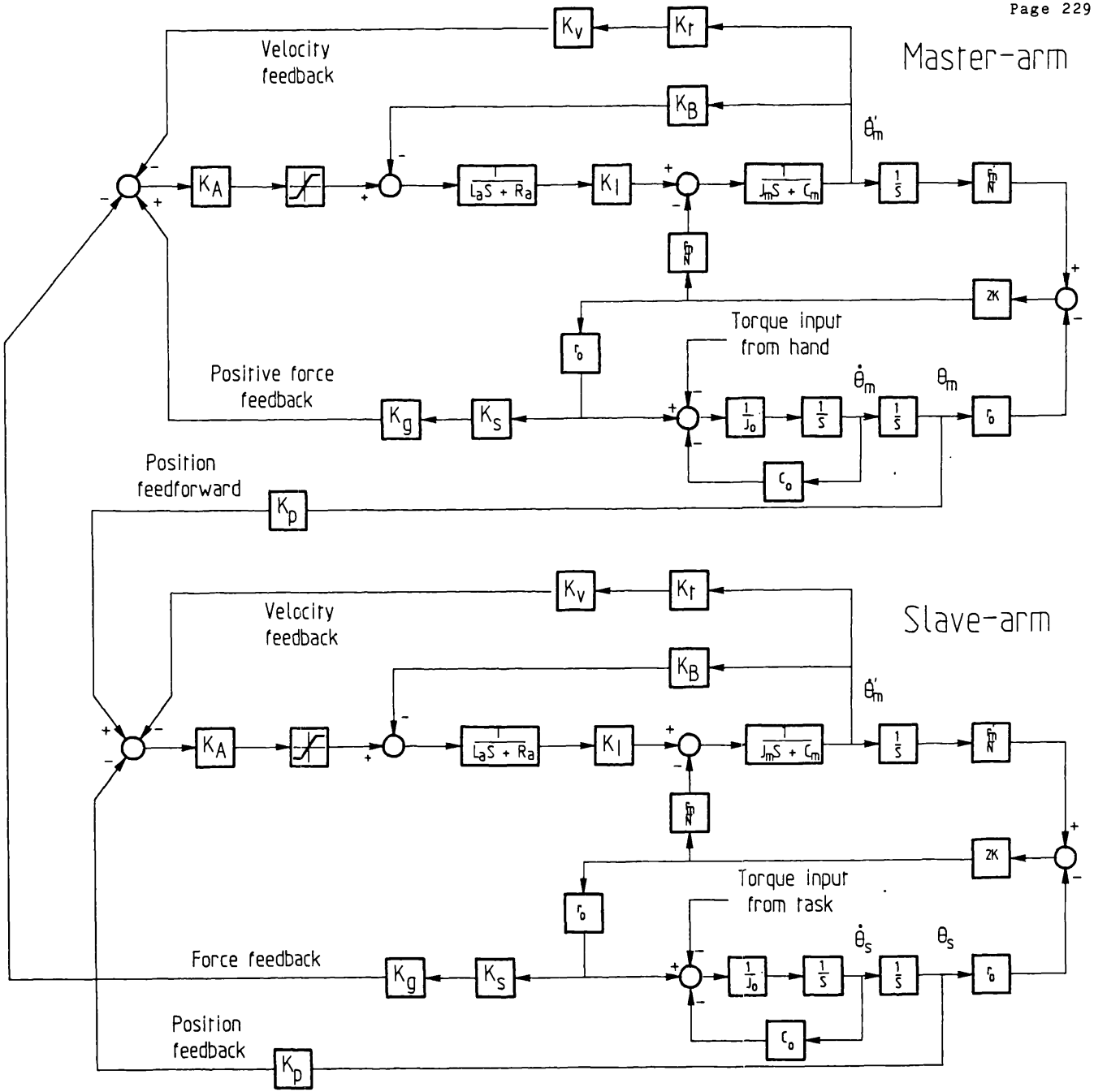

Figure VI.1 Block diagram of ACSL model

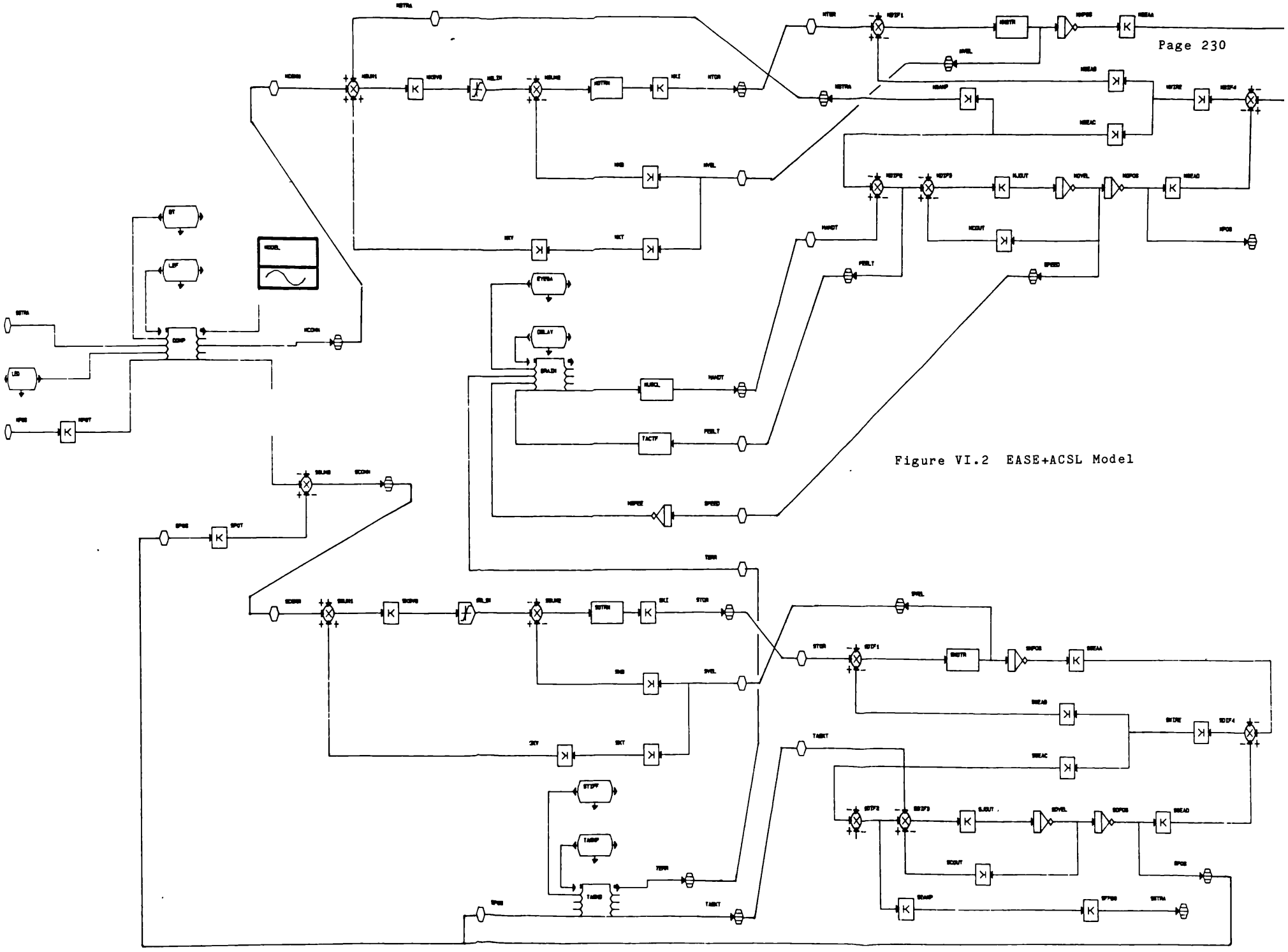

Figure VI.2 EASE+ACSL Model

```
"---->BRAIN SOURCE CODE - NEUROMUSCULAR CONTROL"

      BRAINE=TACTFA-...
      DELAY(TASKDA*EYEGAA,0,DELAYA,2500)

"---->COMP SOURCE CODE - DIGITAL CONTROLLER"

      PROCEDURAL(SSUM31=DTA,...
      MPOTA,LEDA)
      L11 = QNTZR(0.00244,MPOTA)
      L21 = LEDLAG(LEDA,0.0005,L11,0)
      COMPE = ZOH(L21,0,0,DTA)
      END $ 'PROCEDURAL'
      PROCEDURAL(MSUM11=SFFBGA,LEFA)
      COMPC = LEDLAG(LEFA,0.0005,SFFBGA,0)
      END $ 'PROCEDURAL'

"---->                                          CONSTANTS"

      CONSTANT TASKPA    = 0.5                  $"RIGID STOP POSITION (R"
      CONSTANT STIFFA    = -48475.7617          $"TASK STIFFNESS (LINK)"
      CONSTANT EYEGAA    = 1.                   $"EYE GAIN"
      CONSTANT DELAYA    = 0.                   $"NEURO - TIME DELAY"
      CONSTANT DTA       = 0.001                $"DIGITAL SAMPLING PERIO"
      CONSTANT LEDA      = 0.01                 $"POSITION (P+D) DERIVAT"
      CONSTANT LEFA      = 0.01                 $"FORCE(P+D) DERIVATIVE "

"---->                                          SUMMERS (real)"

      MSUM1A    = COMPC  +     MGAMPA + MKVA   $"MASTER SERVO SUMMING J"
      SSUM1A    = SSUM3A +     SKVA            $"SLAVE-ARM SUMMING JUNC"

"---->                                          DIFFERENCE (real)"

      MSUM2A    = MSLIMA -     MKBA            $"MASTER-SERVO SUMMING J"
      MDIF1A    = MKIA   -     MGEABA          $"MASTER ARM SUMMING JUN"
      MDIF4A    = MGEAAA -     MGEADA          $"SUMMING JUNCTION (CABL"
      SSUM3A    = COMPE  -     SPOTA           $"SLAVE POSITION FEEDBAC"
      SSUM2A    = SSLIMA -     SKBA            $"SLAVE-ARM SUMMING JUNC"
      SDIF1A    = SKIA   -     SGEABA          $"SLAVE-ARM SUMMING JUNC"
      SDIF4A    = SGEAAA -     SGEADA          $"SUMMING JUNCTION"
      SDIF2A    = SGEACA                       $"SLAVE LINK SUMMING JUN"
      SDIF3A    = SDIF2A -     TASKDE - SCOUTA $"SLAVE-LINK SUMMING JUN"
      MDIF2A    = MGEACA -     MUSCLA          $"MASTER-LINK SUMMING JU"
      MDIF3A    = MDIF2A -     MCOUTA          $"MASTER-LINK SUMMING JU"
```

Listing continued - ONEDOFMS.CSL

```
"---->                                                  COEFFICIENTS"

      CONSTANT MGEADK    = 35.                          $"RADIUS OF PULLEY"
      MGEADA    = MGEADK *     MOPOSA
      CONSTANT MKBK      = 0.057                        $"MASTER MOTOR BACK EMF "
      MKBA      = MKBK   *     MMOTRA
      CONSTANT MKTK      = 0.0363                       $"MASTER ARM TACHOMETER "
      MKTA      = MKTK   *     MMOTRA
      CONSTANT MKVK      = -0.02                        $"VELOCITY FEEDBACK GAIN"
      MKVA      = MKVK   *     MKTA
      CONSTANT MGAMPK    = -0.0385                      $"MASTER-LINK STRAIN OUT"
      MGAMPA    = MGAMPK *     MGEACA
      CONSTANT MKSVOK    = 46.2                         $"MASTER-SERVO VOLTAGE G"
      MKSVOA    = MKSVOK *     MSUM1A
      CONSTANT MKIK      = 0.048                        $"MASTER MOTOR TORQUE CO"
      MKIA      = MKIK   *     MOTRMA
      CONSTANT MGEABK    = 0.0006                       $"MOTOR TORQUE FEEDBACK"
      MGEABA    = MGEABK *     MWIREA
      CONSTANT MGEAAK    = 0.5787                       $"gearbox & pulley ratio"
      MGEAAA    = MGEAAK *     MMPOSA
      CONSTANT MWIREK    = 542.                         $"wire stiffness (n/mm)"
      MWIREA    = MWIREK *     MDIF4A
      CONSTANT MGEACK    = 0.035                        $"TORQUE DRIVING OUTPUT "
      MGEACA    = MGEACK *     MWIREA
      CONSTANT SGEADK    = 35.                          $"SLAVE LINK PULLEY DIA "
      SGEADA    = SGEADK *     SOPOSA
      CONSTANT SGEABK    = 0.0006                       $"SLAVE MOTOR TORQUE FEE"
      SGEABA    = SGEABK *     SWIREA
      CONSTANT SKTK      = 0.0363                       $"SLAVE MOTOR TACHOMETER"
      SKTA      = SKTK   *     SMOTRA
      CONSTANT SKVK      = -0.05                        $"VELOCITY FEEDBACK (-VE"
      SKVA      = SKVK   *     SKTA
      CONSTANT SPOTK     = 2.48                         $"SLAVE-ARM POSITION POT"
      SPOTA     = SPOTK  *     SOPOSA
      CONSTANT SKSVOK    = 46.2                         $"SLAVE SERVO VOLTAGE GA"
      SKSVOA    = SKSVOK *     SSUM1A
      CONSTANT SKBK      = 0.057                        $"SLAVE MOTOR BACK EMF"
      SKBA      = SKBK   *     SMOTRA
      CONSTANT SKIK      = 0.048                        $"SLAVE MOTOR TORQUE CON"
      SKIA      = SKIK   *     SOTRMA
      CONSTANT SGEAAK    = 0.5787                       $"SLAVE MOTOR OUTPUT TOR"
      SGEAAA    = SGEAAK *     SMPOSA
      CONSTANT SWIREK    = 542.                         $"SLAVE ARM WIRE STIFFNE"
      SWIREA    = SWIREK *     SDIF4A
      CONSTANT SGEACK    = 0.035                        $"SLAVE LINK PULLEY DIA "
      SGEACA    = SGEACK *     SWIREA
      CONSTANT SCOUTK    = 0.2                          $"SLAVE LINK VISCOUS FRI"
      SCOUTA    = SCOUTK *     SOVELA
      CONSTANT SJOUTK    = 68.027                       $"SLAVE LINK INVERSE INE"
      SJOUTA    = SJOUTK *     SDIF3A
      CONSTANT MCOUTK    = 0.2                          $"LINK VISCOUS FRICTION"
```

Listing continued - ONEDOFMS.CSL

```
      MCOUTA     = MCOUTK *      MOVELA
      CONSTANT MJOUTK     = 68.027              $"MASTER LINK INVERSE IN"
      MJOUTA     = MJOUTK *      MDIF3A
      CONSTANT MPOTK      = 2.48                $"MASTER-ARM INPUT POTEN"
      MPOTA      = MPOTK  *      MOPOSA
      CONSTANT SGAMPK     = -0.0385             $"SLAVE-LINK STRAIN OUTP"
      SGAMPA     = SGAMPK *      SDIF2A
      CONSTANT SFFBGK     = 1.                  $"Force feedback gain"
      SFFBGA     = SFFBGK *      SGAMPA

"---->                                          BOUND FUNCTIONS"

      CONSTANT MSLIMN     = -12.7               $"MASTER SERVO SATURATIO"
      CONSTANT MSLIMX     = 11.35
      MSLIMA     = BOUND( MSLIMN,MSLIMX,MKSVOA )

      CONSTANT SSLIMN     = -12.7               $"SLAVE SERVO SATURATION"
      CONSTANT SSLIMX     = 11.35
      SSLIMA     = BOUND( SSLIMN,SSLIMX,SKSVOA )

"---->                                          INTEGRATORS"

      XERROR   MMPOSA     = 0.01                $"MOTOR VELOCITY TO POSI"
      MERROR   MMPOSA     = 0.01
      CONSTANT MMPOSZ     = 0.
      MMPOSA     = INTEG( MMOTRA,MMPOSZ)

      XERROR   HSPEEA     = 0.01                $"MOTION SENSORY FEEDBAC"
      MERROR   HSPEEA     = 0.01
      CONSTANT HSPEEZ     = 0.
      HSPEEA     = INTEG( MOVELA,HSPEEZ)

      XERROR   SMPOSA     = 0.01                $"SLAVE MOTOR VELOCITY T"
      MERROR   SMPOSA     = 0.01
      CONSTANT SMPOSZ     = 0.
      SMPOSA     = INTEG( SMOTRA,SMPOSZ)

      XERROR   SOVELA     = 0.01                $"SLAVE-LINK ACCELERATIO"
      MERROR   SOVELA     = 0.01
      CONSTANT SOVELZ     = 0.
      SOVELA     = INTEG( SJOUTA,SOVELZ)

      XERROR   SOPOSA     = 0.01                $"SLAVE-LINK VELOCITY TO"
      MERROR   SOPOSA     = 0.01
      CONSTANT SOPOSZ     = 0.
      SOPOSA     = INTEG( SOVELA,SOPOSZ)

      XERROR   MOVELA     = 0.01                $"MASTER-LINK ACCELERATI"
      MERROR   MOVELA     = 0.01
      CONSTANT MOVELZ     = 0.
      MOVELA     = INTEG( MJOUTA,MOVELZ)
```

Listing continued - ONEDOFMS.CSL

```
      XERROR   MOPOSA    = 0.01                $"MASTER-LINK VELOCITY T"
      MERROR   MOPOSA    = 0.01
      CONSTANT MOPOSZ    = 0.
      MOPOSA     = INTEG( MOVELA,MOPOSZ)

"---->                                          TRANSFER FUNCTIONS"
MACRO EETRAN(ID, NN, ND, IN)
MACRO IF(NN=0) 100
MACRO ASSIGN N
MACRO MULTIPLY 0
MACRO INCREMENT NN
MACRO INCREMENT 1
ARRAY ID_P(N)
MACRO 100..CONTINUE
MACRO MULTIPLY 0
MACRO INCREMENT ND
MACRO INCREMENT 1
ARRAY ID_Q(N)
TRAN(ID_A=NN, ND, ID_P, ID_Q, IN)
MACRO END

      CONSTANT MOTRMP    = 1.
      CONSTANT MOTRMQ    = 0.0012,1.2
      EETRAN( "MOTRM",0,1,MSUM2A )              $"MASTER MOTOR ELECTRICA"

      CONSTANT MMOTRP    = 1.
      CONSTANT MMOTRQ    = 4.1000e-005,0.0002
      EETRAN( "MMOTR",0,1,MDIF1A )              $"MASTER MOTOR DYNAMICS"

      CONSTANT TACTFP    = 1.
      CONSTANT TACTFQ    = 8.0000e-004,1.
      EETRAN( "TACTF",0,1,MDIF2A )              $"TACTILE FORCE FEEDBACK"

      CONSTANT SOTRMP    = 1.
      CONSTANT SOTRMQ    = 0.0012,1.2
      EETRAN( "SOTRM",0,1,SSUM2A )              $"SLAVE-MOTOR ELECTRICAL"

      CONSTANT SMOTRP    = 1.
      CONSTANT SMOTRQ    = 4.1000e-005,0.0002
      EETRAN( "SMOTR",0,1,SDIF1A )              $"SLAVE-MOTOR DYNAMICS"

      CONSTANT MUSCLP    = 40.
      CONSTANT MUSCLQ    = 0.2198,1.
      EETRAN( "MUSCL",0,1,BRAINE )              $"MUSCLE TRANSFER FUNCTI"

END $"OF DERIVATIVE"

END $"OF DYNAMIC"

END $"OF PROGRAM"
```

APPENDIX VII

CRANK-TURNING TASK : FORTRAN SOURCE CODE

Appendix VII.1 - Data logging Program CRANK.FOR

Appendix VII.2 - Analysis Program ANALYZE.FOR

Appendix VII.1 - Listing of Crank data logging program CRANK.FOR

```
      PROGRAM CRANK
C
C
C     ***     PROGRAM TO CAPTURE DATA FROM CRANK       ***
C     ***     TURNING TEST USING FORCE INFORMATION     ***
C     ***     AND CRANK ANGLE                          ***
C
C     ***     SUBROUTINES USED BASED ON AMPLICON       ***
C     ***     PC30 A/D & D/A BOARD: AS FOLLOWS         ***
C     ***                                              ***

C     ***     [1]  PC30-FOR.ASM - 4 CH, 12 BIT A/D &   ***
C     ***          16 BIT DIGITAL INPUT.               ***
C     ***     [2]  DACPC30.ASM - 2 CH, 12 BIT D/A      ***
C
C
      INTEGER*2 THETA,FORCEX,FORCEY,M,N,F3,F2,TORQUE
      DIMENSION M(1020,2)
      CHARACTER*64 STORE,AGAIN
      REAL*4 TORQ
C
C
C     *       SET FILENAME TO WRITE DATA TO      *
C
2     WRITE (*,100)
      WRITE (*,610)
      READ  (*,600) STORE
      OPEN  (2,FILE=STORE,STATUS='NEW')
C
C     *       SET OUTPUT TORQUE IN THE RANGE 0 - 10 NM        *
C
      WRITE(*,100)
5     WRITE(*,620)
      READ (*,400) TORQ
C
      IF (TORQ.LT.0. OR .TORQ.GT.10) GOTO 5
C
C     ***     CONVERT TO DIGITAL VALUE         ***
C
C
      TORQUE= INT(TORQ*25) - 2
C
C     ***     CALL D/A SUBROUTINE              ***
C
      CALL DAC(TORQUE,TORQUE)
C
```

Listing continued - CRANK.FOR

```
C       ***     GET PRESENT CRANK ANGLE         ***
C       ***     IF LESS THAN 20 JUMP BACK       ***
        N=0
10      CALL ADC(THETA,FORCEX,FORCEY,F2,F3)
        IF (THETA.LT.20) GOTO 20
        GOTO 10
C
C       ***     TURN TWICE BEFORE PROCEEDING    ***
C
20      N = N + 1
        IF (N.EQ.2) GOTO 30
        GOTO 10
C
C       ***     BEGIN TO CAPTURE DATA IE.       ***
C       ***     FORCEX,FORCEY AND ANGLE         ***
C       ***     STARTING AT INDEX - 10          ***
C
30      WRITE(*,100)
        WRITE(*,630)
35      CALL ADC(THETA,FORCEX,FORCEY,F2,F3)
        IF (THETA.LT.990) GOTO 35
C
C       ***     START HERE      ***
C
40      CALL ADC(THETA,FORCEX,FORCEY,F2,F3)
        IF (THETA.LT.900) GOTO 45
        M(THETA-989,1) = FORCEX
        M(THETA-989,2) = FORCEY
        GOTO 40
C
C       ***     AND CONTINUE FROM INDEX         ***
C
43      CALL ADC(THETA,FORCEX,FORCEY,F2,F3)
        IF (THETA.GT.950) GOTO 50
45      M(THETA+11,1) = FORCEX
        M(THETA+11,2) = FORCEY
        GOTO 43
C
C       ***     FULL REVOLUTION                 ***
C
48      CALL ADC(THETA,FORCEX,FORCEY,F2,F3)
        IF (THETA.LT.900) GOTO 55
50      M(THETA+11,1) = FORCEX
        M(THETA+11,2) = FORCEY
        GOTO 48
C
C       ***     AND ON UNTIL INDEX + 10         ***
C
53      CALL ADC(THETA,FORCEX,FORCEY,F2,F3)
        IF (THETA.GT.11) GOTO 60
55      M(THETA+1011,1) = FORCEX
        M(THETA+1011,2) = FORCEY
```

Listing continued - CRANK.FOR

```
        GOTO 53
C
C       ***     ALL DATA COLLECTED      ***
C
60      WRITE(*,100)
        WRITE (*,640)
        N = 5
C
C       ***     WRITE FILE STATUS TO DISK       ***
C
        WRITE(2,400) TORQ
C
C       ***   NOW WRITE DATA TO FILE    ***
C
70      WRITE (2,500) N - 10,M(N,1),M(N,2)
        N=N+1
        IF (N.LE.1015) GOTO 70
C
C
C
C       ***     ANOTHER TEST    ***
C
80      WRITE(*,100)
        WRITE (*,700)
        READ (*,600) AGAIN
        IF (AGAIN.EQ.'Y') GOTO 2
        IF (AGAIN.EQ.'y') GOTO 2
C
100     FORMAT (2H+*)
400     FORMAT (F8.4)
500     FORMAT (3I5)
600     FORMAT (A)
610     FORMAT (' ENTER FILENAME TO WRITE DATA TO -  '\)
620     FORMAT (' ENTER DESIRED CRANK TORQUE (0-10NM) -  '\)
630     FORMAT (' START SAMPLING DATA ')
640     FORMAT (' END DATA SAMPLING ')
700     FORMAT (' IF ANOTHER RUN IS WANTED ANSWER YES - (Y) '\)
        STOP
        END
```

Appendix VII.2 - Listing of Analysis Program ANALYZE.FOR

```
      PROGRAM  ANALYZE
C
C     ***     PROGRAM TO ANALYZE CRANK DATA            ***
C     ***                                              ***
C     ***     TEST REQUIRES TO DEFINE A OUTPUT FILE    ***
C     ***     AND TO PRESET REQUIRED CRANK TORQUE.     ***
C     ***     FILE TO WRITE DATA TO, IE ANGLE,FORCEX   ***
C     ***     & FORCEY, OVER 1000 +/- 10 INCREMENTS    ***
C     ***                                              ***
C     ***     THIS PROGRAM READS SAME DATA AND         ***
C     ***     ANALYZES IT TO DETERMINE RADIAL AND      ***
C     ***     TANGENTIAL FORCE ON CRANK AS A           ***
C     ***     FUNCTION OF CRANK ANGLE.                 ***
C     ***                                              ***
C     ***     FURTHER ANALYSIS IS CARRIED OUT TO       ***
C     ***     ESTIMATE MEAN ERROR ON RADIAL AND        ***
C     ***     TANGENTIAL FORCES                        ***
C     ***                                              ***
C
      INTEGER*2       N,TORQUE,X,THETA,FORCEX,FORCEY
      REAL*4          MEANR,MEANT,RESULT,ANGLE,STHETA,TEMP,
     1                CTHETA,AVERAR,AVERAT,RAD,TORQ,DATA
      CHARACTER*64    STORE,AGAIN
      DIMENSION       DATA(1011,3),RESULT(1011,7)
C
C     ***             DEFINE FILE NAME AS 'STORE'      ***
C
1     FORMAT(2H+*)
50    WRITE(*,1)
      WRITE(*,600)
      READ(*,610)  STORE
      OPEN (2,FILE=STORE,ACCESS='SEQUENTIAL',STATUS='OLD')
C
C
C     ***     READ DATA FROM FILE     ***
C
C     *       READ TORQUE SETTING FIRST       *
C
      READ (2,620)    TORQ
C
      N = 1
70    READ (2,300) THETA,FORCEX,FORCEY
      DATA(N,1) = THETA
      DATA(N,2) = FORCEX
      DATA(N,3) = FORCEY
      N=N+1
      IF (N.LE.1011) GOTO 70
C
C
C     ***     PREPAR TO CONVERT DATA TO RADIAL &       ***
C     ***     TANGENTIAL COMPONENTS OF FORCE           ***
C
```

Listing continued - ANALYZE.FOR

```
          N=1
          RAD=6.283183E-03
 100      ANGLE = DATA(N,1)*RAD
          CTHETA = COS(ANGLE)
          STHETA = SIN(ANGLE)
          RESULT(N,1) =  DATA(N,1)
          RESULT(N,2) =  CTHETA*DATA(N,2) + STHETA*DATA(N,3)
          RESULT(N,3) = -STHETA*DATA(N,2) + CTHETA*DATA(N,3)
          N = N+1
          IF (N.LE.1011) GOTO 100
C
C         ***      PREPARE TO CARRY OUT ANALYSIS    ***
C
          OPEN (3,FILE='RESULTS',ACCESS='SEQUENTIAL',STATUS='OLD')
C
          AVERAT = 0
          AVERAR = 0
          N = 6
 150      MEANT = 0

C
C         ***      DETERMINE MEAN VALUE OF TANGENTIAL FORCES       ***
C
          DO 200 X = N-5, N+5
 200      MEANT = MEANT + RESULT (X,3)
          RESULT (N,5) = MEANT/11
C
C         ***      DETERMINE RELATIVE ERROR BETWEEN ACTUAL ***
C         ***      AND ESTIMATED MEAN VALUE                ***
C
          RESULT (N,7) = ABS(ABS(RESULT(N,3))-ABS(RESULT(N,5)))
C
C         ***      CALCULATE VERTICAL AVERAGES             ***
C
          AVERAR = AVERAR+ABS(RESULT(N,2))
          AVERAT = AVERAT+RESULT(N,7)
          N = N + 1
          IF (N.LE.1006) GOTO 150
          AVERAR = AVERAR/1000
          AVERAT = AVERAT/1000
C
C         ***      WRITE VERTICAL AVERAGES         ***
C
          WRITE(*,1)
          WRITE (*,650)   AVERAR,AVERAT
          WRITE (*,660)   TORQ
          WRITE (3,670)   STORE
          WRITE (3,660)   TORQ
          WRITE(3,1)
          WRITE (3,650)   AVERAR,AVERAT
          WRITE(3,1)
C
```

Lsting continued - ANALYZE.FOR

```
C       ***     ANY MORE ANALYSIS       ***
C
        WRITE (*,700)
        READ (*,610) AGAIN
        IF (AGAIN.EQ.'Y') GOTO 50
        IF (AGAIN.EQ.'y') GOTO 50
C
625     CONTINUE
650     FORMAT (' MEAN RAD ERR=',F6.2,' ,     MEAN TAN ERR=',F6.2)
300     FORMAT (BN,3I5)
400     FORMAT (1H,I5,3F10.4)
500     FORMAT (1H, F10.4)
600     FORMAT (' ENTER FILENAME CONTAINING DATA -  '\)
610     FORMAT (A)
620     FORMAT (BN,F8.4)
660     FORMAT (' CRANK TORQUE = ',F8.4)
670     FORMAT (' FILENAME CONTAINING DATA - ',A)
700     FORMAT (' ANY FURTHER ANALYSIS (THEN ENTER Y) -   '\)
        STOP
        END
```

APPENDIX VIII

MECHANICAL LAYOUT DRAWINGS FOR EXPERIMENTAL RIG

The following layout drawings are contained within the inner pocket :

Pantograph Arm - Main layout
- Terminal joint
- X-Y Cross-slide

Articulated Arm - Main layout
- Gearbox